Draft version 0.5

ATLAS NOTE

February 10, 2017

Search for new phenomena with the ATLAS detector in monophoton events from pp collisions at $\sqrt{s} = 13$ TeV collected in 2015 and 2016

Leonard Aubry[2], Leonardo Carminati[1], Donatella Cavalli[1], Marie-Helene Genest[2], Maria Giulia Ratti[1], Silvia Resconi[1]

[1]*Milan*
[2]*LPSC Grenoble*

Abstract

This note presents the search for new physics with the ATLAS detector in the γ + missing transverse momentum final state using 36.4 fb^{-1}of pp collision data at $\sqrt{s} = 13$ TeV recorded in 2015 and 2016. Events are selected by requiring the presence of a single isolated photon and missing transverse momentum. The results of the search are interpreted within the framework of various new physics models.

Contents

List of contributions

L. Aubry [LPSC Grenoble]: electron faking photons, implementation of multi-bin fit, Signal Regions yields and uncertainties, data/MC comparisons, Zgamma limits.

L. Carminati [Milan]: jet faking photons, supervisor of M.G. Ratti.

D. Cavalli [Milan]: paper editor, MET studies, MET Significance criteria.

M-H. Genest [LPSC Grenoble]: paper editor, electrons faking photons, trigger turn-on, DM signal and background generation, derivation framework, limit settings for DM and Zgamma models, supervisor of L. Aubry.

M.G. Ratti [Milan]: support for analysis code and PDF systematics.

S. Resconi [Milan]: analysis contact, analysis code development, jet faking photons, gamma-jet background, mini-trees production, supervisor of M.G. Ratti.

List of changes

Main changes to the note are overviewed in the following.

Draft version 0.1 First description of the 2016 analysis.

- Section 2: new signal grid for axial-vector simplified model of dark matter production at NLO
- Section 4: new signal region optimization studies to reduce γ + jet background in SR (more details in Appendix A).
- Section 5: first estimations for photon fakes background based on a data sample of $13.9 fb^{-1}$, data/MC comparisons in CRs (more plots in Appendix C and D).
- Section 7 and 8: same as in last year note, should be updated in next versions.

Draft version 0.2 moved to full 2015+2016 luminosity (36.4 fb^{-1})

- Section 2: new Feynman diagrams for axial-vector simplified model of dark matter production at NLO.
- Section 4: new definition of inclusive and exclusive SRs corresponding to increasing MET thresholds. Updated trigger efficiency for full 2015+2016 luminosity.
- Section 5: updated data/MC pre-fit distributions, New table to explain probe-electron control regions used to estimate the electron-to-photon fake background. Updated electron and jet fakes estimates for inclusive/exclusive SRs for full 2015+2016 luminosity.
- Section 6: new results for full 2015+2016 luminosity obtained performing a HistFitter background only fit in the inclusive and exclusive SRs . New post-fit distributions for main kinematic variables.
- Section 7: new post-fit breakdown of systematics for the inclusive and exclusive SRs.
- Section 8: new table with signal expected event yields for the inclusive SRs.

Draft version 0.3 for circulation to the JDM subgroup

- implemented EB comments related to Draft version 0.2.
- Section 5: added kinematic distributions for leptons in CRs.
- Section 6: first check with simplified shape fit performed on all exclusive SRs. For the moment added only k-factors.
- Section 7: summary table for breakdown of systematics, pull plots for systematic nuisance parameters and correlation matrices for all inclusive and exclusive SRs.
- Appendix E: pre-fit breakdown of systematics for all inclusive and exclusive SRs.

Draft version 0.4 for circulation to the Exotics group

- Section 6: updated all results in inclusive and exclusive SRs fixing a problem in one MC sample in which only a part of events were processed (this was causing a tension between k_Zmumu and k_Zee).
- Section 8: New model independent limit on visible cross-secition, new exclusion limit for simplified model with axial-vector mediator, new limit on suppression scale M_* for a dimension-7 operator EFT model. Updated signal systematics uncertainty.
- Appendix D: check of the impact of adding 1eleCR in the simultaneous fit.

- Appendix F: checks on expected limits between single bin fit on inclusive SRs and simplified shape fit on exclusive SRs to assess the analysis strategy.
- Appendix G: checks to show that the recommended various choices of couplings for axial-vector and vector mediators models only affect the cross-section and not the acceptance of the analysis.

Draft version 0.5 for circulation to ATLAS

- Section 6: moved to post-fit distributions with 3 bins (the same used in the multiple-bin fit).
- Section 8: model independent limit on fiducial cross-section, limits for simplified model, for EFT and for Zgamma.

1 Introduction

The analysis presented in this note consists in a search for an excess in events with a final state composed of a single high transverse momentum photon and a consequently large missing transverse momentum ($E_{\mathrm{T}}^{\mathrm{miss}}$) may constitute a striking signature of new physics at the LHC. Various theories involving new physics, as Large Extra Dimensions (LED) theories and models in which Dark Matter (DM) particles are produced in association with a photon, are expected to produce an excess of monophoton events with respect to the SM.

DM can be produced at LHC if it interacts with Standard Model (SM) particles. Since many theories of physics beyond the SM predict a weakly interacting DM candidate, it can be measured only as missing transverse momentum ($E_{\mathrm{T}}^{\mathrm{miss}}$) in the ATLAS detector. To tag those events a detectable physics object is required to be produced in association with DM particles. The tag objects include single photons or jets as well as Z, W or Higgs bosons. Such searches are known as mono-X searches and first results on Run II data taken during 2015 and corresponding to a centre-of-mass energy of 13 TeV have shown a a good complementarity with di-jets searches [1] No deviations from SM predictions have been observed so far but the increased luminosity taken during 2016 will permit to enhance their discovery and exclusion power extending the reach of DM searches.

The monophoton analysis is characterized by a relative clean final state, actually only few processes give such a monophoton final state in the Standard Model (SM). The abundant multijet background is strongly reduced by the large $E_{\mathrm{T}}^{\mathrm{miss}}$ selection and other important backgrounds, such as top quark and W/Z bosons produced in association with a jet, are reduced by asking a high transverse energy photon.

The dominant backgrounds consist in processes with a Z or W boson produced in association with a photon (mainly $Z(\rightarrow \nu\bar{\nu}) + \gamma$). They are estimated by rescaling the MC prediction for those backgrounds with a simultaneous fitting technique, based on control regions built by reverting one or more cuts of the signal region such that one type of process becomes dominant in that region. Other backgrounds, like W/Z + jet, top and diboson, in which electrons or jets can fake photons are estimated with data-driven techniques.

This note presents an analysis of the monophoton final state with the ATLAS detector [1]. The search presented here is performed on events collected in pp collisions at 13 TeV in 2015 and 2016 data-taking (36.4 fb^{-1}) and it is an update of the 2015 analysis (3.2 fb^{-1}) [2].

Section 2 describes the data and the MC simulation samples used for the analysis while Sections 3 and 4 cover the definition of the objects used in this analysis and the event selection, respectively. The background estimation is reviewed in Section 5 . The results in the signal region are described in Section 6 and the systematic uncertainties are reviewed in Section 7. Finally the interpretation of results in the context of the models studied is described in 8. Conclusions are presented in Section 9.

[1] see https://atlas.web.cern.ch/Atlas/GROUPS/PHYSICS/CombinedSummaryPlots/EXOTICS/ATLAS_DarkMatter_Summary/history.htm

2 Data and simulation samples used in this analysis

This analysis is performed on data from proton-proton collision at $\sqrt{s}$ = 13 TeV recorded by the ATLAS experiment at the LHC during 2015 and 2016 with stable proton beams. Only data with a fully functioning calorimeter, inner detector and muon spectrometer are analyzed. The standard detector quality criteria are applied, which reduce the impact of instrumental noise and out-of-time calorimeter deposits from cosmic ray and beam backgrounds. A good run list (GRL) is used in order to select lumi blocks for which all subdetectors were working as expected. The data sample used corresponds to a total integrated luminosity of 36.4 fb^{-1}, collected with a bunch crossing interval (bunch spacing) of 25 ns.

The Monte Carlo (MC) samples used in the analysis are from the official MC15 Monte Carlo production (mc15_13TeV). In particular, the MC15c samples with an updated average number of interactions per event ($< \mu >$) (with respect to the MC15b samples) that reflects the distribution found in the 2016 data, have been used for this note. In this analysis EXOT6 official ATLAS derived samples are used, as explained in 4.1.

The pileup collisions are generated with Pythia8 using the MSTW2008 LO PDF [3] and the ATLAS A2 tune [4]. The pileup interactions are randomly selected for each event, and they are overlaid on the simulated physics process before running event reconstruction. The reconstruction of simulated events proceeds as with data events. The MC simulation samples are weighted such that the distribution of the average number of interactions per bunch crossing matches that observed in the data sample to ensure that the pile-up interactions are accurately described.

2.1 Signal samples

2.1.1 Dark matter models

The MC15 dark matter signal samples follow the recommendations from the joint ATLAS/CMS Dark Matter Forum [5]. There are two types of models considered, illustrated in Figure 1: a simplified model and an effective field theory (EFT) model of type $\gamma\gamma\chi\chi$, as described below.

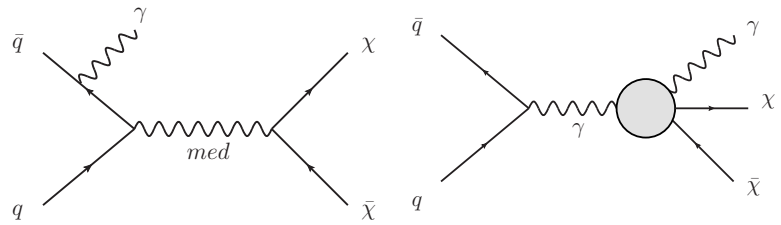

Figure 1: Feynman diagrams corresponding to the DM models considered: the simplified model (left) and the EFT model (right).

Simplified dark matter model

The simplified model considers an s-channel mediator with axial-vector interactions. Only axial-vector interactions are generated as vector and axial-vector models only differ by their cross sections and can hence be rescaled to one another if wanted. There are five free parameters in this kind of models: the mass of the mediator M_{med}, the mass of the dark matter particle m_χ, the coupling of the mediator to the quarks g_q, the coupling of the mediator to the dark matter particle g_χ and the width of the mediator. As recommended in [5], g_q is set to be universal in quark flavour and equal to 0.25, g_χ is set to 1.0, and the width of the mediator is computed as the minimal width allowed given the couplings and masses[2].

[2]The script to compute this width can be found here: https://github.com/noslenwerdna/DarkMatterWidthCalculator

The minimal width assumption implies that the mediator only decays to quarks and the DM particles (the only decays strictly necessary to maintain the self-consistency of the model): the width, computed taking into account only these decay modes, varies from about $\Gamma_{MED}/m_{MED} \approx 2\%$ to $\Gamma_{MED}/m_{MED} \approx 6\%$ as can be seen in Table 2.3 of Reference [5].

As done with the previous analysis for the DM summary plots[3], a rescaling of the cross section of the samples can eventually be used to present the results for other values of these couplings. A grid in the m_χ/M_{med} plane is generated, in accordance with the recommendations. The parameters of the samples are reported in Table 1. When the mediator mass is very high, the simplified model behaves like an Effective Field Theory: the mediator can be integrated out of the propagator when its mass is assumed to be much greater than the momentum transfer at the LHC. For this reason no specific EFT model of the type $qq\chi\chi$ is produced.

For this simplified model, the generation was updated with respect to the 2015 analysis: the new implementation of the model at NLO (DMsimp) is used. It allows new diagrams to take part in the event generation, as exemplified in Figure 2. It was cross-checked to give the same cross-section and kinematic distributions as the previously used LO model (dmA) when used at LO. The acceptance of the analysis was checked when validating the NLO implementation and it was found to be roughly 15% lower for the NLO model than for the LO one; the increased cross section however counterbalances advantageously this loss, leading to an overall increase in the yield of $O(10\%)$ after selection with respect to the LO model.

The set of parton distribution functions used is NNPDF30_nlo_as_0118. The samples[4] are generated with MCProd-19.2.5.14.3 (the samples are now ready, the derivation step is running and is almost done); MADGRAPH 5 v2.4.3 is used in its on-the-fly implementation in conjunction with Pythia 8.212 (with tune A14 NNPDF23LO); a photon with at least 130 GeV of transverse momentum is requested in MADGRAPH . Distributions at truth level were cross checked for validation of the jobOptions[5] before production. As seen in other analyses, the acceptance is seen to be constant as a function of the dark matter candidate mass (within the statistical uncertainties) for a fixed mediator mass in the on-shell regime, see Figure 3. The acceptance and cross section in the on-shell regime was also crossed-checked to be unchanged if one goes from low-mass dark matter at $m_\chi = 10$ GeV to very low-mass dark matter at $m_\chi = 0.1$ GeV (by comparing points at $m_{Med} = 200$, 600 and 1000 GeV). For this reason, no point below $m_\chi = 10$ GeV is requested as the results obtained for $m_\chi = 10$ GeV will be valid down to very low DM masses. Therefore, full simulation is only requested for m_χ=10 GeV for the various mediator masses well into the on-shell space. Full simulation is also requested near the diagonal $m_{Med} = 2m_\chi$ and for a few points in the off-shell region of the parameter space in order to allow good interpolation of the limit near the diagonal. The cross-section being very low in the off-shell region (see Figure 3), the analysis is only expected to be sensitive to this region at very low mediator masses. In total, 90 points are generated officially, 51 in full simulation (fast simulation leads to discrepancies in some photon quantities such as the isolation) and 39 at truth level only. All samples contain 50000 events.

A preliminary number of events expected for 30 fb^{-1}of data is shown in Figure 4; it is a rough estimate based on the truth-level samples and using a preliminary event selection, using an 80 % reconstruction efficiency for all points. The final yields after simulation can be seen in Section 8. In comparison, as will be shown in Section 6.2, roughly 2300 background events are expected for 30 fb^{-1} in the signal region requiring $E_{\mathrm{T}}^{\mathrm{miss}}$>150 GeV .

[3] https://atlas.web.cern.ch/Atlas/GROUPS/PHYSICS/CombinedSummaryPlots/EXOTICS/ATLAS_DarkMatter_Summary_ModifiedCoupling/history.html

[4] see https://its.cern.ch/jira/browse/ATLMCPROD-3743

[5] See https://twiki.cern.ch/twiki/bin/viewauth/AtlasProtected/MonoPhotDMProductionRun2

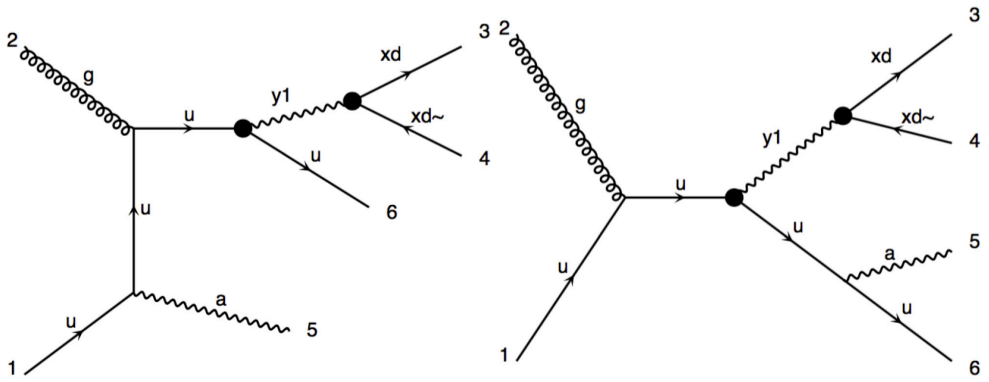

Figure 2: Example of production diagrams considered at NLO for the simplified-model dark-matter production (”y1” is the mediator, ”xd” the dark matter candidate, ”a” the photon and ”u” is a quark in these diagrams).

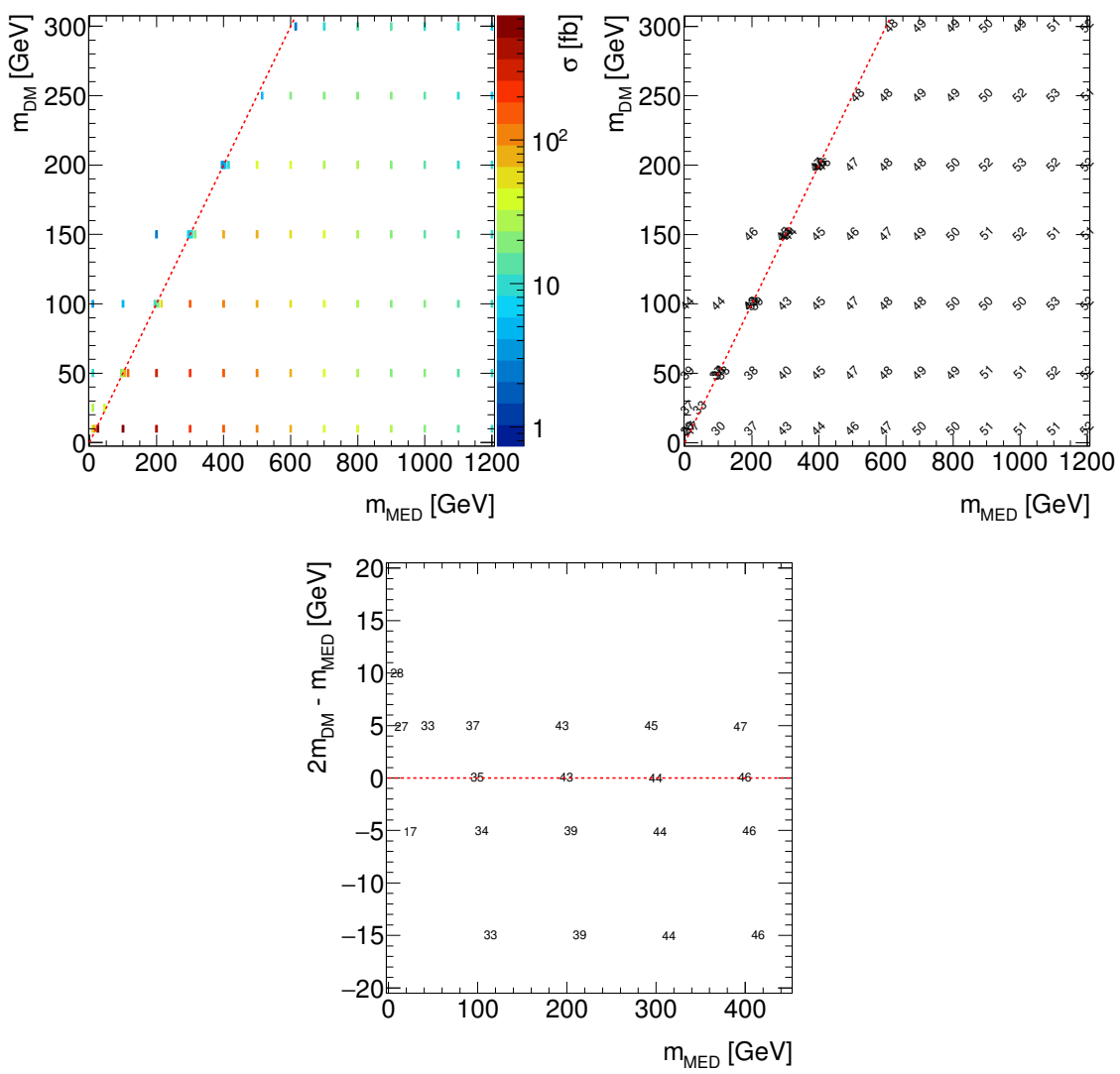

Figure 3: Cross section for the DMsimp axial-vector model for the points generated as a function of the dark matter and the mediator mass (upper left) and truth-level acceptance (in %) of the signal region cuts (upper right). The latter is also shown as a function of $2m_{DM} - m_{MED}$ and m_{MED} for a part of the parameter space scanned in order to show more explicitely the acceptance near the on-shell/off-shell mediator boundary (lower plot). The acceptance is computed with private samples containing 5000 events each (the statistical uncertainty on the acceptance therefore varies from ±1% to ±3% depending on the point). In both plots, the dashed red line separates the on-shell and off-shell regimes.

Dataset ID	m_χ [GeV]	M_{med} [GeV]	Cross-section [fb]
306618	10	10	62.87
306619	10	15	71.04
306620	10	25	734.9
306621	10	100	716.4
306622	10	200	411.4
306623	10	300	239.8
306624	10	400	154.5
306625	10	500	96.84
306626	10	600	67.01
306627	10	700	46.16
306628	10	800	32.91
306629	10	900	23.92
306630	10	1000	17.33
306631	10	1100	12.71
306632	10	1200	9.794
306633	100	10	3.678
306634	100	100	4.397
306635	100	195	10.66
306636	100	200	14.06
306637	100	205	22.35
306638	100	215	47.25
306639*	100	300	150.3
306640*	100	400	122.0
306641*	100	500	86.61
306642*	100	600	60.78
306643*	100	700	42.75
306644*	100	800	30.54
306645*	100	900	22.65
306646*	100	1000	16.85
306647*	100	1100	12.49
306648*	100	1200	9.484
306649	150	200	2.275
306650	150	295	5.952
306651	150	300	7.247
306652	150	305	10.02
306653	150	315	19.30
306654*	150	400	71.03
306655*	150	500	66.63
306656*	150	600	52.13
306657*	150	700	38.29
306658*	150	800	28.37
306659*	150	900	21.07
306660*	150	1000	15.76
306661*	150	1100	12.06
306662*	150	1200	9.114
306663	200	395	3.417
306664	200	400	4.088
306665	200	405	5.340
306666	200	415	9.179
306667*	200	500	35.96
306668*	200	600	38.56
306669*	200	700	32.03
306670*	200	800	25.48
306671*	200	900	19.17
306672*	200	1000	14.38
306673*	200	1100	11.37
306674*	200	1200	8.685
306675	25	10	25.66
306676	25	45	40.15
306677	250	515	4.729
306678*	250	600	19.78
306679*	250	700	22.96
306680*	250	800	20.69
306681*	250	900	16.62
306682*	250	1000	13.29
306683*	250	1100	10.30
306684*	250	1200	7.960
306685	300	615	2.760
306686*	300	700	11.19
306687*	300	800	14.03
306688*	300	900	13.26
306689*	300	1000	11.50
306690*	300	1100	9.274
306691*	300	1200	7.352
306692	50	10	11.10
306693	50	95	23.05
306694	50	100	31.99
306695	50	105	70.17
306696	50	115	168.7
306697*	50	200	325.6
306698*	50	300	226.0
306699*	50	400	147.3
306700*	50	500	95.45
306701*	50	600	65.32
306702*	50	700	46.13
306703*	50	800	32.30
306704*	50	900	23.00
306705*	50	1000	17.11
306706*	50	1100	12.85
306707*	50	1200	9.521

Table 1: Cross-sections for the NLO DM simplified-model samples with axial-vector couplings. The * in the dataset ID column refers to samples which are only generated at truth level: they can be rescaled by cross-section from fully simulated lower-mass DM samples as they have the same acceptance.

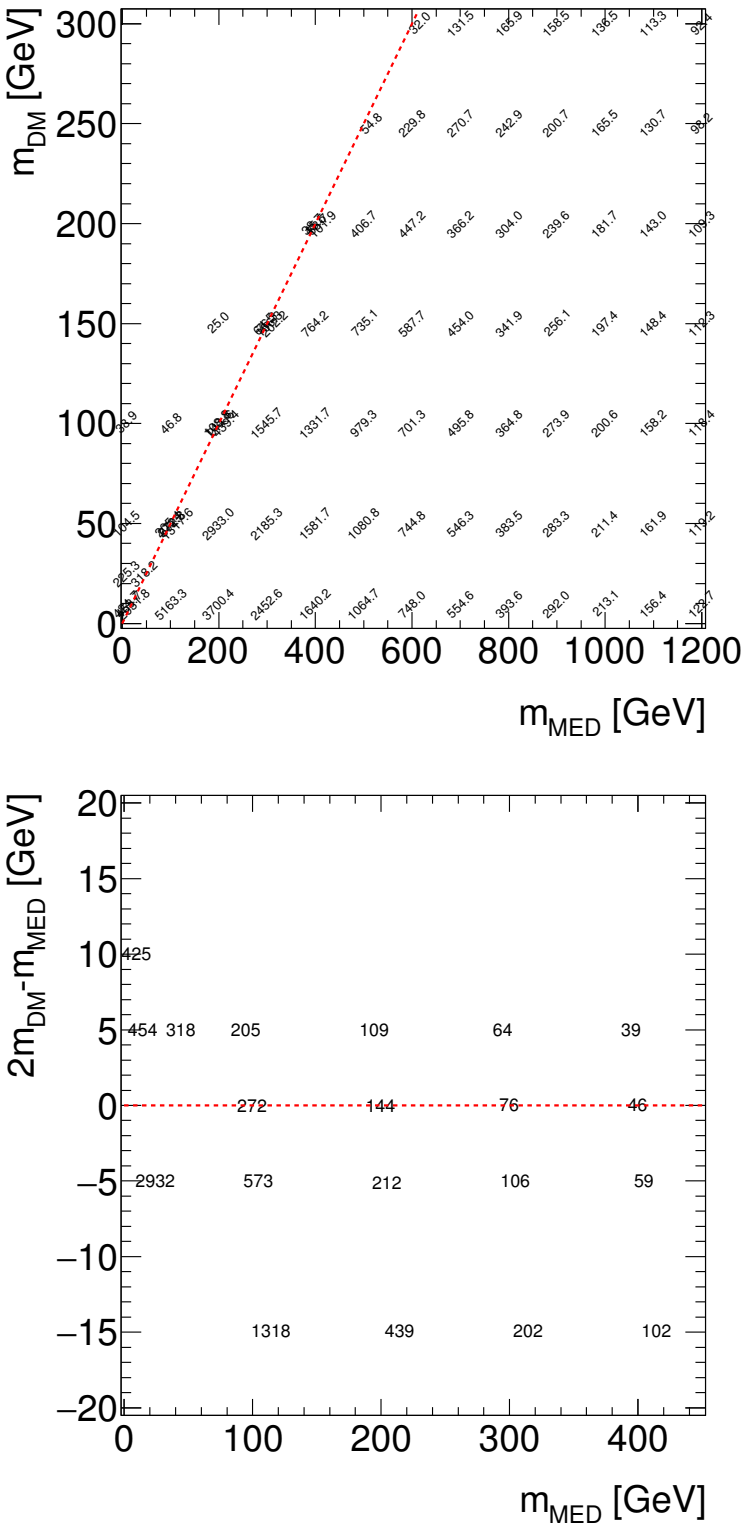

Figure 4: Number of events for 30 fb^{-1}after the signal region cuts are applied at truth level, assuming a reconstruction efficiency of 80% (level seen in the 2015 analysis). The lower plot displays the same information for a part of the parameter space, but plotting the yield as function of $2m_{DM} - m_{MED}$ versus m_{MED} in order to show the on-shell/off-shell mediator boundary better.

Dimension-7 EFT model

The second type of model is a dimension-7 operator EFT model with contact interaction of type $\gamma\gamma\chi\chi$, which was also used in the Run-1 analysis. There are four free parameters in this model: the EW coupling strengths k_1 and k_2, the suppression scale Λ (also referred to as M_*) and the dark matter particle mass m_χ. The detailed description of the model is shown in Section 3.2.2 of [5]. The event generation settings follow the Dark Matter Forum recommendations for the choice of parameters and generators: the parameters which only influence the cross section are set to $k_1 = k_2 = 1.0$ and $\Lambda = 3$ TeV ; these give rise to very small cross sections, but the important point here is to have initial benchmark samples which can be rescaled (as the cross section depends on Λ as $\sigma \propto \Lambda^{-6}$) in order to eventually place limits on the parameter Λ itself, which will be lower than 3 TeV and will thus correspond to higher cross sections. A scan of various values of m_χ is performed. The various samples produced are listed in Table 2. For these models, the set of parton distribution functions used is NNPDF30_lo_as_0130. The release used is MCProd-19.2.4.4.2; MADGRAPH 5 v2.2.3 is used in its on-the-fly implementation in conjunction with Pythia 8.186 (with tune A14 NNPDF23LO); a photon with at least 130 GeV of transverse momentum is requested in MADGRAPH . 10000 events per sample is produced with full simulation.

Run numbers	m_χ [GeV]	Cross-section [fb]
303643	1	1.14E-03
303644	10	1.14E-03
303645	50	1.11E-03
303646	100	1.03E-03
303647	200	8.35E-07
303648	400	4.81E-07
303649	800	1.34E-07
303650	1300	2.41E-08

Table 2: Cross-sections for the DM EFT samples of type $\gamma\gamma\chi\chi$.

2.1.2 Large Extra Dimensions Model

Some $q\bar{q} \rightarrow \gamma G$ datasets were produced in the framework of the large-extra-dimension scenario of Arkani-Hamed, Dimopoulos, and Dvali (ADD)[6]. Figure 5 shows two representative Feynman diagrams corresponding to the ADD model with graviton production.

The generation of these samples is based on the Run-1 setup, but with the new centre-of-mass energy and an updated lower cut on $\hat{p}_T^{min}$ set at 100 GeV . This cut defines the lowest transverse momentum used for generation of the $2 \rightarrow 2$ leading-order matrix elements. The simulation uses the A14 Pythia8 tune i[7] with the NNPDF23LO proton structure function [8]. The events are generated with Pythia 8 using the same tune and PDF as the dark matter samples, and with varying values of the 4+n-dimensional Planck scale, M_D, and number of extra dimensions, n. The available samples are summarized in Table 3.

The implementation of the ADD model in Pythia8 is discussed in [9]. It differs from the original Pythia6 implementations. In particular, it has two parameters, $m0$ (graviton mass) and MD (scale). The case $m0 = MD$ corresponds to the extreme point for the theory to make sense. The current simulation was performed for this extreme setting when $m0 = MD$. As an example, here we show a typical setting of Pythia8 for $m0 = MD = 2000$ GeV used in this analysis:

```
'ExtraDimensionsLED:ffbar2Ggamma = on', # Process type.
'ExtraDimensionsLED:n = 2',             # Number of extra dimensions.
'ExtraDimensionsLED:MD = 2000',         # Choice of the scale, MD.

# Treatment of the effective theory
'ExtraDimensionsLED:CutOffmode = 0'

# 0: all the events.
# 1 : truncate events with s_hat>MDˆ2, with a weight of MDˆ2/s_hatˆ4
'PhaseSpace:pTHatMin = 100.',  # pT Cut at the generator level.

# Choice of factorization scale (3:
# the arithmetic mean of the squared transverse masses
# of the two outgoing particles, default in pythia6)
'SigmaProcess:factorScale2 = 3',

# Choice of renormalization scale (3: the arithmetic mean of the
# squared transverse masses of the two outgoing particles.
# This is default in Pythia6
'SigmaProcess:renormScale2 = 3'

# Central value of the Breit-Wigner mass resonance
'5000039:m0 = 2000.'

# Resonance width
'5000039:mWidth = 1000.
```

To estimate uncertainties on the modelling of ISR/FSR radiation. As example, the Pythia8 was generated by using a new tune "Var3aUp" by replacing the common job option [10]:

```
MC15JobOptions/Pythia8_A14_NNPDF23LO_EvtGen_Common.py
MC15JobOptions/Pythia8_A14_NNPDF23LO_Var3aUp_EvtGen_Common.py
```

Run numbers	n	M_D [GeV]	Cross-section [fb]	Upper Var3aUp
303004	2	2000	78.05	0.07767
303009	2	3000	15.42	0.01548
303005	3	2000	110.0	0.1092
303010	3	3000	14.27	0.01483
303006	4	2000	180.5	0.0869
303011	4	3000	15.9	0.01578
303007	5	2000	328.5	0.3423
303012	5	3000	19.26	0.01927
303008	6	2000	647.4	0.6359
303013	6	3000	25.36	0.02438

Table 3: Cross-sections for the ADD MC15 samples for $n = 2 - 6$ and $MD = 2, 3$ TeV. The last column shows a systematic variation in Pythia8 settings which tests the sensitivity to the ISR/FSR radiation (see the text).

The result of this change in the Pythia8 parameters is shown in the last column of Table 3. The maximum uncertainty which can be attributed to this variation is 4%. But the typical uncertainty is 1%, without a clear trend as a function of the parameters MD and n.

The effect of variations on the acceptance corrections due the ISR/FSR was estimated using the Var3aUp, Var3bUp and Var3cUp Pythia8 settings. The global effect on the acceptance was below 4.1%.

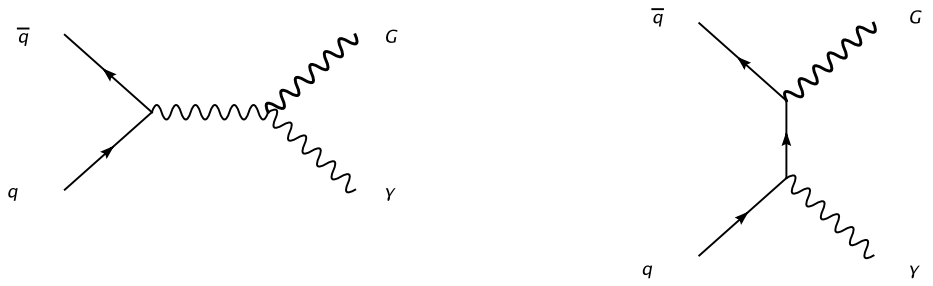

Figure 5: Feynman diagrams corresponding to the ADD model with graviton (G) production.

2.1.3 $Z(\to \nu\nu) + \gamma$ resonance

An interesting possibility for this analysis would also be to search for the production of heavy resonances decaying to the $E_{\mathrm{T}}^{\mathrm{miss}} + \gamma$ final state, such as a scalar decaying to $Z(\to \nu\nu) + \gamma$. The samples used can be seen in Table 4. As the idea would be to put a limit on the cross section for these models, the initial cross section for these samples is irrelevant.

The samples were generated using Powheg-Box with CT10 and Pythia 8.210 for the showering with the AZNLO tune based on CTEQ6L1. They assume the production, through gluon-gluon fusion, of a heavy scalar resonance X of very narrow width (4.07 MeV) which then decays exclusively to $Z\gamma$ (the limit will hence be placed on the production cross section of this resonance times the branching ratio of $X \to Z\gamma$). The Z decay is not limited in the high-mass samples (see Table 4), except for the 1 TeV mass point in which the Z is forced to decay to neutrinos. For this reason, this point will not be used in the

Run numbers	M_H [GeV]	Z decay
305048	1000	$\nu\nu$
341936	2000	inclusive
343586	2500	inclusive
343587	3000	inclusive
343588	3500	inclusive
343589	4000	inclusive
343590	4500	inclusive
343591	5000	inclusive

Table 4: Samples for the heavy scalar resonance decaying to $Z\gamma$

limit setting unless we succeed in having in time the proper derivation for the complementary $Z \to \ell\ell$ decay. It is important to have the leptonic decay channels opened as well because through its $Z(\to \ell\ell)+\gamma$ decay, the signal would contaminate the dileptonic control regions used in this analysis to estimate the major $Z \to \nu\nu$ background (see Section 5.1).

Limits have already been placed by searches conducted via a bump search method in the very sensitive dileptonic channel and the hadronic channel for masses below and above 1.5 TeV , respectively [11]. Although the Z branching ratio to neutrinos is higher than to charged leptons, the presence of $E_{\mathrm{T}}^{\mathrm{miss}}$ makes the search much less sensitive than in the dileponic channel; preliminary studies suggest that the region of interest for the analysis discussed here lies at higher masses, where it could eventually complement the hadronic searches. For a 1.5 TeV signal, assuming an acceptance of about 50% as seen in MC validation studies, one would expect $O(15)$ events per dileptonic control region for 36.4 fb^{-1}of data, if one assumes a cross section at the limit of the exclusion obtained in [11]. These events would sit at high values of $m_{\ell\ell\gamma}$, where almost no background is expected; the contamination of the control region is kept under control by placing an upper limit on $m_{\ell\ell\gamma}$, the request of $m_{\ell\ell\gamma} < 1$ TeV is applied in the analysis selection. This criterion implies a small impact on the CR statistics.

2.2 Background samples

The following Standard Model backgrounds may lead to a final state with a high p_{T} photon and a high $E_{\mathrm{T}}^{\mathrm{miss}}$:

- $\gamma + Z(\to \nu\nu)$: this is the only irreducible SM background;
- $\gamma + W(e\nu)$: the e is not reconstructed, or is reconstructed as a γ;
- $\gamma + W(\mu\nu)$: the μ is not reconstructed;
- $\gamma + W(\tau\nu)$: the τ can either decay leptonically and be missed (see other leptonic channels above) or reconstructed as a jet;
- $\gamma + Z(ll)$: both taus, electrons or muons are missed;
- jet + $Z(\to \nu\nu)$: the jet fakes a γ;
- jet + $W(e\nu)$: the e or a jet fakes a γ;
- jet + $W(\mu\nu)$ and jet + $W(\tau\nu)$: the μ/τ is not reconstructed or the τ is reconstructed as a jet and a jet fakes a γ;
- $t\bar{t}$, single-t and diboson: similar to the W + jet backgrounds;

· *QCD* and γ + jet: a high fake $E_{\mathrm{T}}^{\mathrm{miss}}$ is produced by a miscalibration or misreconstruction of a jet or a γ and a jet fakes a γ in case of QCD.

· $\gamma + t\bar{t}$: leptons from W's are not reconstructed, minor contribution.

Some more details about generation and simulation of the SM background samples are given in the following.

For $W/Z\gamma$ backgrounds, events containing a charged lepton and neutrino or a lepton pair (lepton is an e, μ or τ), together with a photon and associated jets are simulated using the Sherpa 2.1.1 generator [12]. The matrix elements including all diagrams with three electroweak couplings are calculated with up to three partons at LO and merged with Sherpa parton shower [13] using the ME+PS@LO prescription [14]. The CT10 PDF set [15] is used in conjunction with a dedicated parton shower tuning developed by the Sherpa authors. For γ^*/Z events with the Z decaying to charged particles a requirement on the dilepton invariant mass of $m_{\ell\ell} > 10$ GeV is applied at generator level.

Events containing a photon with associated jets are also simulated using Sherpa 2.1.1, generated in several bins of photon p_{T} from 35 GeV up to larger than 4 TeV. The matrix elements are calculated at LO with up to three partons (lowest p_{T} slice) or four partons and merged with Sherpa parton shower using the ME+PS@LO prescription. The CT10 PDF set is used in conjunction with the dedicated parton shower tuning.

For W/Z+jets backgrounds, events containing W or Z bosons with associated jets are again simulated using Sherpa 2.2.0. The matrix elements are calculated for up to two partons at NLO and four partons at LO using the Comix [16] and OpenLoops [17] matrix element generators and merged with Sherpa parton shower using the ME+PS@NLO prescription [18]. As in the case of the γ+jets samples, the CT10 PDF set is used together with the dedicated parton shower tuning. The W/Z+jets events are normalized to NNLO cross sections [**?**]. These samples are also generated in several p_{T} bins.

Multi-jet processes are simulated using the Pythia 8.186 generator. The A14 tune is used together with the NNPDF2.3LO PDF set. The EvtGen v1.2.0 program [19] is used to simulate the bottom and charm hadron decays.

For the generation of $t\bar{t}$ and single top quarks in the Wt and s-channel, the Powheg-Box v2 [20, 21] generator is used, with the CT10 PDF set used in the matrix element calculations. For all top processes, top-quark spin correlations are preserved. For t-channel production, top quarks are decayed using MadSpin [22]. The parton shower, fragmentation, and the underlying event are simulated using Pythia 6.428 [23] with the CTEQ6L1 [24] PDF sets and the corresponding Perugia 2012 tune [25]. The top mass is set to 172.5 GeV. The EvtGen v1.2.0 program is used for properties of the bottom and charm hadron decays.

The simulated event samples for the SM backgrounds are summarized in Tables 5-7. All samples are from the official MC15 production.

Channel	Run numbers	Generator	Cross-section [pb]	k-factor	Filter efficiency
$W(e\nu)$ + jet					
$0 < p_T < 70$ GeV, c-veto/b-veto	361300	Sherpa v2.2.0	21283.	0.90824	0.890724
$0 < p_T < 70$ GeV, c-filter/b-veto	361301	Sherpa v2.2.0	21379.	0.90824	0.049290
$0 < p_T < 70$ GeV, b-filter	361302	Sherpa v2.2.0	21392.	0.90824	0.059786
$70 < p_T < 140$ GeV, c-veto/b-veto	361303	Sherpa v2.2.0	632.99	0.90824	0.728829
$70 < p_T < 140$ GeV, c-filter/b-veto	361304	Sherpa v2.2.0	632.58	0.9082	0.176811
$70 < p_T < 140$ GeV, b-filter	361305	Sherpa v2.2.0	632.58	0.90824	0.096681
$140 < p_T < 280$ GeV, c-veto/b-veto	361306	Sherpa v2.2.0	90.146	0.90824	0.681554
$140 < p_T < 280$ GeV, c-filter/b-veto	361307	Sherpa v2.2.0	89.969	0.90824	0.205907
$140 < p_T < 280$ GeV, b-filter	361308	Sherpa v2.2.0	90.026	0.90824	0.112284
$280 < p_T < 500$ GeV, c-veto/b-veto	361309	Sherpa v2.2.0	6.5305	0.90824	0.652724
$280 < p_T < 500$ GeV, c-filter/b-veto	361310	Sherpa v2.2.0	6.6273	0.90824	0.221526
$280 < p_T < 500$ GeV, b-filter	361311	Sherpa v2.2.0	6.5447	0.90824	0.130994
$500 < p_T < 700$ GeV, c-veto/b-veto	361312	Sherpa v2.2.0	0.41892	0.90824	0.631749
$500 < p_T < 700$ GeV, c-filter/b-veto	361313	Sherpa v2.2.0	0.39861	0.90824	0.243561
$500 < p_T < 700$ GeV, b-filter	361314	Sherpa v2.2.0	0.39684	0.90824	0.155229
$700 < p_T < 1000$ GeV, c-veto/b-veto	361315	Sherpa v2.2.0	0.072864	0.90824	0.609620
$700 < p_T < 1000$ GeV, c-filter/b-veto	361316	Sherpa v2.2.0	0.10164	0.90824	0.202801
$700 < p_T < 1000$ GeV, b-filter	361317	Sherpa v2.2.0	0.077232	0.90824	0.168701
$1000 < p_T < 2000$ GeV, c-veto/b-veto	361318	Sherpa v2.2.0	0.011665	0.90824	0.629245
$1000 < p_T < 2000$ GeV, c-filter/b-veto	361319	Sherpa v2.2.0	0.010676	0.90824	0.237991
$1000 < p_T < 2000$ GeV, b-filter	361320	Sherpa v2.2.0	0.0093154	0.90824	0.173096
$p_T > 2000$ GeV, c-veto/b-veto	361321	Sherpa v2.2.0	0.000034013	0.90824	0.638441
$p_T > 2000$ GeV, c-filter/b-veto	361322	Sherpa v2.2.0	0.00004555	0.90824	0.272781
$p_T > 2000$ GeV, b-filter	361323	Sherpa v2.2.0	0.000052489	0.90824	0.165186
$W(\mu\nu)$ + jet					
$0 < p_T < 70$ GeV, c-veto/b-veto	361324	Sherpa v2.2.0	21392.	0.90824	0.892510
$0 < p_T < 70$ GeV, c-filter/b-veto	361325	Sherpa v2.2.0	21376.	0.90824	0.047370
$0 < p_T < 70$ GeV, b-filter	361326	Sherpa v2.2.0	21363.	0.90824	0.059710
$70 < p_T < 140$ GeV, c-veto/b-veto	361327	Sherpa v2.2.0	635.05	0.90824	0.728418
$70 < p_T < 140$ GeV, c-filter/b-veto	361328	Sherpa v2.2.0	632.11	0.90824	0.175047
$70 < p_T < 140$ GeV, b-filter	361329	Sherpa v2.2.0	632.03	0.90824	0.096687
$140 < p_T < 280$ GeV, c-veto/b-veto	361330	Sherpa v2.2.0	90.022	0.90824	0.684150
$140 < p_T < 280$ GeV, c-filter/b-veto	361331	Sherpa v2.2.0	90.165	0.90824	0.203512
$140 < p_T < 280$ GeV, b-filter	361332	Sherpa v2.2.0	90.301	0.90824	0.112541
$280 < p_T < 500$ GeV, c-veto/b-veto	361333	Sherpa v2.2.0	6.5108	0.90824	0.653631
$280 < p_T < 500$ GeV, c-filter/b-veto	361334	Sherpa v2.2.0	6.4747	0.90824	0.222520
$280 < p_T < 500$ GeV, b-filter	361335	Sherpa v2.2.0	6.5897	0.90824	0.130709
$500 < p_T < 700$ GeV, c-veto/b-veto	361336	Sherpa v2.2.0	0.41351	0.90824	0.631109
$500 < p_T < 700$ GeV, c-filter/b-veto	361337	Sherpa v2.2.0	0.41386	0.90824	0.239840
$500 < p_T < 700$ GeV, b-filter	361338	Sherpa v2.2.0	0.40969	0.90824	0.163529
$700 < p_T < 1000$ GeV, c-veto/b-veto	361339	Sherpa v2.2.0	0.076726	0.90824	0.632602
$700 < p_T < 1000$ GeV, c-filter/b-veto	361340	Sherpa v2.2.0	0.0744	0.90824	0.227699
$700 < p_T < 1000$ GeV, b-filter	361341	Sherpa v2.2.0	0.084611	0.90824	0.160140
$1000 < p_T < 2000$ GeV, c-veto/b-veto	361342	Sherpa v2.2.0	0.010678	0.90824	0.597890
$1000 < p_T < 2000$ GeV, c-filter/b-veto	361343	Sherpa v2.2.0	0.0096763	0.90824	0.236425
$1000 < p_T < 2000$ GeV, b-filter	361344	Sherpa v2.2.0	0.01146	0.90824	0.159623
$p_T > 2000$ GeV, c-veto/b-veto	361345	Sherpa v2.2.0	0.000044057	0.90824	0.617928
$p_T > 2000$ GeV, c-filter/b-veto	361346	Sherpa v2.2.0	0.000058221	0.90824	0.267917
$p_T > 2000$ GeV, b-filter	361347	Sherpa v2.2.0	0.000035509	0.90824	0.192802
$W(\tau\nu)$ + jet					
$0 < p_T < 70$ GeV, c-veto/b-veto	361348	Sherpa v2.2.0	21386.	0.90824	0.891411
$0 < p_T < 70$ GeV, c-filter/b-veto	361349	Sherpa v2.2.0	21378.	0.90824	0.048706
$0 < p_T < 70$ GeV, b-filter	361350	Sherpa v2.2.0	21389.	0.90824	0.059683
$70 < p_T < 140$ GeV, c-veto/b-veto	361351	Sherpa v2.2.0	630.1	0.90824	0.726079
$70 < p_T < 140$ GeV, c-filter/b-veto	361352	Sherpa v2.2.0	635.4	0.90824	0.176273
$70 < p_T < 140$ GeV, b-filter	361353	Sherpa v2.2.0	631.35	0.90824	0.095733
$140 < p_T < 280$ GeV, c-veto/b-veto	361354	Sherpa v2.2.0	90.212	0.90824	0.683964
$140 < p_T < 280$ GeV, c-filter/b-veto	361355	Sherpa v2.2.0	89.89	0.90824	0.204983
$140 < p_T < 280$ GeV, b-filter	361356	Sherpa v2.2.0	90.006	0.90824	0.113070
$280 < p_T < 500$ GeV, c-veto/b-veto	361357	Sherpa v2.2.0	6.3912	0.90824	0.647441
$280 < p_T < 500$ GeV, c-filter/b-veto	361358	Sherpa v2.2.0	6.7398	0.90824	0.218875
$280 < p_T < 500$ GeV, b-filter	361359	Sherpa v2.2.0	6.4933	0.90824	0.132548
$500 < p_T < 700$ GeV, c-veto/b-veto	361360	Sherpa v2.2.0	0.41469	0.90824	0.628862
$500 < p_T < 700$ GeV, c-filter/b-veto	361361	Sherpa v2.2.0	0.41459	0.90824	0.230541
$500 < p_T < 700$ GeV, b-filter	361362	Sherpa v2.2.0	0.41365	0.90824	0.159453
$700 < p_T < 1000$ GeV, c-veto/b-veto	361363	Sherpa v2.2.0	0.07929	0.90824	0.627393
$700 < p_T < 1000$ GeV, c-filter/b-veto	361364	Sherpa v2.2.0	0.07821	0.90824	0.220035
$700 < p_T < 1000$ GeV, b-filter	361365	Sherpa v2.2.0	0.080632	0.90824	0.155527
$1000 < p_T < 2000$ GeV, c-veto/b-veto	361366	Sherpa v2.2.0	0.010612	0.90824	0.607110
$1000 < p_T < 2000$ GeV, c-filter/b-veto	361367	Sherpa v2.2.0	0.010158	0.90824	0.237999
$1000 < p_T < 2000$ GeV, b-filter	361368	Sherpa v2.2.0	0.011285	0.90824	0.175976
$p_T > 2000$ GeV, c-veto/b-veto	361369	Sherpa v2.2.0	0.000048638	0.90824	0.545399
$p_T > 2000$ GeV, c-filter/b-veto	361370	Sherpa v2.2.0	0.00005607	0.90824	0.242272
$p_T > 2000$ GeV, b-filter	361371	Sherpa v2.2.0	0.000043334	0.90824	0.196031

Table 5: Cross-sections for the Standard Model backgrounds considered in this analysis (continued in Tables 6-7). The k-factor and generator filter efficiency are also given when appropriate and should be multiplied by the cross-section.

Channel	Run numbers	Generator	Cross-section [pb]	k-factor	Filter efficiency
$\gamma + V$					
$\gamma + W(e\nu)$, $E_T^\gamma \in 35-70$ GeV	301890	Sherpa v2.1.1	15.348	1	1
$\gamma + W(e\nu)$, $E_T^\gamma \in 70-140$ GeV	301891	Sherpa v2.1.1	1.5282	1	1
$\gamma + W(e\nu)$, $E_T^\gamma > 140$ GeV	301892	Sherpa v2.1.1	0.24155	1	1
$\gamma + W(\mu\nu)$, $E_T^\gamma \in 35-70$ GeV	301893	Sherpa v2.1.1	15.272	1	1
$\gamma + W(\mu\nu)$, $E_T^\gamma \in 70-140$ GeV	301894	Sherpa v2.1.1	1.5235	1	1
$\gamma + W(\mu\nu)$, $E_T^\gamma > 140$ GeV	301895	Sherpa v2.1.1	0.24183	1	1
$\gamma + W(\tau\nu)$, $E_T^\gamma \in 35-70$ GeV	301896	Sherpa v2.1.1	15.297	1	1
$\gamma + W(\tau\nu)$, $E_T^\gamma \in 70-140$ GeV	301897	Sherpa v2.1.1	1.529	1	1
$\gamma + W(\tau\nu)$, $E_T^\gamma > 140$ GeV	301898	Sherpa v2.1.1	0.2426	1	1
$\gamma + Z(ee)$, $E_T^\gamma \in 35-70$ GeV	301899	Sherpa v2.1.1	5.242	1	1
$\gamma + Z(ee)$, $E_T^\gamma \in 70-140$ GeV	301900	Sherpa v2.1.1	0.38455	1	1
$\gamma + Z(ee)$, $E_T^\gamma > 140$ GeV	301901	Sherpa v2.1.1	0.047209	1	1
$\gamma + Z(\mu\mu)$, $E_T^\gamma \in 35-70$ GeV	301902	Sherpa v2.1.1	5.2455	1	1
$\gamma + Z(\mu\mu)$, $E_T^\gamma \in 70-140$ GeV	301903	Sherpa v2.1.1	0.38548	1	1
$\gamma + Z(\mu\mu)$, $E_T^\gamma > 140$ GeV	301904	Sherpa v2.1.1	0.04724	1	1
$\gamma + Z(\tau\tau)$, $E_T^\gamma \in 35-70$ GeV	301905	Sherpa v2.1.1	5.249	1	1
$\gamma + Z(\tau\tau)$, $E_T^\gamma \in 70-140$ GeV	301906	Sherpa v2.1.1	0.38482	1	1
$\gamma + Z(\tau\tau)$, $E_T^\gamma > 140$ GeV	301907	Sherpa v2.1.1	0.047025	1	1
$\gamma + Z(\nu\nu)$, $E_T^\gamma \in 35-70$ GeV	301908	Sherpa v2.1.1	4.0365	1	1
$\gamma + Z(\nu\nu)$, $E_T^\gamma \in 70-140$ GeV	301909	Sherpa v2.1.1	0.97151	1	1
$\gamma + Z(\nu\nu)$, $E_T^\gamma > 140$ GeV	301910	Sherpa v2.1.1	0.17115	1	1
γ + jet					
$E_T^\gamma \in 35-70$ GeV , c-veto/b-veto	361039	Sherpa v2.1.1	34988.	1.	0.41028
$E_T^\gamma \in 35-70$ GeV , c-filter/b-veto	361040	Sherpa v2.1.1	34986.	1.	0.48610
$E_T^\gamma \in 35-70$ GeV , b-filter	361041	Sherpa v2.1.1	35002.	1.	0.10372
$E_T^\gamma \in 70-140$ GeV , c-veto/b-veto	361042	Sherpa v2.1.1	3129	1.	0.39960
$E_T^\gamma \in 70-140$ GeV , c-filter/b-veto	361043	Sherpa v2.1.1	3132.9	1.	0.48201
$E_T^\gamma \in 70-140$ GeV , b-filter	361044	Sherpa v2.1.1	3135.2	1.	0.11728
$E_T^\gamma \in 140-280$ GeV , c-veto/b-veto	361045	Sherpa v2.1.1	247.41	1.	0.39265
$E_T^\gamma \in 140-280$ GeV , c-filter/b-veto	361046	Sherpa v2.1.1	247.39	1.	0.47826
$E_T^\gamma \in 140-280$ GeV , b-filter	361047	Sherpa v2.1.1	249.37	1.	0.12874
$E_T^\gamma \in 280-500$ GeV , c-veto/b-veto	361048	Sherpa v2.1.1	13.648	1.	0.38607
$E_T^\gamma \in 280-500$ GeV , c-filter/b-veto	361049	Sherpa v2.1.1	13.617	1.	0.47349
$E_T^\gamma \in 280-500$ GeV , b-filter	361050	Sherpa v2.1.1	13.874	1.	0.14065
$E_T^\gamma \in 500-1000$ GeV , c-veto/b-veto	361051	Sherpa v2.1.1	0.92334	1.	0.37922
$E_T^\gamma \in 500-1000$ GeV , c-filter/b-veto	361052	Sherpa v2.1.1	0.92185	1.	0.47149
$E_T^\gamma \in 500-1000$ GeV , b-filter	361053	Sherpa v2.1.1	0.93819	1.	0.14811
$E_T^\gamma \in 1000-2000$ GeV , c-veto/b-veto	361054	Sherpa v2.1.1	0.018432	1.	0.37058
$E_T^\gamma \in 1000-2000$ GeV , c-filter/b-veto	361055	Sherpa v2.1.1	0.018388	1.	0.46648
$E_T^\gamma \in 1000-2000$ GeV , b-filter	361056	Sherpa v2.1.1	0.019046	1.	0.15750
$E_T^\gamma \in 2000-4000$ GeV , c-veto/b-veto	361057	Sherpa v2.1.1	7.9163×10^{-5}	1.	0.38039
$E_T^\gamma \in 2000-4000$ GeV , c-filter/b-veto	361058	Sherpa v2.1.1	8.0515×10^{-5}	1.	0.45148
$E_T^\gamma \in 2000-4000$ GeV , b-filter	361059	Sherpa v2.1.1	8.2153×10^{-5}	1.	0.16548
$E_T^\gamma > 4000$ GeV , c-veto/b-veto	361060	Sherpa v2.1.1	2.4843×10^{-9}	1.	0.40351
$E_T^\gamma > 4000$ GeV , c-filter/b-veto	361061	Sherpa v2.1.1	2.5134×10^{-9}	1.	0.41612
$E_T^\gamma > 4000$ GeV , b-filter	361062	Sherpa v2.1.1	2.5431×10^{-9}	1.	0.14831
$Z(\nu\nu)$ + jet					
$0 < p_T < 70$ GeV, c-veto/b-veto	361344	Sherpa v2.2.0	11937.	0.9141	0.778461
$0 < p_T < 70$ GeV, c-filter/b-veto	361345	Sherpa v2.2.0	11933.	0.9141	0.140128
$0 < p_T < 70$ GeV, b-filter	361346	Sherpa v2.2.0	11949.	0.9141	0.080032
$70 < p_T < 140$ GeV, c-veto/b-veto	361347	Sherpa v2.2.0	428.25	0.9141	0.649624
$70 < p_T < 140$ GeV, c-filter/b-veto	361448	Sherpa v2.2.0	427.67	0.9141	0.218402
$70 < p_T < 140$ GeV, b-filter	361449	Sherpa v2.2.0	428.59	0.9141	0.132849
$140 < p_T < 280$ GeV, c-veto/b-veto	361450	Sherpa v2.2.0	65.902	0.9141	0.613840
$140 < p_T < 280$ GeV, c-filter/b-veto	361451	Sherpa v2.2.0	65.796	0.9141	0.239057
$140 < p_T < 280$ GeV, b-filter	361452	Sherpa v2.2.0	66.149	0.9141	0.147665
$280 < p_T < 500$ GeV, c-veto/b-veto	361453	Sherpa v2.2.0	4.8378	0.9141	0.585661
$280 < p_T < 500$ GeV, c-filter/b-veto	361454	Sherpa v2.2.0	4.8408	0.9141	0.260628
$280 < p_T < 500$ GeV, b-filter	361455	Sherpa v2.2.0	4.8839	0.9141	0.161749
$500 < p_T < 700$ GeV, c-veto/b-veto	361456	Sherpa v2.2.0	0.29329	0.9141	0.555049
$500 < p_T < 700$ GeV, c-filter/b-veto	361457	Sherpa v2.2.0	0.30096	0.9141	0.274948
$500 < p_T < 700$ GeV, b-filter	361458	Sherpa v2.2.0	0.30345	0.9141	0.164931
$700 < p_T < 1000$ GeV, c-veto/b-veto	361459	Sherpa v2.2.0	0.053341	0.9141	0.557693
$700 < p_T < 1000$ GeV, c-filter/b-veto	361460	Sherpa v2.2.0	0.054118	0.9141	0.303868
$700 < p_T < 1000$ GeV, b-filter	361461	Sherpa v2.2.0	0.056399	0.9141	0.163096
$1000 < p_T < 2000$ GeV, c-veto/b-veto	361462	Sherpa v2.2.0	0.0076507	0.9141	0.534707
$1000 < p_T < 2000$ GeV, c-filter/b-veto	361463	Sherpa v2.2.0	0.0084891	0.9141	0.312154
$1000 < p_T < 2000$ GeV, b-filter	361464	Sherpa v2.2.0	0.0078858	0.9141	0.197191
$p_T > 2000$ GeV, c-veto/b-veto	361465	Sherpa v2.2.0	0.000034976	0.9141	0.543622
$p_T > 2000$ GeV, c-filter/b-veto	361466	Sherpa v2.2.0	0.000021126	0.9141	0.345637
$p_T > 2000$ GeV, b-filter	361467	Sherpa v2.2.0	0.000032459	0.9141	0.215729

Table 6: Cross-sections for the Standard Model backgrounds considered in this analysis (continued from Table 5 and in Table 7). The k-factor and generator filter efficiency are also given when appropriate and should be multiplied by the cross-section.

Channel	Run numbers	Generator	Cross-section [pb]	k-factor	Filter efficiency
$Z(ee)$ + jet					
$0 < p_T < 70$ GeV, c-veto/b-veto	361372	Sherpa v2.2.0	2206.7	0.90105	0.778989
$0 < p_T < 70$ GeV, c-filter/b-veto	361373	Sherpa v2.2.0	2206.5	0.90105	0.142259
$0 < p_T < 70$ GeV, b-filter	361374	Sherpa v2.2.0	2203.	0.90105	0.079669
$70 < p_T < 140$ GeV, c-veto/b-veto	361375	Sherpa v2.2.0	75.523	0.90105	0.646932
$70 < p_T < 140$ GeV, c-filter/b-veto	361376	Sherpa v2.2.0	75.621	0.90105	0.218226
$70 < p_T < 140$ GeV, b-filter	361377	Sherpa v2.2.0	76.658	0.90105	0.131146
$140 < p_T < 280$ GeV, c-veto/b-veto	361378	Sherpa v2.2.0	11.785	0.90105	0.617229
$140 < p_T < 280$ GeV, c-filter/b-veto	361379	Sherpa v2.2.0	11.49	0.90105	0.244908
$140 < p_T < 280$ GeV, b-filter	361380	Sherpa v2.2.0	11.552	0.90105	0.150367
$280 < p_T < 500$ GeV, c-veto/b-veto	361381	Sherpa v2.2.0	0.84832	0.90105	0.588874
$280 < p_T < 500$ GeV, c-filter/b-veto	361382	Sherpa v2.2.0	0.84494	0.90105	0.261732
$280 < p_T < 500$ GeV, b-filter	361383	Sherpa v2.2.0	0.85285	0.90105	0.156212
$500 < p_T < 700$ GeV, c-veto/b-veto	361384	Sherpa v2.2.0	0.053805	0.90105	0.577255
$500 < p_T < 700$ GeV, c-filter/b-veto	361385	Sherpa v2.2.0	0.054017	0.90105	0.271427
$500 < p_T < 700$ GeV, b-filter	361386	Sherpa v2.2.0	0.056207	0.90105	0.168468
$700 < p_T < 1000$ GeV, c-veto/b-veto	361387	Sherpa v2.2.0	0.010097	0.90105	0.566055
$700 < p_T < 1000$ GeV, c-filter/b-veto	361388	Sherpa v2.2.0	0.0097667	0.90105	0.300167
$700 < p_T < 1000$ GeV, b-filter	361389	Sherpa v2.2.0	0.010265	0.90105	0.182922
$1000 < p_T < 2000$ GeV, c-veto/b-veto	361390	Sherpa v2.2.0	0.001263	0.90105	0.536884
$1000 < p_T < 2000$ GeV, c-filter/b-veto	361391	Sherpa v2.2.0	0.0014567	0.90105	0.309836
$1000 < p_T < 2000$ GeV, b-filter	361392	Sherpa v2.2.0	0.0012455	0.90105	0.191868
$p_T > 2000$ GeV, c-veto/b-veto	361393	Sherpa v2.2.0	0.0000057359	0.90105	0.519728
$p_T > 2000$ GeV, c-filter/b-veto	361394	Sherpa v2.2.0	0.0000092786	0.90105	0.393222
$p_T > 2000$ GeV, b-filter	361395	Sherpa v2.2.0	0.000013172	0.90105	0.222083
$Z(\mu\mu)$ + jet					
$0 < p_T < 70$ GeV, c-veto/b-veto	361396	Sherpa v2.2.0	2205.8	0.90105	0.778381
$0 < p_T < 70$ GeV, c-filter/b-veto	361397	Sherpa v2.2.0	2205.7	0.90105	0.141881
$0 < p_T < 70$ GeV, b-filter	361398	Sherpa v2.2.0	2203.4	0.90105	0.079624
$70 < p_T < 140$ GeV, c-veto/b-veto	361399	Sherpa v2.2.0	75.822	0.90105	0.649106
$70 < p_T < 140$ GeV, c-filter/b-veto	361400	Sherpa v2.2.0	75.936	0.90105	0.219295
$70 < p_T < 140$ GeV, b-filter	361401	Sherpa v2.2.0	75.977	0.90105	0.130293
$140 < p_T < 280$ GeV, c-veto/b-veto	361402	Sherpa v2.2.0	11.599	0.90105	0.610026
$140 < p_T < 280$ GeV, c-filter/b-veto	361403	Sherpa v2.2.0	11.599	0.90105	0.241249
$140 < p_T < 280$ GeV, b-filter	361404	Sherpa v2.2.0	11.705	0.90105	0.148024
$280 < p_T < 500$ GeV, c-veto/b-veto	361405	Sherpa v2.2.0	0.869	0.90105	0.580841
$280 < p_T < 500$ GeV, c-filter/b-veto	361406	Sherpa v2.2.0	0.87544	0.90105	0.272103
$280 < p_T < 500$ GeV, b-filter	361407	Sherpa v2.2.0	0.86458	0.90105	0.163024
$500 < p_T < 700$ GeV, c-veto/b-veto	361408	Sherpa v2.2.0	0.05564	0.90105	0.566372
$500 < p_T < 700$ GeV, c-filter/b-veto	361409	Sherpa v2.2.0	0.056776	0.90105	0.265874
$500 < p_T < 700$ GeV, b-filter	361410	Sherpa v2.2.0	0.056196	0.90105	0.176439
$700 < p_T < 1000$ GeV, c-veto/b-veto	361411	Sherpa v2.2.0	0.010459	0.90105	0.561305
$700 < p_T < 1000$ GeV, c-filter/b-veto	361412	Sherpa v2.2.0	0.0095255	0.90105	0.288730
$700 < p_T < 1000$ GeV, b-filter	361413	Sherpa v2.2.0	0.0093901	0.90105	0.178631
$1000 < p_T < 2000$ GeV, c-veto/b-veto	361414	Sherpa v2.2.0	0.0013495	0.90105	0.549132
$1000 < p_T < 2000$ GeV, c-filter/b-veto	361415	Sherpa v2.2.0	0.0015595	0.90105	0.282508
$1000 < p_T < 2000$ GeV, b-filter	361416	Sherpa v2.2.0	0.0014846	0.90105	0.198009
$p_T > 2000$ GeV, c-veto/b-veto	361417	Sherpa v2.2.0	0.0000073382	0.90105	0.597261
$p_T > 2000$ GeV, c-filter/b-veto	361418	Sherpa v2.2.0	0.0000064214	0.90105	0.325784
$p_T > 2000$ GeV, b-filter	361419	Sherpa v2.2.0	0.000011932	0.90105	0.246649
$Z(\tau\tau)$ + jet					
$0 < p_T < 70$ GeV, c-veto/b-veto	361320	Sherpa v2.2.0	2196.4	0.90105	0.778140
$0 < p_T < 70$ GeV, c-filter/b-veto	361321	Sherpa v2.2.0	2204.	0.90105	0.142335
$0 < p_T < 70$ GeV, b-filter	361322	Sherpa v2.2.0	2207.8	0.90105	0.079215
$70 < p_T < 140$ GeV, c-veto/b-veto	361323	Sherpa v2.2.0	76.229	0.90105	0.647945
$70 < p_T < 140$ GeV, c-filter/b-veto	361424	Sherpa v2.2.0	76.079	0.90105	0.222003
$70 < p_T < 140$ GeV, b-filter	361425	Sherpa v2.2.0	76.318	0.90105	0.131225
$140 < p_T < 280$ GeV, c-veto/b-veto	361426	Sherpa v2.2.0	11.468	0.90105	0.614503
$140 < p_T < 280$ GeV, c-filter/b-veto	361427	Sherpa v2.2.0	11.624	0.90105	0.241705
$140 < p_T < 280$ GeV, b-filter	361428	Sherpa v2.2.0	11.645	0.90105	0.142080
$280 < p_T < 500$ GeV, c-veto/b-veto	361429	Sherpa v2.2.0	0.85864	0.90105	0.581019
$280 < p_T < 500$ GeV, c-filter/b-veto	361430	Sherpa v2.2.0	0.86366	0.90105	0.255775
$280 < p_T < 500$ GeV, b-filter	361431	Sherpa v2.2.0	0.90216	0.90105	0.158859
$500 < p_T < 700$ GeV, c-veto/b-veto	361432	Sherpa v2.2.0	0.054666	0.90105	0.563903
$500 < p_T < 700$ GeV, c-filter/b-veto	361433	Sherpa v2.2.0	0.055443	0.90105	0.270431
$500 < p_T < 700$ GeV, b-filter	361434	Sherpa v2.2.0	0.055614	0.90105	0.170454
$700 < p_T < 1000$ GeV, c-veto/b-veto	361435	Sherpa v2.2.0	0.008835	0.90105	0.560184
$700 < p_T < 1000$ GeV, c-filter/b-veto	361436	Sherpa v2.2.0	0.0098863	0.90105	0.298414
$700 < p_T < 1000$ GeV, b-filter	361437	Sherpa v2.2.0	0.011322	0.90105	0.180118
$1000 < p_T < 2000$ GeV, c-veto/b-veto	361438	Sherpa v2.2.0	0.0011582	0.90105	0.563610
$1000 < p_T < 2000$ GeV, c-filter/b-veto	361439	Sherpa v2.2.0	0.0012131	0.90105	0.348277
$1000 < p_T < 2000$ GeV, b-filter	361440	Sherpa v2.2.0	0.0015868	0.90105	0.168462
$p_T > 2000$ GeV, c-veto/b-veto	361441	Sherpa v2.2.0	0.0000050133	0.90105	0.595406
$p_T > 2000$ GeV, c-filter/b-veto	361442	Sherpa v2.2.0	0.0000056335	0.90105	0.359953
$p_T > 2000$ GeV, b-filter	361443	Sherpa v2.2.0	0.0000076959	0.90105	0.250846

Table 7: Cross sections for the Standard Model backgrounds considered in this analysis (continued from Tables 5 and 6). The k-factor and generator filter efficiency are also given when appropriate and should be multiplied by the cross section.

3 Object definition

The object definition follows the recommendations from the various combined performance groups implemented in the SUSTools version SUSYTools-00-08-20 with AnalysisBase 2.4.21 (including METUtilities-00-02-35).

3.1 Photon definition

Photons are reconstructed from clusters in the electromagnetic calorimeter measured in projective towers of $N_1 \times N_2$ cells in $\eta \times \phi$ of the second layer of the calorimeter. Clusters without matching tracks are classified as unconverted photon candidates. A photon containing clusters that can be matched to tracks is considered as a converted photon candidate [26]. The final energy measurement is made using clusters of size 3×5 cells (3×7 cells) in the barrel calorimeter for non-converted photons (converted photons). In the endcap, clusters of size 5×5 are used for all photon candidates. Cleaning cuts are applied on photon candidates in order to identify bad quality or fake clusters coming from instrumental problems. A photon is flagged as bad if it contains or edges dead/masked cells.

The photon energy in data is corrected by applying the energy scales measured on well-known resonances ($Z \to e^+e^-$, $J/\psi \to e^+e^-$) or E/p studies using isolated electrons from $W \to e\nu$. For MC events, the photon transverse energy is smeared to reproduce the energy resolution measured on data.

Identification cuts are applied in order to separate the photon candidates from the contamination coming from π^0 or other neutral hadrons decaying to two photons. The photon identification is based on the profile of the energy deposit in the first (strip) and second (middle) layer of the electromagnetic calorimeter. The differences observed between data and MC in the isEM discriminating variables are measured comparing the shower shape distributions, and parametrized as simple shifts. These so-called fudge factors are computed as the difference between the means of a given variable in data and MC; they are then applied to the photon discriminating variables in MC samples in order to obtain corrected efficiencies. Fudge factors are applied following the recommendations in [27].

A transverse energy isolation cut is applied on $TopoEtcone40$ variable that is computed as the sum of the three-dimensional calorimeter topological cluster (TopoCluster) transverse energies (calibrated at the electromagnetic scale [6]) within a cone around the cluster barycenter of radius $\Delta R = \sqrt{(\Delta\eta)^2 + (\Delta\phi)^2} = 0.4$. Corrections to the isolation energy accounting for the leakage of the photon energy outside of the central core and for the soft energy deposits from pileup interactions depending on the amount of activity in a given event are also applied. A track isolation criteria on $ptcone20$ variable is also requested following recommendations in [28]. The "$FixedCutTight$" isolation working point is adopted in 2016 analysis that corresponds to the following criteria: $TopoEtcone40 < 0.022 p_{\mathrm{T}}^{\gamma} + 2.45$ GeV and $ptcone20/p_{\mathrm{T}}^{\gamma} < 0.05$. All the reconstructed photons of loose quality with $E_{\mathrm{T}} > 10\,\mathrm{GeV}$ (after energy rescaling) and $|\eta| < 2.37$ are considered as photon candidates, or "preselected" photons.

3.2 Electron definition

Electrons are reconstructed from clusters in the electromagnetic calorimeter matched to a track in the ID [29]. The "preselected" electrons are required to pass a variant of the "medium" selection (called "mediumLH') of [29], to have $p_{\mathrm{T}} > 7$ GeV and $|\eta| < 2.47$. It is also required that the significance of the transverse impact parameter, defined as the transverse impact parameter d_0 divided by its estimated uncertainty, σ_{d_0}, of tracks with respect to the primary vertex satisfies $|d_0|/\sigma_{d_0} < 5.0$. The longitudinal impact parameter z_0 must be $|z_0| \sin\theta < 0.5$ mm.

[6] This scale provides a good representation of the electron or photon energy in the calorimeter, but does not correct for energy losses associated with hadronic showers.

"Selected" electrons are defined as the "preselected" ones, but in addition are required to satisfy the "loose" isolation working point[7].

3.3 Muon definition

Muons are identified either as a combined track in the muon spectrometer (MS) and ID systems, or as an ID track matching with a MS segment [30, 31]. Muons are selected according to the "medium" recommendation, similar to the criteria used in Run-1 [32] and are required to have $p_{\mathrm{T}} > 6$ GeV and $|\eta| < 2.7$. It is also required that $|d_0|/\sigma_{d_0} < 3.0$ and that $|z_0| \sin\theta < 0.5$ mm.
"Selected" muons are defined as the "preselected" ones, but in addition are required to satisfy the "loose" isolation working point[8].

3.4 Jet definition

Jets are reconstructed from TopoClusters calibrated at the electromagnetic energy scale. The anti-k_t algorithm [33, 34] with distance parameter $R = 0.4$ is employed. The jets are fully calibrated using the EM+JES scheme [35], corrected for pileup [36]. "Preselected" jets must have $p_{\mathrm{T}} > 20$ GeV .
"Selected" jets must have $p_{\mathrm{T}} > 30$ GeV and $|\eta| < 4.5$. In addition, to remove jets originating from pileup, a cut on the jet vertex tagger variable (JVT) [37] of JVT > 0.59 is applied to jets with $|\eta| < 2.4$ and 30 GeV $< p_{\mathrm{T}} < 60$ GeV . Quality criteria are applied to clean jets from detector effects, beam background and cosmics. The jet cleaning applied rejects events with any *LooseBad* jet, overlapping with neither leptons nor photons, with calibrated $p_{\mathrm{T}} > 20$ GeV [38].

3.5 Missing transverse momentum

The $E_{\mathrm{T}}^{\mathrm{miss}}$ calculation used in this analysis is based on reconstructed and calibrated physics objects. In particular "preselected" leptons, photons and jets are given as input to the $E_{\mathrm{T}}^{\mathrm{miss}}$ rebuilding. Energy deposits in the calorimeters and/or tracks are associated with a reconstructed and identified high-p_{T} parent object in a specific order: electrons with $p_{\mathrm{T}}>$ 10 GeV , photons with $p_{\mathrm{T}}>$ 10 GeV and jets with $p_{\mathrm{T}}>$ 20 GeV . Energy deposits/tracks not associated with any such objects are also taken into account in the $E_{\mathrm{T}}^{\mathrm{miss}}$ calculation [39]. Muons with $p_{\mathrm{T}}>$ 10 GeV are also added in the standard $E_{\mathrm{T}}^{\mathrm{miss}}$ computation.

The $E_{\mathrm{T}}^{\mathrm{miss}}$ is calculated as the sum of the following terms:

$$E_{x(y)}^{\mathrm{miss}} = E_{x(y)}^{\mathrm{miss},e} + E_{x(y)}^{\mathrm{miss},\gamma} + E_{x(y)}^{\mathrm{miss,jets}} + E_{x(y)}^{\mathrm{miss,SoftTerm}} + E_{x(y)}^{\mathrm{miss},\mu}, \quad (1)$$

where each term is calculated as the negative sum of the calibrated reconstructed objects, projected onto the x and y directions and from the "Soft Term" that is calculated from energy deposits/tracks that are not matched to selected hard objects. In Run-1 analysis, a "Calorimeter Soft Term" (CST) [40] was used, but due to the high pileup environment of the LHC from 2012 onwards, the soft component suffers from a high degree of contamination from interactions besides the hard scatter (HS) vertex of interest. In the present analysis, the recommended "Track Soft Term" (TST), calculated from the tracks from the primary vertex that are not matched to selected hard objetcs, which provides a more robust measurement against pileup, is used [41].

The quantity ΣE_T, which is used in the calculation of MET_Signif in Sec. 4.2.1, is calculated as the scalar sum of all p_{T} from the objects and the tracks contributing to $E_{\mathrm{T}}^{\mathrm{miss}}$ reconstruction described above.

[7] https://twiki.cern.ch/twiki/bin/view/AtlasProtected/IsolationSelectionTool#Leptons.
[8] https://twiki.cern.ch/twiki/bin/view/AtlasProtected/IsolationSelectionTool#Leptons.

3.6 Overlap Removal

To resolve amibiguities which can happen in the object reconstruction, an overlap removal procedure is performed, following the recommendations by the Harmonization effort [42]. The procedure is performed suing the official on "preselected" objects as described in the previous sections and in the following order:

- if an electron shares its inner detector track with a muon, the electron is removed and the muon is kept, in order to remove electron candidates coming from muon bremstrahlung followed by photon conversion.
- If a photon and an electron are found within $\Delta R < 0.4$ the object is interpreted as an electron and the photon is removed, with $\Delta R = \sqrt{(\Delta y)^2 + (\Delta\phi)^2}$, where y is the rapidity. This permits to reduce the electron to photon fake rate.
- If a photon and a muon are found within $\Delta R < 0.4$ the object is interpreted as a muon and the overlapping photon is removed from the event.
- If a jet and an electron are found within $\Delta R < 0.2$ the object is interpreted as an electron and the jet is removed from the event.
- If a jet and an electron are found within $0.2 < \Delta R < 0.4$ the object is interpreted as a jet and the electron is removed from the event.
- if a jet and a muon are found within $\Delta R < 0.4$, then the muon is removed from the event, except if the number of tracks with $p_{\mathrm{T}} > 0.5$ GeV associated with the jet is less than 3.
- If a photon and a jet are found within $\Delta R < 0.4$ the object is interpreted as a photon and the overlapping jet is removed from the event.

4 Event Selection

4.1 Derivation and analysis code

During Run-2 ATLAS has developed the so called "derivation framework" to provide an intermediate data format (referred to as derivation) produced centrally to all the analyses. For this analysis a specific derivation called "EXOT6" has been implemented in collaboration with the exotic photon+jet analysis based on the following skimming selection:

1. trigger: the event must pass one of the following trigger request: `HLT_g140_loose`, `HLT_g160_loose`, `HLT_xe90_tc_lcw_L1XE50`, `HLT_xe90_mht`, `HLT_xe100_mht_L1XE50`, `HLT_xe_100`, `HLT_xe90_mht_L1XE50`, `HLT_xe110_mht_L1XE50`.

2. offline selection: the event must have one loose photon with $p_{\mathrm{T}} > 80$ GeV or one loose electron with $p_{\mathrm{T}} > 100$ GeV. The second request is needed for the in-situ estimate of the electron faking photons background described in Sec. 5.3.

Note that this analysis is based solely on the unprescaled trigger `HLT_g140_loose`, the $E_{\mathrm{T}}^{\mathrm{miss}}$ triggers only being used to compute the gamma trigger efficiency, as discussed in Section 4.3.

The analysis code is based on SUSYTools [43], to handle all necessary physics objects corrections recommended by Combined Performance groups. Version SUSYTools-00-08-20, based on AnalysisBase 2.4.21 (including METUtilities-00-02-35) has been used for the full luminosity results. The analysis code is maintained in a common svn [9] repository and common ROOT mini-trees are produced to expedite the analysis team progress.

4.2 Selection in Signal Region

The selection in the signal region (SR) is mainly based on the 2015 Run-2 analysis, events are pre–selected by requiring:

1. data quality: the event must be in the good run list (GRL);

2. trigger: the event must have passed the `HLT_g140_loose` trigger requirement;

3. good vertex: a primary vertex must be reconstructed with at least two associated good-quality tracks (see [44]) with $p_{\mathrm{T}} > 400$ MeV and $|\eta| < 2.5$ [10]

4. jet cleaning: reject events with any *LooseBad* jet, overlapping with neither leptons nor photons, with calibrated $p_{\mathrm{T}} > 20$ GeV [38];

Candidates in the SR are selected by requiring:

1. $E_{\mathrm{T}}^{\mathrm{miss}} > 150$ GeV (lowest $E_{\mathrm{T}}^{\mathrm{miss}}$ threshold; different SRs defined with increasing $E_{\mathrm{T}}^{\mathrm{miss}}$ thresholds as explained below);

2. at least 1 loose photon with $p_{\mathrm{T}} > 150$ GeV, $|\eta| < 2.37$ excluding the calorimeter crack region $1.37 < |\eta| < 1.52$;

3. MET significance > 8.5 GeV $^{1/2}$, adopted in 2016 analysis, see more details in Sec. 4.2.1;

4. the leading photon must be tight;

[9] https://svnweb.cern.ch/trac/atlasphys-exo/browser/Physics/Exotic/JDM/MonoPhoton/Run2/Code

[10] The signal efficiency for this requirement is about 100%

5. the leading photon must be isolated: $TopoEtcone40 < 2.45$ GeV $+ 0.022 p_{\mathrm{T}}^{\gamma}$ GeV, $ptcone20/p_{\mathrm{T}}^{\gamma} <$ 0.05 ("*FixedCutTight*" isolation working point);

6. the leading photon must not overlap with $E_{\mathrm{T}}^{\mathrm{miss}}$: $\Delta\phi(\gamma, E_{\mathrm{T}}^{\mathrm{miss}}) > 0.4$;

7. photon pointing: the z coordinate pointed by the photon with respect to the identified primary vertex, < 250 mm. This criteria was optimized in 2015 to suppress the anomalous rate of unconverted photons caused by beam-induced background in the tight-4 and isolated region of the 2-dimensional matrix method described in Sec. 5.4.;

8. jet veto: events with at most one "selected" jet are retained; if there is a jet, this jet must have $\Delta\phi(E_{\mathrm{T}}^{\mathrm{miss}}, \mathrm{jet}) > 0.4$;

9. lepton veto: events with any "preselected" electron or muon are discarded.

The 2016 dataset has a small number of mistimed events that have corrected calorimeter energy but incorrect tracking and muon information, it was checked that none of these events pass the SR selection.

Thanks to the increased statistics recorded during 2016 data-taking, it is possible to define different SRs with increasing $E_{\mathrm{T}}^{\mathrm{miss}}$ threshold. In particular, inclusive and exclusive SRs have been defined for different $E_{\mathrm{T}}^{\mathrm{miss}}$ bins as shown in Table 8.

Inclusive SR	$E_{\mathrm{T}}^{\mathrm{miss}}$> 150 GeV	$E_{\mathrm{T}}^{\mathrm{miss}}$> 225 GeV	$E_{\mathrm{T}}^{\mathrm{miss}}$> 300 GeV
Exclusive SR	150 < $E_{\mathrm{T}}^{\mathrm{miss}}$< 225 GeV	225 < $E_{\mathrm{T}}^{\mathrm{miss}}$< 300 GeV	

Table 8: Definitions of inclusive and exclusive SRs for different $E_{\mathrm{T}}^{\mathrm{miss}}$ bins.

4.2.1 MET Significance

The $E_{\mathrm{T}}^{\mathrm{miss}}$ significance, defined as $E_{\mathrm{T}}^{\mathrm{miss}}/\sigma(E_{\mathrm{T}}^{\mathrm{miss}})$, gives the significance of $E_{\mathrm{T}}^{\mathrm{miss}}$ with respect to its resolution ($\sigma(E_{\mathrm{T}}^{\mathrm{miss}})$) and is a powerful quantity for the separation of events with true $E_{\mathrm{T}}^{\mathrm{miss}}$ from events where the $E_{\mathrm{T}}^{\mathrm{miss}}$ is fake. In the absence, up to now, of an official recommendation for the $E_{\mathrm{T}}^{\mathrm{miss}}$ significance definition, the $E_{\mathrm{T}}^{\mathrm{miss}}$ significance calculated as: MET_Signif = $\mathrm{E}_{\mathrm{T}}^{\mathrm{miss}}/\sqrt{\Sigma E_T}$ (where $E_{\mathrm{T}}^{\mathrm{miss}}$ and ΣE_T were defined in Section 3.5) has been adopted, because the scaling of the Emiss resolution due to purely calorimetric measurements is approximately as $\sqrt{\Sigma E_T}$. This quantity allows a very good separation between γ + jet events and events with true $E_{\mathrm{T}}^{\mathrm{miss}}$.

Figure 6 shows the $E_{\mathrm{T}}^{\mathrm{miss}}$ significance distribution for MC background events in the SR region, selected according the criteria listed in Sec. 4.2. It can be seen that the γ+jet events are mostly concentrated in the small significance region, as expected because the $E_{\mathrm{T}}^{\mathrm{miss}}$ is fake in these events.

The agreement between the shapes of the MET_Signif distributions in data and MC simulation was checked in two control regions. Figure 7 shows the $E_{\mathrm{T}}^{\mathrm{miss}}$ significance distribution for MC background events and data in the Photon-Jet and in the Single-Muon control regions, selected according the criteria listed in Sec. 5.1. It can be seen that the MET_Signif values are always small in PhJetCR because the $E_{\mathrm{T}}^{\mathrm{miss}}$ is fake and also because there is an upper cut on the $E_{\mathrm{T}}^{\mathrm{miss}}$ in this region; the MET_Signif values are larger in 1muCR because the muon term is subtracted in the computation of $E_{\mathrm{T}}^{\mathrm{miss}}$ as explained in Sec. 5.1, so all events have a "true" $E_{\mathrm{T}}^{\mathrm{miss}}$.

Table 9 shows that in the SR with $E_{\mathrm{T}}^{\mathrm{miss}} > 150$ GeV a cut MET_Signif > 8.5 can reduce the γ + jet background from 13% to the 2015 level (6%) with a small suppression on the other backgrounds and a small effect on the total event number. The efficiency of this cut on the signal samples described in Sec. 2.1 ranges from 98.5% to 99.9%.

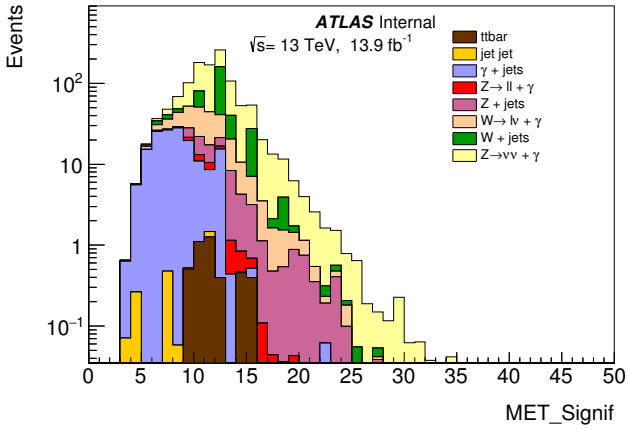

Figure 6: Distribution of $E_{\mathrm{T}}^{\mathrm{miss}}$ significance MET_Signif = $\mathrm{E}_{\mathrm{T}}^{\mathrm{miss}}/\sqrt{\Sigma E_T}$ for MC background events in the SR region for an integrated luminosity of 13.9 fb^{-1}.

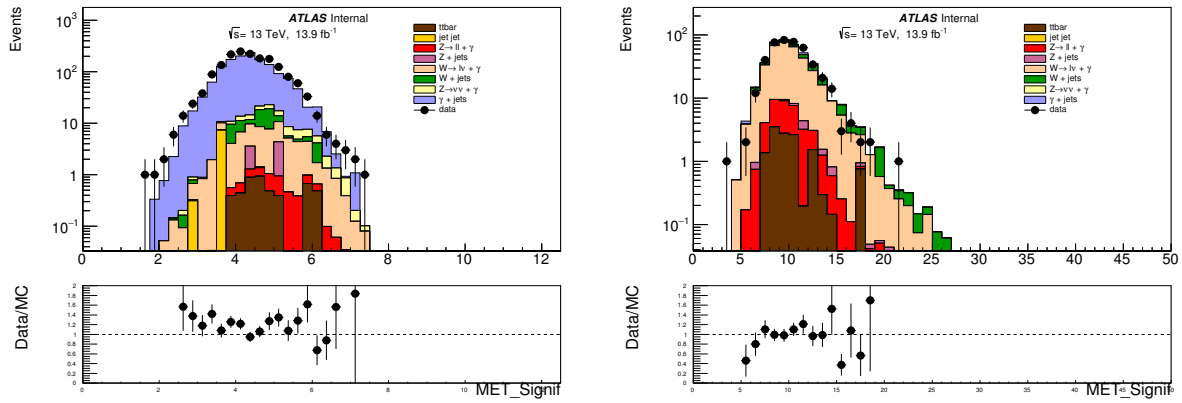

(a) PhJetCR (b) 1muCR

Figure 7: Distribution of $E_{\mathrm{T}}^{\mathrm{miss}}$ significance for MC background events and data in the PhJetCR region and the 1muCR for an integrated luminosity of 13.9 fb^{-1}. The lower panel shows the ratio of data to expected background event yields.

	SR	MET_Signif>8.0	MET_Signif>8.5	MET_Signif>9.0
$Z(\rightarrow \nu\nu)\gamma$	594 (51%)	584 (55%)	576 (56%)	563 (57%)
$W(\rightarrow \ell\nu)\gamma$	159 (14%)	144 (14%)	137 (13%)	128 (13%)
$Z(\rightarrow \ell\ell)\gamma$	11.0 (0.9%)	10.1 (0.9%)	9.5 (0.9%)	8.9 (0.9%)
γ + jet	152 (13%)	80 (7.5%)	62 (6%)	52 (5.2%)
Fake photons	252 (22%)	241 (23%)	241 (23%)	234 (24%)
Total MC background	1167	1058	1026	990

Table 9: Expected event yields from SM backgrounds in 13.9 fb^{-1} in the signal region with $E_{\mathrm{T}}^{\mathrm{miss}}$ > 150 GeV using different MET_Signif cuts. Fake photons include the contribution from W/Z + jets, top and di-jets backgrounds, calculated from the pure MC simulation. For each column, the percentages of each background with respect to the total is also reported.

4.3 Trigger efficiency

The efficiency of the *HLT_g140_loose* trigger has been measured as a function of the calibrated p_{T} of the offline leading photon, satisfying the tight identification criteria, the isolation requirement and $|\eta| < 2.37$ (excluding the calorimeter crack region). No matching is applied between the offline photon and the triggered photon. The events are selected based on the following criteria: only data with a fully functional calorimeter, ID and MS are analysed, events with at least one jet arising from detector noise or out-of-time energy deposits in the calorimeter are removed, the events must have a reconstructed primary vertex and a reconstructed photon with the characteristics described above. The turn-on curve is shown in Figure 8 for data and in Figure 9 for the Monte Carlo (all the background MC samples are added according to their weight). The efficiency in those plots is measured using the orthogonality of the photon and $E_{\mathrm{T}}^{\mathrm{miss}}$ triggers as:

$$\epsilon = \frac{\text{Events passing } HLT\_g140\_loose \text{ AND } HLT\_MET}{\text{Events passing } HLT\_MET} \tag{2}$$

where HLT_MET is an OR of the various $E_{\mathrm{T}}^{\mathrm{miss}}$ triggers to cover the lowest unprescaled trigger which changed with time in 2015/2016 (*HLT_xe*100, *HLT_xe*90*_tc_lcw_L*1*XE*50, *HLT_xe*90*_mht_L*1*XE*50, *HLT_xe*100*_mht_L*1*XE*50, *HLT_xe*110*_mht_L*1*XE*50)

The trigger is more than 98.5% efficient for all the photons selected in this analysis. The small difference in the $p_{\mathrm{T}} > 150$ GeV region between the data and MC will be treated as a systematic uncertainty.

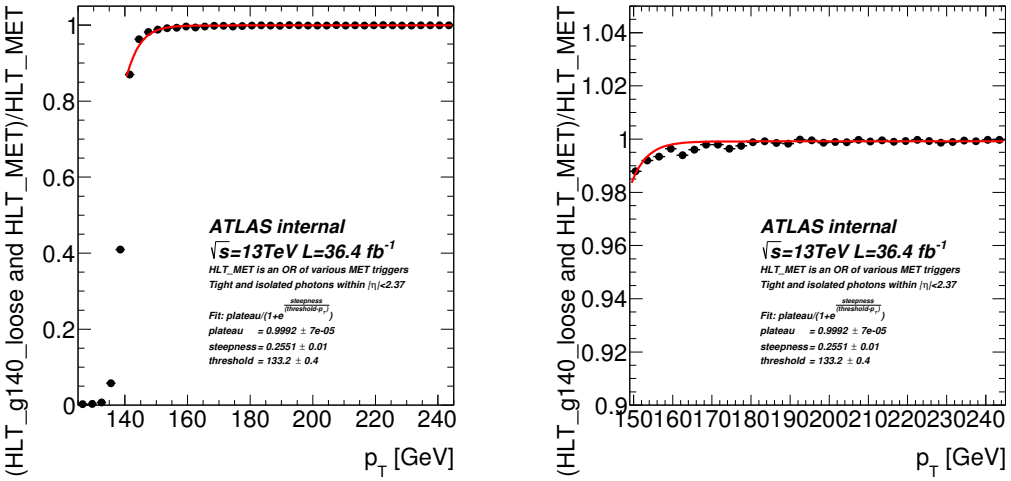

Figure 8: Trigger efficiency in data for the *HLT_g140_loose* trigger shown as a function of the offline leading photon p_{T} (left). A zoom into the region of interest is shown on the right.

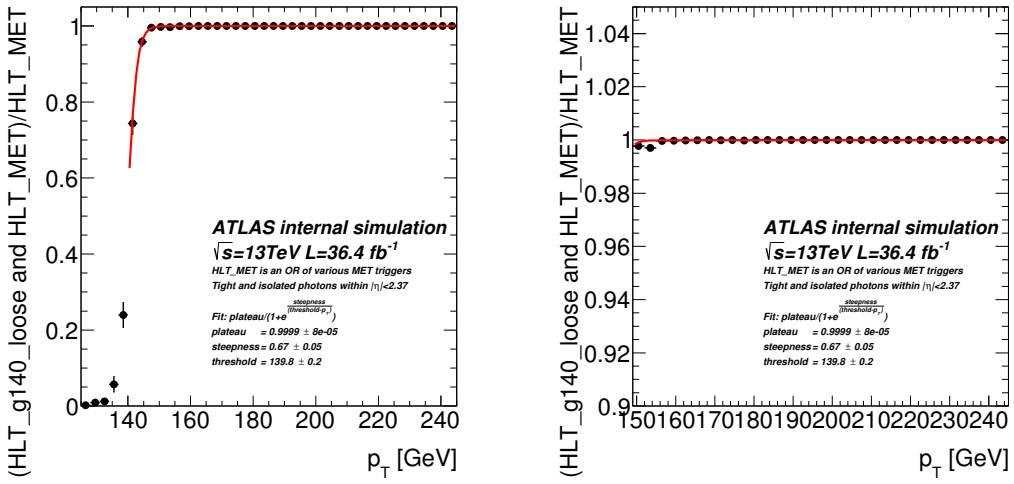

Figure 9: Trigger efficiency in the Monte Carlo background samples for the *HLT_g*140*_loose* trigger shown as a function of the offline leading photon p_{T} (left). A zoom into the region of interest is shown on the right.

5 Background estimation

The Standard Model background in the signal region is composed by different sources, as listed in Section 2.2. All dominant backgrounds are evaluated using data control regions.

For the dominant background $Z(\rightarrow \nu\nu)+\gamma$ and secondary contributions, like $W(\rightarrow \ell\nu)+\gamma$, $Z(\rightarrow \ell\ell)+\gamma$ and γ + jet, control regions are built reverting one or more cuts used to define the Signal Region, allowing one of these processes to become dominant. The corresponding cuts are described in Sec. 5.1. The control regions are fitted simultaneously using MC predictions rescaled such to match the data yields as explained in Sec. 5.2.

The W/Z + jet, top and diboson contributions are estimated with data driven techniques based on electron/jet photon–fake studies described in Sec. 5.3 and Sec. 5.4.

Beam-induced background is highly suppressed by applying the jet cleaning and the photon pointing criteria described in Sec. 4.

5.1 Definition of the control regions used to estimate the real-γ background

Four control regions (CR) are defined to constrain the normalization of $W\gamma$, $Z\gamma$ and γ + jet backgrounds.

- **Single-Muon Control Region**: the same selection of the SR is applied, except for the muon veto: it is required that exactly one "selected" muon is present in the event. For this control region the the $E_{\mathrm{T}}^{\mathrm{miss}}$ is defined as described in 3.5, but the muon term is subtracted from the computation, i.e. the muons are treated as invisible particles. This control region is used to extract the normalization of the $W(\rightarrow \ell\nu) + \gamma$ background in the signal region.

- **Two-Muon (Two-Electron) Control Region** : the same selection of the SR is applied, except for the lepton veto: it is required that exactly two "selected" muons (electrons) are present in the event and no "pre-selected" electron (muon). As in the Single-Muon CR the muon (electron) term is subtracted from the $E_{\mathrm{T}}^{\mathrm{miss}}$ computation, such that muons (electrons) are treated as invisible particles. The two-muon (two-electron) invariant mass is required to be greater than 10 GeV to be coherent with the generator level cut of the $W\gamma$, $Z\gamma$ background samples. This second kind of control regions is used to constrain the normalization of both the $Z(\rightarrow \nu\nu) + \gamma$ and the $Z(\rightarrow ll) + \gamma$ in the SR; both two-muon and two-electron CRs are considered, in order to improve the statistics of the sample.

- **Photon-Jet Control Region**: the same selection of the SR is applied except for a lower $E_{\mathrm{T}}^{\mathrm{miss}}$ range: $85\,\mathrm{GeV} < E_{\mathrm{T}}^{\mathrm{miss}} < 110\,\mathrm{GeV}$ to enrich this region of γ + jet background. The request $\Delta\phi(\gamma, E_{\mathrm{T}}^{\mathrm{miss}}) < 3.0$ is applied to reduce possible signal contamination. This specific photon-jet CR has been defined in Run-2 to constrain the normalization of γ + jet background.

In the single and two-muon CRs the muons are treated as invisible particles in the $E_{\mathrm{T}}^{\mathrm{miss}}$ computation. Similarly in the two-electron CR the electrons are treated as invisible. In this way it is possible to ensure that the $E_{\mathrm{T}}^{\mathrm{miss}}$ spectrum in all the CRs is similar to the one in the SR.

Comparisons between data and MC simulations have been made on a data sample corresponding to 36.4 fb^{-1}. Distributions of $E_{\mathrm{T}}^{\mathrm{miss}}$, photon p_{T}^{γ} and η^{γ} are shown for all CRs in Figures 11, 12, 10 and 13. Distributions of muon and electron p_{T}, η and ϕ are shown for the leptonic CRs in Figures 14, 15, 20, 18, 19. More kinematic distributions can be found in Appendix C. For the one-electron CR, defined in a similar way than one-muon CR, main kinematic distributions can be found in Appendix D.

Distributions of MC background processes in SR corresponding to $E_{\mathrm{T}}^{\mathrm{miss}} > 150$ GeV are shown in fig. 21, more distributions can be found in Appendix C.

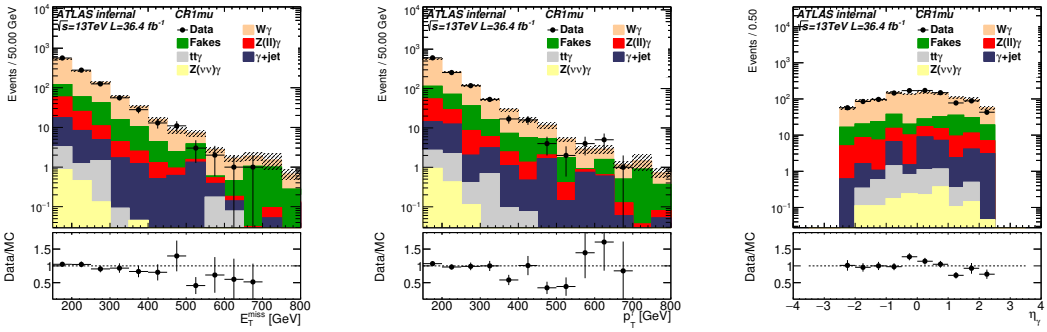

Figure 10: Pre-fit distributions of $E_{\mathrm{T}}^{\mathrm{miss}}$, photon p_{T}^{γ} and η^{γ} in the one-muon CR for 36.4 fb^{-1}of data (black dots) and SM background processes. The dashed bands include only statistical uncertainties associated to the events from the SM MC generation. The fakes are estimated by using W/Z + jet, $t\bar{t}$and di-jet samples instead of data-driven methods. The lower part of the figure shows the ratios of data to pre-fit background event yields. Negative bins from fakes are set to 0 but the error on them are conserved.

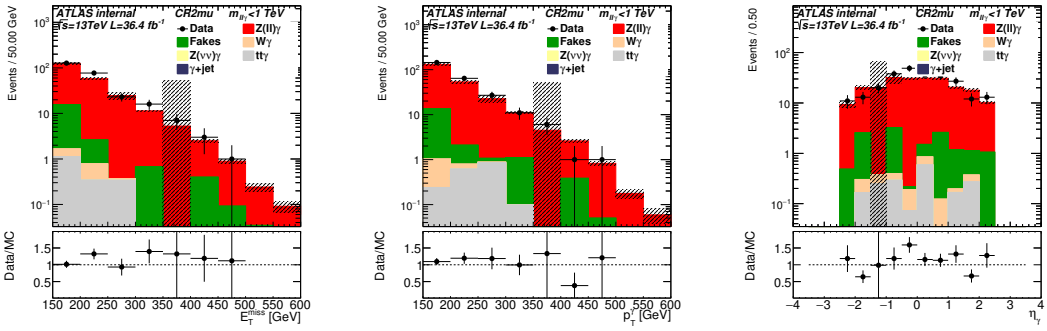

Figure 11: Pre-fit distributions of $E_{\mathrm{T}}^{\mathrm{miss}}$, photon p_{T}^{γ} and η^{γ} in the two-muons CR for 36.4 fb^{-1}of data (black dots) and SM background processes. The dashed bands include only statistical uncertainties associated to the events from the SM MC generation. The fakes are estimated by using W/Z + jet, $t\bar{t}$and di-jet samples instead of data-driven methods. The lower part of the figure shows the ratios of data to pre-fit background event yields. Negative bins from fakes are set to 0 but the error on them are conserved.

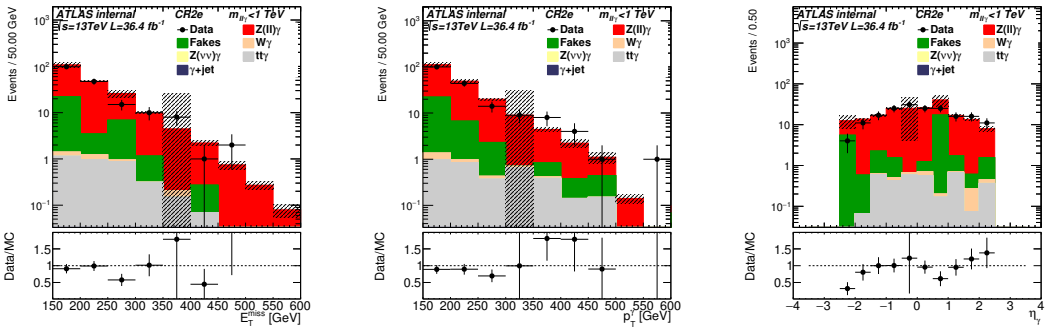

Figure 12: Pre-fit distributions of $E_{\mathrm{T}}^{\mathrm{miss}}$, photon p_{T}^{γ} and η^{γ} in the two-electrons CR for 36.4 fb^{-1}of data (black dots) and SM background processes. The dashed bands include only statistical uncertainties associated to the events from the SM MC generation. The fakes are estimated by using W/Z + jet, $t\bar{t}$and di-jet samples instead of data-driven methods. The lower part of the figure shows the ratios of data to pre-fit background event yields. Negative bins from fakes are set to 0 but the error on them are conserved.

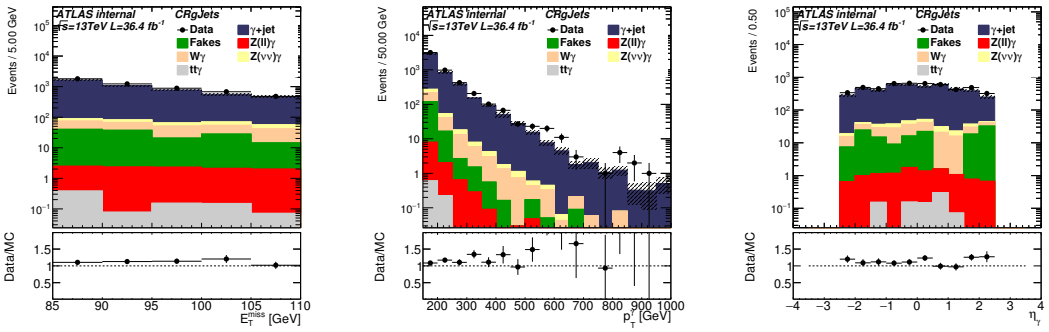

Figure 13: Pre-fit distributions of $E_{\mathrm{T}}^{\mathrm{miss}}$, photon p_{T}^{γ} and η^{γ} in the Photon-Jet CR for 36.4 fb^{-1}of data (black dots) and SM background processes. The dashed bands include only statistical uncertainties associated to the events from the SM MC generation. The fakes are estimated by using W/Z + jet, $t\bar{t}$and di-jet samples instead of data-driven methods. The lower part of the figure shows the ratios of data to pre-fit background event yields. Negative bins from fakes are set to 0 but the error on them are conserved.

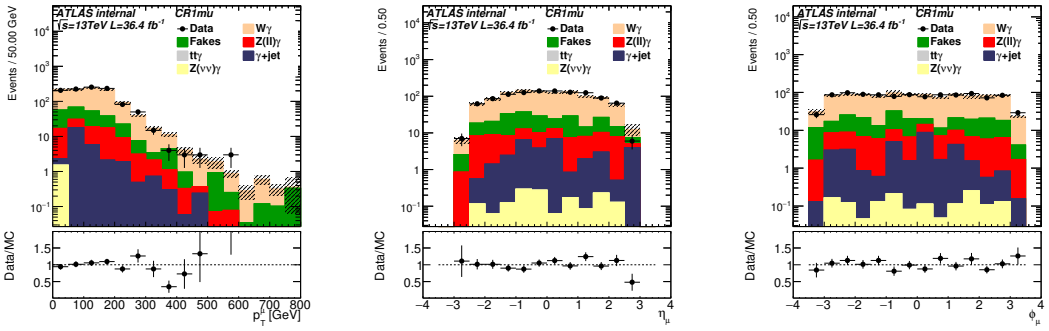

Figure 14: Pre-fit distributions of muon p_{T}, η,and ϕ in the one-muon CR for 36.4 fb^{-1}of data (black dots) and SM background processes. The dashed bands include only statistical uncertainties associated to the events from the SM MC generation. The fakes are estimated by using W/Z + jet, $t\bar{t}$and di-jet samples instead of data-driven methods. The lower part of the figure shows the ratios of data to pre-fit background event yields. Negative bins from fakes are set to 0 but the error on them are conserved.

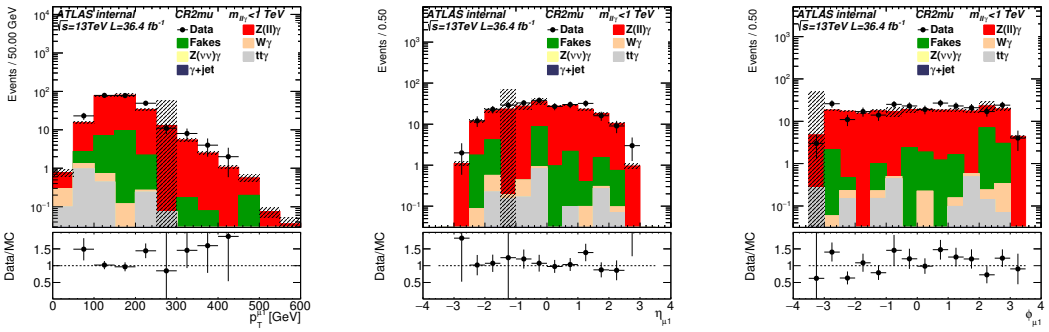

Figure 15: Pre-fit distributions of leading muon p_{T}, η,and ϕ in the two-muon CR for 36.4 fb^{-1}of data (black dots) and SM background processes. The dashed bands include only statistical uncertainties associated to the events from the SM MC generation. The fakes are estimated by using W/Z + jet, $t\bar{t}$and di-jet samples instead of data-driven methods. The lower part of the figure shows the ratios of data to pre-fit background event yields. Negative bins from fakes are set to 0 but the error on them are conserved.

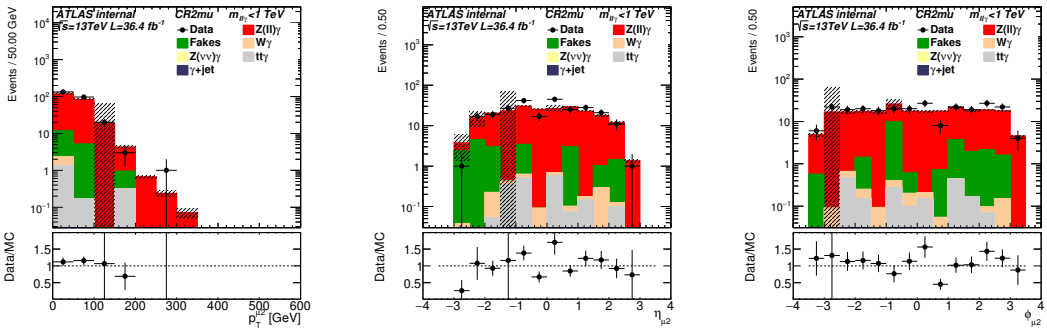

Figure 16: Pre-fit distributions of subleading muon p_{T}, η,and ϕ in the two-muon CR for 36.4 fb^{-1}of data (black dots) and SM background processes. The dashed bands include only statistical uncertainties associated to the events from the SM MC generation. The fakes are estimated by using W/Z + jet, $t\bar{t}$and di-jet samples instead of data-driven methods. The lower part of the figure shows the ratios of data to pre-fit background event yields. Negative bins from fakes are set to 0 but the error on them are conserved.

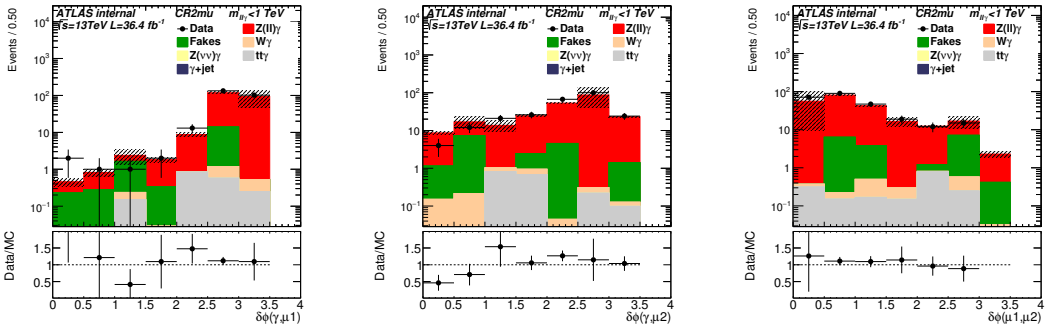

Figure 17: Pre-fit angular distributions in the two-muon CR for 36.4 fb^{-1}of data (black dots) and SM background processes. The dashed bands include only statistical uncertainties associated to the events from the SM MC generation. The fakes are estimated by using W/Z + jet, $t\bar{t}$and di-jet samples instead of data-driven methods. The lower part of the figure shows the ratios of data to pre-fit background event yields. Negative bins from fakes are set to 0 but the error on them are conserved.

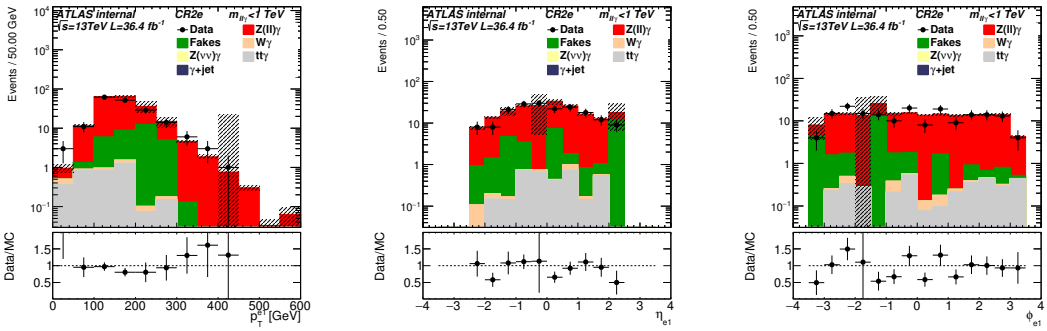

Figure 18: Pre-fit distributions of leading electron p_{T}, η,and ϕ in the two-electron CR for 36.4 fb^{-1}of data (black dots) and SM background processes. The dashed bands include only statistical uncertainties associated to the events from the SM MC generation. The fakes are estimated by using W/Z + jet, $t\bar{t}$and di-jet samples instead of data-driven methods. The lower part of the figure shows the ratios of data to pre-fit background event yields. Negative bins from fakes are set to 0 but the error on them are conserved.

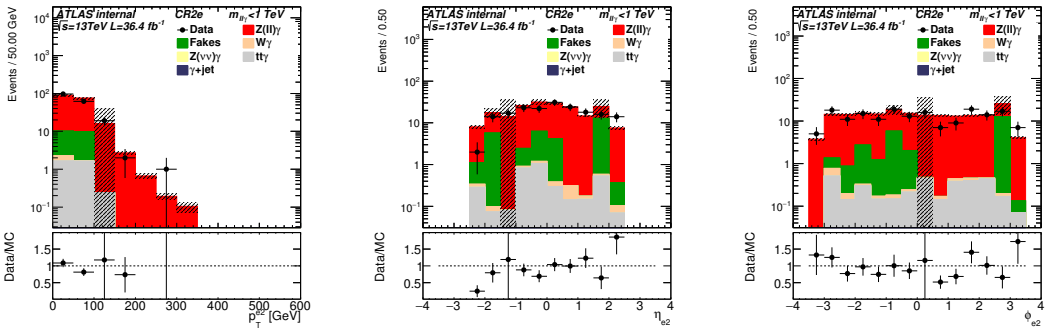

Figure 19: Pre-fit distributions of subleading electron p_{T}, η,and ϕ in the two-electron CR for 36.4 fb^{-1}of data (black dots) and SM background processes. The dashed bands include only statistical uncertainties associated to the events from the SM MC generation. The fakes are estimated by using W/Z + jet, $t\bar{t}$and di-jet samples instead of data-driven methods. The lower part of the figure shows the ratios of data to pre-fit background event yields. Negative bins from fakes are set to 0 but the error on them are conserved.

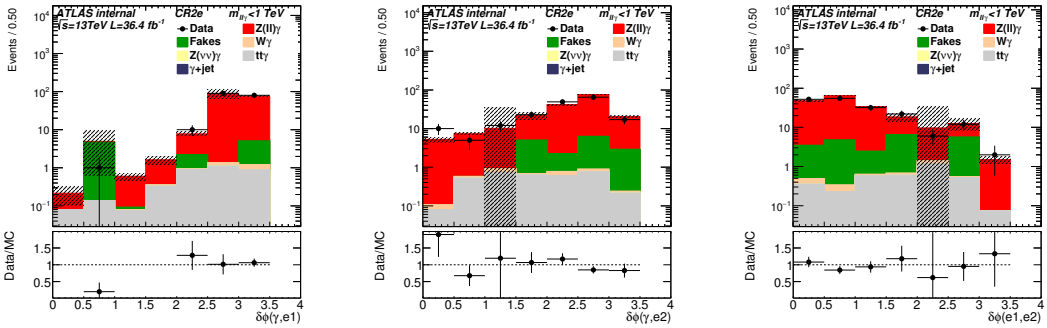

Figure 20: Pre-fit angular distributions in the two-electron CR for 36.4 fb^{-1}of data (black dots) and SM background processes. The dashed bands include only statistical uncertainties associated to the events from the SM MC generation. The fakes are estimated by using W/Z + jet, $t\bar{t}$and di-jet samples instead of data-driven methods. The lower part of the figure shows the ratios of data to pre-fit background event yields. Negative bins from fakes are set to 0 but the error on them are conserved.

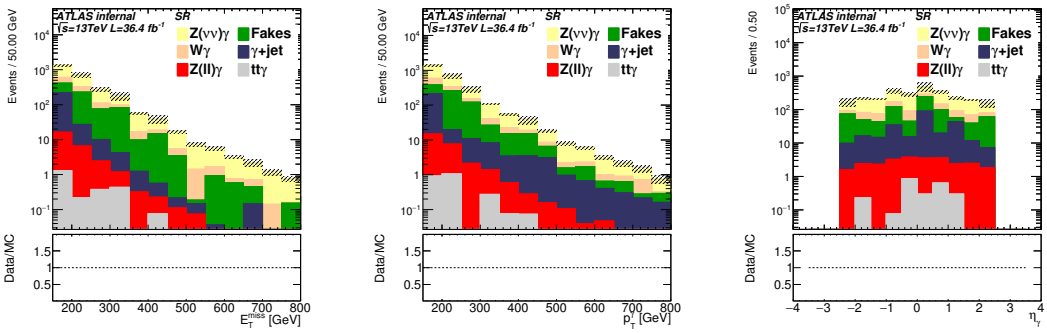

Figure 21: Pre-fit distributions of $E_{\mathrm{T}}^{\mathrm{miss}}$, photon p_{T}^{γ} and η^{γ} in the SR corresponding to $E_{\mathrm{T}}^{\mathrm{miss}} > 150$ GeV for 36.4 fb^{-1}of SM background processes. The dashed bands include only statistical uncertainty associated to the events from the SM MC generation. The fakes are estimated by using W/Z+jets, ttbar and di-jet samples instead of data-driven methods for fake electrons and fake jets. Negative bins from fakes are set to 0 but the error on them are conserved.

5.2 Simultaneous fitting technique

The simultaneous fitting technique is used as the baseline technique for the background estimation and for the signal interpretation. This technique enables the signal and background yields estimation in both CRs and SR exploiting the data constrain in all these regions at the same time. Using a simultaneous fit technique allows a straightforward combination of multiple CRs and permits a coherent treatment of the correlation of the systematic uncertainties across the different regions.

The predicted event yield in each region R (either the signal region or a control region) is described as a random variable which follows a Poisson distribution,

$$\begin{aligned} N_R(\text{data}) \propto \text{Pois}\Bigg(& N_R(\text{data}) | L \times \sigma \times (A \times \epsilon)_R \\ & + k_{Z\gamma} N_R(Z(\to \nu\nu) + \gamma) \\ & + k_{W\gamma} N_R(W(\to \ell\nu) + \gamma) \\ & + k_{Z\gamma} N_R(Z(\to \ell\ell) + \gamma) \\ & + k_{\gamma+\text{jet}} N_R(\gamma + \text{jet}) \\ & + \sum_{B \neq V\gamma, Z\gamma, \gamma+\text{jet}} N_R(B) \Bigg), \end{aligned} \tag{3}$$

whose expectation value is given by the sum of:

- the signal yield in the region R, given by the product of the integrated luminosity, signal cross section, acceptance and efficiency $L \times \sigma \times (A \times \epsilon)$:
- the expected (MC) yield for the $Z(\to \nu\nu) + \gamma$ background, rescaled by a factor $k_{Z\gamma}$;
- the expected (MC) yield for the $W(\to \ell\nu) + \gamma$ background, rescaled by a factor $k_{W\gamma}$;
- the expected (MC) yield for the $Z(\to \ell\ell) + \gamma$ background, rescaled by a factor $k_{Z\gamma}$ (i.e. the same used to rescale $Z(\to \nu\nu) + \gamma$);
- the expected (MC) yield for the γ + jet background, rescaled by a factor $k_{\gamma+\text{jet}}$;
- the yields expected for the additional backgrounds.

The free parameters of the fit are the signal yield and the three k factors: $k_{Z\gamma}$, $k_{W\gamma}$, $k_{\gamma+\text{jet}}$. Uncertainties on each of the background components are taken into account, for each region, by multiplying Eq. (3) by log–normal constraints. Each yield N_R is replaced by $N_R(1 + \sum_i \Delta_i)$, where Δ_i is the nuisance parameter associated to a given systematic variation, and a multiplicative constraint term on Δ_i is added to the likelihood. A simultaneous likelihood is then built, by multiplying the likelihoods obtained for each region. More detail about the treatment of the systematic uncertainties in the likelihood can be found in Section 7.

The simultaneous fit is performed separately in each of the inclusive regions shown in Table 8 to extract the final result for each inclusive SR. Moreover a simultaneous fit is performed using all the exclusive $E_{\text{T}}^{\text{miss}}$ regions shown in Table 8, this permits to extract different k-factors in each $E_{\text{T}}^{\text{miss}}$ bin to correct the $E_{\text{T}}^{\text{miss}}$ shape to data, allowing more information in an exclusion fit than is available just with inclusive SRs. This technique is known as "simplified shape fit".

Technically, the implementation of the likelihood and the statistical treatment of the results is performed by means of the HistFitter package [45]. Various fit strategies, described in [45], are employed in the analysis:

- Background-only fit: it is performed on all CRs to estimate the k-factors needed to evaluate the background yields in the SR before unblinding, as described in Sec. 6.

- Model dependent signal fit: it is performed on all CRs plus the SR including a signal component to set exclusion/discovery fits. This strategy will be employed after the unblinding of the SR for the interpretation of the results in Sec. 6.

5.3 Electrons faking photons

Electrons and photons have very similar signatures in the EM calorimeters. Some photons (the "converted photons") also leave a signal in the tracking system. These two effects make the electron/photon separation difficult and a fraction of electrons are mistakenly being identified as photons. In order to derive the contribution of such electron fakes to the event yield, a two-step approach is taken.

In the first step, the probability of electrons to fake photons ("fake rate") is measured. The electron fake rate is measured through a tag-and-probe method which selects events with one good electron (tag) and one electron/photon (probe); the tag-and-probe invariant mass is required to be compatible with the Z mass. The "fake rate" is calculated as the ratio of the number of electron-photon pairs over the number of electron-electron pairs and it is derived as a function of p_{T} and η.

In the second step, the background contribution coming from electrons faking photons is derived by using the fake rate to scale control regions, called probe-electron control regions, in which the requirement of having one signal photon is replaced by the requirement to have a probe electron.

To estimate this background in the signal region, a probe-electron control region is hence selected in a similar way as the mono-photon signal region, except that a single probe electron is required instead of the photon. Similarly, a probe-electron control region with one muon is used to estimate the electron fakes in the one-muon plus photon control region. The same logic applies to the other real-γ control regions (see Section 5.1), as summarised in Table 10; if more than one probe electron is present in one given probe-electron region (as can be the case in the probe-e $2e$ CR), all possibilities of an electron faking a photon are taken into account.

Region in which the e-to-γ BG is to be evaluated	Corresponding probe-e CR
Signal region (γ+$E_{\mathrm{T}}^{\mathrm{miss}}$)	probe-e SR (probe-e+$E_{\mathrm{T}}^{\mathrm{miss}}$)
1μ CR (γ + μ+$E_{\mathrm{T}}^{\mathrm{miss}}$)	probe-e 1μ CR (probe-e + μ+$E_{\mathrm{T}}^{\mathrm{miss}}$)
2μ CR (γ + 2μ+$E_{\mathrm{T}}^{\mathrm{miss}}$)	probe-e 2μ CR (probe-e + 2μ+$E_{\mathrm{T}}^{\mathrm{miss}}$)
$2e$ CR (γ + $2e$+$E_{\mathrm{T}}^{\mathrm{miss}}$)	probe-e $2e$ CR (probe-e + $2e$+$E_{\mathrm{T}}^{\mathrm{miss}}$)
PhJet CR (γ+$E_{\mathrm{T}}^{\mathrm{miss}}$at low $E_{\mathrm{T}}^{\mathrm{miss}}$)	probe-e PhJet CR (probe-e+$E_{\mathrm{T}}^{\mathrm{miss}}$at low $E_{\mathrm{T}}^{\mathrm{miss}}$)

Table 10: The various probe-electron control regions used to estimate the electron-to-photon fake background in the signal and $V\gamma$ / γ+jet control regions.

5.3.1 Electron-to-photon fake rate

As mentioned above, the probability of electrons to fake photons is measured through a tag-and-probe procedure. In this method the following selections are used:

- For the electrons:

  - The *tag* electrons are required to be identified using the mediumLH requirement, to have p_{T}> 25 GeV , η< 2.47, and to pass cuts on the transverse (longitudinal) impact parameter.

675 – The *probe* electrons are requested to have p_T> 150 GeV , be outside the crack region, be iden-
676 tified using the mediumLH requirement and be isolated, using the Loose isolation working
677 point.

678 – To evaluate the "real fake rate" in the MC, used to assess systematic uncertainties, the *true*
679 electrons are electrons passing the probe requirements at reconstruction level which are also
680 associated at truth level to an isolated electron (value of the *truth type* of 2) coming from a Z
681 boson, or from a W boson when evaluating the "real fake rate" in a $W(e\nu)$+jets sample (value
682 of the *truth origin* of 13 or 12).

683 · For the photons:

684 – The *probe* photons are selected in the same way as the signal photons used in this analysis,
685 starting at p_T> 150 GeV .

686 – To evaluate the "real fake rate" in the MC, used to assess systematic uncertainties, the *true*
687 photons are photons passing the probe requirements at reconstruction level which are also
688 associated at truth level to an isolated electron or to final state radiation (value of the *truth*
689 *type* of 2 or 15) coming from a Z (or W) boson or final state radiation (value of the *truth*
690 *origin* of 13 (12) or 40).

691 The tag-and-probe selection accepts events if they satisfy $E_T^{miss} < 40$ GeV and if they contain at least
692 one tag-and-probe pair (either a probe electron or photon) within 10 GeV or the Z boson mass.

693 The fake rate reported here is measured using 36.4 fb^{-1}of data and the MC15 simulation samples.
694 The invariant mass distribution measured in data is compared to the one obtained by using simulation
695 samples from $Z(ee)$+jets in Figure 22. The Monte Carlo is not used to derive the fake rate value, but is
696 used in estimating the systematic on the fake rate as described later. One can note that there seems to be a
697 higher tail contribution in $e\gamma$ data on both sides of the Z peak, suggesting some QCD contamination of the
698 tag-and-probe sample, which will be addressed by fitting the sidebands and subtracting this contribution
699 from the peak.

700 In this dataset, 620 $e + \gamma$ tag-and-probe events are found in the Z mass window, while 38185 ee
701 events are found, amounting to a global fake rate of (1.62 ± 0.07)% (without the eventual background
702 subtraction and with statistical uncertainty only). The fake rate obtained in Monte Carlo samples, by
703 looking at the truth information, is (1.15 ± 0.06)% for $Z(ee)$ events and (1.22 ± 0.05)% for $W(e\nu)$ events.

704 The global fake rate reported above is not the one used in the analysis, as the fake rate is seen to
705 vary as a function of p_T and η, as can be seen in Figure 23, where the data is shown before sideband
706 subtraction. For information, the conversion type of the selected photons is also shown in this Figure,
707 showing rather good agreement between data and MC, within uncertainties: fake photons can either be
708 converted or unconverted, with about the same probability.

709 Fake rates were also estimated using $W(e\nu)$ events at truth level. Based on the $W(e\nu)$ expectation and
710 because of the relatively low statistics in data (620 $e\gamma$ events in total), the fake rate is then measured in
711 fours different bins: two bins in η, $|\eta| < 1.37$ and $|\eta| > 1.52$, times two bins in p_T, 150 <p_T< 200 GeV
712 and p_T> 200 GeV .

713 In each region, the BG to the $e\gamma$ sample is estimated using by fitting a first-order polynomial in the Z
714 mass sidebands, being either:

715 · 66 to 81 GeV and 101 to 116 GeV (sideband subtraction 1)

716 · 66 to 76 GeV and 106 to 116 GeV (sideband subtraction 2)

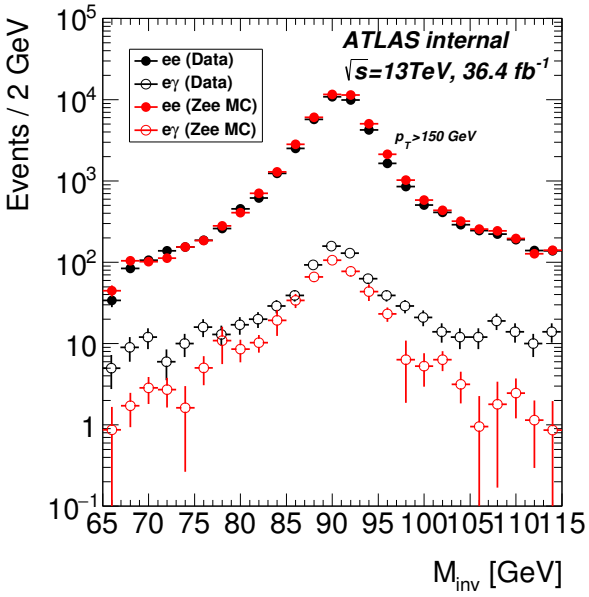

Figure 22: Invariant mass distribution of the tag-and-probe pair as measured in the data and in the $Z(ee)$+jets Monte Carlo samples, for electron and photon probes. A mass window of 10 GeV around the Z mass is used to evaluate the fake rate.

and subtracting the extrapolation of this fit inside the Z mass window[11].

The values measured in data with the various methods are reported in Table 11, while the values found in the MC can be found in Table 12. The invariant mass in each p_{T}/η bin can be seen in Figure 24. The addition of the $ptcone20/p_{\mathrm{T}}< 0.05$ requirement on the signal photon with respect to the isolation criteria used in the 2015 analysis was shown to reduce the measured fake rate by 15-30% (depending on the regions) in studies based on 13.9 fb^{-1} of data and was thus adopted throughout.

$\lvert\eta\rvert$	p_{T}[GeV]	T&P no SBS	T&P SBS1	T&P SBS2
<1.37	< 200	1.46 ± 0.09	1.07 ± 0.07	1.10 ± 0.08
	> 200	1.0 ± 0.1	0.59 ± 0.08	0.59 ± 0.08
> 1.52	< 200	2.9 ± 0.2	2.5 ± 0.2	2.6 ± 0.2
	> 200	2.9 ± 0.3	2.4 ± 0.3	2.3 ± 0.3

Table 11: Electron-to-photon fake rates, in %, as measured in data for various methods. The uncertainty shown here is statistical only.

The following sources of systematic uncertainties on the measured fake rates are considered and added in quadrature:

- The difference between the fake rates measured in $Z(ee)$ and $W(e\nu)$ MC samples using the truth information, as most of the electron-to-photon background in the SR is expected to come from $W(e\nu)$ events
- The difference between the fake rate as measured using the tag-and-probe method on the $Z(ee)$ MC

[11] An unconstrained double-sided Crystal Ball (Z peak) + Gaussian fit (BG) is performed in the e/gamma group to estimate fake rates at lower p_{T} values. This approach was tried, but the large number of free parameters combined with the relatively low statistics makes this approach difficult at the large p_{T} values we are probing.

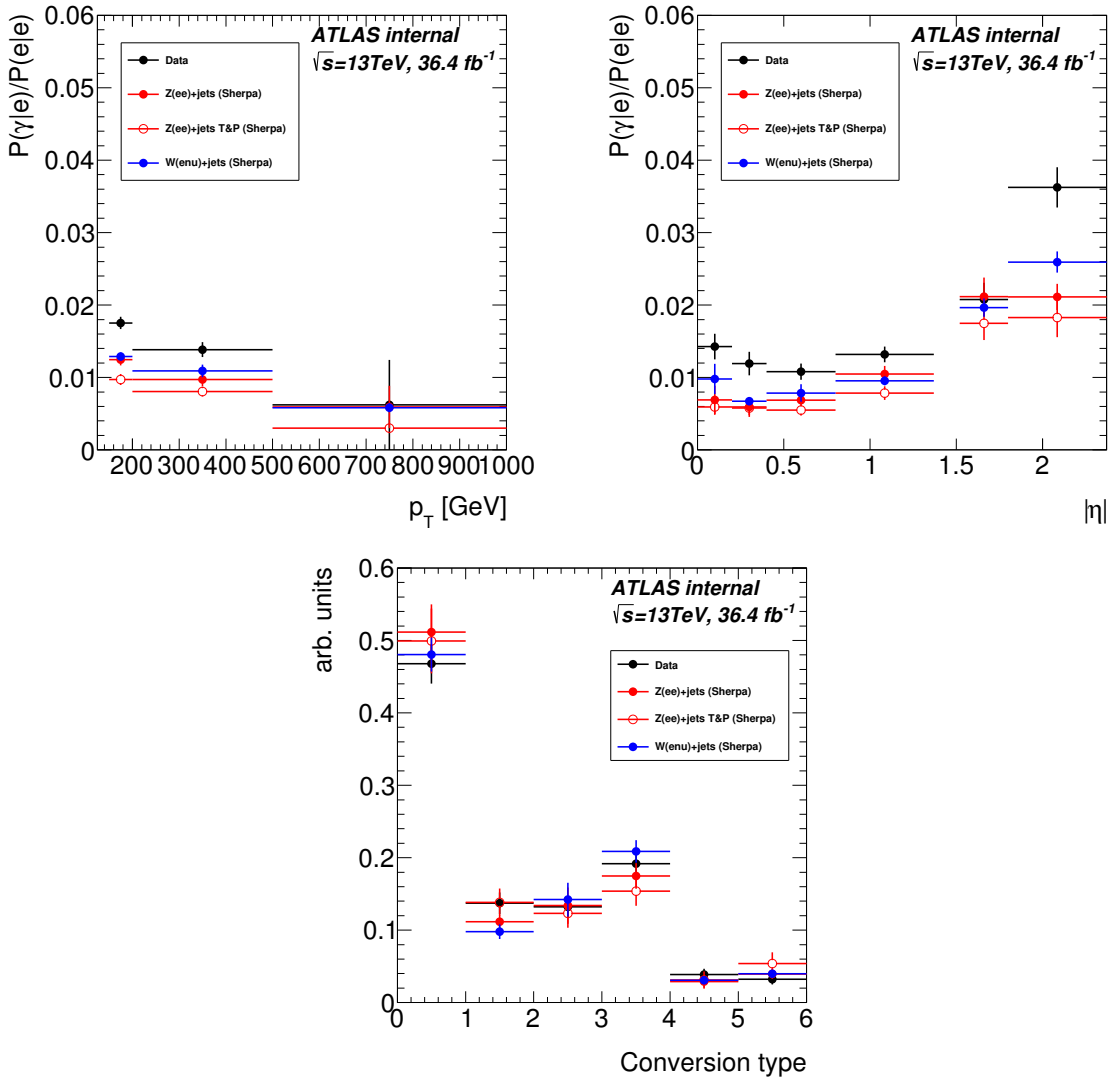

Figure 23: Fake rate obtained as a function of p_{T} (top left) and η (top right), as measured in the data (without BG subtraction from sidebands) and in Monte Carlo samples (see the text). The conversion type of the fake photons is also shown (bottom), normalized to unity; the conversion types are 0:unconverted, 1:singleSi, 2:singleTRT, 3:doubleSi, 4:doubleTRT, 5:doubleSiTRT.

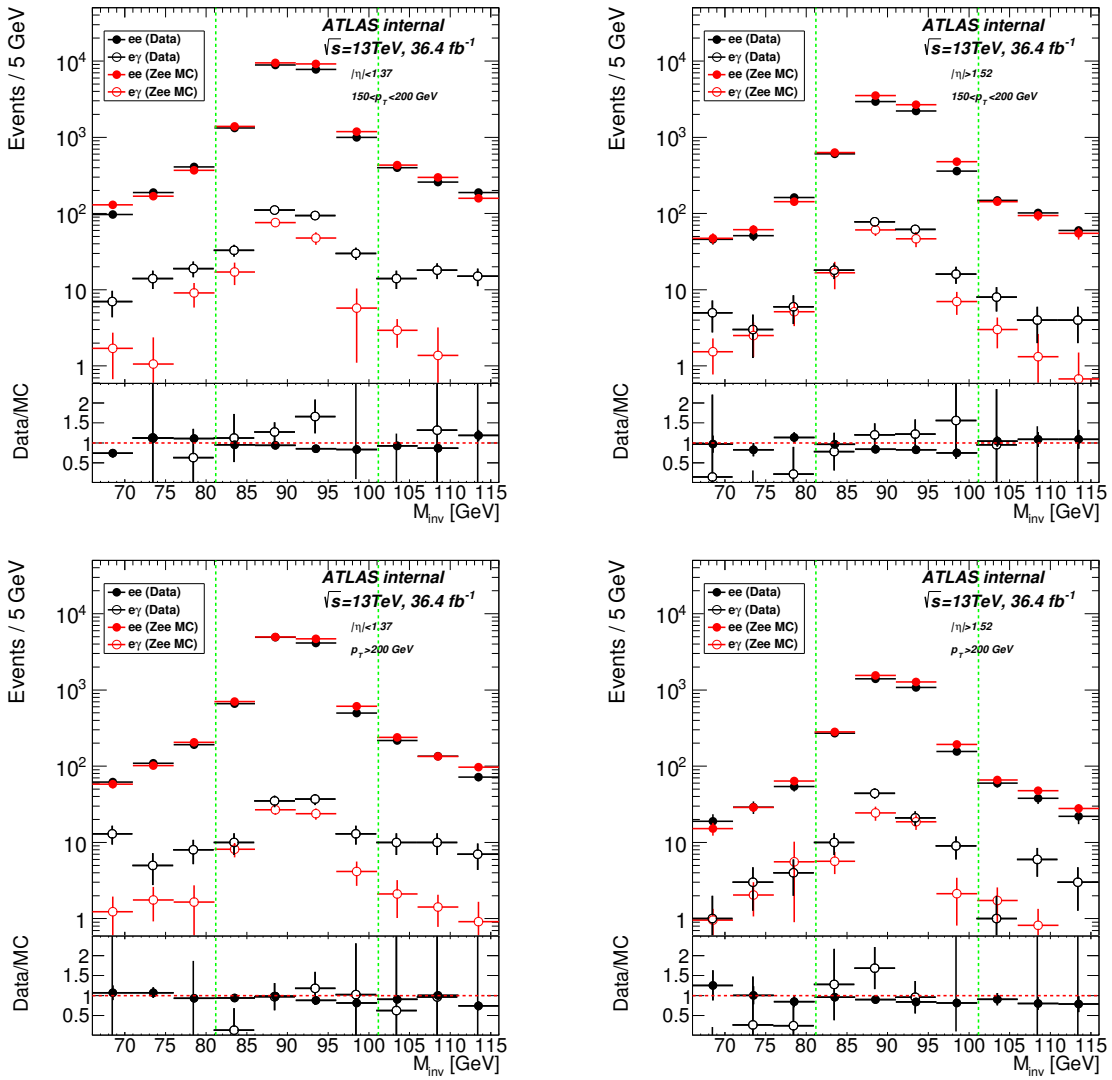

Figure 24: Invariant mass distribution of the tag-and-probe pair as measured in the data and in the $Z(ee)$+jets Monte Carlo samples, for electron and photon probes, for the various p_{T}/η bins used to derive the fake rate: $|\eta| < 1.37$ (left column), $|\eta| > 1.52$ (right column), 150 $< p_{\mathrm{T}} <$ 200 GeV (top row) and $p_{\mathrm{T}} >$ 200 GeV (bottom row). A mass window of 10 GeV around the Z mass is used to evaluate the fake rate, sidebands are used to subtract the BG. The ratio plot is shown after subtraction.

$\|\eta\|$	p_T[GeV]	$W(e\nu)$ truth	$Z(ee)$ truth	$Z(ee)$ T&P no SBS	$Z(ee)$ T&P SBS1
<1.37	< 200	0.92 ± 0.07	0.89 ± 0.08	0.69 ± 0.07	0.67 ± 0.06
	> 200	0.76 ± 0.10	0.68 ± 0.10	0.58 ± 0.06	0.52 ± 0.07
> 1.52	< 200	2.2 ± 0.1	2.1 ± 0.2	1.8 ± 0.2	1.7 ± 0.2
	> 200	2.2 ± 0.2	1.8 ± 0.2	1.5 ± 0.2	1.4 ± 0.2

Table 12: Electron-to-photon fake rates, in %, as measured in Monte Carlo samples for various methods. The uncertainty shown here is statistical only.

samples and the fake rate measured in the same samples but using truth information (non-closure), in order to cover for any bias which could come from applying the tag-and-probe method

· The difference between the fake rate measured in the $Z(ee)$ MC sample using tag-and-probe with or without background subtraction, in order to cover from any bias which could come from the background subtraction method

· The difference between the fake rates measured in data using the two sideband definitions

The final fake rate with statistical and systematic uncertainties can be found in Table 13.

$\|\eta\|$	p_T[GeV]	Fake rate ± stat ± syst
<1.37	< 200	1.07 ± 0.07 ± 0.21
	> 200	0.59 ± 0.08 ± 0.14
> 1.52	< 200	2.5 ± 0.2 ± 0.3
	> 200	2.4 ± 0.3 ± 0.5

Table 13: Electron-to-photon fake rates measured in data, in %, as used in this analysis with statistical and systematic uncertainties.

5.3.2 Probe-electron Control Regions

In order to estimate the electron-to-photon fake background in the signal regions and in the control regions used to estimate the $V\gamma$ and γ+jet backgrounds (see Section 5.1), a probe-electron control region is built for each signal or control region, as was summarised in Table 10. As mentioned before, these probe-electron control regions use the same selection as their corresponding signal or control region except that a probe electron is required instead of a photon. This means for example that in the probe-electron control region used to estimate the e-to-γ fake background in the signal region, $W(e\nu)$+jets is the dominant process.

The numbers of selected events in data for the various probe-electron regions are given in Table 14.

E_T^{miss} bins	Probe-e SR	Probe-e 1μ CR	Probe-e 2μ CR	Probe-e 2e CR	Probe-e PhJet CR
> 150 GeV	15368	1378	41	6	
> 225 GeV	4557	407	16	4	5306
> 300 GeV	1455	112	4	4	
150 – 225 GeV	10811	971	25	2	
225 – 300 GeV	3102	295	12	0	

Table 14: Number of selected events in the probe-electron control regions for 36.4 fb^{-1}of data. The PhJet CR being defined at low E_T^{miss} values, there is no splitting in various E_T^{miss} bins for this region.

If one considers models with dark matter production with a photon emitted as ISR, one is also compelled to consider the emission of a W in the same way: this could lead to a signal contamination of

the probe-e SR if the W decays to $e\nu$. This was checked on a truth sample produced using an official jobOption (DSID 304212) which uses a mono-W axial-vector production model (with the same quark and dark matter mediator couplings as the axial-vector model used in this analysis). For m_{DM} = 1 GeV and m_{med} = 500 GeV (chosen to be roughly in the middle of the expected exclusion reach in m_{med}), the contamination is found to be negligible (around 0.8%, assuming an optimistic reconstruction efficiency of 100%).

5.3.3 Results in Signal Regions and Control Regions

Table 15 shows the final estimate for the electron-to-photon fake background in the various regions, as obtained by scaling the various probe-electron control regions by the fake rates. In this table, the statistical uncertainty is expressed by two terms: the first one is related to the statistics of each probe-electron control region and the second one, to the statistics in tag-and-probe events used to compute the electron fake rate.

$E_{\mathrm{T}}^{\mathrm{miss}}$ bins	SR	1μ CR	2μ CR	2e CR	PhJet CR
> 150 GeV	198.5 ± 1.8 ± 18.0 ± 35.5	16.7 ± 0.5 ± 1.5 ± 3.1	0.50 ± 0.09 ± 0.04 ± 0.09	0.09 ± 0.04 ± 0.01 ± 0.01	
> 225 GeV	46.7 ± 0.9 ± 5.7 ± 10.0	4.2 ± 0.2 ± 0.4 ± 0.9	0.17 ± 0.05 ± 0.02 ± 0.04	0.052 ± 0.030 ± 0.004 ± 0.009	71.6 ± 1.1 ± 6.1 ± 12.4
> 300 GeV	13.1 ± 0.4 ± 1.7 ± 2.9	1.1 ± 0.1 ± 0.1 ± 0.2	0.028 ± 0.015 ± 0.003 ± 0.006	0.052 ± 0.030 ± 0.004 ± 0.009	
150 – 225 GeV	151.8 ± 1.6 ± 12.3 ± 25.5	12.4 ± 0.4 ± 1.0 ± 2.2	0.32 ± 0.07 ± 0.02 ± 0.06	0.036 ± 0.027 ± 0.003 ± 0.005	
225 – 300 GeV	33.6 ± 0.7 ± 4.0 ± 7.1	3.1 ± 0.2 ± 0.3 ± 0.6	0.14 ± 0.05 ± 0.02 ± 0.03	0	

Table 15: Electron-to-photon fakes estimated in the SR and its CRs for an integrated luminosity of 36.4 fb^{-1}. The uncertainty is expressed in three terms: The first term is the statistical uncertainty related to the number of events found in the probe-e CR; the second and third terms are the statistical and systematic uncertainties related to the electron fake, respectively. The PhJet CR being defined at low $E_{\mathrm{T}}^{\mathrm{miss}}$ values, there is no splitting in various $E_{\mathrm{T}}^{\mathrm{miss}}$ bins for this region.

5.4 Jets faking photons

Hadronic jets can also be reconstructed as photons. This background is suppressed by requiring tight photon identification and isolation criteria. The remaining jet contribution is estimated with a 2-dimensional matrix method applied to each of the analysis regions, SR and all CRs. This method was studied and adopted for the 2015 analysis, a brief remind of the method and results for the 2016 analysis are described in the following.

5.4.1 Description of the method

The 2-dimensional side-band matrix is defined by inverting or loosening the isolation and identification requirements on the photon. Tight-n photons are defined as photons which are non tight and fail one or more among n of the cuts in the tight menu. In Appendix B the variables used for the definition of the tight menu of the photons are reported with a brief description. Following the 2015, the inverted cuts are:

- for tight-3: F_{side}, ΔE, w_{s_3}
- for tight-4: F_{side}, ΔE, w_{s_3}, E_{ratio}
- for tight-5: F_{side}, ΔE, w_{s_3}, E_{ratio}, $w_{s_{tot}}$

Isolated photons are defined by the requirement: $TopoEtCone40 - 0.022\, p_T^{\gamma} - 2.45\ \mathrm{GeV} < 0$.
Non-isolated photons are defined by the requirement: $3\ \mathrm{GeV} < TopoEtCone40 - 0.022\, p_T^{\gamma} - 2.45\ \mathrm{GeV} < 27\ \mathrm{GeV}$.

776 N_A is defined as the number of events with tight and isolated photons (signal photons), N_B, M_A and
777 M_B correspond to tight and non-isolated, tight-4 and isolated, tight-4 and non-isolated photons (back-
778 ground photons), as illustrated in Figure 25.
779
780 Assuming that in CR1, CR2 and CR3 the component of signal photons is negligible and that for
781 background photons the correlation between isolation and identification is negligible, the number of
782 background photons in each region of the analysis can be estimated as:

$$N^A_{bkg} = \frac{N^B M^A}{M_B} \tag{4}$$

783 and consequently the number of signal photons in each region is:

$$N^A_{sign} = N_A - \frac{N^B M^A}{M_B} \tag{5}$$

784 with the purity defined as:

$$P = \frac{N^A_{sign}}{N^A} \tag{6}$$

785 A correction to the method is added in order to take into account the leakage of the signal photons to
786 the control regions; signal leakage coefficients are defined as:

$$\frac{N^B_{sign}}{N^A_{sign}} = c_1, \quad \frac{M^A_{sign}}{N^A_{sign}} = c_2, \quad \frac{M^B_{sign}}{N^A_{sign}} = c_3 \tag{7}$$

787 A schematic representation of the signal leakage coefficients is given in Figure 26.
788 When applying the correction to Equation 5, one obtains:

$$N^A_{sign} = N^A - \left(N^B - N^A_{sign} \cdot c_1\right) \frac{\left(M^A - N^A_{sign} \cdot c_2\right)}{\left(M^B - N^A_{sign} \cdot c_3\right)} = \left(N_A - \frac{N^B M^A}{M_B}\right) \frac{1}{1 + \frac{c_3 N^A - c_2 N^B - c_1 M^A}{M^B}} \tag{8}$$

789 which equals to Equation 5 if $c_1 = c_2 = c_3 = 0$. The correction is similarly propagated to the number
790 of estimated background events.
791 Signal leakage coefficients are evaluated from MC15 $V + \gamma$ samples. The systematic uncertainty on the
792 method is evaluated by varying the definition of the CRs, namely the tight-3 and tight-5 are used instead
793 of tight-4, and the energy gap between isolated and non-isolated regions is varied from 2 to 4 GeV instead
794 of 3 GeV.
795 To check the impact of the lower threshold to define Non-isolated photons an optimization study
796 based on the purity and its statistical error was done varying the threshold from 0 to 140 GeV. It was
797 found that the best threshold is 5 GeV but moving to it provides no significant impact on the final
798 estimates and uncertainties. On the basis of these checks it was decided to keep the 3 GeV threshold.
799 To overcome the problem of low statistics of the non-tight regions of the two-muon and two-electron
800 CRs a *reduced* method was validated and applied in the 2015 analysis. The idea is to apply the ratio
801 $r = \frac{M^A}{M^B}$ evaluated from the SR and single-muon CR (with more events) to the two-muon and two-electron
802 CRs. The number of signal events in the signal region (corrected for signal leakage) is:

$$N^A_{sign} = \frac{N^A - N^B r}{1 - c_1 r} \tag{9}$$

803 and the number of background events is:

$$N^A_{bkg} = \frac{\left(c_1 N^A - N^B\right) r}{r c_1 - 1} \tag{10}$$

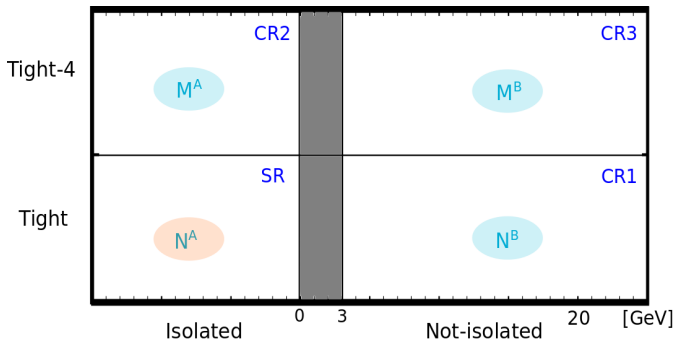

Figure 25: Illustration of the two dimensional plane, defined with the isolation and a subset of the photon Id variables. The jet background in the signal region N^A is estimated from the three control regions N^B, M^A and M^B.

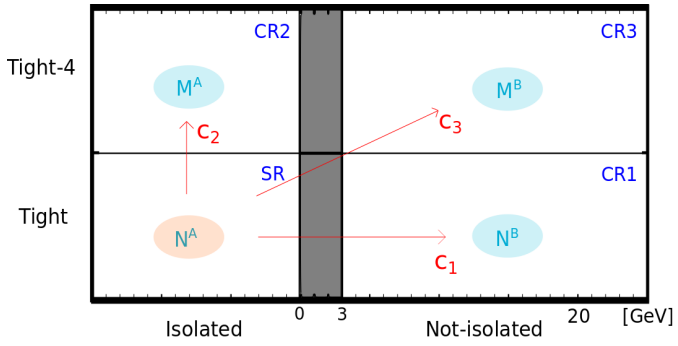

Figure 26: Illustration of the signal leakage coefficients in the two dimensional plane.

5.4.2 Results in Signal Regions and Control Regions

The *reduced* method has been applied on the full 2015+2016 data sample corresponding to 36.4 fb^{-1} to obtain the jet fakes estimates in SR and its CRs. The results for the inclusive SR corresponding to $E_{\mathrm{T}}^{\mathrm{miss}} >$ 150 GeV and related CRs. are shown in Figure 27(a) for data and MC samples. A good compatibility between data and MC estimates is shown.

As a cross-check the results corresponding to the complete method are shown in Figure 27(b). The results are in agreement within the erros with the *reduced* method but the complete method is characterized by large statistical uncertainty in the two-muon and two-electron CRs due to too low statistics in those CRs as shown in table Table 16. This confirms that the *reduced* method is preferable and will be adopted also for the 2016 analysis.

Figure 28 shows the purity evaluated with the *reduced* method. A high level of purity (> 90%) is obtained both in the SR and its CRs.

Tab. 17 shows the jet to photon fake estimates for the all the SRs and its associated CRs corresponding to different $E_{\mathrm{T}}^{\mathrm{miss}}$ bins with their statistic and systematic uncertainties obtained with the *reduced* method. The corresponding signal leakage coefficients for the inclusive SR corresponding to $E_{\mathrm{T}}^{\mathrm{miss}} >$ 150 GeV are reported in the Table 18. It has been checked that the other SRs provide values of signal leakage coefficients of the same order of magnitude.

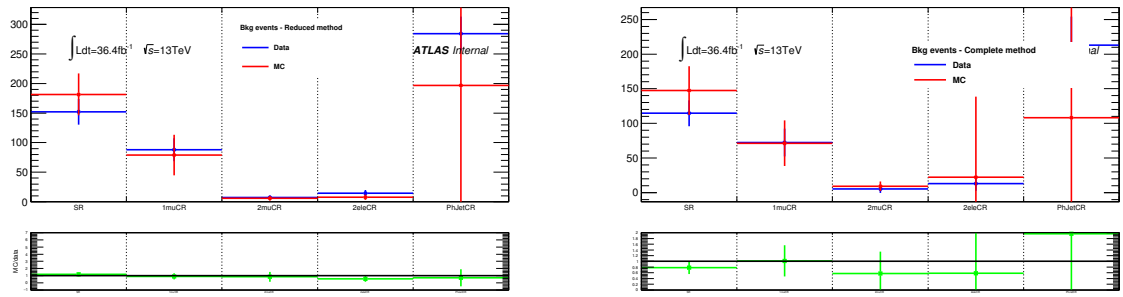

(a) *reduced* method (b) complete method

Figure 27: Comparison between data and MC for jet-to-photon fakes estimated for the inclusive SR corresponding to $E_{\mathrm{T}}^{\mathrm{miss}} >$ 150 GeV and related CRs for the *reduced* and complete methods. The data sample corresponds to 36.4 fb^{-1}.

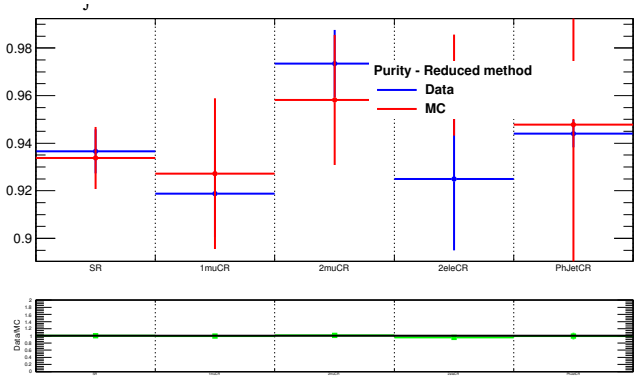

Figure 28: Purity evaluated with the reduced method for data and MC samples for the inclusive SR corresponding to $E_{\mathrm{T}}^{\mathrm{miss}} >$ 150 GeV and related CRs. The data sample corresponds to 36.4 fb^{-1}.

$E_{\mathrm{T}}^{\mathrm{miss}}$bins	M^A	M^B	N^B
SR	245	235	211
Single-muon CR	138	162	138
Two-muon CR	15	12	14
Two-electron CR	14	11	19
PhJet CR	468	728	597

Table 16: Number of events in the M^A, M^B, N^B regions for the inclusive SR corresponding to $E_{\mathrm{T}}^{\mathrm{miss}} >$ 150 GeV and related CRs. The data sample corresponds to 36.4 fb^{-1}

$E_{\mathrm{T}}^{\mathrm{miss}}$bins	SR	Single-muon CR	Two-muon CR	Two-electron CR	PhJet CR
$E_{\mathrm{T}}^{\mathrm{miss}}$> 150 GeV	152.1 ± 21.3 ± 4.2	88.1 ± 14.8 ± 12.6	7.2 ± 3.7 ± 0.5	14.3 ± 4.5 ± 3.2	284.4 ± 24.4 ± 15
$E_{\mathrm{T}}^{\mathrm{miss}}$> 225 GeV	36.7 ± 9 ± 12.2	23.4 ± 7.2 ± 7.4	4.8 ± 2.4 ± 1.3	5.4 ± 2.5 ± 1.7	284.4 ± 24.4 ± 15
$E_{\mathrm{T}}^{\mathrm{miss}}$> 300 GeV	9.6 ± 4.4 ± 9	3.4 ± 2.1 ± 2.9	1.0 ± 0.9 ± 0.8	1.6 ± 1.1 ± 1.5	284.4 ± 24.4 ± 15
150 < $E_{\mathrm{T}}^{\mathrm{miss}}$< 225 GeV	114.6 ± 19.7 ± 13.7	64.9 ± 13 ± 8.8	0.9 ± 2.4 ± 0.7	7.8 ± 3.5 ± 2	284.4 ± 24.4 ± 15
225 < $E_{\mathrm{T}}^{\mathrm{miss}}$< 300 GeV	27 ± 7.9 ± 4.8	20.5 ± 7.5 ± 6.6	3.5 ± 2.2 ± 0.7	3.1 ± 2.0 ± 0.9	284.4 ± 24.4 ± 15

Table 17: Jet-to-photon fakes estimated in all the SRs and their associated CRs with their statistical and systematic uncertainties for different $E_{\mathrm{T}}^{\mathrm{miss}}$ bins. The data sample corresponds to 36.4 fb^{-1}

Signal Leakage Coefficients	
SR	single-muon CR
$c_1 = 2.89\% \pm 0.07\%$	$c_1 = 3.46\% \pm 0.11\%$
$c_2 = 2.68\% \pm 0.009\%$	$c_2 = 2.64\% \pm 0.014\%$
$c_3 = 0.11\% \pm 0.0004\%$	$c_3 = 0.35\% \pm 0.002\%$
di-muon CR	di-electron CR
$c_1 = 2.41\% \pm 0.09\%$	$c_1 = 2.27\% \pm 0.09\%$
$c_2 = 2.57\% \pm 0.01\%$	$c_2 = 2.57\% \pm 0.015\%$
$c_3 = 0.11\% \pm 0.0006\%$	$c_3 = 0.12\% \pm 0.0007\%$
ph-Jet CR	
$c_1 = 3.2\% \pm 0.20\%$	
$c_2 = 2.4\% \pm 0.03\%$	
$c_3 = 0.16\% \pm 0.002\%$	

Table 18: Signal leakage coefficients for the inclusive SR corresponding to $E_{\mathrm{T}}^{\mathrm{miss}} > 150$ GeV with their statistical uncertainty in the SR and its CRs. The data sample corresponds to 36.4fb^{-1}.

6 Results

The full 2015+2016 dataset has been analyzed using two GRLs[12] for 2015 and for 2016 data corresponding to a total integrated luminosity of 36.4 fb^{-1}.

6.1 Results in Signal Regions and Control Regions from single bin fit

A background-only single-bin fit, as described in Sec. 5.2, is performed to estimate the normalization factors (k-factors) used to predict the background yields in the inclusive SRs and in their associated CRs. The in-situ estimates for electrons and jets faking photons reported in Sec. 5.3.3 and in Sec. 5.4.2 are included in the fit.

The estimated k-factors after the fit for each inclusive SR, defined for different $E_{\mathrm{T}}^{\mathrm{miss}}$ bins, are reported in Table 19. The different k-factors are stable and in agreement within uncertainties among the different $E_{\mathrm{T}}^{\mathrm{miss}}$ bins.

HistFitter tables 20, 21, 22 report the expected background yields with their uncertainties before and after the fit and the number of observed events in data in the CRs.

$E_{\mathrm{T}}^{\mathrm{miss}}$bins	$k_{Z\gamma}$	$k_{W\gamma}$	$k_{\gamma+\mathrm{jet}}$
$E_{\mathrm{T}}^{\mathrm{miss}}$> 150 GeV	1.10 ± 0.09	1.05 ± 0.09	1.07 ± 0.25
$E_{\mathrm{T}}^{\mathrm{miss}}$> 225 GeV	1.14 ± 0.13	1.04 ± 0.11	1.06 ± 0.25
$E_{\mathrm{T}}^{\mathrm{miss}}$> 300 GeV	1.27 ± 0.23	1.04 ± 0.15	1.06 ± 0.24

Table 19: Normalization factors (k-factors) obtained from a background only single-bin fit performed in each inclusive SR for an integrated luminosity of 36.4 fb^{-1}. The errors shown include both the statistical and systematic uncertainties.

6.2 Results in Signal Regions and Control Regions from simplified shape fit

A background-only simplified shape fit, as described in Sec. 5.2, is performed using all exclusive $E_{\mathrm{T}}^{\mathrm{miss}}$ regions defined in Table 8. The in-situ estimates for electrons and jets faking photons reported in Sec. 5.3.3 and in Sec. 5.4.2 are included in the fit.

The estimated k-factors after the simplified shape fit for each exclusive SR are reported in Table 23. It's possible to notice that the different k-factors are very similar to ones obtained from a single-bin fit in Table 19.

HistFitter tables 24, 25, 26, report the expected background yields with their uncertainties before and after the fit and the number of observed events in data for each of the exclusive $E_{\mathrm{T}}^{\mathrm{miss}}$ bin. Figures 29 and 30 shows the post-fit $E_{\mathrm{T}}^{\mathrm{miss}}$ and photon p_{T} distributions in SR from the simplified shape fit corresponding to $E_{\mathrm{T}}^{\mathrm{miss}} > 150$ GeV .

[12] GRL_2015: data15_13TeV.periodAllYear_DetStatus-v73-pro19-08_DQDefects-00-01-02_PHYS_StandardGRL_All_Good_25ns.xml, GRL_2016: data16_13TeV.periodAllYear_DetStatus-v83-pro20-15_DQDefects-00-02-04_PHYS_StandardGRL_All_Good_25ns.xml

table.results.yields channel	SR	ONEmuCR	TWOmuCR	TWOeleCR	PhJetCR
Observed events	2400	1083	254	181	5064
Fitted bkg events	2637.80 ± 160.55	1083.02 ± 32.91	242.53 ± 12.80	192.83 ± 10.32	5063.83 ± 72.13
Fitted Znunugamma events	1614.97 ± 107.65	1.70 ± 0.19	0.00 ± 0.00	0.00 ± 0.00	80.91 ± 5.67
Fitted Zgamma events	34.48 ± 2.75	77.14 ± 4.64	233.05 ± 12.96	179.69 ± 10.41	12.75 ± 0.85
Fitted Wgamma events	389.91 ± 24.38	866.49 ± 39.58	1.08 ± 0.35	0.68 ± 0.12	162.44 ± 9.43
Fitted gammajets events	247.79 ± 79.59	32.89 ± 8.49	0.00 ± 0.00	0.00 ± 0.00	4451.69 ± 79.64
Fitted JetFakes events	152.10 ± 21.72	88.14 ± 19.32	7.89 ± 3.77	12.37 ± 4.72	284.41 ± 28.49
Fitted EleFakes events	198.53 ± 39.82	16.67 ± 3.40	0.50 ± 0.13	0.09 ± 0.04	71.63 ± 13.81
MC exp. SM events	2442.02 ± 203.99	1024.60 ± 71.74	218.45 ± 15.31	180.52 ± 13.34	4789.39 ± 989.02
MC exp. Znunugamma events	1460.60 ± 112.23	1.54 ± 0.16	0.00 ± 0.00	0.00 ± 0.00	73.17 ± 5.55
MC exp. Zgamma events	31.17 ± 3.04	69.58 ± 5.07	209.71 ± 14.66	165.49 ± 12.10	11.54 ± 0.82
MC exp. Wgamma events	368.85 ± 34.88	818.20 ± 60.68	1.01 ± 0.37	0.67 ± 0.12	153.69 ± 13.39
MC exp. gammajets events	230.78 ± 76.18	30.48 ± 6.28	0.00 ± 0.00	0.00 ± 0.00	4194.96 ± 987.64
MC exp. JetFakes events	152.10 ± 21.72	88.14 ± 19.45	7.24 ± 3.78	14.27 ± 5.54	284.40 ± 28.68
MC exp. EleFakes events	198.53 ± 39.82	16.67 ± 3.42	0.50 ± 0.13	0.09 ± 0.04	71.63 ± 13.91

Table 20: Results of the background estimation in the SR defined with $E_{\mathrm{T}}^{\mathrm{miss}} > 150$ GeV and in its CRs for an integrated luminosity of 36.4 fb^{-1}. Results are obtained with a background-only fit in the CRs. Each background component is reported before (bottom) and after the fit (top). The errors shown include both the statistical and systematics uncertainties.

table.results.yields channel	SR	ONEmuCR	TWOmuCR	TWOeleCR	PhJetCR
Observed events	729	343	86	59	5064
Fitted bkg events	765.46 ± 59.07	342.98 ± 18.52	80.67 ± 7.18	64.37 ± 5.86	5063.82 ± 72.31
Fitted Znunugamma events	543.97 ± 54.52	0.42 ± 0.10	0.00 ± 0.00	0.00 ± 0.00	82.74 ± 9.15
Fitted Zgamma events	7.82 ± 0.85	20.87 ± 2.18	75.16 ± 7.33	59.57 ± 5.91	13.09 ± 1.38
Fitted Wgamma events	108.69 ± 9.08	284.03 ± 21.53	0.00 ± 0.00	0.17 ± 0.05	158.49 ± 13.83
Fitted gammajets events	21.58 ± 6.92	9.97 ± 2.12	0.00 ± 0.00	0.00 ± 0.00	4453.47 ± 81.77
Fitted JetFakes events	36.68 ± 15.16	23.44 ± 10.26	5.34 ± 2.86	4.58 ± 2.57	284.40 ± 28.49
Fitted EleFakes events	46.73 ± 11.48	4.24 ± 1.00	0.17 ± 0.07	0.05 ± 0.03	71.63 ± 13.81
MC exp. SM events	695.85 ± 44.29	330.29 ± 22.95	70.74 ± 4.63	58.63 ± 4.86	4789.39 ± 989.02
MC exp. Znunugamma events	479.96 ± 30.64	0.37 ± 0.09	0.00 ± 0.00	0.00 ± 0.00	73.17 ± 5.55
MC exp. Zgamma events	6.90 ± 0.54	18.40 ± 1.37	65.75 ± 3.71	53.02 ± 3.77	11.54 ± 0.82
MC exp. Wgamma events	105.11 ± 8.13	274.40 ± 18.79	0.00 ± 0.00	0.17 ± 0.05	153.69 ± 13.39
MC exp. gammajets events	20.47 ± 6.26	9.43 ± 1.06	0.00 ± 0.00	0.00 ± 0.00	4194.96 ± 987.64
MC exp. JetFakes events	36.68 ± 15.16	23.44 ± 10.33	4.82 ± 2.76	5.39 ± 3.05	284.40 ± 28.68
MC exp. EleFakes events	46.73 ± 11.48	4.24 ± 1.01	0.17 ± 0.07	0.05 ± 0.03	71.63 ± 13.91

Table 21: Results of the background estimation in the SR defined with $E_{\mathrm{T}}^{\mathrm{miss}} > 225$ GeV and in its CRs for an integrated luminosity of 36.4 fb^{-1}. Results are obtained with a background-only fit in the CRs. Each background component is reported before (bottom) and after the fit (top). The errors shown include both the statistical and systematics uncertainties.

table.results.yields channel	SR	ONEmuCR	TWOmuCR	TWOeleCR	PhJetCR
Observed events	236	116	27	21	5064
Fitted bkg events	272.95 ± 36.80	116.00 ± 10.77	26.05 ± 4.03	21.98 ± 3.33	5061.13 ± 71.11
Fitted Znunugamma events	209.34 ± 34.97	0.11 ± 0.04	0.00 ± 0.00	0.00 ± 0.00	93.00 ± 16.06
Fitted Zgamma events	2.18 ± 0.38	7.15 ± 1.21	24.88 ± 4.11	20.45 ± 3.42	14.67 ± 2.47
Fitted Wgamma events	33.45 ± 4.21	98.15 ± 11.69	0.00 ± 0.00	0.06 ± 0.04	159.35 ± 20.64
Fitted gammajets events	5.21 ± 1.11	6.05 ± 1.74	0.00 ± 0.00	0.00 ± 0.00	4438.07 ± 82.68
Fitted JetFakes events	$9.66^{+10.03}_{-9.66}$	$3.44^{+3.56}_{-3.44}$	$1.14^{+1.29}_{-1.14}$	$1.42^{+1.63}_{-1.42}$	284.41 ± 28.49
Fitted EleFakes events	13.11 ± 3.36	1.10 ± 0.29	0.03 ± 0.02	0.05 ± 0.03	71.63 ± 13.81
MC exp. SM events	226.36 ± 17.54	110.58 ± 8.58	20.64 ± 1.97	17.89 ± 2.30	4789.39 ± 989.02
MC exp. Znunugamma events	164.69 ± 11.49	0.09 ± 0.03	0.00 ± 0.00	0.00 ± 0.00	73.17 ± 5.55
MC exp. Zgamma events	1.71 ± 0.17	5.62 ± 0.46	19.54 ± 1.53	16.12 ± 1.21	11.54 ± 0.82
MC exp. Wgamma events	32.25 ± 2.54	94.61 ± 6.92	0.00 ± 0.00	0.06 ± 0.04	153.69 ± 13.39
MC exp. gammajets events	4.93 ± 1.27	5.73 ± 0.96	0.00 ± 0.00	0.00 ± 0.00	4194.96 ± 987.64
MC exp. JetFakes events	$9.66^{+10.03}_{-9.66}$	$3.43^{+3.58}_{-3.43}$	$1.07^{+1.25}_{-1.07}$	$1.66^{+1.95}_{-1.66}$	284.40 ± 28.68
MC exp. EleFakes events	13.11 ± 3.36	1.10 ± 0.29	0.03 ± 0.02	0.05 ± 0.03	71.63 ± 13.91

Table 22: Results of the background estimation in the SR defined with $E_{\mathrm{T}}^{\mathrm{miss}} > 300$ GeV and in its CRs for an integrated luminosity of 36.4 fb^{-1}. Results are obtained with a background-only fit in the CRs. Each background component is reported before (bottom) and after the fit (top). The errors shown include both the statistical and systematics uncertainties.

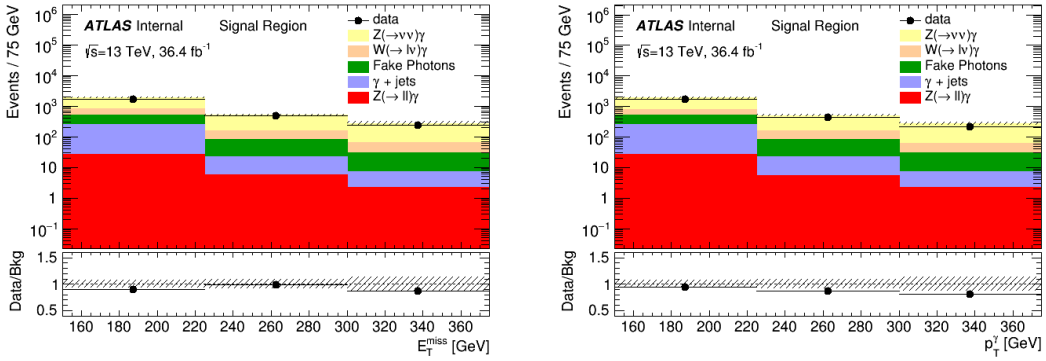

(a) $E_{\mathrm{T}}^{\mathrm{miss}}$in SR

(b) photon p_{T} in SR

Figure 29: Post-fit distributions of $E_{\mathrm{T}}^{\mathrm{miss}}$and photon p_{T} in the SR corresponding for 36.4 fb^{-1}of data and for background predicted from the simplified shape fit. The dashed band includes statistical and systematic uncertainties. Overflows are included in the final bin. The lower part of the figure shows the ratios of data to expected-background event yields.

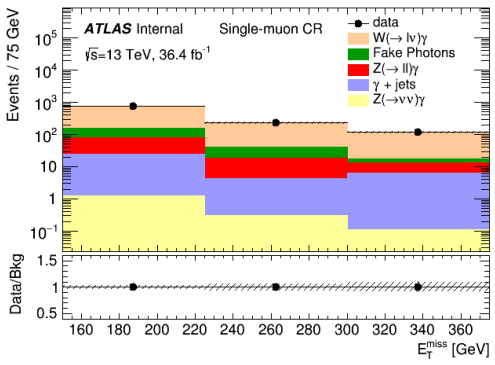

(a) $E_{\mathrm{T}}^{\mathrm{miss}}$in the single-muon CR

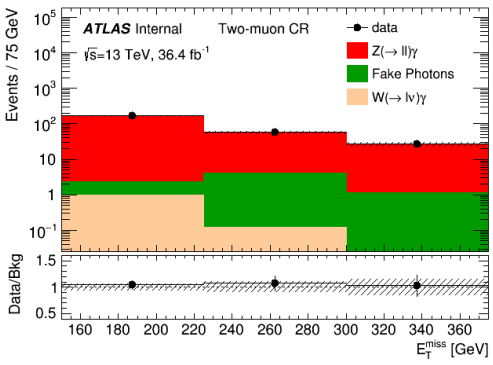

(b) $E_{\mathrm{T}}^{\mathrm{miss}}$ in the two-muon CR

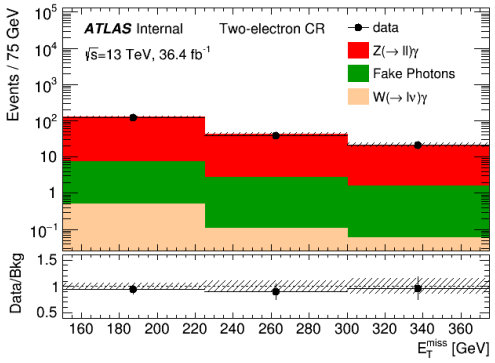

(c) $E_{\mathrm{T}}^{\mathrm{miss}}$ in the two-electron CR

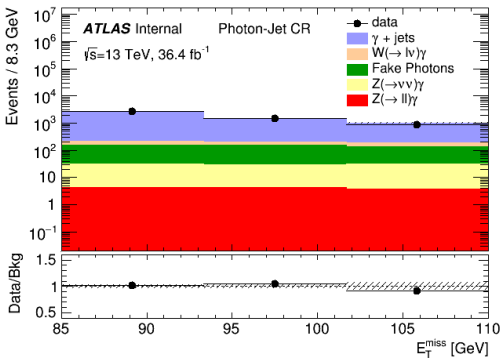

(d) $E_{\mathrm{T}}^{\mathrm{miss}}$ in the photon-jet CR

Figure 30: Post-fit distributions of $E_{\mathrm{T}}^{\mathrm{miss}}$in the four CRs corresponding for 36.4 fb^{-1}of data and for background predicted from the simplified shape fit. The dashed band includes statistical and systematic uncertainties. Overflows are included in the final bin. The lower part of the figure shows the ratios of data to expected-background event yields.

$E_{\mathrm{T}}^{\mathrm{miss}}$bins	$k_{Z\gamma}$	$k_{W\gamma}$	$k_{\gamma+\mathrm{jet}}$
$150 < E_{\mathrm{T}}^{\mathrm{miss}} < 225$ GeV	1.10 ± 0.10	1.06 ± 0.10	1.07 ± 0.25
$225 < E_{\mathrm{T}}^{\mathrm{miss}} < 300$ GeV	1.09 ± 0.14	1.02 ± 0.12	1.07 ± 0.25
$E_{\mathrm{T}}^{\mathrm{miss}} > 300$ GeV	1.27 ± 0.23	1.03 ± 0.14	1.07 ± 0.25

Table 23: Normalization factors (k-factors) obtained from a background-only simplified shape fit performed on all exclusive $E_{\mathrm{T}}^{\mathrm{miss}}$ bins for an integrated luminosity of 36.4 fb^{-1}. The errors shown include both the statistical and systematic uncertainties.

table.results.yields channel	SR1	ONEmuCR1	TWOmuCR1	TWOeleCR1	PhJetCR
Observed events	1671	740	168	122	5064
Fitted bkg events	1878.95 ± 144.49	740.02 ± 27.20	161.36 ± 10.27	128.94 ± 8.12	5063.83 ± 71.95
Fitted Znunugamma events	1078.85 ± 88.73	1.28 ± 0.21	0.00 ± 0.00	0.00 ± 0.00	80.46 ± 6.27
Fitted Zgamma events	26.70 ± 2.54	56.39 ± 3.91	159.07 ± 10.31	121.51 ± 8.15	12.68 ± 0.95
Fitted Wgamma events	281.87 ± 22.26	582.14 ± 32.67	0.97 ± 0.28	0.51 ± 0.13	164.15 ± 11.01
Fitted gammajets events	225.13 ± 79.61	22.88 ± 7.43	0.00 ± 0.00	0.00 ± 0.00	4450.51 ± 79.93
Fitted JetFakes events	114.60 ± 24.05	64.91 ± 15.64	$1.00^{+2.06}_{-1.00}$	6.88 ± 3.60	284.41 ± 28.49
Fitted EleFakes events	151.80 ± 28.39	12.43 ± 2.43	0.32 ± 0.09	0.04 ± 0.03	71.63 ± 13.81
MC exp. SM events	1745.48 ± 172.08	694.53 ± 52.19	146.05 ± 10.63	120.86 ± 9.44	4789.39 ± 989.02
MC exp. Znunugamma events	980.76 ± 85.73	1.17 ± 0.16	0.00 ± 0.00	0.00 ± 0.00	73.17 ± 5.55
MC exp. Zgamma events	24.26 ± 2.64	51.17 ± 3.80	143.96 ± 10.32	112.47 ± 8.49	11.54 ± 0.82
MC exp. Wgamma events	263.76 ± 28.03	543.79 ± 42.79	0.90 ± 0.30	0.50 ± 0.13	153.69 ± 13.39
MC exp. gammajets events	210.31 ± 76.78	21.05 ± 6.22	0.00 ± 0.00	0.00 ± 0.00	4194.96 ± 987.64
MC exp. JetFakes events	114.60 ± 24.05	64.92 ± 15.74	$0.87^{+1.79}_{-0.87}$	7.86 ± 4.10	284.40 ± 28.68
MC exp. EleFakes events	151.80 ± 28.39	12.43 ± 2.45	0.32 ± 0.09	0.04 ± 0.03	71.63 ± 13.91

Table 24: Results of the background estimation from the simplified shape corresponding to the $E_{\mathrm{T}}^{\mathrm{miss}}$ bin [150 GeV; 225 GeV] for an integrated luminosity of 36.4 fb^{-1}. Each background component is reported before (bottom) and after the fit (top). The errors shown include both the statistical and systematics uncertainties.

table.results.yields channel	SR2	ONEmuCR2	TWOmuCR2	TWOeleCR2
Observed events	493	227	59	38
Fitted bkg events	500.71 ± 44.12	226.99 ± 15.06	54.82 ± 5.83	42.12 ± 4.62
Fitted Znunugamma events	342.96 ± 41.03	0.32 ± 0.09	0.00 ± 0.00	0.00 ± 0.00
Fitted Zgamma events	5.64 ± 0.72	13.98 ± 1.70	50.63 ± 5.94	39.42 ± 4.66
Fitted Wgamma events	74.77 ± 7.92	185.11 ± 18.29	0.12 ± 0.11	0.11 ± 0.06
Fitted gammajets events	16.68 ± 6.28	3.93 ± 1.29	0.00 ± 0.00	0.00 ± 0.00
Fitted JetFakes events	27.04 ± 9.24	20.52 ± 9.90	3.93 ± 2.37	2.59 ± 1.88
Fitted EleFakes events	33.62 ± 8.15	3.14 ± 0.74	0.14 ± 0.06	0.00 ± 0.00
MC exp. SM events	469.52 ± 29.41	220.22 ± 16.78	49.97 ± 3.99	40.17 ± 3.44
MC exp. Znunugamma events	315.27 ± 19.69	0.29 ± 0.09	0.00 ± 0.00	0.00 ± 0.00
MC exp. Zgamma events	5.19 ± 0.41	12.78 ± 0.98	46.21 ± 3.22	36.90 ± 2.64
MC exp. Wgamma events	72.85 ± 5.86	179.79 ± 12.38	0.11 ± 0.11	0.11 ± 0.06
MC exp. gammajets events	15.54 ± 5.51	3.70 ± 1.30	0.00 ± 0.00	0.00 ± 0.00
MC exp. JetFakes events	27.04 ± 9.24	20.52 ± 9.97	3.51 ± 2.33	3.16 ± 2.19
MC exp. EleFakes events	33.62 ± 8.15	3.14 ± 0.75	0.14 ± 0.06	0.00 ± 0.00

Table 25: Results of the background estimation from the simplified shape corresponding to the $E_{\mathrm{T}}^{\mathrm{miss}}$ bin [225 GeV; 300 GeV] for an integrated luminosity of 36.4 fb^{-1}. Each background component is reported before (bottom) and after the fit (top). The errors shown include both the statistical and systematics uncertainties.

table.results.yields channel	SR3	ONEmuCR3	TWOmuCR3	TWOeleCR3
Observed events	236	116	27	21
Fitted bkg events	273.81 ± 36.96	116.00 ± 10.77	26.26 ± 4.06	21.76 ± 3.29
Fitted Znunugamma events	210.33 ± 35.13	0.11 ± 0.04	0.00 ± 0.00	0.00 ± 0.00
Fitted Zgamma events	2.19 ± 0.38	7.20 ± 1.22	25.11 ± 4.15	20.18 ± 3.37
Fitted Wgamma events	33.30 ± 4.18	98.02 ± 11.68	0.00 ± 0.00	0.06 ± 0.04
Fitted gammajets events	5.22 ± 1.12	6.13 ± 1.83	0.00 ± 0.00	0.00 ± 0.00
Fitted JetFakes events	$9.66^{+10.03}_{-9.66}$	$3.44^{+3.56}_{-3.44}$	$1.12^{+1.28}_{-1.12}$	$1.47^{+1.68}_{-1.47}$
Fitted EleFakes events	13.11 ± 3.36	1.10 ± 0.29	0.03 ± 0.02	0.05 ± 0.03
MC exp. SM events	226.36 ± 17.54	110.58 ± 8.58	20.64 ± 1.97	17.89 ± 2.30
MC exp. Znunugamma events	164.69 ± 11.49	0.09 ± 0.03	0.00 ± 0.00	0.00 ± 0.00
MC exp. Zgamma events	1.71 ± 0.17	5.62 ± 0.46	19.54 ± 1.53	16.12 ± 1.21
MC exp. Wgamma events	32.25 ± 2.54	94.61 ± 6.92	0.00 ± 0.00	0.06 ± 0.04
MC exp. gammajets events	4.93 ± 1.27	5.73 ± 0.96	0.00 ± 0.00	0.00 ± 0.00
MC exp. JetFakes events	$9.66^{+10.03}_{-9.66}$	$3.43^{+3.58}_{-3.43}$	$1.07^{+1.25}_{-1.07}$	$1.66^{+1.95}_{-1.66}$
MC exp. EleFakes events	13.11 ± 3.36	1.10 ± 0.29	0.03 ± 0.02	0.05 ± 0.03

Table 26: Results of the background estimation from the simplified shape corresponding to the $E_{\mathrm{T}}^{\mathrm{miss}} >$ 300 GeV for an integrated luminosity of 36.4 fb^{-1}. Each background component is reported before (bottom) and after the fit (top). The errors shown include both the statistical and systematics uncertainties.

7 Systematic uncertainties

7.1 Systematic uncertainties on the background

Various sources of experimental uncertainties are taken into account for the background prediction. For the backgrounds estimated with data-driven techniques, the methods used to evaluate the systematic uncertainties have been explained in Sec. 5.3 and Sec. 5.4. For the $Z(\to \nu\nu)+\gamma$, $Z(\to \ell\ell)+\gamma$, $W(\to \ell\nu)+\gamma$ and γ + jet contributions all variations due to the uncertainties provided by the CP groups have been taken into account. These are related to the knowledge of the energy and momentum scale of the physics objects and of their identification, reconstruction and isolation efficiencies, when applicable. For each source of such uncertainties the corresponding variation on the final yield for each process is obtained by varying the relevant quantity (calibration scale, identification and reconstruction scale factor or efficiency), as per CP recommendation, and by propagating its impact through the full analysis chain.
The uncertainty on the calorimetric isolation of the photon is not obtained with the variation of a scale factor, but rather with a data–driven correction as per recommendation[13], i.e. a one-sided shift is applied to the topoetcone40 variable and the corresponding variation on each yield is symmetrized and considered as systematic uncertainty.
Lepton identification/reconstruction efficiency scale factors uncertainties are propagated to the signal region, in terms of veto efficiency scale uncertainties, in the following way:

- the average muon (electron) efficiency scale factor $\langle SF\rangle_{\mu(e)\text{ veto}}$ is evaluated on a control region selected exactly like the signal region, but inverting the muon (electron) veto;
- the number of events in the vetoed muon (electron) region, $N_{\mu(e)\text{ veto}}$, is evaluated;
- the number of events $(1-\langle SF\rangle_{\mu(e)\text{ veto}})N_{\mu(e)\text{ veto}}$ is added to the MC signal region estimate for each sample.

With this procedure, the anticorrelation between lepton identification/reconstruction efficiency and the lepton veto efficiency is automatically taken into account.

Overall uncertainties on the event selection efficiency are also taken into account: ± 4.1 % uncertainty on the integrated luminosity and an uncertainty on the photon trigger efficiency described in Sec. 4.3 that varies from ± 0.5 % to ± 1 % for photons below 180 GeV.
The variation of the background yields due to all the uncertainties described above are treated as nuisance parameters in the fit. Each nuisance parameter is described by a gaussian centered on zero and of width one. Zero corresponds to the nominal rate in all regions, while 1 correspond to the ”up” and ”down” systematic variations. The list of considered sources of uncertainty are listed in Table 27 with a brief description. In the table for each source of uncertainty it is also indicated if that particular uncertainty is treated as correlated or uncorrelated among different regions in the fit.
The listed nuisance parameters are treated as uncorrelated among one another. If residual correlations are found, the final error on the fitted total background in the various regions is estimated by properly taking into account of the correlation matrix between the different errors.

7.1.1 PDF uncertainties on background

PDF uncertainties have an impact on the expected event yields of the $V\gamma$ and γ+jets samples in each region. They are evaluated following the ATLAS PDF recommedations [14] and using the reweighting

[13] https://twiki.cern.ch/twiki/bin/view/AtlasProtected/IsolationLeakageCorrections
[14] https://twiki.cern.ch/twiki/bin/viewauth/AtlasProtected/PDFRecommendations

Name	Description of the uncertainty	Correlation among analysis regions
gamma_stat_REGION	limited MC statistics in each analysis region	no
alpha_LUMI_syst	computation of the integrated luminosity	yes
alpha_JetFake_syst	variation of isolation and identification requirements for estimation of jet fakes	yes
alpha_JetFake_stat_REGION	statistics of the ABCD control regions	no
alpha_EleFake_syst	variation of mass window and difference from MC for estimation of electron fakes	yes
alpha_EleFake_stat	statistics of the data for fake rate	yes
alpha_EleFake_statCR_REGION	statistics of the mono-electron control regions	no
alpha_EG_SCALE alpha_EG_RESO	scale and resolution of all photons and electrons due to egamma calibration procedure (simplified correlation model)	yes
alpha_PH_EFF	identification of leading photon	yes
alpha_PH_EFF_TRKISO	track isolation efficiency	yes
alpha_PH_TRIG_EFF	trigger efficiency on leading photon	yes
alpha_PH_ISO	isolation of leading photon	yes
alpha_EL_EFF_RECO	reconstruction efficiency of electrons	yes
alpha_EL_EFF_ID	identification efficiency of electrons	yes
alpha_EL_EFF_ISO	isolation efficiency of electrons	yes
alpha_MU_EFF_SYST alpha_MU_EFF_STAT alpha_MU_EFF_SYST_LOWPT	reconstruction efficiency of muons	yes
alpha_MU_ISO_SYST alpha_MU_ISO_STAT	isolation efficiency of muons	yes
alpha_MU_ID alpha_MU_MS	resolution of the momentum of the muons	yes
alpha_MU_SCALE	scale of the momentum of the muons	yes
alpha_MU_TTVA_SYST	Track To Vertex Association scale factor	yes
alpha_MU_TTVA_STAT	Track To Vertex Association scale factor	yes
alpha_MET_SCALE	scale of SoftTerm	yes
alpha_MET_RESO_PERP alpha_MET_RESO_PARA	resolution of SoftTerm	yes
alpha_JES	scale of jets due to jet calibration procedure, group 1 parametrization	yes
alpha_JER	resolution of jets due to 2012 calibration procedure	yes
alpha_JVT_EFF	Jet Vertex Tagger efficiency	yes
alpha_PRW_DATASF	variation of data scale factor for pile-up reweighting	yes
PhJet modelling	shape uncertainty on the γ+jets background	yes

Table 27: List and description of the systematic contributions of uncertainty considered for the background estimation.

procedure implemented in the recommended LHAPDF Tool [46]. Intra-PDF uncertainties are obtained by varying the PDF parameters of the PDF set with which the samples were generated. Inter-PDF uncertainties are obtained in the same way except that a different PDF set is used for the reweighting. For inter-PDF uncertainties, two separate PDF families are studied.

The uncertainty on each set of PDFs is obtained with a symmetric Hessian, asymmetric Hessian or standard deviation method according to the PDF set used.[15]

The combination of the intra and inter-PDF uncertainties is finally obtained by combining the uncertainties obtained, following the PDF4LHC recommendation, with three different sets of PDFs: CT10, MMHT2014lo68cl , NNPDF30_lo_as_0130. The central value of the yield is the one obtained with the nominal PDF weight (the one with which the sample was generated), while the uncertainty on the yield is computed as a symmetric overall contribution determined as:

$$\Delta = \frac{1}{2}\left[\max\left(\Delta_{CT10,}{}^{+}, \Delta^{+}_{MMHT}, \Delta^{+}_{NNPDF}\right) - \min\left(\Delta_{CT10,}{}^{-}, \Delta^{-}_{MMHT}, \Delta^{-}_{NNPDF}\right)\right],$$

[15]Note that CT10 / CT14 are provided at 90% CL and thus need to be rescaled by a factor 1.642 in order to be comparable with the uncertainties from the other PDF families which are provided at 68%CL.

where $\Delta^{+,-}$ are the upper and lower uncertainties on the yield (with their + or - sign).
Results from different PDF sets are compared and the total combined uncertainty is taken as the envelope among the three PDF sets considered. Table 28 shows the combined total uncertainties in percentage on $Z\nu\nu\gamma$, $Z+\gamma$, $W\gamma$ and γ+jets samples for each analysis region, these uncertainties are given as an input to the simultaneous fit.

Process	SR	1mu-CR	2mu-CR	2ele-CR	PhJet-CR
$Z\nu\nu\gamma$	(+0.80% – 0.80%)	(+1.28% – 1.28%)	(+0.00% – 0.00%)	(+0.00% – 0.00%)	(+0.92% – 0.92%)
$Z+\gamma$	(+0.65% – 0.65%)	(+0.63% – 0.63%)	(+0.78% – 0.78%)	(+0.78% – 0.78%)	(+0.76% – 0.76%)
$W+\gamma$	(+0.60% – 0.60%)	(+0.76% – 0.76%)	(+2.76% – 2.76%)	(+2.06% – 2.06%)	(+0.65% – 0.65%)
γ+jets	(+1.54% – 1.54%)	(+2.46% – 2.46%)	(+0.00% – 0.00%)	(+0.00% – 0.00%)	(+0.61% – 0.61%)

Table 28: Computed PDF uncertainty in percentage on the event yields for the $V\gamma$ and γ+jet background samples.

7.2 Shape uncertainty on the γ+jets background

The following eight Sherpa variations were studied in order to assign an uncertainty on the extrapolation factor from the PhJet CR to the SRs, as recommended by PMG[16]:

- Renormalisation scale varied by x 2 and x 1/2
- Factorisation scale varied by x 2 and x 1/2
- Resummation scale varied by x 2 and x 1/2
- CKKW matching scale variations to 15 GeV and 30 GeV (the nominal being 20 GeV)

These variations correspond to the official samples with DSIDs ranging from 361050 to 362991. They were produced at EVNT level and the extrapolation uncertainty was hence studied on TRUTH1 DAODs, using the leading jet p_{T} as a proxy to the $E_{\mathrm{T}}^{\mathrm{miss}}$(as it is the bad reconstruction / loss of a high-p_{T} jet which leads γ+jets events to populate the high-$E_{\mathrm{T}}^{\mathrm{miss}}$ region).

The resulting uncertainty is obtained by adding in quadrature the differences coming from each type of the variations listed above. The total uncertainty on the extrapolation factor ($N^{SR}_{MC,\gamma+jets}/N^{PhJetCR}_{MC,\gamma+jets}$), which directly translates into an uncertainty on the event count of γ+jets events in the SRs, varies from 12 to 19 % depending on the signal regions. As the γ+jets background is a rather small background, this does not have a large impact on the total background uncertainty.

7.3 Systematic uncertainties in SRs and CRs from single bin fit

The impact of each source of uncertainty with respect to the total background prediction is evaluated after the simultaneous fit for all inclusive SRs, as reported in Tables 30, 31, 32. The corresponding pre-fit tables for all SRs are reported in Appendix E. An effect of reduction of the uncertainties can be clearly seen by comparing the pre-fit and post-fit tables, this is due to a cancellation of common systematic uncertainties between the numerator and denominator in the estimation of the expected yield with k-factor method.

The impact of each nuisance parameter associated to a given systematic uncertainty is obtained by repeating the background-only fit shifting each time the nuisance parameter to ± one standard deviation and evaluating the impact in terms of the variation of the total yields.

[16] see https://twiki.cern.ch/twiki/bin/view/AtlasProtected/MC15SystematicUncertainties

Table 29 shows the total expected background yields for all the SR with their total uncertainty and the pure statistical uncertainty. The same table summarizes the main contributions (> 0.1 %) from the post-fit systematics breakdown tables.

Figure 31, 32, 33 report the correlation matrices among the various source of uncertainties that are taken into account in the simultaneous fit.

Figure 34, 35, 36 show the post-fit nuisance parameter values and errors for all SRs.

$E_{\mathrm{T}}^{\mathrm{miss}}$	> 150 GeV	> 225 GeV	> 300 GeV	[150,225] GeV	[225, 300] GeV
Total background	2822	829	299	1989	530
Total (statistical+systematic) uncertainty	5.7%	7.2%	11.7%	7.3%	8.9%
Statistical uncertainty only	4.3%	6.2%	10.4%	5.5%	7.8%
Jet fake rate	1.3%	3.0%	5.3%	1.7%	3.3%
Electron fake rate	1.5%	1.5%	1.2%	1.5%	1.6%
Jet energy scale	4.1%	1.9%	1.4%	5.6%	0.6%
Jet energy resolution	0.7%	0.2%	0.5%	0.8%	0.3%
$E_{\mathrm{T}}^{\mathrm{miss}}$ soft term scale and resolution	0.9%	0.4%	0.7%	1.1%	1.0%
Muon reconstruction/isolation efficiency	1.4%	1.3%	1.6%	1.3%	1.4%
Electron reconstruction/identification/isolation efficiency	1.0%	1.3%	1.3%	0.8%	1.2%
Electron and photon energy scale	0.2%	0.5%	0.4%	< 0.1%	< 0.1%
Electron and photon energy resolution	< 0.1%	0.3%	0.2%	0.1%	1.0%
Photon efficiency	0.1%	1.0%	< 0.1%	0.2%	< 0.1%
PhJet modelling	1.5%	0.3%	0.3%	2.3%	0.4%
PRW data scale factor	1.3%	0.3%	0.9%	1.7%	0.3%

Table 29: Total post-fit background uncertainty and breakdown of uncertainties for all SRs.

Systematic	SR	CR1mu	CR2mu	CR2e	CRgjet
alpha_EG_RESO	(−0.00, 0.06)	(−0.00, 0.00)	(0.09, −0.04)	(−0.10, 0.05)	(−0.00, −0.01)
alpha_EG_SCALE	(0.16, −0.13)	(−0.00, 0.00)	(0.09, −0.06)	(−0.12, 0.10)	(−0.00, −0.00)
alpha_EL_EFF_ID	(−0.75, 0.81)	(0.00, −0.02)	(−1.09, 1.11)	(1.38, −1.40)	(−0.00, 0.00)
alpha_EL_EFF_ISO	(−0.36, 0.40)	(−0.00, −0.00)	(−0.53, 0.53)	(0.68, −0.69)	(−0.00, 0.00)
alpha_EL_EFF_RECO	(−0.30, 0.30)	(0.00, −0.00)	(−0.39, 0.40)	(0.52, −0.52)	(−0.00, 0.00)
alpha_EleFake_statCR_ONEmuCR	(−0.02, 0.02)	(0.01, −0.01)	(−0.01, 0.02)	(−0.01, 0.01)	(−0.00, −0.00)
alpha_EleFake_statCR_PhJetCR	(−0.00, 0.00)	(−0.00, 0.00)	(−0.00, 0.00)	(−0.00, 0.00)	(−0.00, −0.00)
alpha_EleFake_statCR_SR	(0.07, −0.07)	(0.00, 0.00)	(0.00, 0.00)	(0.00, 0.00)	(0.00, 0.00)
alpha_EleFake_statCR_TWOeleCR	(−0.00, 0.00)	(−0.00, 0.00)	(−0.00, 0.00)	(0.02, −0.02)	(0.00, 0.00)
alpha_EleFake_statCR_TWOmuCR	(−0.00, 0.01)	(−0.00, 0.00)	(0.03, −0.02)	(−0.00, 0.02)	(0.00, −0.00)
alpha_EleFake_stat_ONEmuCR	(−0.03, 0.02)	(0.01, −0.01)	(0.00, −0.01)	(0.02, −0.02)	(−0.00, −0.00)
alpha_EleFake_stat_PhJetCR	(−0.00, 0.00)	(0.00, −0.00)	(0.00, −0.00)	(0.00, 0.00)	(0.00, −0.00)
alpha_EleFake_stat_SR	(0.68, −0.68)	(0.00, 0.00)	(0.00, 0.00)	(0.00, 0.00)	(0.00, 0.00)
alpha_EleFake_stat_TWOeleCR	(−0.00, 0.00)	(−0.00, 0.00)	(−0.00, 0.00)	(0.00, −0.00)	(−0.00, 0.00)
alpha_EleFake_stat_TWOmuCR	(−0.00, 0.00)	(−0.00, 0.00)	(0.02, −0.02)	(−0.00, 0.00)	(0.00, 0.00)
alpha_EleFake_syst_ONEmuCR	(−0.07, 0.07)	(0.00, −0.01)	(0.01, −0.00)	(0.01, −0.00)	(−0.00, −0.00)
alpha_EleFake_syst_PhJetCR	(−0.01, 0.04)	(−0.00, −0.00)	(0.01, 0.00)	(0.00, −0.00)	(0.00, −0.00)
alpha_EleFake_syst_SR	(1.34, −1.34)	(0.00, 0.00)	(0.00, 0.00)	(0.00, 0.00)	(0.00, 0.00)
alpha_EleFake_syst_TWOeleCR	(−0.00, 0.00)	(−0.00, 0.00)	(−0.00, 0.00)	(0.01, −0.01)	(−0.00, 0.00)
alpha_EleFake_syst_TWOmuCR	(−0.00, 0.01)	(−0.00, 0.00)	(0.03, −0.02)	(−0.00, 0.02)	(0.00, −0.00)
alpha_JER	(−0.56, 0.67)	(−0.00, −0.00)	(−0.11, 0.10)	(0.15, −0.15)	(0.00, 0.00)
alpha_JES	(−4.09, 1.78)	(−0.00, −0.00)	(−0.28, 0.14)	(0.36, −0.17)	(−0.00, −0.00)
alpha_JVT_EFF	(−0.01, 0.04)	(−0.00, 0.01)	(−0.01, 0.00)	(0.01, −0.02)	(−0.00, 0.00)
alpha_JetFake_statCR_ONEmuCR	(−0.27, 0.22)	(0.00, −0.00)	(−0.02, −0.03)	(0.01, −0.02)	(−0.00, −0.00)
alpha_JetFake_statCR_PhJetCR	(−0.03, 0.06)	(0.00, −0.00)	(−0.00, 0.00)	(−0.02, −0.00)	(0.00, −0.00)
alpha_JetFake_statCR_SR	(0.81, −0.81)	(0.00, 0.00)	(0.00, 0.00)	(0.00, 0.00)	(0.00, 0.00)
alpha_JetFake_statCR_TWOeleCR	(−0.46, 0.48)	(−0.00, 0.00)	(−0.67, 0.62)	(1.01, −0.96)	(−0.00, −0.00)
alpha_JetFake_statCR_TWOmuCR	(−0.70, 0.68)	(−0.00, −0.00)	(0.50, −0.48)	(−0.73, 0.72)	(0.00, −0.00)
alpha_LUMI_SYST	(0.04, −0.02)	(−0.00, −0.00)	(−0.01, −0.01)	(−0.03, −0.01)	(0.01, 0.00)
alpha_MET_RESO_PARA	(0.18, −0.10)	(−0.00, −0.00)	(0.02, −0.02)	(−0.03, 0.02)	(−0.00, −0.01)
alpha_MET_RESO_PERP	(0.24, −0.21)	(−0.00, 0.01)	(−0.00, 0.01)	(0.02, −0.02)	(−0.01, 0.01)
alpha_MET_SCALE	(0.84, −0.79)	(0.01, −0.00)	(0.02, 0.03)	(0.01, −0.04)	(−0.00, 0.01)
alpha_MU_EFF_STAT	(−0.13, 0.33)	(−0.01, −0.01)	(0.04, −0.16)	(−0.05, 0.17)	(−0.00, 0.00)
alpha_MU_EFF_SYST	(−0.81, 1.00)	(−0.00, −0.00)	(0.52, −0.63)	(−0.67, 0.78)	(−0.01, −0.00)
alpha_MU_EFF_SYST_LOWPT	(−0.08, 0.28)	(−0.01, −0.01)	(0.02, −0.13)	(−0.01, 0.14)	(−0.00, 0.00)
alpha_MU_ID	(−0.10, 0.20)	(0.00, −0.01)	(−0.01, −0.12)	(0.02, 0.14)	(−0.00, −0.00)
alpha_MU_ISO_STAT	(−0.13, 0.33)	(−0.01, −0.01)	(0.04, −0.16)	(−0.04, 0.17)	(−0.00, 0.00)
alpha_MU_ISO_SYST	(−0.37, 0.60)	(0.00, −0.01)	(0.21, −0.31)	(−0.25, 0.43)	(−0.00, 0.00)
alpha_MU_MS	(−0.04, 0.04)	(−0.01, −0.00)	(−0.01, −0.02)	(0.03, 0.03)	(−0.00, −0.00)
alpha_MU_SCALE	(−0.01, 0.08)	(−0.00, −0.00)	(−0.01, −0.11)	(0.02, 0.13)	(−0.00, −0.00)
alpha_MU_TTVA_STAT	(−0.07, 0.27)	(−0.01, −0.01)	(0.01, −0.13)	(−0.00, 0.13)	(−0.00, 0.00)
alpha_MU_TTVA_SYS	(−0.16, 0.37)	(−0.01, −0.01)	(0.07, −0.19)	(−0.08, 0.21)	(−0.00, 0.00)
alpha_PDF_Comb	(0.06, −0.03)	(0.01, −0.00)	(0.01, −0.00)	(0.01, −0.00)	(0.00, −0.00)
alpha_PH_EFF	(−0.13, −0.00)	(0.01, −0.00)	(−0.03, −0.01)	(0.02, 0.00)	(−0.01, −0.00)
alpha_PH_EFF_TRKISO	(−0.01, 0.04)	(−0.00, 0.01)	(−0.01, 0.00)	(0.01, −0.02)	(−0.00, 0.00)
alpha_PH_ISO_DD	(−0.01, 0.04)	(−0.00, 0.01)	(−0.01, 0.00)	(0.01, −0.02)	(−0.00, 0.00)
alpha_PRW_DATASF	(0.14, −1.31)	(−0.00, −0.00)	(−0.26, 0.06)	(0.35, −0.07)	(0.00, −0.01)
alpha_syst_JetFake_ONEmuCR	(−0.19, 0.19)	(−0.00, −0.00)	(0.00, −0.02)	(−0.00, −0.02)	(−0.00, −0.00)
alpha_syst_JetFake_PhJetCR	(−0.01, 0.05)	(−0.00, −0.00)	(0.01, 0.00)	(0.00, −0.00)	(0.00, −0.00)
alpha_syst_JetFake_SR	(0.16, −0.16)	(0.00, 0.00)	(0.00, 0.00)	(0.00, 0.00)	(0.00, 0.00)
alpha_syst_JetFake_TWOeleCR	(−0.30, 0.31)	(−0.00, 0.00)	(−0.38, 0.41)	(0.62, −0.65)	(−0.00, −0.00)
alpha_syst_JetFake_TWOmuCR	(−0.10, 0.09)	(0.00, −0.01)	(0.08, −0.07)	(−0.11, 0.11)	(−0.00, −0.00)
alpha_syst_PhJet_shape_SR	(−1.50, 1.50)	(0.00, 0.00)	(0.00, 0.00)	(0.00, 0.00)	(0.00, 0.00)

Table 30: Breakdown of the dominant systematic uncertainties expressed in % on background estimates after the fit in the SR defined by $E_{\mathrm{T}}^{\mathrm{miss}} > 150$ GeV and its CRs for an integrated luminosity of 36.4 fb^{-1}. Note that the individual uncertainties can be correlated, and do not necessarily add up quadratically to the total background uncertainty. The percentages show the size of the uncertainty relative to the total expected background.

Systematic	SR	CR1mu	CR2mu	CR2e	CRgjet
alpha_EG_RESO	(0.05, −0.34)	(−0.00, −0.00)	(−0.04, −0.11)	(0.06, 0.13)	(−0.00, −0.00)
alpha_EG_SCALE	(0.47, −0.35)	(−0.00, 0.00)	(0.17, −0.11)	(−0.21, 0.12)	(−0.00, 0.00)
alpha_EL_EFF_ID	(−1.02, 1.02)	(−0.02, 0.02)	(−1.10, 1.11)	(1.34, −1.38)	(−0.00, −0.00)
alpha_EL_EFF_ISO	(−0.70, 0.71)	(−0.01, 0.01)	(−0.75, 0.78)	(0.92, −0.96)	(−0.00, −0.00)
alpha_EL_EFF_RECO	(−0.34, 0.35)	(0.01, −0.02)	(−0.38, 0.40)	(0.50, −0.53)	(−0.00, 0.00)
alpha_EleFake_statCR_ONEmuCR	(−0.02, 0.02)	(0.01, −0.01)	(−0.01, 0.01)	(−0.01, 0.01)	(−0.00, −0.00)
alpha_EleFake_statCR_PhJetCR	(−0.00, 0.00)	(−0.00, 0.00)	(−0.00, 0.00)	(−0.00, 0.00)	(−0.00, −0.00)
alpha_EleFake_statCR_SR	(0.11, −0.11)	(0.00, 0.00)	(0.00, 0.00)	(0.00, 0.00)	(0.00, 0.00)
alpha_EleFake_statCR_TWOeleCR	(−0.00, 0.00)	(−0.00, 0.00)	(−0.00, 0.00)	(0.04, −0.04)	(0.00, 0.00)
alpha_EleFake_statCR_TWOmuCR	(−0.02, 0.02)	(−0.00, 0.00)	(0.03, −0.03)	(−0.02, 0.02)	(−0.00, −0.00)
alpha_EleFake_stat_ONEmuCR	(−0.03, 0.03)	(0.02, −0.02)	(−0.02, 0.02)	(−0.02, 0.02)	(−0.00, −0.00)
alpha_EleFake_stat_PhJetCR	(−0.00, 0.00)	(0.00, −0.01)	(0.00, 0.00)	(0.00, 0.00)	(0.00, −0.00)
alpha_EleFake_stat_SR	(0.74, −0.74)	(0.00, 0.00)	(0.00, 0.00)	(0.00, 0.00)	(0.00, 0.00)
alpha_EleFake_stat_TWOeleCR	(−0.00, 0.00)	(−0.00, 0.00)	(−0.00, 0.00)	(0.01, −0.01)	(−0.00, 0.00)
alpha_EleFake_stat_TWOmuCR	(−0.00, 0.00)	(−0.00, 0.00)	(0.02, −0.02)	(−0.00, 0.00)	(0.00, 0.00)
alpha_EleFake_syst_ONEmuCR	(−0.05, 0.03)	(0.01, −0.01)	(0.01, −0.03)	(0.01, −0.02)	(−0.00, −0.00)
alpha_EleFake_syst_PhJetCR	(−0.00, 0.01)	(0.00, −0.00)	(0.01, 0.00)	(0.01, −0.01)	(0.00, −0.00)
alpha_EleFake_syst_SR	(1.30, −1.30)	(0.00, 0.00)	(0.00, 0.00)	(0.00, 0.00)	(0.00, 0.00)
alpha_EleFake_syst_TWOeleCR	(−0.00, 0.00)	(−0.00, 0.00)	(−0.00, 0.00)	(0.01, −0.01)	(−0.00, 0.00)
alpha_EleFake_syst_TWOmuCR	(−0.00, 0.00)	(−0.00, 0.00)	(0.04, −0.04)	(−0.00, 0.00)	(0.00, 0.00)
alpha_JER	(−0.20, 0.12)	(0.00, −0.00)	(−0.11, 0.11)	(0.13, −0.14)	(−0.01, −0.00)
alpha_JES	(−1.91, 1.11)	(−0.00, 0.01)	(0.56, −0.51)	(−0.71, 0.61)	(−0.00, −0.00)
alpha_JVT_EFF	(−0.06, 0.05)	(−0.00, −0.00)	(0.05, −0.05)	(−0.06, 0.06)	(−0.00, 0.00)
alpha_JetFake_statCR_ONEmuCR	(−0.36, 0.35)	(0.00, −0.00)	(0.02, 0.02)	(−0.02, 0.02)	(−0.00, −0.00)
alpha_JetFake_statCR_PhJetCR	(−0.01, 0.01)	(−0.00, 0.00)	(−0.00, 0.00)	(−0.01, −0.01)	(0.00, −0.00)
alpha_JetFake_statCR_SR	(1.18, −1.18)	(0.00, 0.00)	(0.00, 0.00)	(0.00, 0.00)	(0.00, 0.00)
alpha_JetFake_statCR_TWOeleCR	(−1.03, 1.04)	(−0.02, 0.02)	(−1.10, 1.12)	(1.76, −1.66)	(−0.00, −0.00)
alpha_JetFake_statCR_TWOmuCR	(−1.55, 1.52)	(−0.01, 0.00)	(1.12, −1.05)	(−1.60, 1.60)	(−0.00, −0.00)
alpha_LUMI_SYST	(−0.02, 0.02)	(0.00, −0.01)	(0.00, 0.00)	(−0.01, −0.00)	(−0.00, −0.01)
alpha_MET_RESO_PARA	(0.42, −0.37)	(−0.00, −0.00)	(0.17, −0.14)	(−0.21, 0.19)	(−0.00, 0.01)
alpha_MET_RESO_PERP	(0.10, −0.09)	(−0.00, 0.00)	(0.14, −0.14)	(−0.18, 0.16)	(−0.00, −0.00)
alpha_MET_SCALE	(0.05, −0.04)	(−0.00, −0.00)	(0.17, 0.01)	(−0.21, 0.00)	(−0.01, 0.00)
alpha_MU_EFF_STAT	(−0.07, 0.10)	(0.01, −0.01)	(0.06, −0.08)	(−0.05, 0.03)	(−0.00, 0.00)
alpha_MU_EFF_SYST	(−1.00, 1.20)	(−0.00, −0.00)	(0.73, −0.85)	(−0.85, 1.07)	(−0.00, −0.00)
alpha_MU_EFF_SYST_LOWPT	(−0.06, 0.09)	(−0.00, −0.01)	(0.06, −0.08)	(−0.05, 0.03)	(−0.00, 0.00)
alpha_MU_ID	(−0.11, 0.07)	(0.01, −0.00)	(0.06, −0.05)	(−0.05, 0.06)	(−0.00, −0.00)
alpha_MU_ISO_STAT	(−0.10, 0.30)	(−0.01, −0.02)	(0.07, −0.17)	(−0.08, 0.23)	(−0.00, 0.00)
alpha_MU_ISO_SYST	(−0.12, 0.17)	(0.01, −0.00)	(0.06, −0.06)	(−0.05, 0.07)	(−0.00, 0.00)
alpha_MU_MS	(−0.08, −0.15)	(−0.01, −0.00)	(0.04, −0.05)	(−0.06, 0.05)	(−0.00, −0.00)
alpha_MU_SCALE	(−0.05, 0.05)	(−0.00, −0.01)	(0.05, −0.06)	(−0.06, 0.05)	(−0.00, −0.00)
alpha_MU_TTVA_STAT	(−0.06, 0.09)	(−0.00, −0.01)	(0.06, −0.08)	(−0.05, 0.03)	(−0.00, 0.00)
alpha_MU_TTVA_SYS	(−0.07, 0.10)	(0.01, −0.01)	(0.06, −0.08)	(−0.05, 0.03)	(−0.00, 0.00)
alpha_PDF_Comb	(−0.01, −0.00)	(−0.02, 0.00)	(0.02, 0.00)	(0.01, −0.00)	(0.00, −0.00)
alpha_PH_EFF	(−1.01, 0.85)	(−0.02, 0.00)	(0.80, −0.72)	(−0.98, 0.86)	(−0.01, −0.00)
alpha_PH_EFF_TRKISO	(−0.06, 0.05)	(−0.00, −0.00)	(0.05, −0.05)	(−0.06, 0.06)	(−0.00, 0.00)
alpha_PH_ISO_DD	(−0.06, 0.05)	(−0.00, −0.00)	(0.05, −0.05)	(−0.06, 0.06)	(−0.00, 0.00)
alpha_PRW_DATASF	(−0.14, 0.31)	(0.00, −0.00)	(0.40, −0.39)	(−0.50, 0.47)	(−0.00, −0.00)
alpha_syst_JetFake_ONEmuCR	(−0.37, 0.36)	(0.00, −0.00)	(0.02, 0.02)	(−0.02, 0.02)	(−0.00, −0.00)
alpha_syst_JetFake_PhJetCR	(−0.00, 0.01)	(0.00, −0.00)	(0.01, 0.00)	(0.01, −0.01)	(0.00, −0.00)
alpha_syst_JetFake_SR	(1.59, −1.59)	(0.00, 0.00)	(0.00, 0.00)	(0.00, 0.00)	(0.00, 0.00)
alpha_syst_JetFake_TWOeleCR	(−0.58, 0.66)	(−0.01, 0.01)	(−0.62, 0.72)	(0.98, −1.10)	(−0.00, −0.00)
alpha_syst_JetFake_TWOmuCR	(−0.87, 0.85)	(−0.00, 0.00)	(0.62, −0.60)	(−0.90, 0.90)	(−0.00, −0.00)
alpha_syst_PhJet_shape_SR	(−0.34, 0.34)	(0.00, 0.00)	(0.00, 0.00)	(0.00, 0.00)	(0.00, 0.00)

Table 31: Breakdown of the dominant systematic uncertainties expressed in % on background estimates after the fit in the SR defined by $E_{\mathrm{T}}^{\mathrm{miss}} > 225$ GeV and its CRs for an integrated luminosity of 36.4 fb^{-1}. Note that the individual uncertainties can be correlated, and do not necessarily add up quadratically to the total background uncertainty. The percentages show the size of the uncertainty relative to the total expected background.

Systematic	SR	CR1mu	CR2mu	CR2e	CRgjet
alpha_EG_RESO	(−0.15, −0.19)	(−0.03, −0.02)	(−0.11, −0.09)	(0.07, 0.06)	(−0.00, −0.00)
alpha_EG_SCALE	(−0.38, 0.09)	(−0.03, −0.01)	(0.36, −0.49)	(−0.45, 0.51)	(0.00, −0.00)
alpha_EL_EFF_ID	(−0.95, 0.91)	(0.01, −0.05)	(−1.08, 1.04)	(1.32, −1.38)	(−0.00, 0.00)
alpha_EL_EFF_ISO	(−0.76, 0.72)	(0.01, −0.04)	(−0.86, 0.84)	(1.05, −1.12)	(−0.00, 0.00)
alpha_EL_EFF_RECO	(−0.34, 0.26)	(−0.01, 0.01)	(−0.40, 0.34)	(0.48, −0.58)	(0.00, 0.00)
alpha_EleFake_statCR_ONEmuCR	(−0.04, 0.01)	(0.00, −0.03)	(−0.03, −0.00)	(−0.02, 0.00)	(0.00, 0.00)
alpha_EleFake_statCR_PhJetCR	(−0.01, 0.01)	(−0.01, 0.01)	(−0.01, 0.01)	(−0.01, 0.01)	(0.00, −0.00)
alpha_EleFake_statCR_SR	(0.16, −0.16)	(0.00, 0.00)	(0.00, 0.00)	(0.00, 0.00)	(0.00, 0.00)
alpha_EleFake_statCR_TWOeleCR	(−0.05, 0.00)	(−0.02, 0.00)	(−0.06, 0.01)	(0.06, −0.13)	(0.00, 0.00)
alpha_EleFake_statCR_TWOmuCR	(−0.00, 0.00)	(−0.00, 0.00)	(0.05, −0.05)	(−0.00, 0.00)	(−0.00, 0.00)
alpha_EleFake_stat_ONEmuCR	(−0.03, 0.01)	(0.00, −0.03)	(−0.03, −0.00)	(−0.02, 0.00)	(0.00, 0.00)
alpha_EleFake_stat_PhJetCR	(−0.04, −0.02)	(−0.03, −0.02)	(−0.04, −0.02)	(−0.04, −0.02)	(0.00, −0.00)
alpha_EleFake_stat_SR	(0.61, −0.61)	(0.00, 0.00)	(0.00, 0.00)	(0.00, 0.00)	(0.00, 0.00)
alpha_EleFake_stat_TWOeleCR	(−0.00, 0.00)	(−0.00, 0.00)	(−0.00, 0.00)	(0.02, −0.02)	(−0.00, 0.00)
alpha_EleFake_stat_TWOmuCR	(−0.00, 0.00)	(−0.00, 0.00)	(0.01, −0.01)	(−0.00, 0.00)	(−0.00, 0.00)
alpha_EleFake_syst_ONEmuCR	(−0.06, 0.03)	(0.01, −0.04)	(−0.05, 0.01)	(−0.03, 0.01)	(0.00, 0.00)
alpha_EleFake_syst_PhJetCR	(−0.02, −0.01)	(−0.00, −0.03)	(−0.01, −0.03)	(0.00, −0.02)	(0.00, −0.00)
alpha_EleFake_syst_SR	(1.06, −1.06)	(0.00, 0.00)	(0.00, 0.00)	(0.00, 0.00)	(0.00, 0.00)
alpha_EleFake_syst_TWOeleCR	(−0.00, 0.00)	(−0.00, 0.00)	(−0.00, 0.00)	(0.04, −0.04)	(−0.00, 0.00)
alpha_EleFake_syst_TWOmuCR	(−0.00, 0.00)	(−0.00, 0.00)	(0.02, −0.02)	(−0.00, 0.00)	(−0.00, 0.00)
alpha_JER	(−0.47, 0.35)	(−0.02, −0.01)	(−0.07, 0.04)	(0.02, −0.02)	(−0.00, −0.01)
alpha_JES	(−1.42, −0.39)	(−0.02, −0.01)	(−0.71, 0.38)	(0.77, −0.52)	(−0.00, −0.00)
alpha_JVT_EFF	(0.03, −0.05)	(−0.00, −0.02)	(0.03, −0.04)	(−0.02, 0.02)	(−0.00, 0.00)
alpha_JetFake_statCR_ONEmuCR	(−0.31, 0.24)	(−0.01, −0.02)	(−0.05, −0.02)	(−0.05, −0.00)	(0.00, 0.00)
alpha_JetFake_statCR_PhJetCR	(−0.02, −0.01)	(−0.03, −0.01)	(−0.03, −0.02)	(−0.02, −0.02)	(0.00, −0.00)
alpha_JetFake_statCR_SR	(1.61, −1.61)	(0.00, 0.00)	(0.00, 0.00)	(0.00, 0.00)	(0.00, 0.00)
alpha_JetFake_statCR_TWOeleCR	(−0.95, 1.52)	(0.01, −0.01)	(−1.05, 1.69)	(1.37, −2.23)	(0.00, 0.00)
alpha_JetFake_statCR_TWOmuCR	(−1.84, 1.89)	(−0.03, 0.00)	(1.31, −1.35)	(−1.71, 1.78)	(0.00, 0.00)
alpha_LUMI_SYST	(0.03, −0.02)	(−0.04, −0.02)	(0.00, −0.02)	(0.03, −0.03)	(0.01, 0.00)
alpha_MET_RESO_PARA	(−0.31, 0.17)	(−0.02, −0.02)	(0.07, −0.24)	(−0.13, −0.01)	(−0.00, 0.01)
alpha_MET_RESO_PERP	(−0.51, 0.43)	(−0.02, 0.01)	(0.19, −0.29)	(−0.27, 0.22)	(−0.00, 0.01)
alpha_MET_SCALE	(−0.25, −0.33)	(−0.02, −0.02)	(−0.00, −0.05)	(−0.13, −0.08)	(−0.01, 0.00)
alpha_MU_EFF_STAT	(−0.05, 0.16)	(−0.03, −0.04)	(0.07, −0.22)	(−0.10, 0.22)	(−0.00, 0.00)
alpha_MU_EFF_SYST	(−1.29, 1.44)	(−0.01, −0.04)	(0.89, −1.05)	(−1.11, 1.23)	(−0.00, 0.00)
alpha_MU_EFF_SYST_LOWPT	(0.01, 0.11)	(−0.01, −0.03)	(0.04, −0.17)	(−0.04, 0.18)	(−0.00, 0.00)
alpha_MU_ID	(−0.08, 0.05)	(−0.00, −0.02)	(0.04, −0.13)	(0.01, 0.10)	(−0.00, −0.00)
alpha_MU_ISO_STAT	(−0.14, 0.28)	(−0.01, −0.02)	(0.14, −0.28)	(−0.20, 0.27)	(−0.00, 0.00)
alpha_MU_ISO_SYST	(−0.35, 0.50)	(−0.01, −0.03)	(0.28, −0.41)	(−0.35, 0.44)	(−0.00, 0.00)
alpha_MU_MS	(0.00, 0.17)	(−0.00, −0.01)	(0.03, −0.20)	(−0.03, 0.19)	(−0.00, −0.00)
alpha_MU_SCALE	(0.01, 0.13)	(−0.00, −0.01)	(0.05, −0.18)	(−0.05, 0.16)	(−0.00, −0.00)
alpha_MU_TTVA_STAT	(0.00, 0.12)	(−0.01, −0.03)	(0.05, −0.17)	(−0.04, 0.18)	(−0.00, 0.00)
alpha_MU_TTVA_SYS	(−0.06, 0.17)	(−0.03, −0.04)	(0.08, −0.23)	(−0.11, 0.23)	(−0.00, 0.00)
alpha_PDF_Comb	(−0.06, −0.00)	(−0.02, −0.01)	(−0.06, −0.02)	(−0.02, −0.02)	(0.00, −0.00)
alpha_PH_EFF	(0.00, 0.05)	(−0.02, −0.02)	(0.02, 0.02)	(0.01, −0.11)	(−0.00, −0.00)
alpha_PH_EFF_TRKISO	(0.03, −0.05)	(−0.00, −0.02)	(0.03, −0.04)	(−0.02, 0.02)	(−0.00, 0.00)
alpha_PH_ISO_DD	(0.03, −0.05)	(−0.00, −0.02)	(0.03, −0.04)	(−0.02, 0.02)	(−0.00, 0.00)
alpha_PRW_DATASF	(−0.93, 0.48)	(−0.02, −0.01)	(0.47, −0.19)	(−0.61, 0.13)	(0.00, 0.01)
alpha_syst_JetFake_ONEmuCR	(−0.42, 0.35)	(−0.01, −0.03)	(−0.07, −0.01)	(−0.07, 0.01)	(0.00, 0.00)
alpha_syst_JetFake_PhJetCR	(−0.02, −0.02)	(−0.00, −0.02)	(−0.01, −0.02)	(0.01, −0.02)	(0.00, −0.00)
alpha_syst_JetFake_SR	(3.30, −3.30)	(0.00, 0.00)	(0.00, 0.00)	(0.00, 0.00)	(0.00, 0.00)
alpha_syst_JetFake_TWOeleCR	(−1.97, 2.29)	(−0.04, −0.01)	(−2.17, 2.55)	(3.06, −3.24)	(−0.00, 0.00)
alpha_syst_JetFake_TWOmuCR	(−1.71, 1.73)	(−0.03, 0.00)	(1.22, −1.25)	(−1.59, 1.64)	(0.00, 0.00)
alpha_syst_PhJet_shape_SR	(−0.27, 0.27)	(0.00, 0.00)	(0.00, 0.00)	(0.00, 0.00)	(0.00, 0.00)

Table 32: Breakdown of the dominant systematic uncertainties expressed in % on background estimates after the fit in the SR defined by $E_{\mathrm{T}}^{\mathrm{miss}} > 300$ GeV and its CRs for an integrated luminosity of 36.4 fb^{-1}. Note that the individual uncertainties can be correlated, and do not necessarily add up quadratically to the total background uncertainty. The percentages show the size of the uncertainty relative to the total expected background.

Systematic	SR	CR1mu	CR2mu	CR2e	CRgjet
alpha_EG_RESO	(−0.05, 0.14)	(−0.00, −0.00)	(0.20, 0.06)	(−0.23, −0.08)	(−0.00, −0.00)
alpha_EG_SCALE	(0.00, −0.14)	(−0.00, 0.00)	(0.13, −0.01)	(−0.15, 0.03)	(−0.00, −0.01)
alpha_EL_EFF_ID	(−0.82, 0.89)	(0.00, 0.00)	(−1.32, 1.31)	(1.44, −1.45)	(−0.00, 0.00)
alpha_EL_EFF_ISO	(−0.37, 0.36)	(0.00, 0.00)	(−0.54, 0.54)	(0.61, −0.60)	(−0.00, 0.00)
alpha_EL_EFF_RECO	(−0.34, 0.33)	(0.00, 0.00)	(−0.50, 0.50)	(0.56, −0.55)	(−0.00, 0.00)
alpha_EleFake_statCR_ONEmuCR	(−0.02, 0.02)	(0.01, −0.01)	(−0.02, 0.02)	(−0.01, 0.01)	(−0.00, −0.00)
alpha_EleFake_statCR_PhJetCR	(−0.00, 0.00)	(−0.00, 0.00)	(−0.00, 0.00)	(−0.00, 0.00)	(−0.00, −0.00)
alpha_EleFake_statCR_SR	(0.08, −0.08)	(0.00, 0.00)	(0.00, 0.00)	(0.00, 0.00)	(0.00, 0.00)
alpha_EleFake_statCR_TWOeleCR	(−0.00, 0.00)	(−0.00, 0.00)	(−0.00, 0.00)	(0.02, −0.02)	(0.00, 0.00)
alpha_EleFake_statCR_TWOmuCR	(−0.02, 0.01)	(−0.00, 0.00)	(0.02, −0.03)	(−0.02, 0.02)	(−0.00, −0.00)
alpha_EleFake_stat_ONEmuCR	(−0.03, 0.02)	(0.01, −0.00)	(0.00, −0.01)	(0.01, −0.02)	(0.00, 0.00)
alpha_EleFake_stat_PhJetCR	(−0.01, 0.00)	(0.00, −0.00)	(0.00, −0.00)	(0.00, 0.00)	(0.00, −0.00)
alpha_EleFake_stat_SR	(0.62, −0.62)	(0.00, 0.00)	(0.00, 0.00)	(0.00, 0.00)	(0.00, 0.00)
alpha_EleFake_stat_TWOeleCR	(−0.00, 0.00)	(−0.00, 0.00)	(−0.00, 0.00)	(0.00, −0.00)	(0.00, 0.00)
alpha_EleFake_stat_TWOmuCR	(−0.00, 0.00)	(−0.00, 0.00)	(0.01, −0.01)	(−0.00, 0.00)	(0.00, 0.00)
alpha_EleFake_syst_ONEmuCR	(−0.08, 0.06)	(0.00, −0.00)	(−0.00, −0.01)	(−0.00, −0.00)	(0.00, 0.00)
alpha_EleFake_syst_PhJetCR	(−0.01, 0.06)	(−0.00, −0.00)	(0.01, −0.00)	(0.00, −0.00)	(0.00, −0.00)
alpha_EleFake_syst_SR	(1.28, −1.28)	(0.00, 0.00)	(0.00, 0.00)	(0.00, 0.00)	(0.00, 0.00)
alpha_EleFake_syst_TWOeleCR	(−0.00, 0.00)	(−0.00, 0.00)	(−0.00, 0.00)	(0.00, −0.00)	(0.00, 0.00)
alpha_EleFake_syst_TWOmuCR	(−0.00, 0.00)	(−0.00, 0.00)	(0.03, −0.03)	(−0.01, 0.01)	(0.00, 0.00)
alpha_JER	(−0.72, 0.89)	(0.00, −0.00)	(−0.10, 0.09)	(0.12, −0.13)	(0.00, −0.00)
alpha_JES	(−5.20, 2.16)	(−0.01, −0.01)	(−0.31, 0.23)	(0.36, −0.25)	(−0.01, −0.00)
alpha_JVT_EFF	(−0.02, 0.05)	(−0.00, 0.01)	(−0.01, 0.00)	(0.01, −0.03)	(−0.00, 0.00)
alpha_JetFake_statCR_ONEmuCR	(−0.34, 0.29)	(0.00, −0.00)	(−0.03, −0.03)	(0.00, −0.03)	(0.00, 0.00)
alpha_JetFake_statCR_PhJetCR	(−0.04, 0.08)	(0.01, −0.00)	(−0.01, −0.00)	(−0.03, −0.00)	(0.00, −0.00)
alpha_JetFake_statCR_SR	(0.99, −0.99)	(0.00, 0.00)	(0.00, 0.00)	(0.00, 0.00)	(0.00, 0.00)
alpha_JetFake_statCR_TWOeleCR	(−0.52, 0.40)	(−0.01, 0.00)	(−0.76, 0.59)	(1.21, −0.91)	(−0.00, 0.00)
alpha_JetFake_statCR_TWPmuCR	(−2.64, 0.32)	(0.02, 0.01)	(2.29, −0.29)	(−3.21, 0.38)	(0.00, −0.00)
alpha_LUMI_SYST	(0.14, −0.01)	(0.01, 0.00)	(−0.00, 0.01)	(−0.03, −0.00)	(0.00, −0.00)
alpha_MET_RESO_PARA	(0.00, 0.02)	(0.00, −0.00)	(−0.02, 0.01)	(0.01, −0.03)	(0.00, −0.01)
alpha_MET_RESO_PERP	(0.18, −0.16)	(−0.00, 0.00)	(−0.00, −0.01)	(−0.00, −0.01)	(−0.00, −0.00)
alpha_MET_SCALE	(1.03, −1.05)	(0.00, −0.00)	(0.06, 0.05)	(−0.01, −0.05)	(−0.01, −0.00)
alpha_MU_EFF_STAT	(−0.14, 0.33)	(−0.00, −0.01)	(0.05, −0.19)	(−0.05, 0.19)	(−0.00, 0.00)
alpha_MU_EFF_SYST	(−0.66, 0.83)	(0.00, 0.00)	(0.54, −0.67)	(−0.60, 0.70)	(−0.00, 0.00)
alpha_MU_EFF_SYST_LOWPT	(−0.09, 0.29)	(−0.01, −0.01)	(0.02, −0.16)	(−0.01, 0.16)	(−0.00, 0.00)
alpha_MU_ID	(−0.05, 0.27)	(0.00, −0.00)	(−0.03, −0.15)	(0.03, 0.16)	(−0.00, −0.00)
alpha_MU_ISO_STAT	(−0.12, 0.32)	(−0.01, −0.01)	(0.04, −0.18)	(−0.03, 0.18)	(−0.00, 0.00)
alpha_MU_ISO_SYST	(−0.36, 0.55)	(0.00, −0.01)	(0.26, −0.39)	(−0.26, 0.43)	(−0.00, 0.00)
alpha_MU_MS	(−0.06, 0.21)	(−0.01, −0.00)	(−0.02, −0.03)	(0.04, 0.04)	(−0.00, −0.00)
alpha_MU_SCALE	(−0.02, 0.25)	(−0.00, −0.00)	(−0.02, −0.14)	(0.02, 0.14)	(−0.00, −0.00)
alpha_MU_TTVA_STAT	(−0.09, 0.28)	(−0.01, −0.01)	(0.02, −0.16)	(0.00, 0.15)	(−0.00, 0.00)
alpha_MU_TTVA_SYS	(−0.17, 0.38)	(0.01, −0.01)	(0.12, −0.23)	(−0.09, 0.25)	(−0.00, 0.00)
alpha_PDF_Comb	(0.10, −0.05)	(−0.00, 0.00)	(0.00, −0.01)	(−0.01, −0.01)	(−0.00, −0.00)
alpha_PH_EFF	(−0.02, −0.03)	(−0.00, 0.00)	(−0.01, −0.02)	(0.01, −0.00)	(0.00, −0.00)
alpha_PH_EFF_TRKISO	(−0.02, 0.05)	(−0.00, 0.01)	(−0.01, 0.00)	(0.01, −0.03)	(−0.00, 0.00)
alpha_PH_ISO_DD	(−0.02, 0.05)	(−0.00, 0.01)	(−0.01, 0.00)	(0.01, −0.03)	(−0.00, 0.00)
alpha_PRW_DATASF	(−0.19, −1.59)	(−0.00, −0.00)	(−0.20, −0.05)	(0.22, 0.03)	(−0.00, −0.00)
alpha_syst_JetFake_ONEmuCR	(−0.23, 0.19)	(0.00, −0.00)	(0.02, −0.02)	(0.00, −0.02)	(−0.00, 0.00)
alpha_syst_JetFake_PhJetCR	(−0.01, 0.06)	(−0.00, −0.00)	(0.01, −0.00)	(0.00, −0.00)	(0.00, −0.00)
alpha_syst_JetFake_SR	(0.69, −0.69)	(0.00, 0.00)	(0.00, 0.00)	(0.00, 0.00)	(0.00, 0.00)
alpha_syst_JetFake_TWOeleCR	(−0.19, 0.19)	(−0.00, −0.00)	(−0.26, 0.29)	(0.41, −0.44)	(−0.00, 0.00)
alpha_syst_JetFake_TWOmuCR	(−0.45, 0.27)	(−0.01, 0.01)	(0.37, −0.24)	(−0.52, 0.32)	(0.00, −0.00)

Table 33: Breakdown of the dominant systematic uncertainties expressed in % on background estimates after the fit in the SR defined by $E_{\mathrm{T}}^{\mathrm{miss}} \in [150\ \mathrm{GeV}; 225\ \mathrm{GeV}]$ and its CRs for an integrated luminosity of 36.4 fb^{-1}. Note that the individual uncertainties can be correlated, and do not necessarily add up quadratically to the total background uncertainty. The percentages show the size of the uncertainty relative to the total expected background.

Systematic	SR	CR1mu	CR2mu	CR2e	CRgjet
alpha_EG_RESO	(0.09, −0.27)	(−0.01, −0.00)	(−0.08, −0.27)	(0.10, 0.25)	(−0.00, −0.00)
alpha_EG_SCALE	(0.84, −0.50)	(−0.01, 0.00)	(0.06, 0.02)	(−0.04, −0.05)	(0.01, 0.00)
alpha_EL_EFF_ID	(−1.15, 1.16)	(−0.00, 0.01)	(−1.27, 1.30)	(1.29, −1.35)	(−0.00, 0.00)
alpha_EL_EFF_ISO	(−0.74, 0.76)	(−0.00, 0.01)	(−0.81, 0.85)	(0.83, −0.88)	(−0.00, 0.00)
alpha_EL_EFF_RECO	(−0.42, 0.43)	(0.00, −0.03)	(−0.46, 0.48)	(0.47, −0.51)	(−0.00, 0.00)
alpha_EleFake_statCR_ONEmuCR	(−0.02, 0.02)	(0.01, −0.01)	(−0.01, 0.02)	(−0.01, 0.02)	(−0.00, −0.00)
alpha_EleFake_statCR_PhJetCR	(−0.01, 0.01)	(−0.00, 0.00)	(−0.00, 0.00)	(−0.01, 0.01)	(−0.00, −0.00)
alpha_EleFake_statCR_SR	(0.14, −0.14)	(0.00, 0.00)	(0.00, 0.00)	(0.00, 0.00)	(0.00, 0.00)
alpha_EleFake_statCR_TWOeleCR	(−0.00, −0.00)	(−0.00, −0.00)	(−0.00, −0.00)	(0.00, −0.00)	(−0.00, −0.00)
alpha_EleFake_statCR_TWOmuCR	(−0.04, 0.03)	(−0.00, 0.00)	(0.04, −0.05)	(−0.05, 0.04)	(−0.00, −0.00)
alpha_EleFake_stat_ONEmuCR	(−0.03, 0.03)	(0.02, −0.02)	(−0.02, 0.02)	(−0.01, 0.02)	(−0.00, −0.00)
alpha_EleFake_stat_PhJetCR	(−0.01, 0.01)	(0.01, −0.00)	(0.01, 0.01)	(0.00, −0.01)	(0.00, −0.00)
alpha_EleFake_stat_SR	(0.75, −0.75)	(0.00, 0.00)	(0.00, 0.00)	(0.00, 0.00)	(0.00, 0.00)
alpha_EleFake_stat_TWOeleCR	(−0.00, −0.00)	(−0.00, −0.00)	(−0.00, −0.00)	(0.00, −0.00)	(−0.00, −0.00)
alpha_EleFake_stat_TWOmuCR	(−0.00, 0.00)	(−0.00, 0.00)	(0.03, −0.03)	(−0.00, 0.00)	(−0.00, 0.00)
alpha_EleFake_syst_ONEmuCR	(−0.04, 0.03)	(0.01, −0.00)	(0.02, −0.02)	(0.02, −0.03)	(−0.00, −0.00)
alpha_EleFake_syst_PhJetCR	(−0.01, 0.01)	(0.01, −0.00)	(0.01, 0.01)	(0.00, −0.01)	(0.00, −0.00)
alpha_EleFake_syst_SR	(1.33, −1.33)	(0.00, 0.00)	(0.00, 0.00)	(0.00, 0.00)	(0.00, 0.00)
alpha_EleFake_syst_TWOeleCR	(−0.00, −0.00)	(−0.00, −0.00)	(−0.00, −0.00)	(0.00, −0.00)	(−0.00, −0.00)
alpha_EleFake_syst_TWOmuCR	(−0.00, 0.00)	(−0.00, 0.00)	(0.05, −0.05)	(−0.00, 0.00)	(0.00, 0.00)
alpha_JER	(0.18, −0.23)	(−0.01, 0.01)	(−0.31, 0.33)	(0.37, −0.40)	(0.00, −0.01)
alpha_JES	(−0.29, 0.64)	(−0.01, 0.01)	(−0.36, −0.04)	(0.42, 0.05)	(−0.00, −0.00)
alpha_JVT_EFF	(0.01, −0.01)	(−0.00, 0.00)	(−0.04, 0.05)	(0.04, −0.06)	(−0.00, 0.00)
alpha_JetFake_statCR_ONEmuCR	(−0.55, 0.51)	(−0.00, −0.01)	(0.01, −0.01)	(−0.02, −0.05)	(−0.00, −0.00)
alpha_JetFake_statCR_PhJetCR	(−0.02, 0.01)	(0.01, 0.00)	(−0.00, 0.00)	(−0.03, −0.01)	(0.00, −0.00)
alpha_JetFake_statCR_SR	(1.49, −1.49)	(0.00, 0.00)	(0.00, 0.00)	(0.00, 0.00)	(0.00, 0.00)
alpha_JetFake_statCR_TWOeleCR	(−1.23, 0.86)	(−0.00, 0.01)	(−1.39, 0.98)	(2.27, −1.54)	(−0.00, −0.00)
alpha_JetFake_statCR_TWOmuCR	(−2.64, 2.12)	(−0.03, 0.00)	(2.06, −1.49)	(−3.03, 2.45)	(0.00, −0.00)
alpha_LUMI_SYST	(−0.00, −0.02)	(−0.01, −0.02)	(0.01, −0.01)	(−0.04, −0.03)	(0.00, 0.00)
alpha_MET_RESO_PARA	(0.84, −0.78)	(−0.01, 0.00)	(0.12, −0.11)	(−0.10, 0.07)	(−0.00, −0.01)
alpha_MET_RESO_PERP	(0.34, −0.33)	(−0.02, 0.00)	(0.01, −0.01)	(−0.01, −0.01)	(−0.00, −0.00)
alpha_MET_SCALE	(0.52, −0.03)	(−0.02, 0.00)	(−0.08, 0.07)	(0.16, −0.09)	(−0.00, 0.00)
alpha_MU_EFF_STAT	(−0.06, 0.28)	(0.00, −0.01)	(0.03, −0.15)	(−0.03, 0.21)	(−0.00, 0.00)
alpha_MU_EFF_SYST	(−0.84, 1.03)	(0.00, 0.00)	(0.74, −0.91)	(−0.76, 0.88)	(−0.00, 0.00)
alpha_MU_EFF_SYST_LOWPT	(−0.02, 0.23)	(−0.00, −0.01)	(−0.02, −0.12)	(0.01, 0.17)	(−0.00, 0.00)
alpha_MU_ID	(0.06, 0.14)	(−0.00, −0.00)	(−0.06, −0.12)	(0.06, 0.12)	(−0.00, −0.00)
alpha_MU_ISO_STAT	(−0.07, 0.29)	(0.00, −0.02)	(0.03, −0.16)	(−0.03, 0.22)	(−0.00, 0.00)
alpha_MU_ISO_SYST	(−0.29, 0.49)	(0.00, 0.01)	(0.24, −0.41)	(−0.25, 0.40)	(−0.00, 0.00)
alpha_MU_MS	(0.00, −0.02)	(−0.00, −0.00)	(−0.04, −0.14)	(0.05, 0.14)	(−0.00, −0.00)
alpha_MU_SCALE	(0.07, 0.13)	(−0.00, 0.00)	(−0.06, −0.11)	(0.05, 0.12)	(−0.00, −0.00)
alpha_MU_TTVA_STAT	(−0.01, 0.23)	(−0.00, −0.01)	(−0.02, −0.12)	(0.02, 0.16)	(−0.00, 0.00)
alpha_MU_TTVA_SYS	(−0.08, 0.30)	(0.00, −0.02)	(0.05, −0.17)	(−0.05, 0.23)	(−0.00, 0.00)
alpha_PDF_Comb	(−0.03, −0.00)	(0.00, 0.00)	(−0.01, 0.01)	(−0.02, −0.00)	(0.00, −0.00)
alpha_PH_EFF	(−0.03, 0.01)	(0.02, 0.01)	(−0.05, −0.05)	(0.07, 0.02)	(0.00, −0.00)
alpha_PH_EFF_TRKISO	(0.01, −0.01)	(−0.00, 0.00)	(−0.04, 0.05)	(0.04, −0.06)	(−0.00, 0.00)
alpha_PH_ISO_DD	(0.01, −0.01)	(−0.00, 0.00)	(−0.04, 0.05)	(0.04, −0.06)	(−0.00, 0.00)
alpha_PRW_DATASF	(1.28, −0.64)	(−0.00, 0.01)	(−0.92, 0.41)	(0.92, −0.40)	(−0.00, −0.01)
alpha_syst_JetFake_ONEmuCR	(−0.49, 0.48)	(0.00, −0.01)	(0.01, 0.03)	(−0.02, 0.01)	(−0.00, −0.00)
alpha_syst_JetFake_PhJetCR	(−0.00, 0.01)	(−0.01, 0.00)	(0.02, 0.01)	(0.01, −0.01)	(0.00, −0.00)
alpha_syst_JetFake_SR	(0.90, −0.90)	(0.00, 0.00)	(0.00, 0.00)	(0.00, 0.00)	(0.00, 0.00)
alpha_syst_JetFake_TWOeleCR	(−0.24, 0.28)	(0.02, −0.02)	(−0.26, 0.32)	(0.37, −0.49)	(−0.00, −0.00)
alpha_syst_JetFake_TWOmuCR	(−0.96, 0.92)	(−0.01, 0.02)	(0.72, −0.68)	(−1.10, 1.07)	(0.00, −0.00)

Table 34: Breakdown of the dominant systematic uncertainties expressed in % on background estimates after the fit in the SR defined by $E_{\mathrm{T}}^{\mathrm{miss}} \in [225\ \mathrm{GeV}; 300\ \mathrm{GeV}]$ and its CRs for an integrated luminosity of 36.4 fb^{-1}. Note that the individual uncertainties can be correlated, and do not necessarily add up quadratically to the total background uncertainty. The percentages show the size of the uncertainty relative to the total expected background.

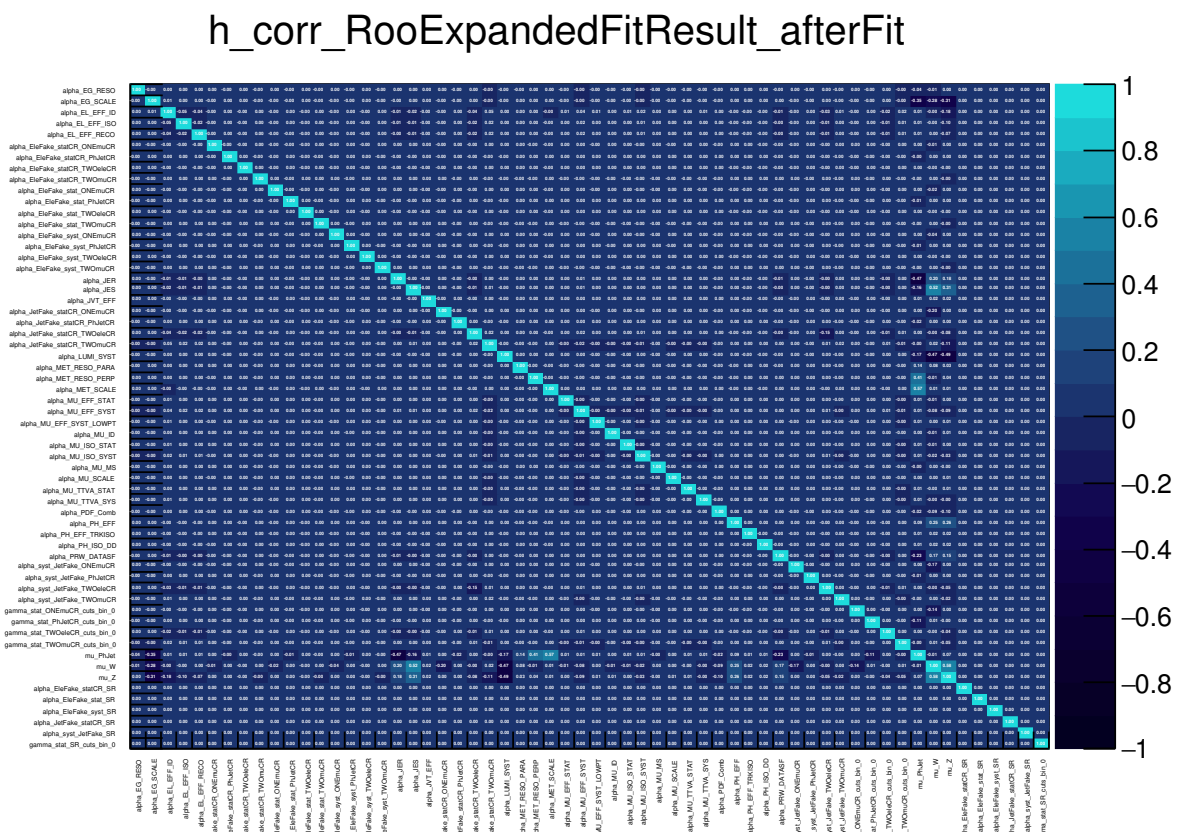

Figure 31: Correlation matrix between the various source of systematic uncertainties that are taken into account in the background-only fit for the SR defined by $E_{\mathrm{T}}^{\mathrm{miss}} > 150$ GeV

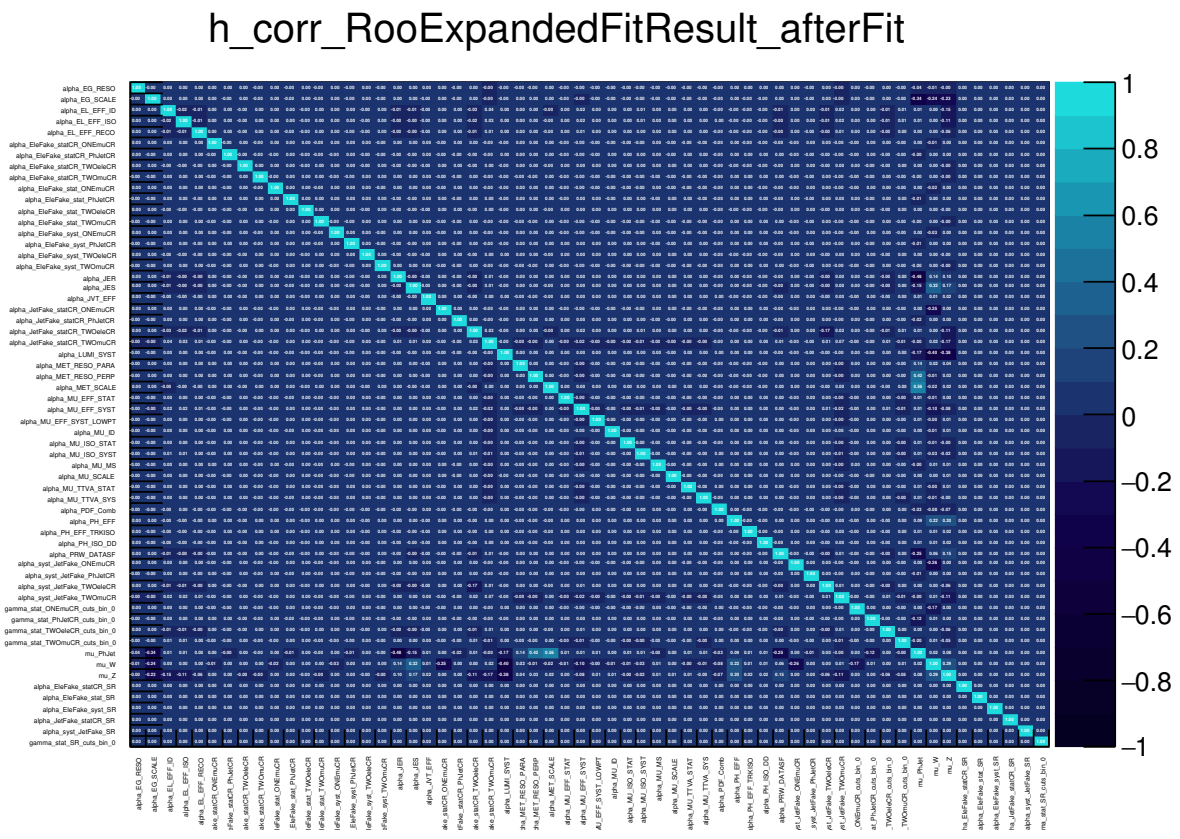

Figure 32: Correlation matrix between the various source of systematic uncertainties that are taken into account in the background-only fit for the SR defined by $E_{\mathrm{T}}^{\mathrm{miss}} > 225$ GeV

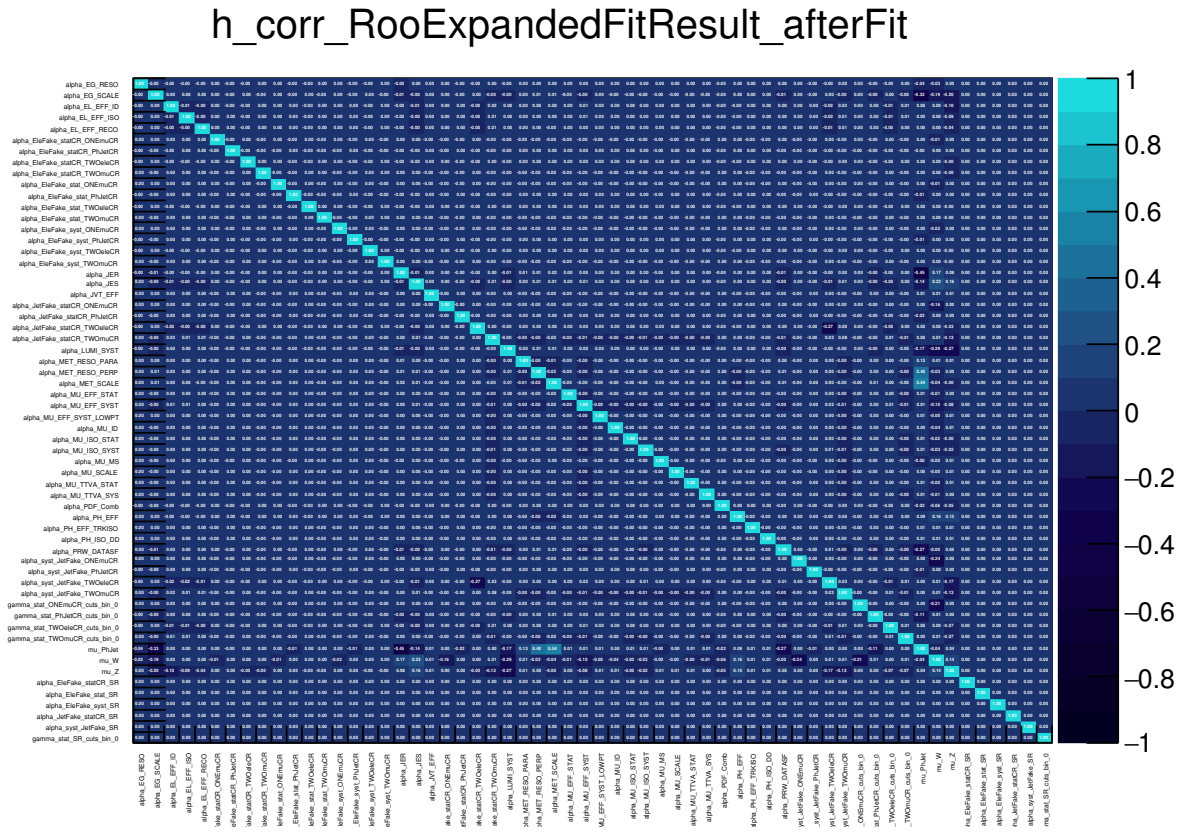

Figure 33: Correlation matrix between the various source of systematic uncertainties that are taken into account in the background-only fit for the SR defined by $E_{\mathrm{T}}^{\mathrm{miss}} > 300$ GeV

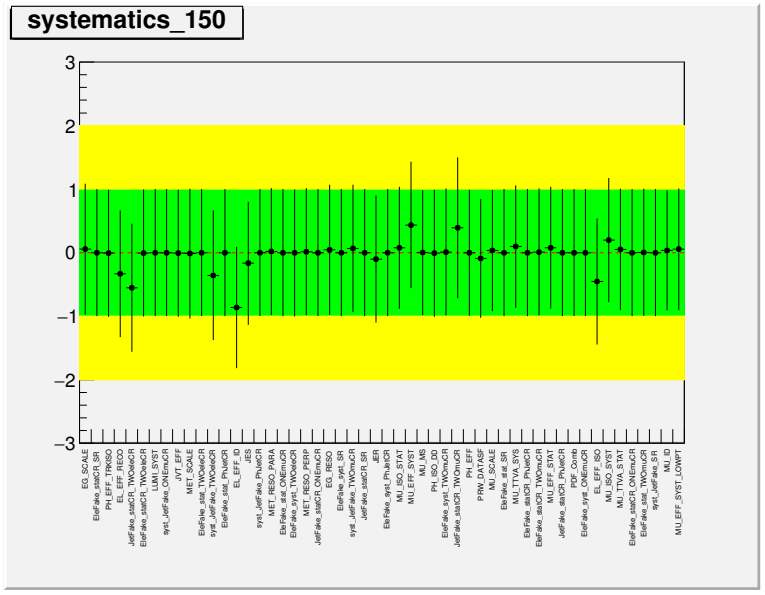

Figure 34: Post-fit nuisance parameter values and errors for SR defined by $E_{\mathrm{T}}^{\mathrm{miss}} > 150$ GeV

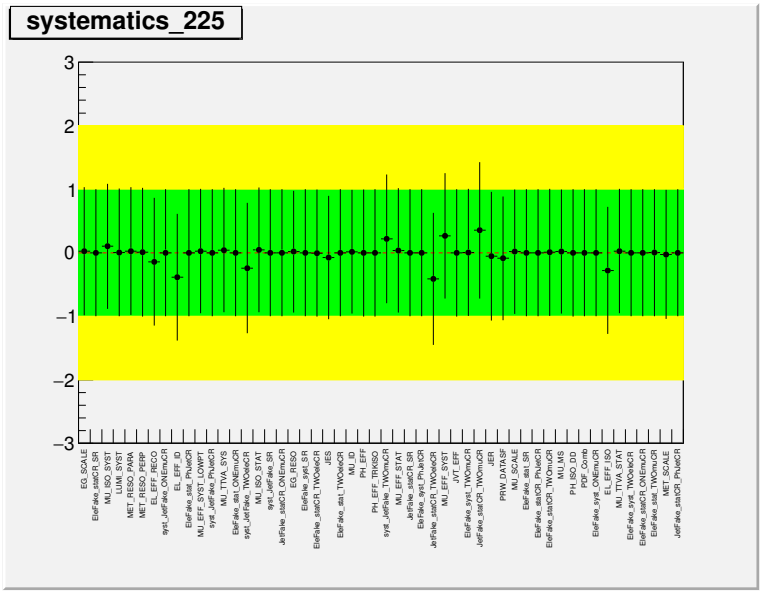

Figure 35: Post-fit nuisance parameter values and errors for SR defined by $E_{\mathrm{T}}^{\mathrm{miss}} > 225$ GeV

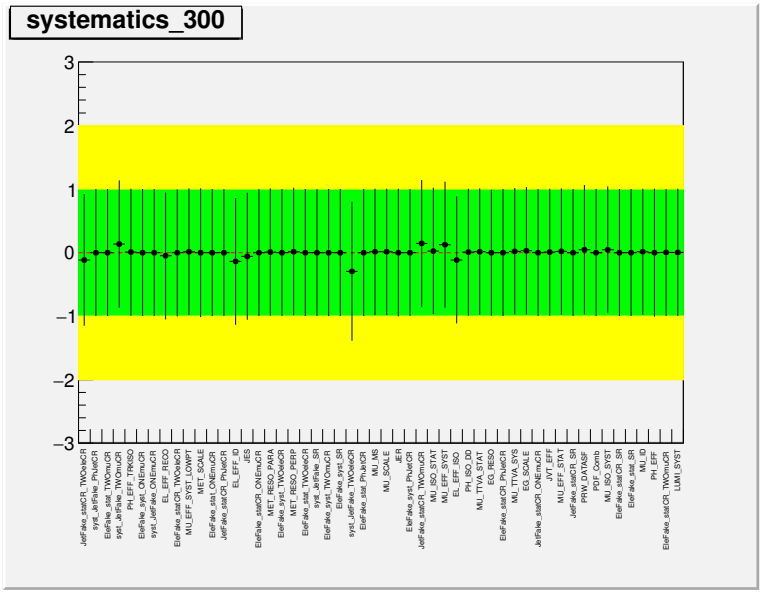

Figure 36: Post-fit nuisance parameter values and errors for SR defined by $E_{\mathrm{T}}^{\mathrm{miss}} > 300$ GeV

7.4 Systematic uncertainties in SRs and CRs from simplified shape fit

The impact of each source of uncertainty with respect to the total background prediction is evaluated after the simplified shape fit for exclusive SRs, as reported in Tables 35, Tables 36, Tables 37.

Figure 37, 38 ,39 show the post-fit nuisance parameter values and errors for all exclusive SRs.

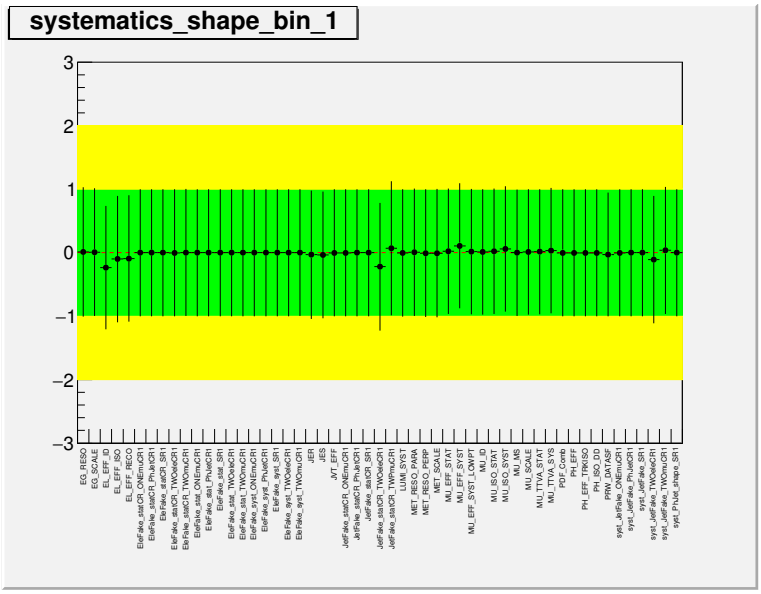

Figure 37: Post-fit nuisance parameter values and errors for exclusive SR defined by 150 GeV $< E_{\mathrm{T}}^{\mathrm{miss}} <$ 225 GeV

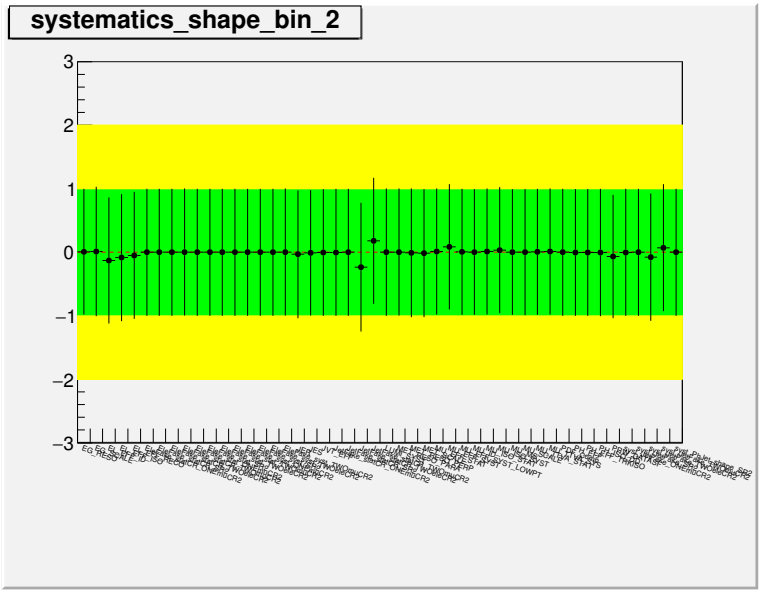

Figure 38: Post-fit nuisance parameter values and errors for exclusive SR defined by 225 GeV $< E_{\mathrm{T}}^{\mathrm{miss}} <$ 300 GeV

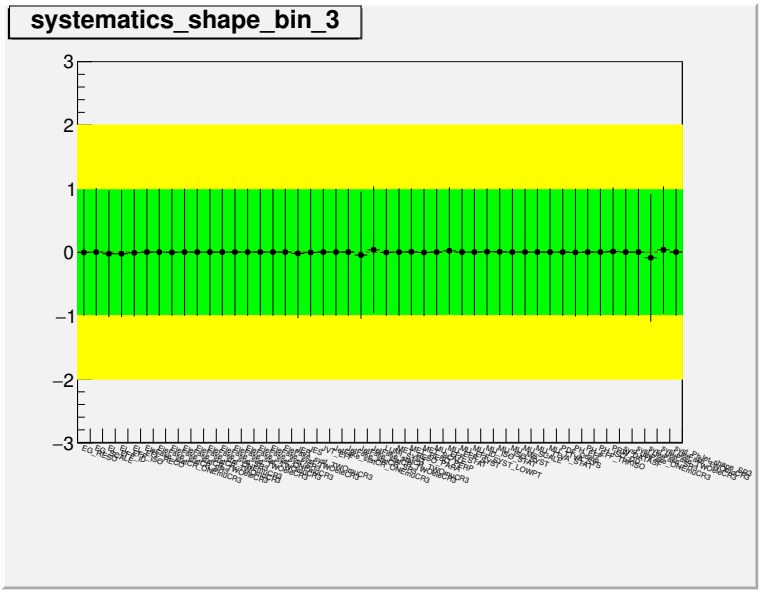

Figure 39: Post-fit nuisance parameter values and errors for exclusive SR defined by $E_{\mathrm{T}}^{\mathrm{miss}} >$ 300 GeV

Systematic	SR	CR1mu	CR2mu	CR2e	CRgjet
alpha_EG_RESO	(−0.05, 0.13)	(−0.01, −0.01)	(0.13, −0.01)	(−0.20, −0.04)	(−0.01, −0.00)
alpha_EG_SCALE	(0.02, −0.07)	(−0.00, −0.00)	(0.06, −0.07)	(−0.10, 0.08)	(−0.01, 0.00)
alpha_EL_EFF_ID	(−0.68, 0.67)	(−0.01, −0.00)	(−1.19, 1.16)	(1.51, −1.52)	(−0.00, 0.00)
alpha_EL_EFF_ISO	(−0.27, 0.27)	(−0.01, −0.00)	(−0.51, 0.48)	(0.63, −0.63)	(−0.00, 0.00)
alpha_EL_EFF_RECO	(−0.24, 0.23)	(−0.01, 0.00)	(−0.47, 0.43)	(0.57, −0.59)	(−0.00, 0.00)
alpha_EleFake_statCR_ONEmuCR1	(−0.01, 0.01)	(−0.00, −0.00)	(−0.00, −0.00)	(−0.00, −0.00)	(−0.00, 0.00)
alpha_EleFake_statCR_PhJetCR1	(−0.00, 0.00)	(0.00, −0.00)	(−0.00, 0.00)	(0.00, −0.00)	(−0.00, 0.00)
alpha_EleFake_statCR_SR1	(0.09, −0.09)	(0.00, 0.00)	(0.00, 0.00)	(0.00, 0.00)	(0.00, 0.00)
alpha_EleFake_statCR_TWOeleCR1	(−0.00, 0.00)	(−0.00, 0.00)	(−0.01, 0.01)	(0.01, −0.01)	(−0.00, 0.00)
alpha_EleFake_statCR_TWOmuCR1	(−0.02, 0.02)	(−0.00, 0.00)	(0.01, −0.01)	(−0.02, 0.02)	(−0.00, 0.00)
alpha_EleFake_stat_ONEmuCR1	(−0.05, 0.02)	(0.01, −0.00)	(−0.06, −0.00)	(−0.02, −0.00)	(0.00, 0.00)
alpha_EleFake_stat_PhJetCR1	(−0.02, 0.02)	(−0.00, −0.00)	(−0.01, 0.00)	(−0.01, 0.00)	(0.00, 0.00)
alpha_EleFake_stat_SR1	(0.66, −0.66)	(0.00, 0.00)	(0.00, 0.00)	(0.00, 0.00)	(0.00, 0.00)
alpha_EleFake_stat_TWOeleCR1	(−0.00, 0.00)	(−0.00, 0.00)	(−0.00, 0.00)	(0.00, −0.00)	(−0.00, 0.00)
alpha_EleFake_stat_TWOmuCR1	(−0.01, 0.01)	(−0.00, 0.00)	(0.00, −0.00)	(−0.01, 0.01)	(−0.00, 0.00)
alpha_EleFake_syst_ONEmuCR1	(−0.08, 0.05)	(−0.01, 0.00)	(−0.04, 0.00)	(−0.02, 0.00)	(0.00, 0.00)
alpha_EleFake_syst_PhJetCR1	(−0.04, 0.02)	(−0.00, 0.01)	(−0.02, −0.04)	(−0.01, −0.02)	(0.00, −0.00)
alpha_EleFake_syst_SR1	(1.36, −1.36)	(0.00, 0.00)	(0.00, 0.00)	(0.00, 0.00)	(0.00, 0.00)
alpha_EleFake_syst_TWOeleCR1	(−0.00, 0.00)	(−0.00, 0.00)	(−0.00, 0.00)	(0.00, −0.00)	(−0.00, 0.00)
alpha_EleFake_syst_TWOmuCR1	(−0.01, 0.01)	(−0.00, 0.00)	(0.01, −0.01)	(−0.02, 0.02)	(−0.00, 0.00)
alpha_JER	(−0.76, 0.84)	(−0.01, −0.01)	(−0.10, 0.09)	(0.13, −0.14)	(0.01, 0.00)
alpha_JES	(−5.62, 2.41)	(−0.01, −0.01)	(−0.29, 0.15)	(0.36, −0.22)	(−0.00, −0.00)
alpha_JVT_EFF	(−0.07, 0.07)	(−0.00, −0.00)	(−0.01, 0.01)	(0.02, −0.02)	(0.00, −0.00)
alpha_JetFake_statCR_ONEmuCR1	(−0.35, 0.34)	(−0.01, −0.01)	(−0.01, −0.00)	(−0.01, −0.01)	(0.00, −0.00)
alpha_JetFake_statCR_PhJetCR1	(−0.06, 0.04)	(−0.01, 0.01)	(−0.01, −0.04)	(−0.00, −0.02)	(−0.00, −0.00)
alpha_JetFake_statCR_SR1	(1.05, −1.05)	(0.00, 0.00)	(0.00, 0.00)	(0.00, 0.00)	(0.00, 0.00)
alpha_JetFake_statCR_TWOeleCR1	(−0.52, 0.50)	(−0.01, −0.01)	(−0.89, 0.86)	(1.31, −1.20)	(−0.00, 0.00)
alpha_JetFake_statCR_TWPmuCR1	(−0.79, 0.23)	(0.00, 0.00)	(0.67, −0.22)	(−1.00, 0.28)	(−0.00, 0.00)
alpha_LUMI_SYST	(0.03, −0.04)	(−0.02, −0.01)	(−0.01, −0.02)	(−0.01, −0.01)	(0.00, 0.00)
alpha_MET_RESO_PARA	(0.01, 0.06)	(−0.01, −0.00)	(−0.00, −0.01)	(−0.02, 0.02)	(−0.00, 0.00)
alpha_MET_RESO_PERP	(0.30, −0.23)	(−0.00, −0.00)	(−0.08, 0.05)	(0.07, −0.08)	(−0.00, 0.00)
alpha_MET_SCALE	(1.03, −1.08)	(−0.01, −0.00)	(−0.01, 0.01)	(−0.02, −0.03)	(−0.00, −0.00)
alpha_MU_EFF_STAT	(−0.14, 0.32)	(−0.00, −0.00)	(0.05, −0.19)	(−0.06, 0.23)	(0.00, 0.00)
alpha_MU_EFF_SYST	(−0.70, 0.89)	(−0.01, −0.01)	(0.48, −0.63)	(−0.64, 0.79)	(−0.00, 0.00)
alpha_MU_EFF_SYST_LOWPT	(−0.10, 0.28)	(−0.00, −0.00)	(0.02, −0.15)	(−0.02, 0.19)	(0.00, 0.00)
alpha_MU_ID	(−0.13, 0.28)	(0.01, −0.00)	(−0.06, −0.14)	(−0.00, 0.18)	(0.00, 0.00)
alpha_MU_ISO_STAT	(−0.13, 0.31)	(−0.00, −0.00)	(0.04, −0.17)	(−0.05, 0.22)	(0.00, 0.00)
alpha_MU_ISO_SYST	(−0.34, 0.54)	(−0.01, −0.00)	(0.22, −0.37)	(−0.30, 0.46)	(−0.00, 0.00)
alpha_MU_MS	(−0.06, 0.15)	(−0.00, 0.01)	(−0.02, −0.08)	(0.03, 0.01)	(0.00, −0.00)
alpha_MU_SCALE	(−0.06, 0.24)	(−0.00, −0.00)	(−0.01, −0.12)	(0.02, 0.16)	(0.00, 0.00)
alpha_MU_TTVA_STAT	(−0.09, 0.27)	(−0.00, −0.00)	(0.01, −0.15)	(−0.01, 0.18)	(0.00, 0.00)
alpha_MU_TTVA_SYS	(−0.19, 0.36)	(−0.00, −0.00)	(0.09, −0.23)	(−0.12, 0.28)	(0.00, 0.00)
alpha_PDF_Comb	(0.09, −0.10)	(−0.01, −0.01)	(−0.01, −0.00)	(−0.01, −0.00)	(−0.00, 0.00)
alpha_PH_EFF	(−0.13, −0.04)	(−0.01, −0.01)	(0.01, −0.02)	(0.03, 0.01)	(−0.00, −0.01)
alpha_PH_EFF_TRKISO	(−0.07, 0.07)	(−0.00, −0.00)	(−0.01, 0.01)	(0.02, −0.02)	(0.00, −0.00)
alpha_PH_ISO_DD	(−0.07, 0.07)	(−0.00, −0.00)	(−0.01, 0.01)	(0.02, −0.02)	(0.00, −0.00)
alpha_PRW_DATASF	(−0.19, −1.72)	(−0.01, −0.01)	(−0.26, −0.00)	(0.33, −0.01)	(−0.00, −0.00)
alpha_syst_JetFake_ONEmuCR1	(−0.21, 0.20)	(−0.01, −0.01)	(−0.01, 0.01)	(−0.01, −0.00)	(−0.00, 0.00)
alpha_syst_JetFake_PhJetCR1	(−0.04, 0.02)	(−0.01, 0.01)	(−0.00, −0.04)	(−0.00, −0.02)	(0.00, −0.00)
alpha_syst_JetFake_SR1	(0.73, −0.73)	(0.00, 0.00)	(0.00, 0.00)	(0.00, 0.00)	(0.00, 0.00)
alpha_syst_JetFake_TWOeleCR1	(−0.23, 0.24)	(−0.00, 0.01)	(−0.39, 0.40)	(0.57, −0.66)	(−0.00, 0.00)
alpha_syst_JetFake_TWOmuCR1	(−0.21, 0.17)	(0.00, 0.00)	(0.19, −0.20)	(−0.27, 0.22)	(−0.00, 0.00)
alpha_syst_PhJet_shape_SR1	(−2.28, 2.28)	(0.00, 0.00)	(0.00, 0.00)	(0.00, 0.00)	(0.00, 0.00)

Table 35: Breakdown of the dominant systematic uncertainties expressed in % on background estimates after the simplified shape fit in the exclusive SR defined by $E_{\mathrm{T}}^{\mathrm{miss}} \in [150\ \mathrm{GeV}; 225\ \mathrm{GeV}]$ and its CRs for an integrated luminosity of 36.4 fb^{-1}. Note that the individual uncertainties can be correlated, and do not necessarily add up quadratically to the total background uncertainty.

Systematic	SR	CR1mu	CR2mu	CR2e	CRgjet
alpha_EG_RESO	(0.06, −0.34)	(−0.01, −0.04)	(0.02, −0.24)	(0.04, 0.20)	(0.28, −0.22)
alpha_EG_SCALE	(1.03, −0.74)	(−0.02, −0.02)	(0.11, 0.09)	(−0.03, −0.06)	(4.27, −6.69)
alpha_EL_EFF_ID	(−0.95, 0.01)	(−0.05, 0.01)	(−1.10, 0.00)	(1.42, −0.01)	(−0.06, −0.00)
alpha_EL_EFF_ISO	(−0.64, 0.71)	(−0.02, −0.02)	(−0.74, 0.81)	(0.86, −0.93)	(−0.05, 0.02)
alpha_EL_EFF_RECO	(−0.38, 0.39)	(−0.03, −0.03)	(−0.42, 0.44)	(0.48, −0.57)	(−0.04, 0.02)
alpha_EleFake_statCR_ONEmuCR2	(−0.06, 0.02)	(−0.04, −0.01)	(−0.04, −0.01)	(−0.08, −0.00)	(−0.02, 0.00)
alpha_EleFake_statCR_SR2	(0.15, −0.15)	(0.00, 0.00)	(0.00, 0.00)	(0.00, 0.00)	(0.00, 0.00)
alpha_EleFake_statCR_TWOeleCR2	(0.00, 0.00)	(0.00, 0.00)	(0.00, 0.00)	(0.00, 0.00)	(−0.00, −0.00)
alpha_EleFake_statCR_TWOmuCR2	(−0.06, 0.04)	(−0.05, 0.00)	(0.02, −0.03)	(−0.12, 0.05)	(−0.03, 0.00)
alpha_EleFake_stat_ONEmuCR2	(−0.07, 0.03)	(−0.04, −0.01)	(−0.04, −0.00)	(−0.08, 0.00)	(−0.02, 0.00)
alpha_EleFake_stat_SR2	(0.80, −0.80)	(0.00, 0.00)	(0.00, 0.00)	(0.00, 0.00)	(0.00, 0.00)
alpha_EleFake_stat_TWOeleCR2	(0.00, 0.00)	(0.00, 0.00)	(0.00, 0.00)	(0.00, 0.00)	(−0.00, −0.00)
alpha_EleFake_stat_TWOmuCR2	(−0.01, 0.01)	(0.00, 0.00)	(0.01, −0.01)	(−0.01, 0.02)	(0.00, 0.00)
alpha_EleFake_syst_ONEmuCR2	(−0.09, 0.07)	(−0.04, 0.00)	(−0.03, 0.00)	(−0.08, 0.01)	(−0.02, 0.00)
alpha_EleFake_syst_SR2	(1.41, −1.41)	(0.00, 0.00)	(0.00, 0.00)	(0.00, 0.00)	(0.00, 0.00)
alpha_EleFake_syst_TWOeleCR2	(0.00, 0.00)	(0.00, 0.00)	(0.00, 0.00)	(0.00, 0.00)	(−0.00, −0.00)
alpha_EleFake_syst_TWOmuCR2	(−0.03, 0.03)	(−0.00, 0.00)	(0.02, −0.02)	(−0.03, 0.03)	(0.00, 0.00)
alpha_JER	(0.23, −0.30)	(−0.04, −0.02)	(−0.19, 0.26)	(0.31, −0.22)	(4.79, −9.63)
alpha_JES	(−0.30, 0.58)	(−0.03, −0.02)	(−0.19, −0.02)	(0.40, 0.05)	(0.77, −3.49)
alpha_JVT_EFF	(−0.00, −0.02)	(0.00, −0.02)	(−0.02, 0.01)	(−0.00, −0.07)	(−0.07, 0.06)
alpha_JetFake_statCR_ONEmuCR2	(−0.56, 0.60)	(−0.02, −0.01)	(0.04, −0.01)	(0.03, 0.00)	(−0.04, 0.02)
alpha_JetFake_statCR_SR2	(1.58, −1.58)	(0.00, 0.00)	(0.00, 0.00)	(0.00, 0.00)	(0.00, 0.00)
alpha_JetFake_statCR_TWOeleCR2	(−1.29, 1.21)	(−0.03, −0.00)	(−1.54, 1.41)	(2.46, −2.01)	(−0.04, 0.03)
alpha_JetFake_statCR_TWOmuCR2	(−1.98, 2.10)	(0.00, −0.04)	(1.56, −1.35)	(−2.30, 2.40)	(0.01, −0.01)
alpha_LUMI_SYST	(0.13, −0.04)	(−0.00, −0.02)	(0.02, 0.03)	(0.02, 0.04)	(2.53, −3.13)
alpha_MET_RESO_PARA	(0.94, −0.84)	(−0.02, −0.01)	(0.09, −0.01)	(0.02, 0.05)	(−1.97, 2.02)
alpha_MET_RESO_PERP	(0.20, −0.19)	(−0.02, −0.02)	(0.09, −0.02)	(−0.01, 0.11)	(−8.23, 4.82)
alpha_MET_SCALE	(0.14, 0.17)	(−0.03, −0.00)	(−0.04, 0.09)	(0.10, −0.05)	(−10.35, 5.16)
alpha_MU_EFF_STAT	(−0.08, 0.28)	(−0.00, 0.01)	(0.02, −0.17)	(−0.04, 0.20)	(−0.06, 0.06)
alpha_MU_EFF_SYST	(−0.91, 1.17)	(−0.04, 0.00)	(0.70, −0.78)	(−0.81, 1.04)	(−0.08, 0.05)
alpha_MU_EFF_SYST_LOWPT	(−0.02, 0.23)	(−0.02, 0.01)	(−0.01, −0.13)	(0.02, 0.15)	(−0.06, 0.06)
alpha_MU_ID	(0.04, 0.15)	(0.01, −0.00)	(−0.06, −0.11)	(0.02, 0.14)	(−0.07, −0.05)
alpha_MU_ISO_STAT	(−0.08, 0.29)	(0.01, 0.01)	(0.04, −0.17)	(−0.04, 0.21)	(−0.06, 0.06)
alpha_MU_ISO_SYST	(−0.35, 0.54)	(−0.04, 0.00)	(0.20, −0.35)	(−0.32, 0.44)	(−0.07, 0.05)
alpha_MU_MS	(−0.02, −0.05)	(0.01, −0.05)	(−0.04, −0.13)	(−0.00, 0.07)	(−0.06, −0.09)
alpha_MU_SCALE	(0.07, 0.13)	(0.00, −0.02)	(−0.03, −0.11)	(0.01, 0.13)	(−0.07, −0.06)
alpha_MU_TTVA_STAT	(−0.02, 0.23)	(−0.01, 0.01)	(−0.01, −0.13)	(0.02, 0.15)	(−0.06, 0.06)
alpha_MU_TTVA_SYS	(−0.09, 0.30)	(0.01, 0.01)	(0.05, −0.19)	(−0.06, 0.22)	(−0.06, 0.06)
alpha_PDF_Comb	(−0.00, 0.04)	(−0.03, −0.00)	(0.01, 0.00)	(−0.00, 0.05)	(0.11, −0.14)
alpha_PH_EFF	(−0.02, 0.04)	(−0.02, −0.03)	(0.00, 0.01)	(0.07, 0.06)	(−1.83, 0.51)
alpha_PH_EFF_TRKISO	(−0.00, −0.02)	(0.00, −0.02)	(−0.02, 0.01)	(−0.00, −0.07)	(−0.07, 0.06)
alpha_PH_ISO_DD	(−0.00, −0.02)	(0.00, −0.02)	(−0.02, 0.01)	(−0.00, −0.07)	(−0.07, 0.06)
alpha_PRW_DATASF	(1.54, −0.70)	(−0.01, −0.02)	(−0.84, 0.37)	(0.95, −0.35)	(3.67, −4.86)
alpha_syst_JetFake_ONEmuCR2	(−0.50, 0.53)	(−0.02, 0.00)	(0.04, −0.03)	(0.03, −0.03)	(−0.03, 0.01)
alpha_syst_JetFake_SR2	(0.96, −0.96)	(0.00, 0.00)	(0.00, 0.00)	(0.00, 0.00)	(0.00, 0.00)
alpha_syst_JetFake_TWOeleCR2	(−0.36, 0.41)	(−0.01, −0.02)	(−0.43, 0.49)	(0.59, −0.78)	(−0.01, 0.01)
alpha_syst_JetFake_TWOmuCR2	(−0.76, 0.86)	(−0.01, 0.03)	(0.56, −0.47)	(−0.87, 0.92)	(0.00, −0.01)
alpha_syst_PhJet_shape_SR2	(−0.40, 0.40)	(0.00, 0.00)	(0.00, 0.00)	(0.00, 0.00)	(0.00, 0.00)

Table 36: Breakdown of the dominant systematic uncertainties expressed in % on background estimates after the simplified shape fit in the exclusive SR defined by $E_{\mathrm{T}}^{\mathrm{miss}} \in$ [225 GeV; 300 GeV] and its CRs for an integrated luminosity of 36.4 fb^{-1}. Note that the individual uncertainties can be correlated, and do not necessarily add up quadratically to the total background uncertainty.

alpha_EG_RESO	(0.00, −0.11)	(0.00, −0.06)	(−0.00, −0.00)	(0.00, 0.10)	(0.00, −0.36)
alpha_EG_SCALE	(−0.26, 0.15)	(−0.00, −0.03)	(0.45, −0.34)	(−0.40, 0.60)	(4.26, −6.09)
alpha_EL_EFF_ID	(−0.96, 1.04)	(−0.05, 0.01)	(−1.08, 1.19)	(1.36, −1.31)	(−0.03, 0.02)
alpha_EL_EFF_ISO	(−0.78, 0.82)	(−0.03, −0.02)	(−0.88, 0.93)	(1.05, −1.09)	(−0.02, 0.02)
alpha_EL_EFF_RECO	(−0.34, 0.37)	(−0.02, −0.02)	(−0.39, 0.43)	(0.50, −0.52)	(−0.02, 0.03)
alpha_EleFake_statCR_ONEmuCR3	(−0.00, 0.00)	(−0.02, −0.02)	(0.01, −0.01)	(0.00, −0.02)	(0.11, 0.01)
alpha_EleFake_statCR_SR3	(0.16, −0.16)	(0.00, 0.00)	(0.00, 0.00)	(0.00, 0.00)	(0.00, 0.00)
alpha_EleFake_statCR_TWOeleCR3	(−0.04, 0.05)	(−0.01, 0.00)	(−0.04, 0.05)	(0.07, −0.06)	(−0.00, 0.00)
alpha_EleFake_statCR_TWOmuCR3	(−0.03, 0.03)	(−0.00, 0.00)	(0.02, −0.02)	(−0.03, 0.03)	(−0.00, 0.00)
alpha_EleFake_stat_ONEmuCR3	(−0.00, 0.00)	(−0.02, −0.02)	(0.01, −0.01)	(0.00, −0.02)	(0.11, 0.00)
alpha_EleFake_stat_SR3	(0.61, −0.61)	(0.00, 0.00)	(0.00, 0.00)	(0.00, 0.00)	(0.00, 0.00)
alpha_EleFake_stat_TWOeleCR3	(−0.01, 0.01)	(−0.00, 0.00)	(−0.01, 0.01)	(0.01, −0.01)	(−0.00, 0.00)
alpha_EleFake_stat_TWOmuCR3	(−0.01, 0.01)	(−0.00, 0.00)	(0.00, −0.00)	(−0.01, 0.01)	(−0.00, 0.00)
alpha_EleFake_syst_ONEmuCR3	(−0.02, 0.02)	(−0.02, −0.02)	(0.01, −0.01)	(−0.00, −0.00)	(0.11, 0.00)
alpha_EleFake_syst_SR3	(1.06, −1.06)	(0.00, 0.00)	(0.00, 0.00)	(0.00, 0.00)	(0.00, 0.00)
alpha_EleFake_syst_TWOeleCR3	(−0.01, 0.01)	(−0.00, 0.00)	(−0.01, 0.02)	(0.02, −0.02)	(0.00, 0.00)
alpha_EleFake_syst_TWOmuCR3	(−0.01, 0.01)	(−0.00, 0.00)	(0.01, −0.01)	(−0.01, 0.01)	(−0.00, 0.00)
alpha_JER	(−0.38, 0.28)	(−0.08, −0.02)	(−0.03, 0.04)	(0.01, −0.04)	(4.62, −9.45)
alpha_JES	(−1.44, −0.35)	(−0.01, −0.00)	(−0.72, 0.44)	(0.77, −0.50)	(0.86, −3.39)
alpha_JVT_EFF	(0.03, −0.04)	(−0.01, −0.01)	(0.01, −0.02)	(−0.06, 0.06)	(−0.08, 0.07)
alpha_JetFake_statCR_ONEmuCR3	(−0.25, 0.35)	(−0.02, −0.03)	(0.03, 0.08)	(0.04, 0.09)	(−0.01, −0.02)
alpha_JetFake_statCR_SR3	(1.61, −1.61)	(0.00, 0.00)	(0.00, 0.00)	(0.00, 0.00)	(0.00, 0.00)
alpha_JetFake_statCR_TWOeleCR3	(−0.89, 1.56)	(0.01, −0.01)	(−1.01, 1.73)	(1.36, −2.21)	(0.00, −0.00)
alpha_JetFake_statCR_TWOmuCR3	(−1.80, 1.91)	(−0.01, 0.00)	(1.36, −1.33)	(−1.70, 1.80)	(0.10, −0.02)
alpha_LUMI_SYST	(−0.07, −0.03)	(0.03, −0.02)	(−0.10, 0.00)	(−0.08, −0.03)	(2.49, −2.75)
alpha_MET_RESO_PARA	(−0.32, 0.34)	(−0.01, 0.01)	(0.09, −0.02)	(−0.12, 0.10)	(−2.38, 2.39)
alpha_MET_RESO_PERP	(−0.58, 0.54)	(−0.02, −0.02)	(0.23, −0.22)	(−0.27, 0.26)	(−8.13, 4.38)
alpha_MET_SCALE	(−0.30, −0.24)	(−0.02, −0.01)	(0.10, 0.01)	(−0.09, −0.07)	(−10.11, 4.90)
alpha_MU_EFF_STAT	(−0.04, 0.20)	(0.01, −0.02)	(0.08, −0.20)	(−0.11, 0.23)	(−0.07, 0.07)
alpha_MU_EFF_SYST	(−1.25, −0.00)	(−0.03, −0.03)	(0.93, 0.01)	(−1.13, 0.00)	(−0.10, 0.01)
alpha_MU_EFF_SYST_LOWPT	(0.01, 0.15)	(−0.01, −0.02)	(0.02, −0.15)	(−0.08, 0.18)	(−0.08, 0.08)
alpha_MU_ID	(−0.05, 0.07)	(−0.04, 0.00)	(0.03, −0.11)	(−0.08, 0.14)	(−0.11, −0.06)
alpha_MU_ISO_STAT	(−0.06, 0.31)	(−0.03, −0.02)	(0.21, −0.25)	(−0.12, 0.31)	(−0.17, 0.08)
alpha_MU_ISO_SYST	(−0.23, 0.53)	(−0.02, −0.02)	(0.41, −0.39)	(−0.27, 0.50)	(−0.16, 0.08)
alpha_MU_MS	(0.01, 0.18)	(−0.01, −0.02)	(0.01, −0.20)	(−0.07, 0.19)	(−0.07, −0.09)
alpha_MU_SCALE	(0.01, 0.16)	(−0.01, −0.02)	(0.03, −0.15)	(−0.09, 0.18)	(−0.08, −0.07)
alpha_MU_TTVA_STAT	(0.00, 0.16)	(−0.01, −0.02)	(0.03, −0.15)	(−0.09, 0.19)	(−0.07, 0.08)
alpha_MU_TTVA_SYS	(−0.05, 0.21)	(0.00, −0.03)	(0.09, −0.20)	(−0.12, 0.24)	(−0.07, 0.07)
alpha_PDF_Comb	(−0.00, 0.04)	(−0.02, −0.04)	(0.01, 0.04)	(0.01, 0.02)	(0.17, −0.29)
alpha_PH_EFF	(0.05, 0.09)	(−0.03, −0.03)	(0.08, 0.05)	(0.03, −0.08)	(−1.05, 1.26)
alpha_PH_EFF_TRKISO	(0.03, −0.04)	(−0.01, −0.01)	(0.01, −0.02)	(−0.06, 0.06)	(−0.08, 0.07)
alpha_PH_ISO_DD	(0.03, −0.04)	(−0.01, −0.01)	(0.01, −0.02)	(−0.06, 0.06)	(−0.08, 0.07)
alpha_PRW_DATASF	(−0.93, 0.50)	(−0.01, −0.00)	(0.50, −0.11)	(−0.67, 0.17)	(3.69, −4.45)
alpha_syst_JetFake_ONEmuCR3	(−0.45, 0.32)	(0.02, 0.02)	(−0.10, −0.05)	(−0.13, −0.04)	(−0.03, −0.01)
alpha_syst_JetFake_SR3	(3.30, −3.30)	(0.00, 0.00)	(0.00, 0.00)	(0.00, 0.00)	(0.00, 0.00)
alpha_syst_JetFake_TWOeleCR3	(−1.90, 2.28)	(−0.01, −0.05)	(−2.13, 2.55)	(3.09, −3.25)	(−0.08, −0.01)
alpha_syst_JetFake_TWOmuCR3	(−1.67, 1.76)	(−0.01, −0.01)	(1.26, −1.21)	(−1.58, 1.66)	(0.10, −0.01)
alpha_syst_PhJet_shape_SR3	(−0.27, 0.27)	(0.00, 0.00)	(0.00, 0.00)	(0.00, 0.00)	(0.00, 0.00)
Systematic	SR	CR1mu	CR2mu	CR2e	CRgjet

Table 37: Breakdown of the dominant systematic uncertainties expressed in % on background estimates after the simplified shape fit in the exclusive SR defined by $E_{\mathrm{T}}^{\mathrm{miss}} > 300$ GeV and its CRs for an integrated luminosity of 36.4 fb^{-1}. Note that the individual uncertainties can be correlated, and do not necessarily add up quadratically to the total background uncertainty.

8 Interpretations

The expected signal yields in 34.6 fb^{-1}of data in each of the inclusive $E_{\mathrm{T}}^{\mathrm{miss}}$ bin is given in Table 38.

Model			$E_{\mathrm{T}}^{\mathrm{miss}}$> 150 GeV	$E_{\mathrm{T}}^{\mathrm{miss}}$> 225 GeV	$E_{\mathrm{T}}^{\mathrm{miss}}$> 300 GeV
ADD	n	M_D [TeV]			
303004	2	2	863.435	554.244	345.819
303005	3	2	1235.71	832.991	560.573
303006	4	2	2100.24	1451.61	948.463
303007	5	2	3713.13	2524.73	1683.47
303008	6	2	7479.85	5271.73	3541.88
303009	2	3	177.312	115.103	73.0536
303010	3	3	162.767	107.473	69.8441
303011	4	3	182.989	128.455	84.9328
303012	5	3	221.2	152.365	101.019
303013	6	3	296.667	202.666	133.269
DM EFT	m_χ [GeV]				
303643	1		0.0219944	0.0205015	0.0182796
303644	10		0.022395	0.0208804	0.0188487
303645	50		0.0215444	0.0200772	0.0181021
303646	100		0.0201204	0.0189617	0.0173907
303647	200		0.0165063	0.0157639	0.0145373
303648	400		0.00938113	0.00908215	0.00858295
303649	800		0.00260216	0.00254742	0.00246363
303650	1300		0.000471596	0.00046376	0.00045048
DM simplified (NLO)	m_χ [GeV]	m_{med} [GeV]			
306618	10	10	485.766	172.56	62.215
306619	10	15	529.172	186.33	68.7737
306620	10	25	3488.84	1105.29	359.906
306621	10	100	6102.48	2046.61	680.378
306622	10	200	4329.06	1644.81	638.095
306623	10	300	2805.97	1175.52	491.22
306624	10	400	1962.65	901.211	395.952
306625	10	500	1294.33	616.111	282.098
306626	10	600	926.572	477.045	231.271
306627	10	700	646.201	341.143	171.212
306628	10	800	459.998	254.973	131.298
306629	10	900	345.194	197.081	105.029
306630	10	1000	252.035	144.063	77.6118
306631	10	1100	188.436	109.947	59.9852
306632	10	1200	136.856	81.7788	46.8677
306633	100	10	47.4093	22.366	10.1282
306634	100	100	55.5265	25.5687	11.8112
306635	100	195	127.474	54.5933	23.2171
306636	100	200	164.684	69.7679	29.3818
306637	100	205	255.975	104.332	42.9579
306638	100	215	537.413	219.13	89.5083
306649	150	200	29.9359	14.9196	7.12482
306650	150	295	76.3036	35.7032	16.2611
306651	150	300	92.8102	43.1237	19.3378
306652	150	305	125.125	57.453	25.0627
306653	150	315	238.873	106.744	46.6473
306663	200	395	45.6419	23.0757	10.8931
306664	200	400	54.4843	26.8321	12.7909
306665	200	405	70.8709	35.0532	16.1476
306666	200	415	120.425	57.7834	26.5593
306676	25	45	367.813	136.826	50.6944
306677	250	515	64.5875	33.1704	16.1299
306685	300	615	38.8657	21.1602	10.6159
306692	50	10	124.574	51.6864	21.6064
306693	50	95	244.172	93.8803	36.6605
306694	50	100	326.783	124.939	46.4069
306695	50	115	655.292	234.413	89.5179

Table 38: Expected yields for 36.4 fb^{-1} for the various signal samples considered and the three inclusive signal regions.

8.1 Model-independent limit

The number of selected events coming from a potential new physics process of cross-section σ is $N_{\mathrm{new}} = L \times \sigma \times A \times \epsilon$, where L is the integrated luminosity and $A \times \epsilon$ is the product of the acceptance and efficiency of the selection criteria. Without any hypothesis on the model of new physics, a limit on the visible cross–section $\sigma \times A \times \epsilon$ is computed. The expected (in absence of new physics) and observed 95% confidence level (CL) limits on $\sigma \times A \times \epsilon = N_{\mathrm{new}}^{\mathrm{lim}}/L$ are shown in Table 39.

$\sigma \times A \times \epsilon$ limit [fb]	$E_{\mathrm{T}}^{\mathrm{miss}}$> 150 GeV	$E_{\mathrm{T}}^{\mathrm{miss}}$> 225 GeV	$E_{\mathrm{T}}^{\mathrm{miss}}$> 300 GeV
95% CL, observed	5.91	2.73	1.45
95% CL, expected ($\pm 1\sigma$)	8.87(12.18, 6.48)	3.31(4.56,2.41)	1.95 (2.66, 1.44)

Table 39: The observed and expected limit at 95% confidence level on the visible cross-section $\sigma \times A \times \epsilon$. The expected limits at $\pm 1\sigma$ are also reported.

8.2 Fiducial limit ($\sigma \times A$)

In order to provide useful constraints on new physics which can be re-interpreted in terms of signal models not covered here, a fiducial region is defined at truth particle level; this region corresponds to the signal region selection.

- photon selection: $E_{T,\gamma} > 10$ GeV, $|\eta_\gamma| < 2.37$, not in $1.37 < |\eta_\gamma| < 1.52$
- electron selection: $p_{T,e} > 7$ GeV, $|\eta_e| < 2.47$
- muon selection: $p_{T,\mu} > 6$ GeV, $|\eta_\mu| < 2.5$
- jet selection: $p_{T,jet} > 30$ GeV, $|\eta_{jet}| < 4.5$, not overlapping with electron or photon by $\Delta R > 0.4$
- $E_{\mathrm{T}}^{\mathrm{miss}} > 150$ GeV, $E_{\mathrm{T}}^{\mathrm{miss}} > 225$ GeV , or $E_{\mathrm{T}}^{\mathrm{miss}} > 300$ GeV depending on the inclusive signal region
- leading photon with $E_T > 150$ GeV, $\Delta\phi(\gamma, E_{\mathrm{T}}^{\mathrm{miss}}) > 0.4$
- $E_{\mathrm{T}}^{\mathrm{miss}} / \sqrt{\Sigma E_T} > 8.5$ GeV $^{1/2}$
- No electron, no muon, $N_{jets} <= 1$, $\Delta\phi(jet, E_{\mathrm{T}}^{\mathrm{miss}}) > 0.4$ if any.

The total signal efficiency can be decomposed into fiducial acceptance and fiducial reconstruction efficiency.

$$\mathrm{Eff}_{total} = \frac{N_{reco}}{N_{total}} = \mathrm{Acc}_{fiducial} \times \mathrm{Eff}_{fiducial}, \tag{11}$$

$$\mathrm{Acc}_{fiducial} = \frac{N_{fiducial}}{N_{total}}, \tag{12}$$

$$\mathrm{Eff}_{fiducial} = \frac{N_{reco}}{N_{fiducial}}, \tag{13}$$

where N_{total} is the total number of generated events, $N_{fiducial}$ is the number of events passing truth-level fiducial selection and N_{reco} is the number of events passing signal region selection at reconstruction level. $\mathrm{Eff}_{fiducial}$ therefore includes the reconstruction efficiency and the difference between truth-level and reconstruction-level selections. Given $\mathrm{Eff}_{fiducial}$, one can easily convert the visible cross section limit ($\sigma \times A \times \epsilon$) into fiducial cross section limits, which may be used to set constraints on other signals not considered in this analysis.

The efficiency found for the dark matter simplified models can be found in Table 40 for the three inclusive regions. For $E_{\mathrm{T}}^{\mathrm{miss}} > 150$ GeV , > 225 GeV and > 300 GeV it ranges from 84 to 95%, 73 to 86% and 64 to 85%, respectively. The lowest efficiency for each signal region is used in a conservative way to set the fiducial cross section limit.

m_{DM} (GeV)	m_{MED} (GeV)	$\epsilon_{E_{\mathrm{T}}^{\mathrm{miss}}>150\ \mathrm{GeV}}$	$\epsilon_{E_{\mathrm{T}}^{\mathrm{miss}}>225\ \mathrm{GeV}}$	$\epsilon_{E_{\mathrm{T}}^{\mathrm{miss}}>300\ \mathrm{GeV}}$
10	10	0.919	0.754	0.68
50	10	0.902	0.766	0.723
100	10	0.913	0.848	0.85
10	15	0.934	0.775	0.739
10	25	0.952	0.765	0.641
25	45	0.896	0.814	0.738
50	95	0.904	0.794	0.78
10	100	0.944	0.801	0.687
50	100	0.926	0.801	0.752
50	105	0.888	0.752	0.797
50	115	0.94	0.755	0.687
100	100	0.883	0.803	0.769
100	195	0.876	0.769	0.73
10	200	0.895	0.768	0.804
100	200	0.851	0.749	0.683
150	200	0.875	0.797	0.729
100	205	0.915	0.802	0.788
100	215	0.93	0.855	0.754
150	295	0.872	0.804	0.736
10	300	0.864	0.757	0.74
150	300	0.907	0.782	0.806
150	305	0.873	0.768	0.772
150	315	0.881	0.767	0.763
200	395	0.855	0.745	0.712
10	400	0.893	0.801	0.791
200	400	0.868	0.784	0.796
200	405	0.879	0.816	0.791
200	415	0.866	0.749	0.764
10	500	0.881	0.763	0.69
250	515	0.855	0.768	0.787
10	600	0.904	0.829	0.81
300	615	0.873	0.813	0.777
10	700	0.84	0.781	0.738
10	800	0.85	0.774	0.751
10	900	0.853	0.786	0.799
10	1000	0.845	0.761	0.732
10	1100	0.854	0.774	0.709
10	1200	0.795	0.731	0.711

Table 40: Efficiencies for the dark matter simplified models in the three inclusive signal regions.

$\sigma \times A$ limit [fb]	$E_{\mathrm{T}}^{\mathrm{miss}}>$ 150 GeV	$E_{\mathrm{T}}^{\mathrm{miss}}>$ 225 GeV	$E_{\mathrm{T}}^{\mathrm{miss}}>$ 300 GeV
95% CL, observed	7.04	3.74	2.27
95% CL, expected ($\pm 1\sigma$)	10.6(14.5, 7.7)	4.53 (6.25, 3.30)	3.05(4.16, 2.25)

Table 41: The observed and expected limit at 95% confidence level on the fiducial cross-section $\sigma \times A$. The expected limits at $\pm 1\sigma$ are also reported.

8.3 Interpretation in the Dark Matter Models

The results shown in 6.2 are interpreted in the context of two dark matter models described in Sec. 2.1.1: the Simplified Model and a dimension-7 operator EFT model with contact interaction of type $\gamma\gamma\chi\chi$.

8.3.1 Signal systematic uncertainties

The PDF and scale uncertainties on the cross section and the acceptance for the dark-matted simplified model are reported in Table 42. The PDF uncertainty is taken from the envelope of the 100 variations of the NNPDF30_nlo_as0118 set, the variations of this set to alternative α_s values (0.115, 0.117, 0.119 and 0.121) and also the difference to the other PDF sets MMHT2014nlo68cl and CT14nlo. The factorization and renormalization scales are independently varied by a factor of 2 up and down; the scale uncertainty is taken as the largest deviation amongst these 8 variations. Table 43 reports the uncertainties coming from the choice of Pythia8 tune, using the official variations[17], which cover different aspect of extra jet production and jet structure effects.

The PDF, scale and tune uncertainties described above are included in the fit (and hence in the limit setting) when they affect the signal acceptance - the uncertainties affecting the cross section are not included in the fit.

Table 44 reports the computed PDF uncertainties on the acceptance for the EW EFT model. In this case, the PDF sets considered at NNPDF30_lo_as_0130, MMHT2014lo69cl and CT14nlo. The factorization and renormalization scale uncertainties are also reported in this Table; they are obtained by varying the scales up and down by a factor of two. The Table also reports the uncertainties coming from the choice of Pythia8 tune.

All the experimental uncertainties on the prediction, including a trigger efficiency uncertainty of 1%, are included when deriving limits on specific models.

8.3.2 Limits

The analysis strategy chosen to extract limits on physics models has been studied comparing expected limits from single bin fit from various inclusive regions and from the simplified shape fit. All checks are reported in Appendix F, where it is shown that the simplified shape fit allows to set better expected limits than any of the inclusive signal regions. It will thus be adopted to set model-dependent limits.

For the simplified model with an axial-vector mediator, Fig. 40 shows the observed and expected contours corresponding to a 95% CL exclusion as a function of m_{med} and m_χ for $g_q = 0.25$ and $g_\chi = 1$. The region of the plane under the limit curves is excluded. The region not allowed due to perturbative unitarity violation is to the left of the line defined by $m_\chi = \sqrt{\pi/2} m_{\text{med}}$. The line corresponding to the DM thermal relic abundance is also indicated in the figure. The search excludes mediator masses below 1200 GeV for χ masses below 340 GeV.

Following LHC Dark Matter Working Group recommendations results for both axial-vector and vector mediators are also presented for different choices of couplings as reported in Appendix G. Fig. 41 shows the observed and expected contours corresponding to a 95% CL exclusion as a function of m_{med} and m_χ with couplings also to leptons: $g_\chi = 1.0$, $g_q = g_\ell = 0.1$. The search excludes mediator masses below 750 GeV for χ masses below 230 GeV. Fig. 42 shows the observed and expected contours corresponding to a 95% CL exclusion as a function of m_{med} and m_χ for a vector mediator with couplings $g_\chi = 1.0$, $g_q = 0.25$, $g_\ell = 0.$. The search excludes mediator masses below 1200 GeV for χ masses below 480 GeV. Finally, Fig. 43 shows the observed and expected contours corresponding to a 95% CL exclusion as a function of m_{med} and m_χ for a vector mediator having also small couplings to leptons: $g_\chi = 1.0$, $g_q = 0.1$, $g_\ell = 0.01$. The search excludes mediator masses below 750 GeV for χ masses below 320 GeV.

[17] https://twiki.cern.ch/twiki/bin/viewauth/AtlasProtected/MCTuningRecommendations

m_{DM}	m_{med}	ΔA^{PDF} (%)			$\Delta\sigma^{PDF}$ (%)	$\Delta A^{\mathrm{scale}}$ (%)			$\Delta\sigma^{\mathrm{scale}}$ (%)
(GeV)	(GeV)	SR1	SR2	SR3		SR1	SR2	SR3	
10	10	1.1	1.0	2.6	3.9	3.1	2.4	3.5	5.0
10	15	0.9	1.3	3.0	3.9	3.4	3.2	2.3	5.4
10	25	1.7	1.9	3.2	3.7	5.5	4.8	5.4	7.3
10	100	0.9	2.3	2.5	4.1	2.5	2.8	2.5	4.3
10	200	0.7	0.9	5.3	4.3	1.2	0.9	1.8	2.9
10	300	0.9	1.4	3.3	4.3	1.1	0.7	0.6	2.9
10	400	0.6	0.7	2.3	4.6	0.7	0.6	0.5	3.0
10	500	0.8	0.8	1.5	4.7	1.1	0.8	0.6	2.5
10	600	1.4	2.1	1.3	5.0	0.7	0.6	0.8	2.4
10	700	0.6	2.2	1.1	5.3	0.6	0.4	0.8	2.5
10	800	0.7	0.8	1.0	5.2	0.8	0.3	1.4	2.5
10	900	0.6	0.6	1.2	5.2	0.5	0.4	1.0	2.8
10	1000	1.4	0.5	1.6	5.3	0.9	0.6	0.7	2.3
10	1100	0.5	1.3	1.3	5.4	0.8	0.1	1.2	2.6
10	1200	1.7	2.2	1.3	5.4	0.8	0.2	0.3	2.6
100	10	0.5	0.6	1.7	4.5	1.1	0.3	0.5	2.9
100	100	1.2	1.0	2.4	4.6	1.5	1.1	0.7	2.9
100	195	0.8	0.8	2.7	4.2	1.3	0.3	1.6	2.8
100	200	1.1	1.3	2.1	4.3	0.8	0.6	1.0	3.3
100	205	0.6	1.1	2.4	4.3	1.6	0.5	2.0	3.3
100	215	0.7	0.9	1.6	4.3	1.8	1.1	1.8	2.9
150	200	0.7	0.8	1.8	4.8	1.7	0.3	1.4	2.8
150	295	0.6	3.0	1.7	4.7	0.8	1.3	1.4	2.8
150	300	1.1	1.1	1.8	4.5	1.3	0.2	1.1	2.7
150	305	0.9	1.1	1.7	4.7	1.0	0.5	0.2	2.7
150	315	0.5	0.7	1.8	4.5	1.4	0.7	2.1	3.1
200	395	0.8	1.0	1.8	4.9	0.8	0.7	1.6	2.4
200	400	1.3	1.2	1.6	4.7	1.3	0.4	1.0	2.7
200	405	1.0	0.5	1.8	4.8	0.5	0.7	0.9	2.7
200	415	1.4	0.8	2.5	4.8	1.3	0.6	0.9	2.5
25	10	0.7	1.2	3.2	4.2	2.3	1.7	1.7	4.1
25	45	0.7	1.2	2.1	4.0	2.3	1.9	1.6	4.0
250	515	0.4	0.9	1.7	4.9	1.0	0.5	1.0	2.4
300	615	2.4	1.0	1.4	5.3	1.3	1.2	0.7	2.8
50	10	0.7	1.0	2.0	4.2	2.2	1.2	1.1	3.3
50	95	0.6	0.8	2.5	4.1	1.6	1.3	2.4	3.5
50	100	0.8	1.3	2.3	4.0	2.1	1.7	2.5	3.5
50	105	0.8	1.9	2.0	4.1	2.0	1.3	1.5	4.2
50	115	0.8	1.1	2.6	4.0	2.7	1.7	3.1	3.9

Table 42: Effect of the PDF and scale uncertainties, in %, on the acceptance and the cross section of simplified dark matter models.

The limits for the model A1 are largely improved with respect to the limits obtained with the 2015 data only [2] that excluded mediator masses below 710 GeV for χ masses below 150 GeV.

Figure 44 shows the observed exclusion on the χ-proton cross section, where the plane on the left side of the black curve is excluded. Bounds on the χ-proton cross section are obtained following the procedure and equations described in Ref. [47]. The spin-dependent results (axial-vector mediator) are compared with the 90% CL exclusion curves from PICO-60 [48], PICO-2L [49] and LUX [50], while the spin-independent results (vector mediator) are compared with the 90% CL exclusion curves from PandaX [51], LUX [52], CDMS [53] , CRESST [54]. LHC allows to complement the limits on the χ-proton scattering cross section in the low DM mass region where the direct DM search experiments have less sensitivity due to the very low-energy recoils that such low-mass dark matter particles would induce.

Figure 45 shows the observed and expected 95% CL limit on suppression scale M_* for a dimension-7 operator EFT model with contact interaction of type $\gamma\gamma\chi\chi$ at different m_χ points. The search excludes model values of M_* up to about 790 GeV, which is a more stringent limit than the one placed in earlier searches [2].

m_{DM} (GeV)	m_{med} (GeV)	ΔA^{Tune} (%) SR1	SR2	SR3
10	10	4.8	2.3	4.7
10	15	4.2	3.6	9.4
10	25	4.7	5.0	3.4
10	100	5.1	2.3	7.8
10	200	4.1	4.4	7.3
10	300	4.5	5.1	5.2
10	400	4.3	2.7	1.3
10	500	4.3	2.7	4.1
10	600	5.6	3.0	5.6
10	700	3.1	1.9	2.4
10	800	5.0	3.0	2.0
10	900	5.4	3.6	3.3
10	1000	5.5	5.1	5.2
10	1100	5.3	3.2	3.6
10	1200	4.9	3.7	4.0
100	10	6.3	3.4	4.3
100	100	4.2	2.7	3.1
100	195	4.6	3.5	4.9
100	200	5.4	3.7	4.7
100	205	5.4	4.2	3.0
100	215	5.2	3.5	6.6
150	200	6.4	4.7	5.5
150	295	4.4	2.8	1.9
150	300	5.7	2.6	1.9
150	305	5.4	3.6	6.1
150	315	4.0	1.9	2.2
200	395	4.7	1.0	1.4
200	400	4.6	1.5	3.1
200	405	4.6	2.5	1.3
200	415	4.5	3.9	3.9
25	10	4.0	2.7	1.4
25	45	4.8	2.6	4.1
250	515	4.7	4.6	5.8
300	615	3.9	2.9	3.4
50	10	3.4	1.9	3.3
50	95	3.8	3.2	6.1
50	100	6.9	3.4	3.1
50	105	6.3	2.7	5.5
50	115	5.7	2.6	3.9

Table 43: Effect of the tune uncertainties, in %, on the acceptance of simplified dark matter models.

The EFT is not always valid and a truncation procedure is applied, as done in the 2015 analysis [2], following the procedure described in Ref. [55]. In this procedure, the scale at which the EFT description becomes invalid, M_{cut} , is assumed to be related to M_* through $M_{\text{cut}} = g^* M_*$, where g^* is the EFT coupling.

For a given g^* and m_χ the truncation procedure proceeds as a scan over M_{cut}; for each value of M_{cut}:

- the fraction f of valid events is computed, where a valid event is one for which $\sqrt{\hat{s}} < M_{\text{cut}}$.
- the visible cross section is computed as $\sigma(M_{\text{cut}}) = \sigma_0 \times f(\sqrt{\hat{s}} < M_{\text{cut}}) \times (g^* \times M_0/M_{\text{cut}})^6$, where σ_0 and M_0 are the cross section and suppression scale corresponding to the original MC sample
- the visible cross section obtained is compared to the excluded cross section; if $\sigma(M_{\text{cut}}) > \sigma_{\text{excluded}}$, then this M_{cut} value is excluded.
- Using the assumed relationship $M_{\text{cut}} = g^* \times M_*$, this can be translated into an exclusion on M_*.

Figure 45 shows the effect of truncation, applying the procedure described, for two representative values of g^* : if one assumes the maximal coupling value of 4π, the nominal limit is mostly valid, while

m_{DM} (GeV)	ΔA^{tune}	ΔA^{scale}	ΔA^{PDF}
1	5,0	0,3	18,1
10	5,6	1,5	6,4
50	3,4	1,0	6,3
100	4,2	0,2	6,2
200	4,2	0,7	4,4
400	4,9	1,3	10,0
800	4,3	1,0	10,1
1300	4,7	0,1	1,1

Table 44: Tune, scale and PDF uncertainties, in %, on the acceptance of the EW EFT dark matter models, in % for the signal region with $E_{\text{T}}^{\text{miss}} > 300$GeV which contains most of the signal events for this model.

for lower coupling values (e.g. 3), the exclusion limits are confined to smaller area of the parameter space. For even lower coupling values (e.g. 1), no exclusion can be set.

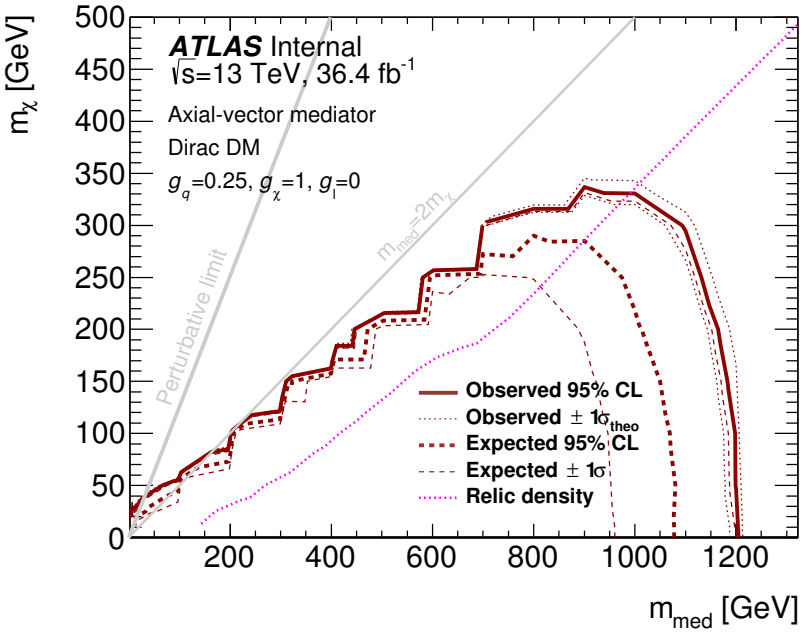

Figure 40: The observed and expected 95% CL exclusion limit for a simplified model of dark matter production involving an axial-vector operator, Dirac DM and couplings $g_q = 0.25$, $g_\chi = 1$ and $g_\ell = 0$ as a function of the dark matter mass m_χ. The plane under the limit curve is excluded.

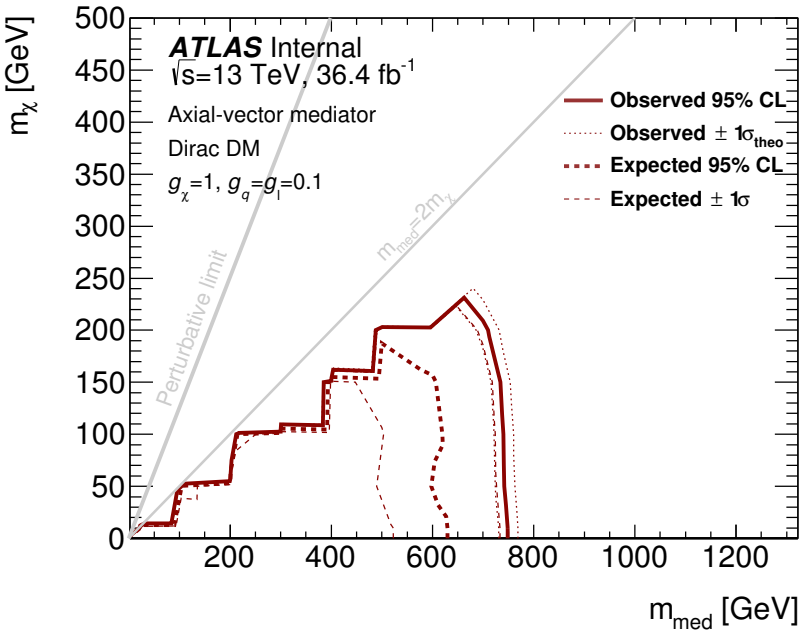

Figure 41: The observed and expected 95% CL exclusion limit for a simplified model of dark matter production involving an axial-vector operator, Dirac DM and with also couplings to leptons: $g_\chi = 1.0$, $g_q = g_\ell = 0.1$ as a function of the dark matter mass m_χ. The plane under the limit curve is excluded.

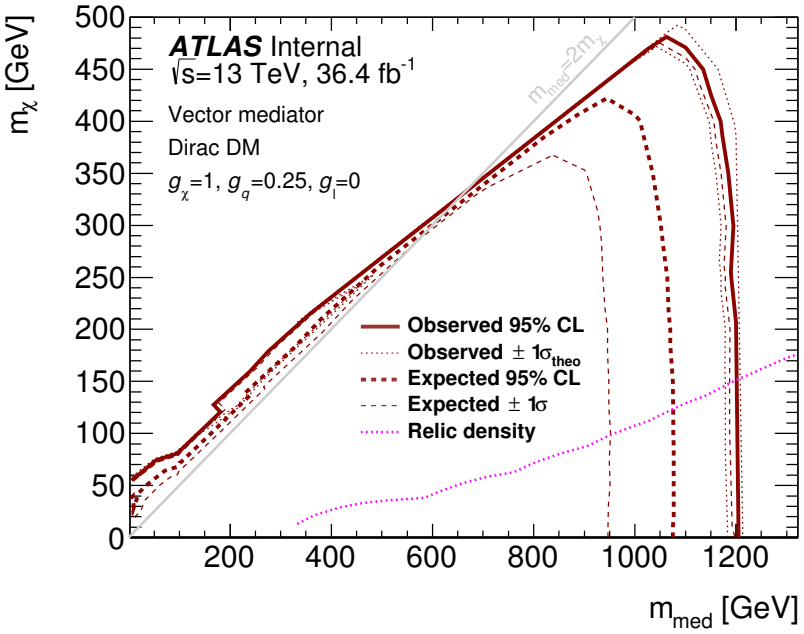

Figure 42: The observed and expected 95% CL exclusion limit for a simplified model of dark matter production involving a vector operator, Dirac DM and with also couplings to leptons: $g_\chi = 1.0$, $g_q = 0.25$, $g_\ell = 0.$ as a function of the dark matter mass m_χ. The plane under the limit curve is excluded.

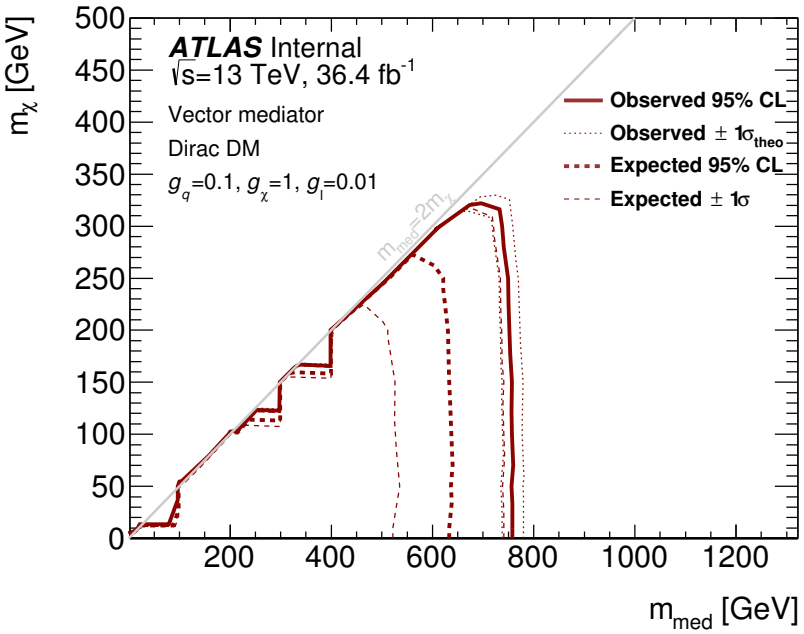

Figure 43: The observed and expected 95% CL exclusion limit for a simplified model of dark matter production involving a vector operator, Dirac DM and with also couplings to leptons: $g_\chi = 1.0$, $g_q = 0.1$, $g_\ell = 0.01$ as a function of the dark matter mass m_χ. The plane under the limit curve is excluded.

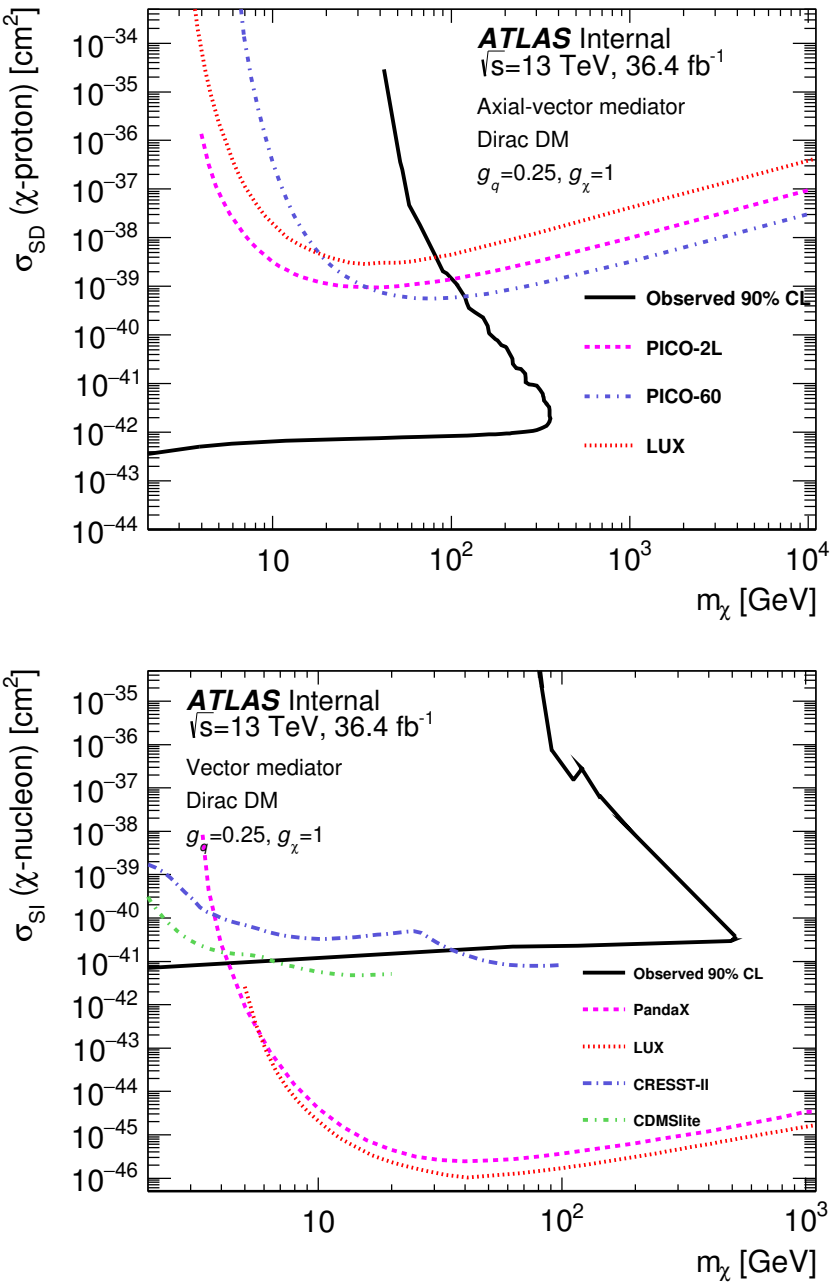

Figure 44: The 90% CL exclusion limit on the on the χ–proton scattering cross section as a function of the dark matter mass m_χ for spin-dependent interaction for the axial-vector mediator (top) and spin-independent interaction with the vector mediator V1 (bottom). The plane on the left of the black curve is excluded.

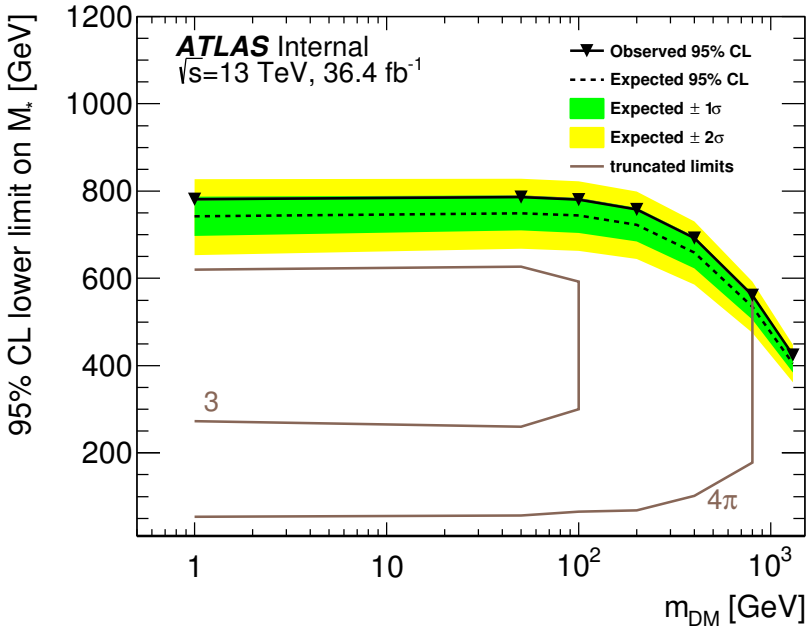

Figure 45: The observed and expected 95% CL limits on M_* for a dimension-7 operator EFT model with contact interaction of type $\gamma\gamma\chi\chi$ at different m_χ points for 36.4 fb^{-1}. Results where EFT truncation is applied are also shown, assuming representative coupling values of 3 and 4π.

8.4 Interpretation in terms of a $Z\gamma$ resonance

The results are also interpreted in terms of a limit on the cross section for the production of a narrow resonance X times the branching ratio of its decay to $Z\gamma$, as described in Section 2.1.3.

The limit is produced in exactly the same way as for the other signal samples, that is looking for an excess of events in the three exclusive signal regions by using the multiple-bin fit. Contrarly to the analyses looking for $X \to Z(\to \ell\ell)\gamma$ or $X \to Z(q\bar{q})\gamma$, the analysis here does not scan for a bump over the falling background spectrum, but merely for an excess in the signal regions. The heavy resonances will mainly populate the $E_{\mathrm{T}}^{\mathrm{miss}} > 300$ GeV signal region as they tend to have a very hard $E_{\mathrm{T}}^{\mathrm{miss}}$ spectrum.

The theoretical uncertainties due to scales and tune variations are reported in Table 45. The PDF uncertainties, calculated as explained in Section 7.1.1, are shown in Table 46.

m_{res} (GeV)	ΔA (%)		
	SR1	SR2	SR3
1000	0.9	0.9	1.3
2000	3.5	3.4	3.4
2500	1.0	1.1	1.0
3000	1.6	1.6	1.7
3500	1.0	1.0	1.0
4000	0.4	0.4	0.4
4500	1.4	1.4	1.4
5000	0.8	0.8	0.8

Table 45: Theoretical uncertainties, in %, on the acceptance for the $Z\gamma$ resonance models, computed by varying the scale and tune parameters.

As mentioned in Section 2.1.3, the sample with a mass of 1 TeV is only generated with the $Z \to \nu\nu$ decay switched on (the other points contain all possible Z decays); its possible signal contamination in the CRs cannot be properly assessed. A complementary sample where $Z \to \ell\ell$ is being processed, but for the moment, the limit will be drawn starting from 2 TeV , see Fig. 46.

Process	ΔA
$ggH1000$	$(+13.3\% - 13.3\%)$
$ggH2000$	$(+6.1\% - 6.1\%)$
$ggH2500$	$(+8.2\% - 8,2\%)$
$ggH3000$	$(+10.7\% - 10.7\%)$
$ggH3500$	$(+13.7\% - 13.7\%)$
$ggH4000$	$(+22.1\% - 22.1\%)$
$ggH4500$	$(+30.2\% - 30.2\%)$
$ggH5000$	$(+33.3\% - 33.3\%)$

Table 46: Computed PDF uncertainty in percentage on the event yields for the $Z\gamma$ samples

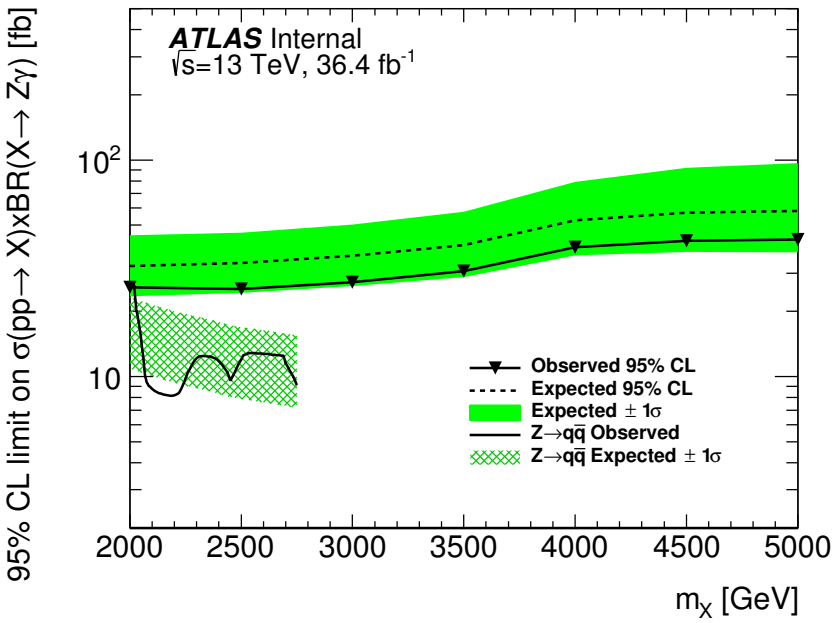

Figure 46: The observed and expected 95% CL limits on the production cross section of a narrow resonance X decaying to $Z\gamma$ for 36.4 fb^{-1}.

9 Conclusions

A search was performed for new phenomena in events with a high-p_{T} photon and large missing transverse momentum in pp collisions at $\sqrt{s}$ = 13 TeV at the LHC, using data collected by the ATLAS experiment in 2015 and 2016 corresponding to an integrated luminosity of 36.4 fb^{-1}.

The observed data are well consistent with Standard Model expectations. The observed (expected) upper limits on the fiducial cross section for the production of events with a photon and large missing transverse momentum are 7.0/2.3(10.6/3.0) fb at 95% CL for $E_{\mathrm{T}}^{\mathrm{miss}}$ thresholds of 150 GeV. For the simplified DM model considered, the search excludes masses below 1200 GeV for an axial-vector (vector) mediator for χ masses below 340/480 GeV. For the EW-EFT model values of M_* up to 790 GeV are excluded and the effect of truncation for various coupling values is reported. The observed (expected) limit at 95% CL on the production of a $Z\gamma$ resonance is provided for masses of 2000/5000 GeV.

References

[1] ATLAS Collaboration, *The ATLAS Experiment at the CERN Large Hadron Collider*, JINST **3** (2008) .

[2] ATLAS Collaboration, ATLAS Collaboration, *Search for new phenomena in events with a photon and missing transverse momentum in pp collisions at $\sqrt{s}$ = 13 TeV with the ATLAS detector*, JHEP (2016) , arXiv:1604.01306 [hep-ex].

[3] A. Martin, W. Stirling, R. Thorne, and G. Watt, *Parton distributions for the LHC*, Eur.Phys.J. **C63** (2009) 189–285, arXiv:0901.0002 [hep-ph].

[4] ATLAS Collaboration, *Further ATLAS tunes of Pythia 6 and Pythia 8*, ATL-PHYS-PUB-2011-014 (2011) , https://cds.cern.ch/record/1400677.

[5] D. Abercrombie et al., *Dark Matter Benchmark Models for Early LHC Run-2 Searches: Report of the ATLAS/CMS Dark Matter Forum*, arXiv:1507.00966 [hep-ex].

[6] N. Arkani-Hamed, S. Dimopoulos, and G. Dvali, *The Hierarchy problem and new dimensions at a millimeter*, Phys. Lett. B **429** (1998) 263–272, arXiv:hep-ph/9803315 [hep-ph].

[7] *ATLAS Run 1 Pythia8 tunes*, Tech. Rep. ATL-PHYS-PUB-2014-021, CERN, Geneva, Nov, 2014. http://cds.cern.ch/record/1966419.

[8] NNPDF Collaboration, R. D. Ball, V. Bertone, S. Carrazza, L. Del Debbio, S. Forte, A. Guffanti, N. P. Hartland, and J. Rojo, *Parton distributions with QED corrections*, Nucl. Phys. **B877** (2013) 290–320, arXiv:1308.0598 [hep-ph].

[9] S. Ask, *Simulation of Z plus Graviton/Unparticle Production at the LHC*, Eur. Phys. J. **C60** (2009) 509–516, arXiv:0809.4750 [hep-ph].

[10] ATLAS, *Recommendations for MC tunes: systematic uncertainties and non-pQCD corrections*, tech. rep., CERN, Geneva, July, 2015. https://twiki.cern.ch/twiki/bin/view/AtlasProtected/MCTuningRecommendations#Prescription_to_estimate_PS_and.

[11] ATLAS Collaboration, ATLAS Collaboration, *Search for heavy resonances decaying to a Z boson and a photon in pp collisions at $\sqrt{=}$13 TeV with the ATLAS detector*, arXiv:1607.06363 [hep-ex].

[12] T. Gleisberg et al., *Event generation with SHERPA 1.1*, J. High Energy Phys. **02** (2009) 007, arXiv:0811.4622 [hep-ph].

[13] S. Schumann and F. Krauss, *A Parton shower algorithm based on Catani-Seymour dipole factorisation*, JHEP **03** (2008) 038, arXiv:0709.1027 [hep-ph].

[14] S. Höche, F. Krauss, S. Schumann, and F. Siegert, *QCD matrix elements and truncated showers*, JHEP **05** (2009) 053, arXiv:0903.1219 [hep-ph].

[15] H.-L. Lai et al., *New parton distributions for collider physics*, Phys. Rev. D **82** (2010) 074024, arXiv:1007.2241 [hep-ph].

[16] T. Gleisberg and S. Höche, *Comix, a new matrix element generator*, JHEP **12** (2008) 039, arXiv:0808.3674 [hep-ph].

[17] F. Cascioli, P. Maierhofer, and S. Pozzorini, *Scattering Amplitudes with Open Loops*, Phys. Rev. Lett. **108** (2012) 111601, arXiv:1111.5206 [hep-ph].

[18] S. Höche, F. Krauss, M. Schönherr, and F. Siegert, *QCD matrix elements + parton showers: The NLO case*, JHEP **04** (2013) 027, arXiv:1207.5030 [hep-ph].

[19] D. J. Lange, *The EvtGen particle decay simulation package*, Nucl. Instrum. Meth. A **462** (2001) 152.

[20] S. Alioli, P. Nason, C. Oleari, and E. Re, *A general framework for implementing NLO calculations in shower Monte Carlo programs: the POWHEG BOX*, JHEP **06** (2010) 043, arXiv:1002.2581 [hep-ph].

[21] S. Alioli, P. Nason, C. Oleari, and E. Re, *NLO single-top production matched with shower in POWHEG: s- and t-channel contributions*, JHEP **09** (2009) 111, arXiv:0907.4076 [hep-ph]. [Erratum: JHEP02,011(2010)].

[22] P. Artoisenet, R. Frederix, O. Mattelaer, and R. Rietkerk, *Automatic spin-entangled decays of heavy resonances in Monte Carlo simulations*, JHEP **03** (2013) 015, arXiv:1212.3460 [hep-ph].

[23] T. Sjostrand, S. Mrenna, and P. Skands, *PYTHIA 6.4 physics and manual*, J. High Energy Phys. **05** (2006) 026, arXiv:hep-ph/0603175.

[24] J. Pumplin et al., *New generation of parton distributions with uncertainties from global QCD analysis*, J. High Energy Phys. **07** (2002) 012, arXiv:hep-ph/0201195 [hep-ph].

[25] P. Z. Skands, *Tuning Monte Carlo Generators: The Perugia Tunes*, Phys. Rev. D **82** (2010) 074018, arXiv:1005.3457 [hep-ph].

[26] ATLAS Collaboration, *Electron and photon reconstruction and identification in ATLAS: expected performance at high energy and results at 900 GeV*, ATLAS-CONF-2010-005 (2010) . http://cdsweb.cern.ch/record/1273197.

[27] C. Anastopoulos, L. Aperio Bella, M. F. Bessner, P. G. Hamnett, G. Marchiori, S. M. Mazza, F. Monticelli, E. Petit, M. Pitt, K. Tackmann, and G. Unal, *Photon identification pre-recommendations for run 2*, Tech. Rep. ATL-COM-PHYS-2015-496, CERN, Geneva, Jun, 2015. https://cds.cern.ch/record/2022342.

[28] ATLAS, *IsolationSelectionTool*, tech. rep., CERN, Geneva, 2015. https://twiki.cern.ch/twiki/bin/view/AtlasProtected/IsolationSelectionTool.

[29] ATLAS Collaboration, *Electron performance measurements with the ATLAS detector using the 2010 LHC proton-proton collision data*, arXiv:1110.3174 [hep-ex].

[30] ATLAS Collaboration, *A measurement of the ATLAS muon reconstruction and trigger efficiency using J/psi decays*, ATLAS-CONF-2011-021 (2011) . http://cdsweb.cern.ch/record/1336750.

[31] ATLAS Collaboration, *Muon reconstruction efficiency in reprocessed 2010 LHC proton-proton collision data recorded with the ATLAS detector*, ATLAS-CONF-2011-063, (2011) . http://cdsweb.cern.ch/record/1345743.

[32] ATLAS Collaboration, *Measurement of the muon reconstruction performance of the ATLAS detector using 2011 and 2012 LHC proton-proton collision data*, arXiv:1407.3935 [hep-ex]. (Submitted to Eur. Phys. J. C).

[33] M. Cacciari, G. P. Salam, and G. Soyez, *The anti-k_t jet clustering algorithm*, J. High Energy Phys. **04** (2008) 063, arXiv:0802.1189 [hep-ph].

[34] M. Cacciari and G. P. Salam, *Dispelling the N^3 myth for the k_t jet-finder*, Phys. Lett. B **641** (2006) 57–61, arXiv:hep-ph/0512210.

[35] ATLAS Collaboration, *Data-driven determination of the energy scale and resolution of jets reconstructed in the ATLAS calorimeters using dijet and multijet events at $\sqrt{s} = 8$ TeV*, . https://cds.cern.ch/record/2008678.

[36] ATLAS Collaboration, *Jet Calibration and Systematic Uncertainties for Jets Reconstructed in the ATLAS Detector at $\sqrt{s} = 13$ TeV*, . https://cds.cern.ch/record/2018215.

[37] ATLAS Collaboration, *Tagging and suppression of pileup jets with the ATLAS detector*, ATLAS-CONF-2014-018, (2012) . https://cds.cern.ch/record/1700870/. http://cdsweb.cern.ch/record/1700870.

[38] N. Makovec and E. Tolley, *Selection of jets produced in proton-proton collisions with the ATLAS detector using 2015 data*, Tech. Rep. ATLAS-COM-CONF-2015-024, CERN, Geneva, May, 2015. https://cds.cern.ch/record/2016323.

[39] ATLAS Collaboration, *Performance of Missing Transverse Momentum Reconstruction in ATLAS studied in Proton-Proton Collisions recorded in 2012 at 8 TeV*, ATLAS-CONF-2013-082, (2013) . http://cdsweb.cern.ch/record/1570993.

[40] ATLAS Collaboration, *Performance of Missing Transverse Momentum Reconstruction in Proton-Proton Collisions at 7 TeV with ATLAS*, Eur. Phys. J. C **72** (2012) 1844, arXiv:1108.5602 [hep-ex].

[41] ATLAS Collaboration, *Expected performance of missing transverse momentum reconstruction for the ATLAS detector at $\sqrt{s} = 13$ TeV*, . https://cds.cern.ch/record/2013489/.

[42] D. Adams and others, *Recommendations of the Physics Objects and Analysis Harmonisation Study Groups 2014*, Tech. Rep. ATLAS-PHYS-INT-2014-018, CERN, Geneva, Jul, 2014.

[43] SUSYTools, *SUSYTools Object Definitions (rel20)*, tech. rep., CERN, Geneva, July, 2015. https://twiki.cern.ch/twiki/bin/viewauth/AtlasProtected/SusyObjectDefinitionsr2013TeV.

[44] ATLAS Collaboration, *Vertex Reconstruction Performance of the ATLAS Detector at $\sqrt{s} = 13$ TeV*, Tech. Rep. ATL-PHYS-PUB-2015-026, July, 2015.

[45] M. Baak et al., *HistFitter software framework for statistical data analysis*, Eur.Phys.J. **C75** (2015) 153, arXiv:1410.1280 [hep-ex].

[46] A. Buckley et al., *LHAPDF6: parton density access in the LHC precision era*, arXiv:1412.7420 [hep-ph].

[47] A. Boveia et al., *Recommendations on presenting LHC searches for missing transverse energy signals using simplified s-channel models of dark matter*, arXiv:1603.04156 [hep-hp].

[48] PICO Collaboration, C. Amole et al., *Dark matter search results from the PICO-60 CF_3I bubble chamber*, Phys. Rev. **D93** (2016) no. 5, 052014, arXiv:1510.07754 [hep-ex].

[49] PICO-2L Collaboration Collaboration, C. Amole and others (PICO-2L Collaboration), *Dark Matter Search Results from the PICO-2L C3F8 Bubble Chamber*, Phys. Rev. Lett. **114** (2015) 231302, arXiv:1503.00008 [astro-ph.CO].

[50] LUX Collaboration, D. S. Akerib et al., *First spin-dependent WIMP-nucleon cross section limits from the LUX experiment*, arXiv:1602.03489 [hep-ex].

[51] PandaX-II Collaboration, A. Tan et al., *Dark Matter Results from First 98.7 Days of Data from the PandaX-II Experiment*, Phys. Rev. Lett. **117** (2016) no. 12, 121303, arXiv:1607.07400 [hep-ex].

[52] LUX Collaboration, D. S. Akerib et al., *Results from a search for dark matter in the complete LUX exposure*, Phys. Rev. Lett. **118** (2017) no. 2, 021303, arXiv:1608.07648 [astro-ph.CO].

[53] CDMS Collaboration Collaboration, Z. Ahmed et al., *Results from a low-energy analysis of the CDMS II Germanium data*, Phys. Rev. Lett. **106** (2011) 131302, arXiv:1011.2482 [astro-ph.CO].

[54] CRESST Collaboration, G. Angloher, et al., *Results on light dark matter particles with a low-threshold CRESST-II detector*, Eur. Phys. J. **C76** (2016) no. 1, 25, arXiv:1509.01515 [astro-ph.CO].

[55] D. Racco, A. Wulzer, F. Zwirner, *Robust collider limits on heavy-mediator Dark Matter*, J. High Energy Phys. **05** (2015) 009, arXiv:1502.04701 [hep-ph].

A $E_{\mathrm{T}}^{\mathrm{miss}}$ studies in γ + jet background

Studies of $E_{\mathrm{T}}^{\mathrm{miss}}$ based on MC samples have shown an anomalous tail in the Track Soft Term (TST) distribution of γ + jet background as shown in Figure 47(a). The problem is related to photons treatment in $E_{\mathrm{T}}^{\mathrm{miss}}$ reconstruction. It can happen, for photons classified as ambiguous, that high p_{T} tracks are not treated as conversions and because they are not associated to any physics object in the event they are added to the TST. This is due to the fact that the track quality requirements for conversions are tighter than the ones adopted for $E_{\mathrm{T}}^{\mathrm{miss}}$ TST, in particular tracks with no pixel hits are not classified as conversion. A fix has been implemented in $E_{\mathrm{T}}^{\mathrm{miss}}$ reconstruction, it flags the tracks associated to electrons overlapping photons so that they are not added to TST calculation. Applying the $E_{\mathrm{T}}^{\mathrm{miss}}$ fix permits to kill the tail in γ + jet events as shown in Figure 47(b). A similar result is obtained applying the recommended track isolation criteria to the leading photon at analysis level: $ptcone20/p_{\mathrm{T}} < 0.05$, as shown in Figure 47(c). This permits to remove events populating the tail of the TST, this criteria becomes ineffective when applied on top of the $E_{\mathrm{T}}^{\mathrm{miss}}$ fix, as shown in Figure 47(d). The track isolation criteria is in any case adopted in 2016 analysis because it permits to reduce the jet and electrons faking photons background as show in Sec. 5.3 and Sec. 5.4.

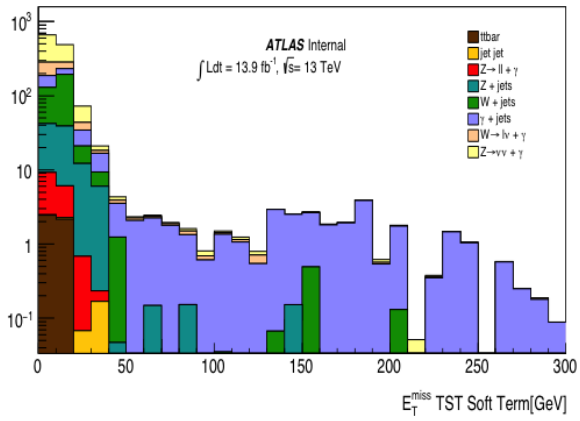

(a) TST before $E_{\mathrm{T}}^{\mathrm{miss}}$ fix

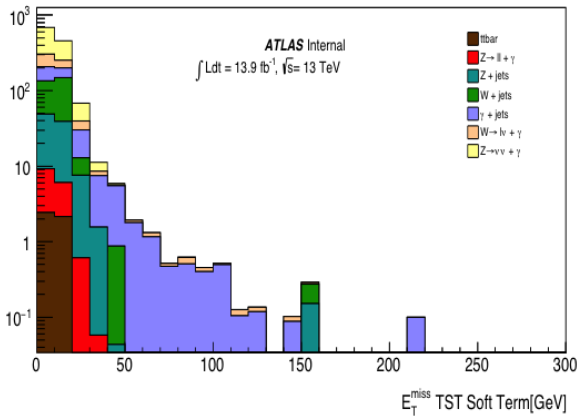

(b) TST after $E_{\mathrm{T}}^{\mathrm{miss}}$ fix

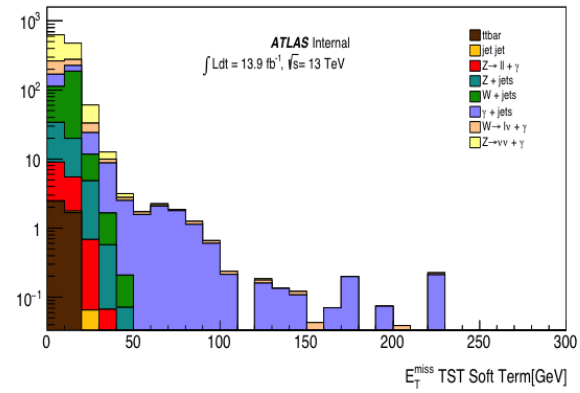

(c) TST before $E_{\mathrm{T}}^{\mathrm{miss}}$ fix adding ptcone20 criteria

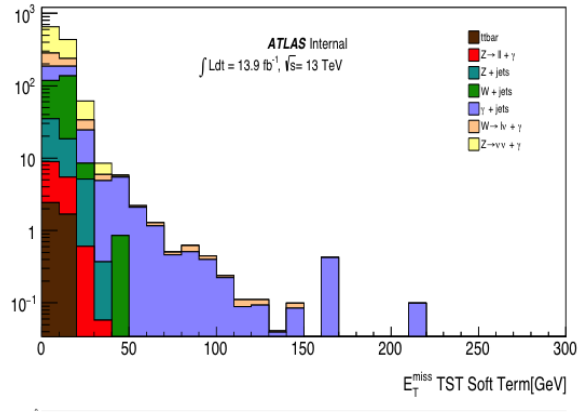

(d) TST after $E_{\mathrm{T}}^{\mathrm{miss}}$ fix adding ptcone20 criteria

Figure 47: Distribution of Track Soft Term (TST) for MC background samples corresponding to an integrated luminosity of 13.9 fb^{-1}.

B Photon Identification Menu

Table 47 reports the list of variables that are used for the identification of loose and tight photons with the description of each variable.

Category	Name	Description	Loose	Tight
Hadronic Leakage	R_{had_1}	Ratio of E_{T} in the first sampling of the hadronic calorimeter to E_{T} of the EM cluster (used over the range $\lvert\eta\rvert < 0.8$ or $\lvert\eta\rvert > 1.37$)	✓	✓
	R_{had}	Ratio of E_{T} in all the hadronic calorimeter to E_{T} of the EM cluster (used over the range $0.8 < \lvert\eta\rvert < 1.37$)	✓	✓
EM Middle Layer	R_{η}	Ratio in η of cell energies in 3×7 over 7×7	✓	✓
	w_{η_2}	Later width of the shower	✓	✓
	R_{ϕ}	Ratio in ϕ of cell energies in 3×7 over 7×7		✓
EM Strip Layer	w_{s_3}	Shower width for three strips around the strip with maximum energy deposit		✓
	$w_{s_{\mathrm{tot}}}$	Total lateral shower width		✓
	F_{side}	Energy outside the core of the three central strips but within seven strips divided by energy within the three central strips		✓
	ΔE	Difference between the energy associated with the second maximum in the strip layer and the energy reconstructed in the strip with the minimal value found between the first and second maxima		✓
	E_{ratio}	Ratio of the energy difference associated with the largest and second largest energy deposits over the sum of these energies		✓

Table 47: Variables used for loose and tight photon identification.

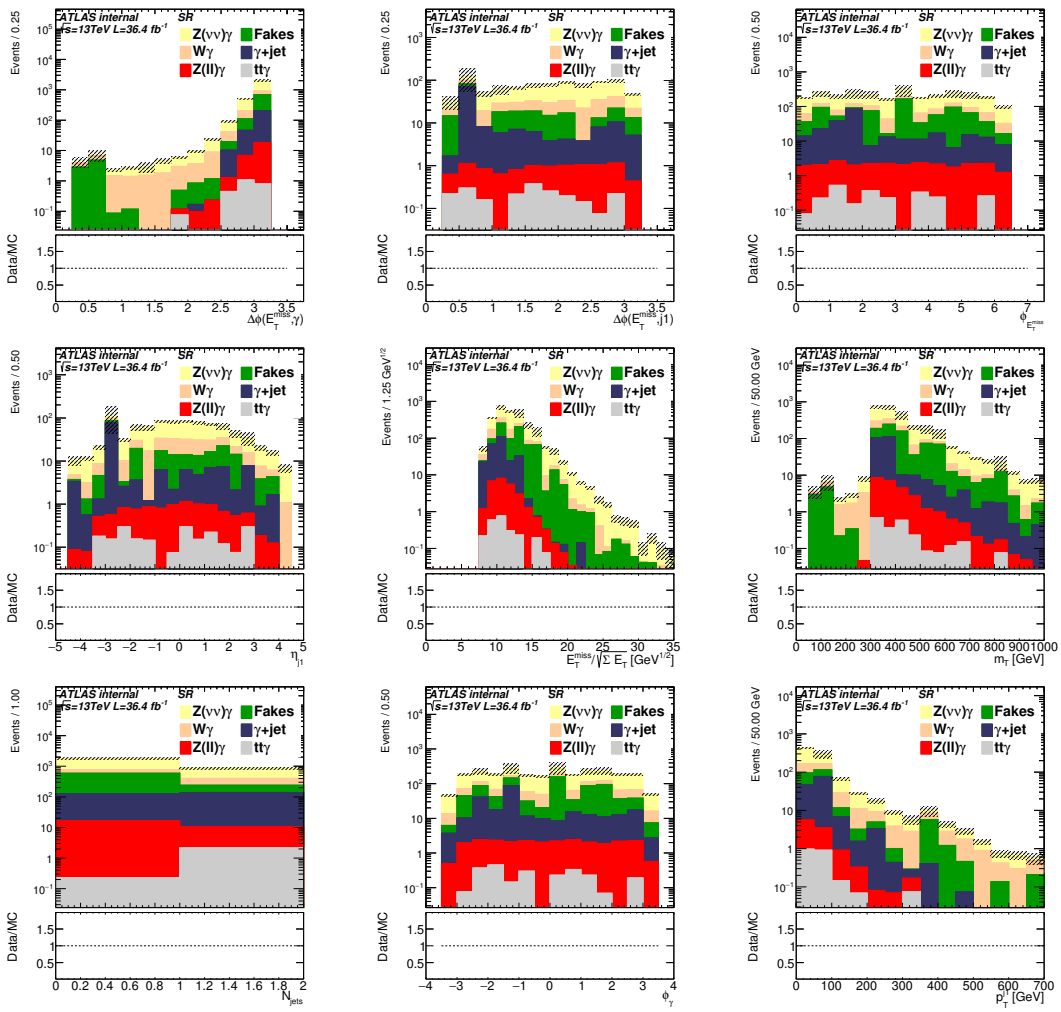

Figure 48: Pre-fit distributions in the SR for 36.4 fb^{-1}of SM background processes. The dashed bands include only statistical uncertainty. The fakes are estimated by using wzjet, ttbar and di-jet samples instead of data-driven methods for fake electrons and fake jets. Negative bins from fakes are set to 0 but the error on them are conserved.

C Data/MC Comparison in CRs and MC in SR

Distributions of SM processes in SR are shown in fig. 48: Comparison between data and MC simulations are shown in fig. 49, 50, 51 and 52 in all the CRs.

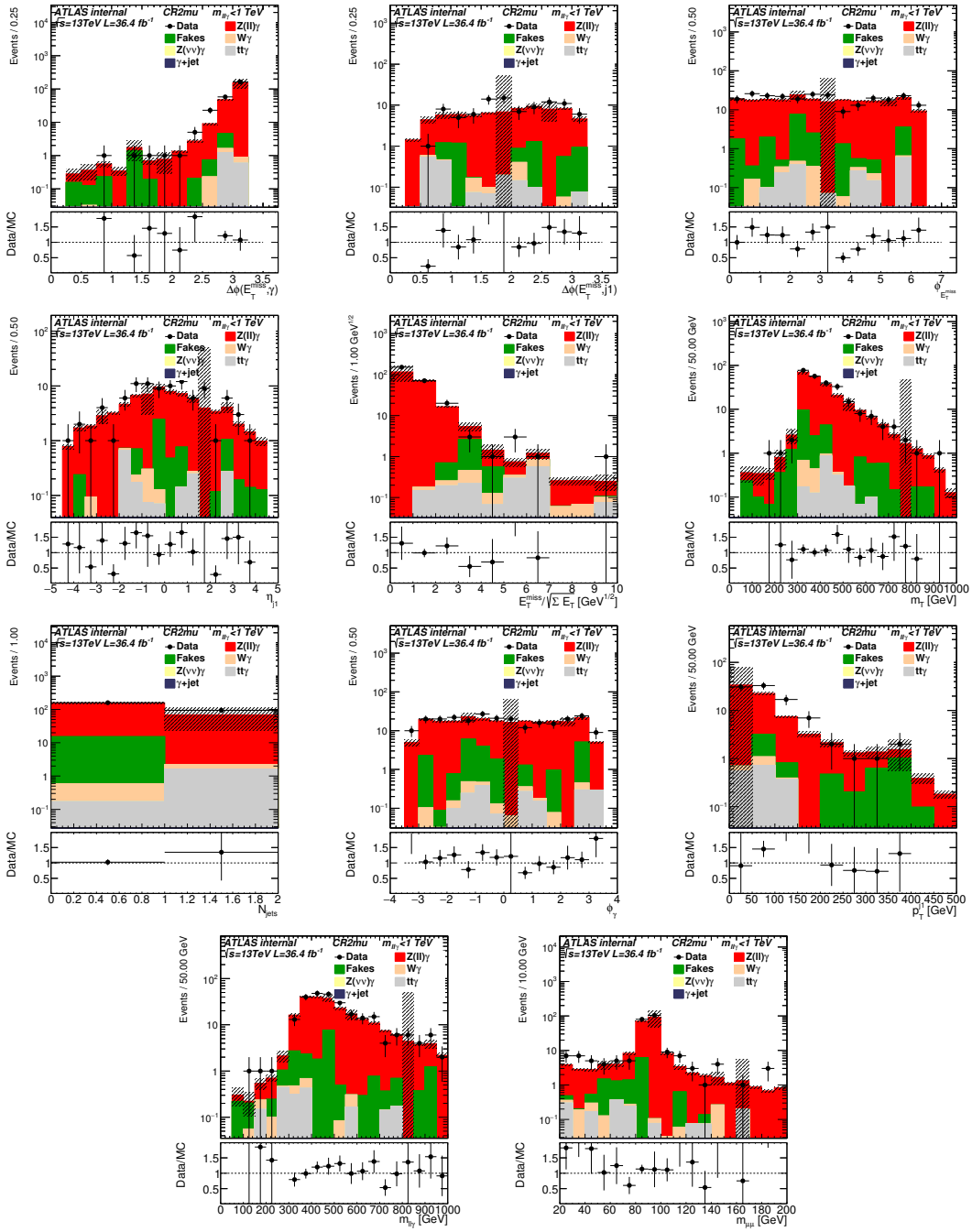

Figure 49: Pre-fit distributions in the two-muons CR for 36.4 fb^{-1} of data (black dots) and SM background processes. The dashed bands include only statistical uncertainty. The fakes are estimated by using W/Z + jet, $t\bar{t}$ and di-jet samples instead of data-driven methods for fake electrons and fake jets. The lower part of the figure shows the ratios of data to pre-fit background event yields. MET_Signif = $\mathrm{E_T^{miss}}/\sqrt{\Sigma E_T}$ is computed using the true $E_{\mathrm{T}}^{\mathrm{miss}}$ and not considering muons as invisible particles. Negative bins from fakes are set to 0 but the error on them are conserved.

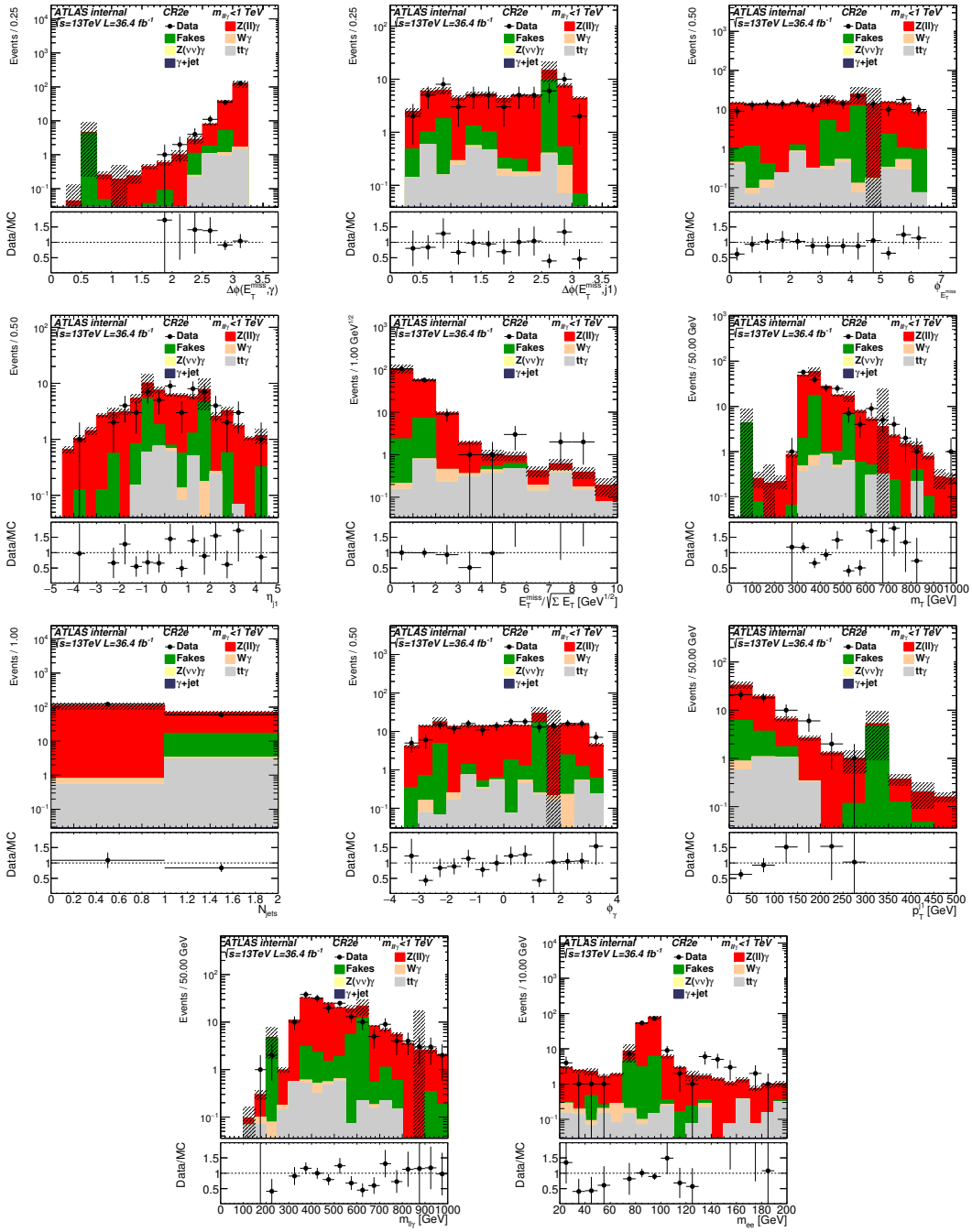

Figure 50: Pre-fit distributions in the two-electrons CR for 36.4 fb^{-1}of data (black dots) and SM background processes. The dashed bands include only statistical uncertainty. The fakes are estimated by using W/Z + jet, $t\bar{t}$and di-jet samples instead of data-driven methods for fake electrons and fake jets. The lower part of the figure shows the ratios of data to pre-fit background event yields. MET_Signif = $\mathrm{E_T^{miss}}/\sqrt{\Sigma E_T}$ is computed using the true $E_{\mathrm{T}}^{\mathrm{miss}}$ and not considering electrons as an invisible particles. Negative bins from fakes are set to 0 but the error on them are conserved.

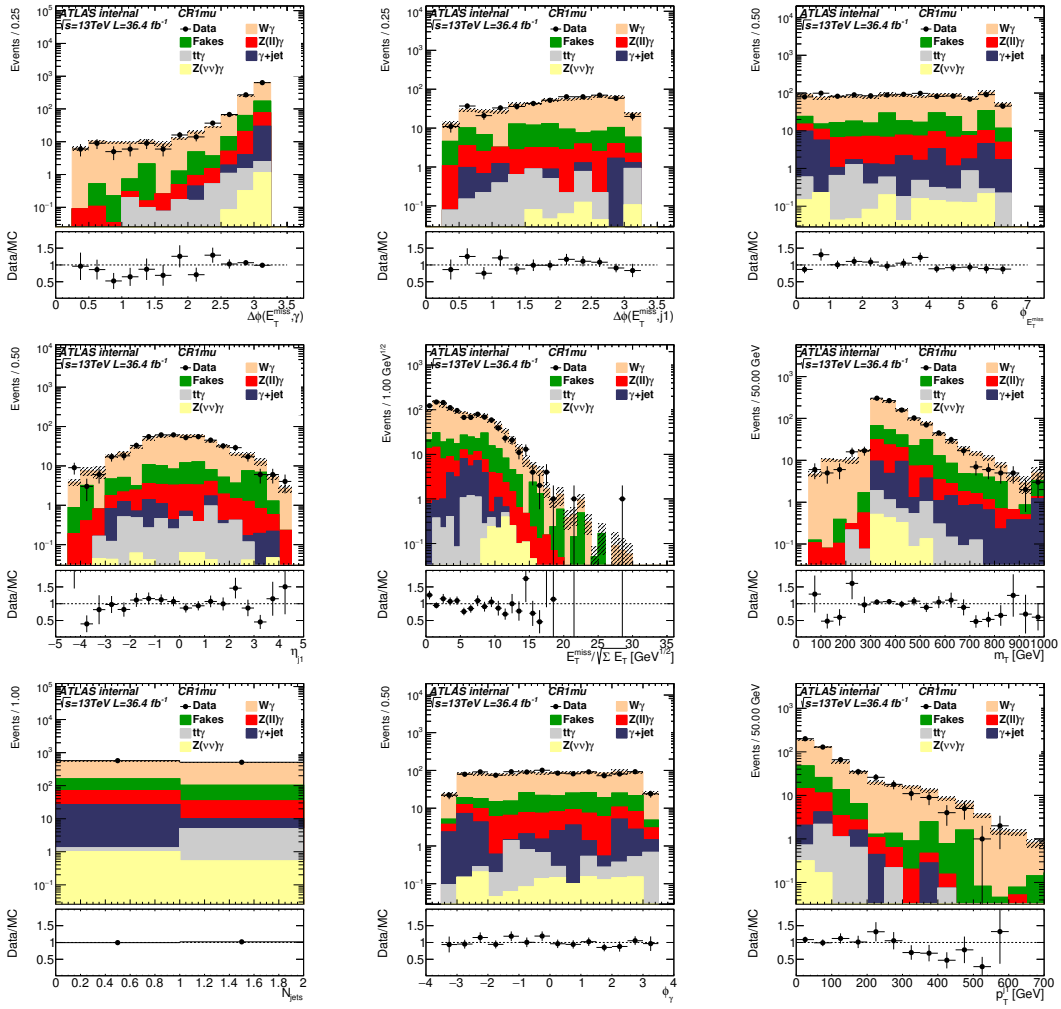

Figure 51: Pre-fit distributions in the one-muon CR for 36.4 fb^{-1} of data (black dots) and SM background processes. The dashed bands include only statistical uncertainty. The fakes are estimated by using W/Z + jet, $t\bar{t}$ and di-jet samples instead of data-driven methods for fake electrons and fake jets. The lower part of the figure shows the ratios of data to pre-fit background event yields. MET_Signif = $E_T^{miss}/\sqrt{\Sigma E_T}$ is computed using the true E_T^{miss} and not considering the muon as an invisible particle. Negative bins from fakes are set to 0 but the error on them are conserved.

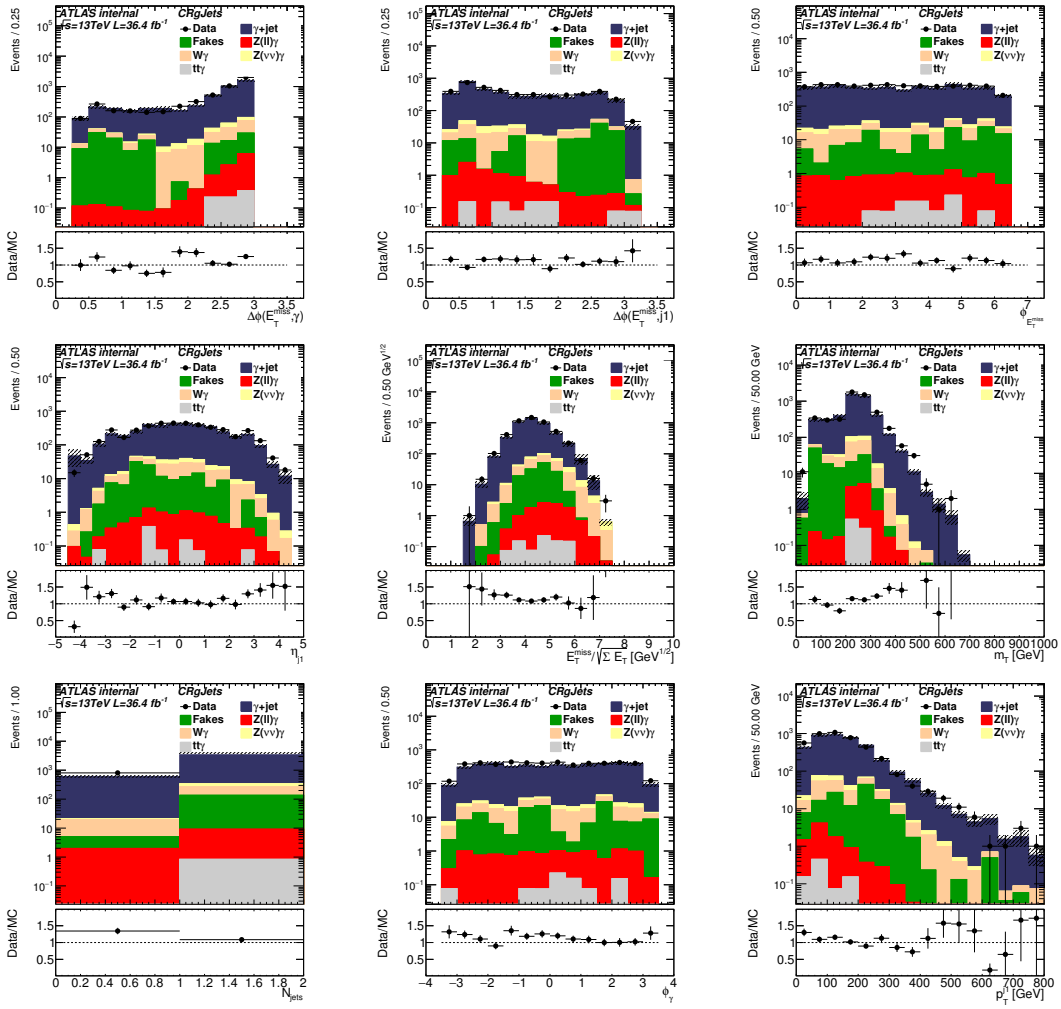

Figure 52: Pre-fit distributions in the Photon-Jet CR for 36.4 fb^{-1} of data (black dots) and SM background processes. The dashed bands include only statistical uncertainty. The fakes are estimated by using W/Z + jet, $t\bar{t}$ and di-jet samples instead of data-driven methods for fake electrons and fake jets. The lower part of the figure shows the ratios of data to pre-fit background event yields. Negative bins from fakes are set to 0 but the error on them are conserved.

D One-Electron Control Region

In fig. 53 are presented the kinematic distributions of SM processes in one-electron CR defined as for the one-muon but requesting the presence of exactly one electron instead of one muon. This CR is characterized by the contamination of γ + jet background which is not present in the 1muCR.

This region has been added to the simultaneous fit to cross-check $W(\rightarrow \ell\nu)+\gamma$ background estimation and to understand if this would improve the uncertainty of the $k_{W\gamma}$. The check has been done in the inclusive SR with $E_{\mathrm{T}}^{\mathrm{miss}} > 150$ GeV and the resulting normalization factors are shown in Table 48 showing that the $k_{W\gamma}$ uncertainty doesn't improve and it is the same as the one obtained without adding the one-electron CR in the fit (see Table 19). There is a slight increase of the $k_{\gamma+\mathrm{jet}}$ due to the contamination of γ + jet background in the one-electron CR, as shown in Table 49. For the 2015+2016 analysis it is preferred to use the one-muon CR only, providing a more pure background composition, to estimate the $k_{W\gamma}$ composition.

$E_{\mathrm{T}}^{\mathrm{miss}}$bins	$k_{Z\gamma}$	$k_{W\gamma}$	$k_{\gamma+\mathrm{jet}}$
$E_{\mathrm{T}}^{\mathrm{miss}}$> 150 GeV	1.10 ± 0.09	1.05 ± 0.09	1.18 ± 0.20

Table 48: Normalization factors (k-factors) obtained from a background-only single bin fit performed on the inclusive SR with $E_{\mathrm{T}}^{\mathrm{miss}} > 150$ GeV including the ONEeleCR for an integrated luminosity of 36.4 fb^{-1}. The errors shown include both the statistical and systematic uncertainties.

table.results.yields channel	SR	ONEmuCR	ONEeleCR	TWOmuCR	TWOeleCR	PhJetCR
Observed events	2400	1083	1502	254	181	5064
Fitted bkg events	2654.73 ± 157.53	1087.51 ± 32.17	1495.00 ± 37.34	242.17 ± 12.77	193.23 ± 10.31	5065.71 ± 73.50
Fitted Znunugamma events	1614.37 ± 107.64	1.66 ± 0.17	1.13 ± 0.11	0.00 ± 0.00	0.00 ± 0.00	80.15 ± 5.48
Fitted Zgamma events	34.14 ± 2.64	76.57 ± 4.53	86.69 ± 5.34	232.58 ± 12.92	180.13 ± 10.40	12.72 ± 0.84
Fitted Wgamma events	392.41 ± 24.21	870.82 ± 39.31	785.95 ± 41.93	1.18 ± 0.32	0.70 ± 0.12	164.02 ± 9.18
Fitted gammajets events	263.19 ± 75.30	35.27 ± 8.22	383.13 ± 58.14	0.00 ± 0.00	0.00 ± 0.00	4453.17 ± 81.34
Fitted JetFakes events	152.10 ± 21.72	86.56 ± 18.89	87.90 ± 17.05	7.91 ± 3.77	12.31 ± 4.70	284.10 ± 28.47
Fitted EleFakes events	198.53 ± 39.82	16.62 ± 3.39	150.19 ± 29.51	0.50 ± 0.13	0.09 ± 0.04	71.56 ± 13.80
MC exp. SM events	2442.02 ± 203.99	1024.60 ± 71.74	1368.81 ± 97.73	218.45 ± 15.31	180.52 ± 13.34	4789.39 ± 989.02
MC exp. Znunugamma events	1460.60 ± 112.23	1.54 ± 0.16	1.03 ± 0.14	0.00 ± 0.00	0.00 ± 0.00	73.17 ± 5.55
MC exp. Zgamma events	31.17 ± 3.04	69.58 ± 5.07	78.69 ± 6.04	209.71 ± 14.66	165.49 ± 12.10	11.54 ± 0.82
MC exp. Wgamma events	368.85 ± 34.88	818.20 ± 60.68	738.80 ± 60.28	1.01 ± 0.37	0.67 ± 0.12	153.69 ± 13.39
MC exp. gammajets events	230.78 ± 76.18	30.48 ± 6.28	317.76 ± 36.85	0.00 ± 0.00	0.00 ± 0.00	4194.96 ± 987.64
MC exp. JetFakes events	152.10 ± 21.72	88.14 ± 19.45	86.53 ± 17.16	7.24 ± 3.78	14.27 ± 5.54	284.40 ± 28.68
MC exp. EleFakes events	198.53 ± 39.82	16.67 ± 3.42	146.01 ± 29.99	0.50 ± 0.13	0.09 ± 0.04	71.63 ± 13.91

Table 49: Results of the background estimation in the SR defined with $E_{\mathrm{T}}^{\mathrm{miss}} > 150$ GeV and in its CRs including the ONEeleCR, for an integrated luminosity of 36.4 fb^{-1}. Results are obtained with a background-only fit in the CRs. Each background component is reported before (bottom) and after the fit (top). The errors shown include both the statistical and systematics uncertainties.

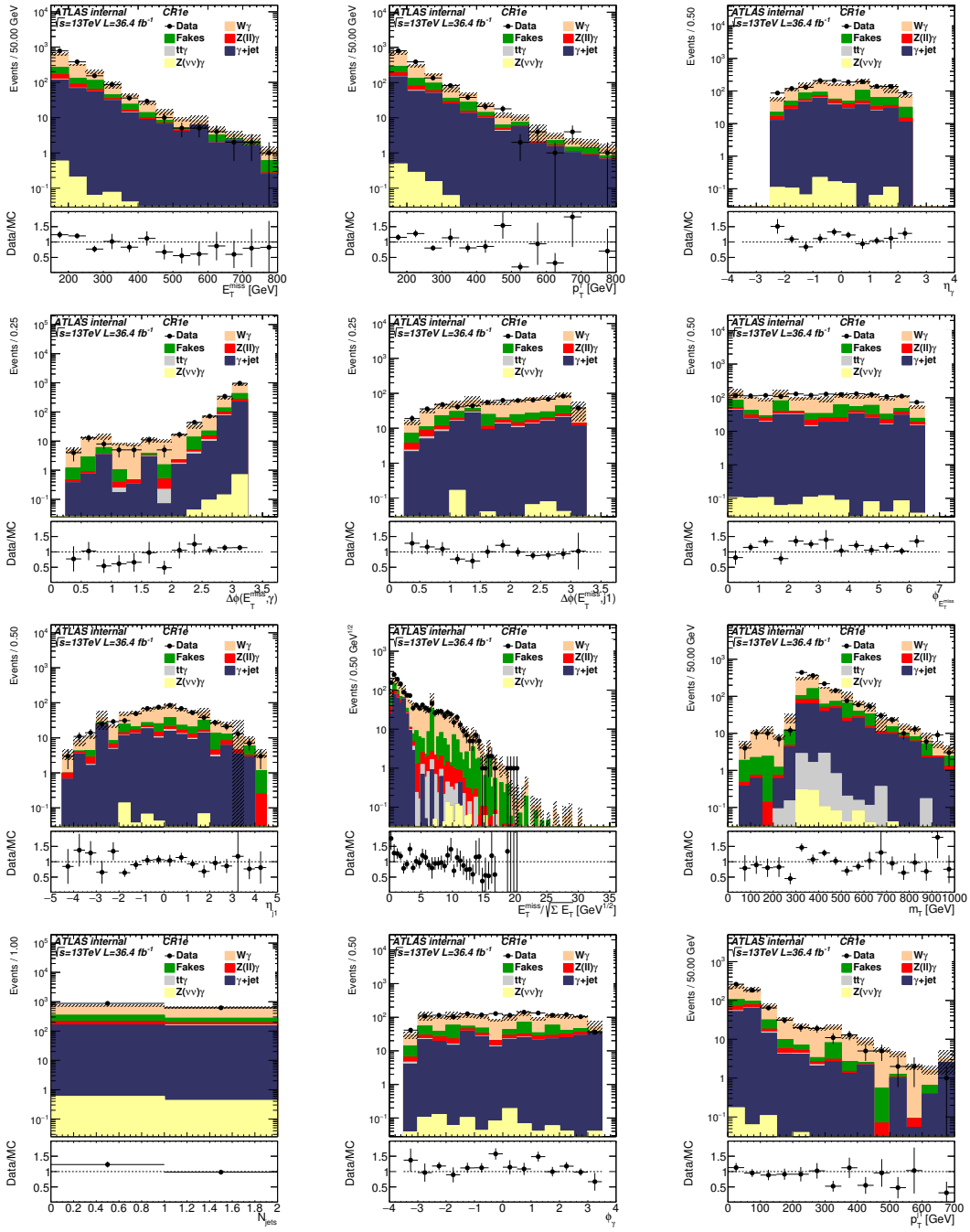

Figure 53: Pre-fit distributions in the one-electron CR for 36.4 fb^{-1}of data (black dots) and SM background processes. The dashed bands include only statistical uncertainty. The fakes are estimated by using W/Z + jet, $t\bar{t}$and di-jet samples instead of data-driven methods for fake electrons and fake jets. The lower part of the figure shows the ratios of data to pre-fit background event yields. Negative bins from fakes are set to 0 but the error on them are conserved.

E Systematics Before Fit

Systematic	SR	CR1mu	CR2mu	CR2e	CRgjet
alpha_EG_RESO	(0.06, 0.11)	(0.19, 0.27)	(−0.00, 0.07)	(0.12, −0.15)	(−0.57, 1.06)
alpha_EG_SCALE	(−2.65, 2.79)	(−2.11, 2.34)	(−2.44, 2.38)	(−2.16, 2.04)	(−6.48, 7.57)
alpha_EL_EFF_ID	(−0.00, 0.01)	(0.01, −0.02)	(−0.01, 0.01)	(−1.94, 4.22)	(0.03, −0.06)
alpha_EL_EFF_ISO	(−0.00, 0.01)	(0.01, −0.02)	(−0.01, 0.01)	(−1.27, 1.86)	(0.04, −0.05)
alpha_EL_EFF_RECO	(−0.00, 0.01)	(0.01, −0.02)	(−0.01, 0.01)	(−1.02, 1.36)	(0.04, −0.05)
alpha_EleFake_statCR_ONEmuCR	(0.00, 0.00)	(−0.05, 0.05)	(0.00, 0.00)	(0.00, 0.00)	(0.00, 0.00)
alpha_EleFake_statCR_PhJetCR	(0.00, 0.00)	(0.00, 0.00)	(0.00, 0.00)	(0.00, 0.00)	(−0.02, 0.02)
alpha_EleFake_statCR_SR	(−0.07, 0.07)	(0.00, 0.00)	(0.00, 0.00)	(0.00, 0.00)	(0.00, 0.00)
alpha_EleFake_statCR_TWOeleCR	(0.00, 0.00)	(0.00, 0.00)	(0.00, 0.00)	(−0.02, 0.02)	(0.00, 0.00)
alpha_EleFake_statCR_TWOmuCR	(0.00, 0.00)	(0.00, 0.00)	(−0.04, 0.04)	(0.00, 0.00)	(0.00, 0.00)
alpha_EleFake_stat_ONEmuCR	(0.00, 0.00)	(−0.13, 0.13)	(0.00, 0.00)	(0.00, 0.00)	(0.00, 0.00)
alpha_EleFake_stat_PhJetCR	(0.00, 0.00)	(0.00, 0.00)	(0.00, 0.00)	(0.00, 0.00)	(−0.12, 0.12)
alpha_EleFake_stat_SR	(−0.68, 0.68)	(0.00, 0.00)	(0.00, 0.00)	(0.00, 0.00)	(0.00, 0.00)
alpha_EleFake_stat_TWOeleCR	(0.00, 0.00)	(0.00, 0.00)	(0.00, 0.00)	(−0.00, 0.00)	(0.00, 0.00)
alpha_EleFake_stat_TWOmuCR	(0.00, 0.00)	(0.00, 0.00)	(−0.02, 0.02)	(0.00, 0.00)	(0.00, 0.00)
alpha_EleFake_syst_ONEmuCR	(0.00, 0.00)	(−0.28, 0.28)	(0.00, 0.00)	(0.00, 0.00)	(0.00, 0.00)
alpha_EleFake_syst_PhJetCR	(0.00, 0.00)	(0.00, 0.00)	(0.00, 0.00)	(0.00, 0.00)	(−0.25, 0.25)
alpha_EleFake_syst_SR	(−1.34, 1.34)	(0.00, 0.00)	(0.00, 0.00)	(0.00, 0.00)	(0.00, 0.00)
alpha_EleFake_syst_TWOeleCR	(0.00, 0.00)	(0.00, 0.00)	(0.00, 0.00)	(−0.01, 0.01)	(0.00, 0.00)
alpha_EleFake_syst_TWOmuCR	(0.00, 0.00)	(0.00, 0.00)	(−0.04, 0.04)	(0.00, 0.00)	(0.00, 0.00)
alpha_JER	(0.68, −0.72)	(1.16, −1.23)	(1.48, −1.56)	(1.11, −1.18)	(−9.60, 10.13)
alpha_JES	(3.50, −7.31)	(4.00, −4.16)	(2.57, −3.86)	(2.11, −2.85)	(−3.76, 1.85)
alpha_JVT_EFF	(0.19, −0.20)	(0.14, −0.14)	(0.18, −0.18)	(0.15, −0.15)	(0.20, −0.20)
alpha_JetFake_statCR_ONEmuCR	(0.00, 0.00)	(−1.37, 1.37)	(0.00, 0.00)	(0.00, 0.00)	(0.00, 0.00)
alpha_JetFake_statCR_PhJetCR	(0.00, 0.00)	(0.00, 0.00)	(0.00, 0.00)	(0.00, 0.00)	(−0.48, 0.48)
alpha_JetFake_statCR_SR	(−0.81, 0.81)	(0.00, 0.00)	(0.00, 0.00)	(0.00, 0.00)	(0.00, 0.00)
alpha_JetFake_statCR_TWOeleCR	(0.00, 0.00)	(0.00, 0.00)	(0.00, 0.00)	(−1.57, 2.91)	(0.00, 0.00)
alpha_JetFake_statCR_TWOmuCR	(0.00, 0.00)	(0.00, 0.00)	(−1.81, 1.28)	(0.00, 0.00)	(0.00, 0.00)
alpha_LUMI_SYST	(−3.57, 3.54)	(−3.72, 3.69)	(−3.97, 3.94)	(−3.85, 3.82)	(−3.83, 3.80)
alpha_MET_RESO_PARA	(0.44, −0.43)	(0.69, −0.69)	(0.23, −0.22)	(0.28, −0.28)	(2.93, −2.90)
alpha_MET_RESO_PERP	(0.89, −0.92)	(0.27, −0.27)	(0.36, −0.37)	(0.32, −0.33)	(8.57, −8.79)
alpha_MET_SCALE	(0.37, −0.66)	(0.38, −0.63)	(0.00, −0.23)	(−0.07, −0.24)	(11.93, −11.15)
alpha_MU_EFF_STAT	(0.20, −0.19)	(−0.24, −0.06)	(−0.36, −0.02)	(0.15, −0.14)	(0.21, −0.19)
alpha_MU_EFF_SYST	(0.23, −0.16)	(−1.13, 0.54)	(−2.10, 1.15)	(0.17, −0.12)	(0.24, −0.16)
alpha_MU_EFF_SYST_LOWPT	(0.20, −0.19)	(−0.17, −0.12)	(−0.26, −0.11)	(0.15, −0.14)	(0.21, −0.20)
alpha_MU_ID	(0.14, −0.19)	(−0.11, 0.11)	(−0.21, −0.20)	(0.15, −0.14)	(−0.15, −0.21)
alpha_MU_ISO_STAT	(0.20, −0.19)	(−0.24, −0.06)	(−0.36, −0.02)	(0.15, −0.14)	(0.21, −0.19)
alpha_MU_ISO_SYST	(0.21, −0.18)	(−0.49, 0.15)	(−0.93, 0.45)	(0.16, −0.13)	(0.22, −0.18)
alpha_MU_MS	(−0.16, −0.20)	(−0.11, −0.16)	(−0.23, −0.20)	(−0.15, −0.15)	(−0.24, −0.18)
alpha_MU_SCALE	(−0.03, −0.19)	(−0.14, −0.15)	(−0.19, −0.20)	(0.15, −0.14)	(−0.21, −0.20)
alpha_MU_TTVA_STAT	(0.20, −0.19)	(−0.17, −0.12)	(−0.25, −0.12)	(0.15, −0.14)	(0.21, −0.20)
alpha_MU_TTVA_SYS	(0.20, −0.19)	(−0.24, −0.05)	(−0.46, 0.07)	(0.15, −0.14)	(0.21, −0.19)
alpha_PDF_Comb	(−0.73, 0.73)	(−0.73, 0.73)	(−0.77, 0.77)	(−0.74, 0.74)	(−0.57, 0.57)
alpha_PH_EFF	(1.69, −2.07)	(1.82, −2.12)	(1.90, −2.28)	(1.86, −2.17)	(1.82, −2.23)
alpha_PH_EFF_TRKISO	(0.19, −0.20)	(0.14, −0.14)	(0.18, −0.18)	(0.15, −0.15)	(0.20, −0.20)
alpha_PH_ISO_DD	(0.19, −0.20)	(0.14, −0.14)	(0.18, −0.18)	(0.15, −0.15)	(0.20, −0.20)
alpha_PRW_DATASF	(−0.84, −0.81)	(0.97, −1.84)	(1.21, −2.25)	(1.01, −1.32)	(−5.06, 6.26)
alpha_syst_JetFake_ONEmuCR	(0.00, 0.00)	(−1.17, 1.16)	(0.00, 0.00)	(0.00, 0.00)	(0.00, 0.00)
alpha_syst_JetFake_PhJetCR	(0.00, 0.00)	(0.00, 0.00)	(0.00, 0.00)	(0.00, 0.00)	(−0.30, 0.30)
alpha_syst_JetFake_SR	(−0.16, 0.16)	(0.00, 0.00)	(0.00, 0.00)	(0.00, 0.00)	(0.00, 0.00)
alpha_syst_JetFake_TWOeleCR	(0.00, 0.00)	(0.00, 0.00)	(0.00, 0.00)	(−1.22, 1.80)	(0.00, 0.00)
alpha_syst_JetFake_TWOmuCR	(0.00, 0.00)	(0.00, 0.00)	(−0.23, 0.22)	(0.00, 0.00)	(0.00, 0.00)
alpha_syst_PhJet_shape_SR	(1.50, −1.50)	(0.00, 0.00)	(0.00, 0.00)	(0.00, 0.00)	(0.00, 0.00)

Table 50: Breakdown of the dominant systematic uncertainties expressed in % on background estimates before the fit in the SR defined by $E_{\mathrm{T}}^{\mathrm{miss}}$ sup 150 GeV and its CRs for an integrated luminosity of 36.4 fb^{-1}. Note that the individual uncertainties can be correlated, and do not necessarily add up quadratically to the total background uncertainty. The percentages show the size of the uncertainty relative to the total expected background.

Systematic	SR	CR1mu	CR2mu	CR2e	CRgjet
alpha_EG_RESO	(−0.24, 0.16)	(0.01, 0.21)	(0.00, 0.00)	(0.31, 0.13)	(−0.56, 1.07)
alpha_EG_SCALE	(−2.76, 2.91)	(−2.37, 2.41)	(−2.55, 2.59)	(−2.25, 2.11)	(−6.44, 7.62)
alpha_EL_EFF_ID	(−0.00, 0.00)	(−0.00, 0.00)	(0.00, 0.00)	(−2.49, 3.42)	(0.04, −0.05)
alpha_EL_EFF_ISO	(−0.00, 0.00)	(−0.00, 0.00)	(0.00, 0.00)	(−1.84, 2.26)	(0.04, −0.05)
alpha_EL_EFF_RECO	(−0.00, 0.00)	(−0.00, 0.00)	(0.00, 0.00)	(−1.07, 1.15)	(0.04, −0.05)
alpha_EleFake_statCR_ONEmuCR	(0.00, 0.00)	(−0.07, 0.07)	(0.00, 0.00)	(0.00, 0.00)	(0.00, 0.00)
alpha_EleFake_statCR_PhJetCR	(0.00, 0.00)	(0.00, 0.00)	(0.00, 0.00)	(0.00, 0.00)	(−0.02, 0.02)
alpha_EleFake_statCR_SR	(−0.11, 0.11)	(0.00, 0.00)	(0.00, 0.00)	(0.00, 0.00)	(0.00, 0.00)
alpha_EleFake_statCR_TWOeleCR	(0.00, 0.00)	(0.00, 0.00)	(0.00, 0.00)	(−0.05, 0.05)	(0.00, 0.00)
alpha_EleFake_statCR_TWOmuCR	(0.00, 0.00)	(0.00, 0.00)	(−0.06, 0.06)	(0.00, 0.00)	(0.00, 0.00)
alpha_EleFake_stat_ONEmuCR	(0.00, 0.00)	(−0.13, 0.13)	(0.00, 0.00)	(0.00, 0.00)	(0.00, 0.00)
alpha_EleFake_stat_PhJetCR	(0.00, 0.00)	(0.00, 0.00)	(0.00, 0.00)	(0.00, 0.00)	(−0.12, 0.12)
alpha_EleFake_stat_SR	(−0.74, 0.74)	(0.00, 0.00)	(0.00, 0.00)	(0.00, 0.00)	(0.00, 0.00)
alpha_EleFake_stat_TWOeleCR	(0.00, 0.00)	(0.00, 0.00)	(0.00, 0.00)	(−0.01, 0.01)	(0.00, 0.00)
alpha_EleFake_stat_TWOmuCR	(0.00, 0.00)	(0.00, 0.00)	(−0.02, 0.02)	(0.00, 0.00)	(0.00, 0.00)
alpha_EleFake_syst_ONEmuCR	(0.00, 0.00)	(−0.25, 0.25)	(0.00, 0.00)	(0.00, 0.00)	(0.00, 0.00)
alpha_EleFake_syst_PhJetCR	(0.00, 0.00)	(0.00, 0.00)	(0.00, 0.00)	(0.00, 0.00)	(−0.25, 0.25)
alpha_EleFake_syst_SR	(−1.30, 1.30)	(0.00, 0.00)	(0.00, 0.00)	(0.00, 0.00)	(0.00, 0.00)
alpha_EleFake_syst_TWOeleCR	(0.00, 0.00)	(0.00, 0.00)	(0.00, 0.00)	(−0.01, 0.01)	(0.00, 0.00)
alpha_EleFake_syst_TWOmuCR	(0.00, 0.00)	(0.00, 0.00)	(−0.05, 0.05)	(0.00, 0.00)	(0.00, 0.00)
alpha_JER	(0.60, −0.61)	(0.89, −0.90)	(0.86, −0.87)	(0.56, −0.57)	(−9.79, 9.90)
alpha_JES	(2.16, −2.68)	(3.15, −2.96)	(0.00, 0.00)	(1.54, −1.42)	(−4.15, 1.43)
alpha_JVT_EFF	(0.13, −0.13)	(0.14, −0.14)	(0.00, 0.00)	(0.14, −0.14)	(0.20, −0.20)
alpha_JetFake_statCR_ONEmuCR	(0.00, 0.00)	(−2.10, 2.10)	(0.00, 0.00)	(0.00, 0.00)	(0.00, 0.00)
alpha_JetFake_statCR_PhJetCR	(0.00, 0.00)	(0.00, 0.00)	(0.00, 0.00)	(0.00, 0.00)	(−0.48, 0.48)
alpha_JetFake_statCR_SR	(−1.18, 1.18)	(0.00, 0.00)	(0.00, 0.00)	(0.00, 0.00)	(0.00, 0.00)
alpha_JetFake_statCR_TWOeleCR	(0.00, 0.00)	(0.00, 0.00)	(0.00, 0.00)	(−2.82, 4.57)	(0.00, 0.00)
alpha_JetFake_statCR_TWOmuCR	(0.00, 0.00)	(0.00, 0.00)	(−3.59, 2.60)	(0.00, 0.00)	(0.00, 0.00)
alpha_LUMI_SYST	(−3.66, 3.65)	(−3.77, 3.77)	(−3.82, 3.82)	(−3.81, 3.80)	(−3.82, 3.81)
alpha_MET_RESO_PARA	(−0.12, 0.12)	(0.25, −0.24)	(0.00, 0.00)	(0.46, −0.44)	(2.99, −2.85)
alpha_MET_RESO_PERP	(0.32, −0.31)	(0.22, −0.21)	(0.00, 0.00)	(0.38, −0.37)	(8.81, −8.60)
alpha_MET_SCALE	(0.28, −0.47)	(0.12, −0.34)	(0.00, 0.00)	(−0.00, −0.44)	(12.14, −10.99)
alpha_MU_EFF_STAT	(0.13, −0.13)	(−0.22, −0.06)	(0.00, 0.00)	(0.14, −0.14)	(0.20, −0.20)
alpha_MU_EFF_SYST	(0.14, −0.11)	(−1.37, 0.86)	(−2.37, 1.63)	(0.15, −0.12)	(0.22, −0.18)
alpha_MU_EFF_SYST_LOWPT	(0.13, −0.13)	(−0.16, −0.12)	(0.00, 0.00)	(0.14, −0.14)	(0.20, −0.20)
alpha_MU_ID	(0.10, −0.12)	(−0.04, 0.18)	(0.00, 0.00)	(0.14, −0.14)	(−0.15, −0.21)
alpha_MU_ISO_STAT	(0.13, −0.13)	(−0.27, −0.01)	(−0.39, 0.05)	(0.14, −0.13)	(0.20, −0.20)
alpha_MU_ISO_SYST	(0.13, −0.13)	(−0.49, 0.20)	(0.00, 0.00)	(0.14, −0.14)	(0.20, −0.20)
alpha_MU_MS	(−0.12, −0.15)	(−0.05, −0.21)	(0.00, 0.00)	(0.14, −0.14)	(−0.24, −0.18)
alpha_MU_SCALE	(0.08, −0.12)	(−0.12, −0.14)	(0.00, 0.00)	(0.14, −0.14)	(−0.21, −0.20)
alpha_MU_TTVA_STAT	(0.13, −0.13)	(−0.17, −0.11)	(0.00, 0.00)	(0.14, −0.14)	(0.20, −0.20)
alpha_MU_TTVA_SYS	(0.13, −0.13)	(−0.22, −0.06)	(0.00, 0.00)	(0.14, −0.14)	(0.20, −0.20)
alpha_PDF_Comb	(−0.70, 0.70)	(−0.74, 0.74)	(−0.73, 0.73)	(−0.73, 0.73)	(−0.57, 0.57)
alpha_PH_EFF	(2.10, −1.90)	(2.14, −1.96)	(0.00, 0.00)	(2.13, −1.95)	(2.05, −2.00)
alpha_PH_EFF_TRKISO	(0.13, −0.13)	(0.14, −0.14)	(0.00, 0.00)	(0.14, −0.14)	(0.20, −0.20)
alpha_PH_ISO_DD	(0.13, −0.13)	(0.14, −0.14)	(0.00, 0.00)	(0.14, −0.14)	(0.20, −0.20)
alpha_PRW_DATASF	(0.59, −0.52)	(0.23, −1.01)	(0.00, 0.00)	(1.13, −1.04)	(−5.65, 5.59)
alpha_syst_JetFake_ONEmuCR	(0.00, 0.00)	(−2.16, 2.16)	(0.00, 0.00)	(0.00, 0.00)	(0.00, 0.00)
alpha_syst_JetFake_PhJetCR	(0.00, 0.00)	(0.00, 0.00)	(0.00, 0.00)	(0.00, 0.00)	(−0.30, 0.30)
alpha_syst_JetFake_SR	(−1.59, 1.59)	(0.00, 0.00)	(0.00, 0.00)	(0.00, 0.00)	(0.00, 0.00)
alpha_syst_JetFake_TWOeleCR	(0.00, 0.00)	(0.00, 0.00)	(0.00, 0.00)	(−2.08, 2.77)	(0.00, 0.00)
alpha_syst_JetFake_TWOmuCR	(0.00, 0.00)	(0.00, 0.00)	(−1.88, 1.57)	(0.00, 0.00)	(0.00, 0.00)
alpha_syst_PhJet_shape_SR	(0.34, −0.34)	(0.00, 0.00)	(0.00, 0.00)	(0.00, 0.00)	(0.00, 0.00)

Table 51: Breakdown of the dominant systematic uncertainties expressed in % on background estimates before the fit in the SR defined by $E_{\mathrm{T}}^{\mathrm{miss}}$ sup 225 GeV and its CRs for an integrated luminosity of 36.4 fb^{-1}. Note that the individual uncertainties can be correlated, and do not necessarily add up quadratically to the total background uncertainty. The percentages show the size of the uncertainty relative to the total expected background.

Systematic	SR	CR1mu	CR2mu	CR2e	CRgjet
alpha_EG_RESO	(0.03, 0.18)	(−0.39, 0.32)	(0.24, 0.20)	(0.41, 0.43)	(−0.55, 1.08)
alpha_EG_SCALE	(−2.50, 2.91)	(−2.60, 2.99)	(−3.18, 3.90)	(−1.95, 2.77)	(−6.38, 7.66)
alpha_EL_EFF_ID	(0.00, −0.00)	(0.00, 0.00)	(0.03, −0.03)	(−2.81, 2.96)	(0.04, −0.05)
alpha_EL_EFF_ISO	(0.00, −0.00)	(0.00, 0.00)	(0.03, −0.03)	(−2.29, 2.35)	(0.04, −0.05)
alpha_EL_EFF_RECO	(0.00, −0.00)	(0.00, 0.00)	(0.03, −0.03)	(−1.09, 1.05)	(0.04, −0.05)
alpha_EleFake_statCR_ONEmuCR	(0.00, 0.00)	(−0.11, 0.11)	(0.00, 0.00)	(0.00, 0.00)	(0.00, 0.00)
alpha_EleFake_statCR_PhJetCR	(0.00, 0.00)	(0.00, 0.00)	(0.00, 0.00)	(0.00, 0.00)	(−0.02, 0.02)
alpha_EleFake_statCR_SR	(−0.16, 0.16)	(0.00, 0.00)	(0.00, 0.00)	(0.00, 0.00)	(0.00, 0.00)
alpha_EleFake_statCR_TWOeleCR	(0.00, 0.00)	(0.00, 0.00)	(0.00, 0.00)	(−0.14, 0.14)	(0.00, 0.00)
alpha_EleFake_statCR_TWOmuCR	(0.00, 0.00)	(0.00, 0.00)	(−0.06, 0.06)	(0.00, 0.00)	(0.00, 0.00)
alpha_EleFake_stat_ONEmuCR	(0.00, 0.00)	(−0.10, 0.10)	(0.00, 0.00)	(0.00, 0.00)	(0.00, 0.00)
alpha_EleFake_stat_PhJetCR	(0.00, 0.00)	(0.00, 0.00)	(0.00, 0.00)	(0.00, 0.00)	(−0.12, 0.12)
alpha_EleFake_stat_SR	(−0.61, 0.61)	(0.00, 0.00)	(0.00, 0.00)	(0.00, 0.00)	(0.00, 0.00)
alpha_EleFake_stat_TWOeleCR	(0.00, 0.00)	(0.00, 0.00)	(0.00, 0.00)	(−0.02, 0.02)	(0.00, 0.00)
alpha_EleFake_stat_TWOmuCR	(0.00, 0.00)	(0.00, 0.00)	(−0.01, 0.01)	(0.00, 0.00)	(0.00, 0.00)
alpha_EleFake_syst_ONEmuCR	(0.00, 0.00)	(−0.20, 0.20)	(0.00, 0.00)	(0.00, 0.00)	(0.00, 0.00)
alpha_EleFake_syst_PhJetCR	(0.00, 0.00)	(0.00, 0.00)	(0.00, 0.00)	(0.00, 0.00)	(−0.25, 0.25)
alpha_EleFake_syst_SR	(−1.06, 1.06)	(0.00, 0.00)	(0.00, 0.00)	(0.00, 0.00)	(0.00, 0.00)
alpha_EleFake_syst_TWOeleCR	(0.00, 0.00)	(0.00, 0.00)	(0.00, 0.00)	(−0.04, 0.04)	(0.00, 0.00)
alpha_EleFake_syst_TWOmuCR	(0.00, 0.00)	(0.00, 0.00)	(−0.02, 0.02)	(0.00, 0.00)	(0.00, 0.00)
alpha_JER	(1.38, −1.37)	(1.57, −1.55)	(1.13, −1.12)	(1.03, −1.02)	(−9.86, 9.75)
alpha_JES	(1.88, −4.03)	(2.49, −3.70)	(2.83, −3.40)	(1.65, −1.57)	(−3.89, 1.67)
alpha_JVT_EFF	(0.12, −0.12)	(0.12, −0.12)	(0.14, −0.14)	(0.23, −0.23)	(0.20, −0.20)
alpha_JetFake_statCR_ONEmuCR	(0.00, 0.00)	(−1.81, 1.81)	(0.00, 0.00)	(0.00, 0.00)	(0.00, 0.00)
alpha_JetFake_statCR_PhJetCR	(0.00, 0.00)	(0.00, 0.00)	(0.00, 0.00)	(0.00, 0.00)	(−0.48, 0.48)
alpha_JetFake_statCR_SR	(−1.61, 1.61)	(0.00, 0.00)	(0.00, 0.00)	(0.00, 0.00)	(0.00, 0.00)
alpha_JetFake_statCR_TWOeleCR	(0.00, 0.00)	(0.00, 0.00)	(0.00, 0.00)	(−4.32, 4.82)	(0.00, 0.00)
alpha_JetFake_statCR_TWOmuCR	(0.00, 0.00)	(0.00, 0.00)	(−3.80, 3.48)	(0.00, 0.00)	(0.00, 0.00)
alpha_LUMI_SYST	(−3.76, 3.75)	(−3.95, 3.93)	(−3.92, 3.91)	(−3.83, 3.82)	(−3.82, 3.80)
alpha_MET_RESO_PARA	(0.29, −0.29)	(0.22, −0.22)	(−0.18, 0.18)	(0.06, −0.06)	(2.91, −2.91)
alpha_MET_RESO_PERP	(0.35, −0.35)	(0.14, −0.14)	(−0.60, 0.60)	(−0.00, 0.00)	(8.67, −8.67)
alpha_MET_SCALE	(−0.05, −0.39)	(0.10, −0.23)	(0.11, 0.03)	(0.05, −0.15)	(12.00, −11.04)
alpha_MU_EFF_STAT	(0.12, −0.12)	(−0.19, −0.04)	(−0.29, 0.00)	(0.23, −0.23)	(0.20, −0.20)
alpha_MU_EFF_SYST	(0.12, −0.11)	(−1.54, 1.25)	(−2.58, 2.21)	(0.23, −0.22)	(0.21, −0.20)
alpha_MU_EFF_SYST_LOWPT	(0.12, −0.12)	(−0.13, −0.10)	(−0.18, −0.10)	(0.23, −0.23)	(0.20, −0.20)
alpha_MU_ID	(0.10, −0.10)	(−0.09, 0.78)	(−0.06, −0.15)	(0.23, −0.23)	(−0.15, −0.21)
alpha_MU_ISO_STAT	(0.12, −0.12)	(−0.32, 0.08)	(−0.47, 0.18)	(0.23, −0.23)	(0.20, −0.20)
alpha_MU_ISO_SYST	(0.12, −0.12)	(−0.50, 0.26)	(−0.87, 0.57)	(0.23, −0.22)	(0.20, −0.20)
alpha_MU_MS	(0.13, −0.13)	(−0.14, −0.11)	(−0.25, −0.13)	(0.23, −0.23)	(−0.24, −0.18)
alpha_MU_SCALE	(0.12, −0.12)	(−0.12, −0.12)	(−0.20, −0.09)	(0.23, −0.23)	(−0.21, −0.20)
alpha_MU_TTVA_STAT	(0.12, −0.12)	(−0.14, −0.09)	(−0.20, −0.09)	(0.23, −0.23)	(0.20, −0.20)
alpha_MU_TTVA_SYS	(0.12, −0.12)	(−0.20, −0.04)	(−0.31, 0.03)	(0.23, −0.23)	(0.20, −0.20)
alpha_PDF_Comb	(−0.72, 0.72)	(−0.81, 0.81)	(−0.75, 0.75)	(−0.74, 0.73)	(−0.57, 0.57)
alpha_PH_EFF	(1.99, −2.23)	(2.08, −2.32)	(2.03, −2.32)	(1.83, −2.29)	(1.82, −2.22)
alpha_PH_EFF_TRKISO	(0.12, −0.12)	(0.12, −0.12)	(0.14, −0.14)	(0.23, −0.23)	(0.20, −0.20)
alpha_PH_ISO_DD	(0.12, −0.12)	(0.12, −0.12)	(0.14, −0.14)	(0.23, −0.23)	(0.20, −0.20)
alpha_PRW_DATASF	(0.40, −0.85)	(−0.36, 0.29)	(−0.17, 0.50)	(0.19, −0.85)	(−5.36, 5.86)
alpha_syst_JetFake_ONEmuCR	(0.00, 0.00)	(−2.50, 2.50)	(0.00, 0.00)	(0.00, 0.00)	(0.00, 0.00)
alpha_syst_JetFake_PhJetCR	(0.00, 0.00)	(0.00, 0.00)	(0.00, 0.00)	(0.00, 0.00)	(−0.30, 0.30)
alpha_syst_JetFake_SR	(−3.30, 3.30)	(0.00, 0.00)	(0.00, 0.00)	(0.00, 0.00)	(0.00, 0.00)
alpha_syst_JetFake_TWOeleCR	(0.00, 0.00)	(0.00, 0.00)	(0.00, 0.00)	(−6.14, 7.78)	(0.00, 0.00)
alpha_syst_JetFake_TWOmuCR	(0.00, 0.00)	(0.00, 0.00)	(−3.50, 3.23)	(0.00, 0.00)	(0.00, 0.00)
alpha_syst_PhJet_shape_SR	(0.27, −0.27)	(0.00, 0.00)	(0.00, 0.00)	(0.00, 0.00)	(0.00, 0.00)

Table 52: Breakdown of the dominant systematic uncertainties expressed in % on background estimates before the fit in the SR defined by $E_{\mathrm{T}}^{\mathrm{miss}}$ sup 300 GeV and its CRs for an integrated luminosity of 36.4 fb^{-1}. Note that the individual uncertainties can be correlated, and do not necessarily add up quadratically to the total background uncertainty. The percentages show the size of the uncertainty relative to the total expected background.

Systematic	SR	CR1mu	CR2mu	CR2e	CRgjet
alpha_EG_RESO	(0.18, 0.09)	(0.27, 0.29)	(0.09, 0.08)	(0.03, −0.31)	(−0.57, 1.06)
alpha_EG_SCALE	(−2.58, 2.76)	(−1.97, 2.33)	(−2.39, 2.35)	(−2.11, 2.05)	(−6.44, 7.62)
alpha_EL_EFF_ID	(−0.00, 0.01)	(0.01, −0.03)	(−0.00, 0.01)	(−1.97, 4.34)	(0.03, −0.06)
alpha_EL_EFF_ISO	(−0.00, 0.01)	(0.02, −0.02)	(−0.00, 0.01)	(−1.08, 1.62)	(0.04, −0.05)
alpha_EL_EFF_RECO	(−0.00, 0.01)	(0.02, −0.02)	(−0.00, 0.01)	(−1.05, 1.43)	(0.04, −0.05)
alpha_EleFake_statCR_ONEmuCR1	(0.00, 0.00)	(−0.06, 0.06)	(0.00, 0.00)	(0.00, 0.00)	(0.00, 0.00)
alpha_EleFake_statCR_PhJetCR1	(0.00, 0.00)	(0.00, 0.00)	(0.00, 0.00)	(0.00, 0.00)	(−0.02, 0.02)
alpha_EleFake_statCR_SR1	(−0.09, 0.09)	(0.00, 0.00)	(0.00, 0.00)	(0.00, 0.00)	(0.00, 0.00)
alpha_EleFake_statCR_TWOeleCR1	(0.00, 0.00)	(0.00, 0.00)	(0.00, 0.00)	(−0.02, 0.02)	(0.00, 0.00)
alpha_EleFake_statCR_TWOmuCR1	(0.00, 0.00)	(0.00, 0.00)	(−0.04, 0.04)	(0.00, 0.00)	(0.00, 0.00)
alpha_EleFake_stat_ONEmuCR1	(0.00, 0.00)	(−0.14, 0.14)	(0.00, 0.00)	(0.00, 0.00)	(0.00, 0.00)
alpha_EleFake_stat_PhJetCR1	(0.00, 0.00)	(0.00, 0.00)	(0.00, 0.00)	(0.00, 0.00)	(−0.12, 0.12)
alpha_EleFake_stat_SR1	(−0.66, 0.66)	(0.00, 0.00)	(0.00, 0.00)	(0.00, 0.00)	(0.00, 0.00)
alpha_EleFake_stat_TWOeleCR1	(0.00, 0.00)	(0.00, 0.00)	(0.00, 0.00)	(−0.00, 0.00)	(0.00, 0.00)
alpha_EleFake_stat_TWOmuCR1	(0.00, 0.00)	(0.00, 0.00)	(−0.02, 0.02)	(0.00, 0.00)	(0.00, 0.00)
alpha_EleFake_syst_ONEmuCR1	(0.00, 0.00)	(−0.30, 0.30)	(0.00, 0.00)	(0.00, 0.00)	(0.00, 0.00)
alpha_EleFake_syst_PhJetCR1	(0.00, 0.00)	(0.00, 0.00)	(0.00, 0.00)	(0.00, 0.00)	(−0.25, 0.25)
alpha_EleFake_syst_SR1	(−1.36, 1.36)	(0.00, 0.00)	(0.00, 0.00)	(0.00, 0.00)	(0.00, 0.00)
alpha_EleFake_syst_TWOeleCR1	(0.00, 0.00)	(0.00, 0.00)	(0.00, 0.00)	(−0.00, 0.00)	(0.00, 0.00)
alpha_EleFake_syst_TWOmuCR1	(0.00, 0.00)	(0.00, 0.00)	(−0.03, 0.03)	(0.00, 0.00)	(0.00, 0.00)
alpha_JER	(0.73, −0.77)	(1.29, −1.38)	(1.74, −1.85)	(1.39, −1.48)	(−9.55, 10.18)
alpha_JES	(4.23, −8.99)	(4.66, −4.49)	(3.11, −4.43)	(2.53, −3.44)	(−3.78, 1.82)
alpha_JVT_EFF	(0.22, −0.22)	(0.15, −0.15)	(0.19, −0.20)	(0.15, −0.15)	(0.20, −0.20)
alpha_JetFake_statCR_ONEmuCR1	(0.00, 0.00)	(−1.76, 1.76)	(0.00, 0.00)	(0.00, 0.00)	(0.00, 0.00)
alpha_JetFake_statCR_PhJetCR1	(0.00, 0.00)	(0.00, 0.00)	(0.00, 0.00)	(0.00, 0.00)	(−0.48, 0.48)
alpha_JetFake_statCR_SR1	(−1.05, 1.05)	(0.00, 0.00)	(0.00, 0.00)	(0.00, 0.00)	(0.00, 0.00)
alpha_JetFake_statCR_TWOeleCR1	(0.00, 0.00)	(0.00, 0.00)	(0.00, 0.00)	(−2.10, 3.29)	(0.00, 0.00)
alpha_JetFake_statCR_TWPmuCR1	(0.00, 0.00)	(0.00, 0.00)	(−0.61, 1.50)	(0.00, 0.00)	(0.00, 0.00)
alpha_LUMI_SYST	(−3.53, 3.50)	(−3.69, 3.66)	(−4.08, 4.05)	(−3.89, 3.86)	(−3.83, 3.80)
alpha_MET_RESO_PARA	(0.67, −0.66)	(0.90, −0.89)	(0.17, −0.17)	(0.20, −0.20)	(2.93, −2.90)
alpha_MET_RESO_PERP	(1.13, −1.16)	(0.30, −0.30)	(0.49, −0.50)	(0.30, −0.30)	(8.58, −8.78)
alpha_MET_SCALE	(0.40, −0.74)	(0.50, −0.77)	(−0.06, −0.12)	(−0.11, −0.15)	(11.88, −11.17)
alpha_MU_EFF_STAT	(0.23, −0.21)	(−0.24, −0.06)	(−0.38, −0.02)	(0.16, −0.15)	(0.21, −0.19)
alpha_MU_EFF_SYST	(0.27, −0.18)	(−0.98, 0.43)	(−1.92, 1.00)	(0.18, −0.12)	(0.24, −0.16)
alpha_MU_EFF_SYST_LOWPT	(0.23, −0.22)	(−0.17, −0.12)	(−0.28, −0.11)	(0.16, −0.15)	(0.21, −0.20)
alpha_MU_ID	(0.16, −0.22)	(−0.37, 0.07)	(−0.25, −0.19)	(0.16, −0.15)	(−0.15, −0.21)
alpha_MU_ISO_STAT	(0.23, −0.22)	(−0.22, −0.08)	(−0.34, −0.05)	(0.16, −0.15)	(0.21, −0.19)
alpha_MU_ISO_SYST	(0.24, −0.20)	(−0.48, 0.14)	(−0.96, 0.45)	(0.17, −0.14)	(0.22, −0.18)
alpha_MU_MS	(−0.01, −0.22)	(−0.14, −0.13)	(−0.24, −0.22)	(−0.16, −0.15)	(−0.24, −0.18)
alpha_MU_SCALE	(0.15, −0.22)	(−0.14, −0.15)	(−0.21, −0.21)	(0.15, −0.15)	(−0.21, −0.20)
alpha_MU_TTVA_STAT	(0.23, −0.22)	(−0.17, −0.12)	(−0.26, −0.13)	(0.16, −0.15)	(0.21, −0.20)
alpha_MU_TTVA_SYS	(0.23, −0.21)	(−0.25, −0.05)	(−0.50, 0.09)	(0.16, −0.15)	(0.21, −0.19)
alpha_PDF_Comb	(−0.74, 0.74)	(−0.72, 0.72)	(−0.79, 0.79)	(−0.75, 0.75)	(−0.57, 0.57)
alpha_PH_EFF	(1.61, −2.06)	(1.78, −2.09)	(1.92, −2.32)	(1.87, −2.18)	(1.82, −2.23)
alpha_PH_EFF_TRKISO	(0.22, −0.22)	(0.15, −0.15)	(0.19, −0.20)	(0.15, −0.15)	(0.20, −0.20)
alpha_PH_ISO_DD	(0.22, −0.22)	(0.15, −0.15)	(0.19, −0.20)	(0.15, −0.15)	(0.20, −0.20)
alpha_PRW_DATASF	(−1.40, −0.90)	(1.33, −2.24)	(1.05, −2.27)	(1.00, −1.44)	(−4.97, 6.36)
alpha_syst_JetFake_ONEmuCR1	(0.00, 0.00)	(−1.19, 1.19)	(0.00, 0.00)	(0.00, 0.00)	(0.00, 0.00)
alpha_syst_JetFake_PhJetCR1	(0.00, 0.00)	(0.00, 0.00)	(0.00, 0.00)	(0.00, 0.00)	(−0.30, 0.30)
alpha_syst_JetFake_SR1	(−0.73, 0.73)	(0.00, 0.00)	(0.00, 0.00)	(0.00, 0.00)	(0.00, 0.00)
alpha_syst_JetFake_TWOeleCR1	(0.00, 0.00)	(0.00, 0.00)	(0.00, 0.00)	(−1.27, 1.56)	(0.00, 0.00)
alpha_syst_JetFake_TWOmuCR1	(0.00, 0.00)	(0.00, 0.00)	(−0.48, 0.45)	(0.00, 0.00)	(0.00, 0.00)
alpha_syst_PhJet_shape_SR1	(2.28, −2.28)	(0.00, 0.00)	(0.00, 0.00)	(0.00, 0.00)	(0.00, 0.00)

Table 53: Breakdown of the dominant systematic uncertainties expressed in % on background estimates before the simplified shape fit in the SR defined by $E_{\mathrm{T}}^{\mathrm{miss}} \in$ [150 GeV; 225 GeV] and its CRs for an integrated luminosity of 36.4 fb^{-1}. Note that the individual uncertainties can be correlated, and do not necessarily add up quadratically to the total background uncertainty. The percentages show the size of the uncertainty relative to the total expected background.

Systematic	SR	CR1mu	CR2mu	CR2e	CRgjet
alpha_EG_RESO	(−0.38, 0.13)	(0.22, 0.16)	(−0.36, 0.01)	(0.20, 0.06)	(−0.69, 1.19)
alpha_EG_SCALE	(−2.88, 2.92)	(−2.24, 2.12)	(−2.23, 2.01)	(−2.41, 1.86)	(−7.21, 8.54)
alpha_EL_EFF_ID	(−0.00, 0.00)	(−0.00, 0.00)	(−0.02, 0.05)	(−1.93, 4.15)	(0.04, −0.08)
alpha_EL_EFF_ISO	(−0.00, 0.00)	(−0.00, 0.00)	(−0.03, 0.04)	(−1.61, 2.31)	(0.04, −0.07)
alpha_EL_EFF_RECO	(−0.00, 0.00)	(−0.00, 0.00)	(−0.03, 0.04)	(−1.01, 1.28)	(0.05, −0.06)
alpha_EleFake_statCR_ONEmuCR2	(0.00, 0.00)	(−0.09, 0.09)	(0.00, 0.00)	(0.00, 0.00)	(0.00, 0.00)
alpha_EleFake_statCR_SR2	(−0.15, 0.15)	(0.00, 0.00)	(0.00, 0.00)	(0.00, 0.00)	(0.00, 0.00)
alpha_EleFake_statCR_TWOeleCR2	(0.00, 0.00)	(0.00, 0.00)	(0.00, 0.00)	(−0.00, 0.00)	(0.00, 0.00)
alpha_EleFake_statCR_TWOmuCR2	(0.00, 0.00)	(0.00, 0.00)	(−0.09, 0.09)	(0.00, 0.00)	(0.00, 0.00)
alpha_EleFake_stat_ONEmuCR2	(0.00, 0.00)	(−0.14, 0.14)	(0.00, 0.00)	(0.00, 0.00)	(0.00, 0.00)
alpha_EleFake_stat_SR2	(−0.80, 0.80)	(0.00, 0.00)	(0.00, 0.00)	(0.00, 0.00)	(0.00, 0.00)
alpha_EleFake_stat_TWOeleCR2	(0.00, 0.00)	(0.00, 0.00)	(0.00, 0.00)	(−0.00, 0.00)	(0.00, 0.00)
alpha_EleFake_stat_TWOmuCR2	(0.00, 0.00)	(0.00, 0.00)	(−0.03, 0.03)	(0.00, 0.00)	(0.00, 0.00)
alpha_EleFake_syst_ONEmuCR2	(0.00, 0.00)	(−0.28, 0.28)	(0.00, 0.00)	(0.00, 0.00)	(0.00, 0.00)
alpha_EleFake_syst_SR2	(−1.41, 1.41)	(0.00, 0.00)	(0.00, 0.00)	(0.00, 0.00)	(0.00, 0.00)
alpha_EleFake_syst_TWOeleCR2	(0.00, 0.00)	(0.00, 0.00)	(0.00, 0.00)	(−0.00, 0.00)	(0.00, 0.00)
alpha_EleFake_syst_TWOmuCR2	(0.00, 0.00)	(0.00, 0.00)	(−0.06, 0.06)	(0.00, 0.00)	(0.00, 0.00)
alpha_JER	(0.20, −0.22)	(0.52, −0.56)	(0.90, −0.96)	(0.36, −0.38)	(−10.96, 11.69)
alpha_JES	(1.90, −2.45)	(2.87, −3.29)	(1.15, −2.38)	(1.23, −1.62)	(−4.60, 2.31)
alpha_JVT_EFF	(0.13, −0.13)	(0.15, −0.15)	(0.18, −0.18)	(0.10, −0.10)	(0.22, −0.22)
alpha_JetFake_statCR_ONEmuCR2	(0.00, 0.00)	(−3.29, 3.29)	(0.00, 0.00)	(0.00, 0.00)	(0.00, 0.00)
alpha_JetFake_statCR_SR2	(−1.58, 1.58)	(0.00, 0.00)	(0.00, 0.00)	(0.00, 0.00)	(0.00, 0.00)
alpha_JetFake_statCR_TWOeleCR2	(0.00, 0.00)	(0.00, 0.00)	(0.00, 0.00)	(−3.47, 5.84)	(0.00, 0.00)
alpha_JetFake_statCR_TWOmuCR2	(0.00, 0.00)	(0.00, 0.00)	(−4.75, 3.39)	(0.00, 0.00)	(0.00, 0.00)
alpha_LUMI_SYST	(−3.62, 3.59)	(−3.69, 3.66)	(−3.81, 3.78)	(−3.86, 3.83)	(−4.12, 4.08)
alpha_MET_RESO_PARA	(−0.36, 0.36)	(0.26, −0.26)	(0.56, −0.56)	(0.63, −0.63)	(3.34, −3.31)
alpha_MET_RESO_PERP	(0.29, −0.30)	(0.25, −0.25)	(0.41, −0.41)	(0.54, −0.55)	(9.73, −9.96)
alpha_MET_SCALE	(0.43, −0.52)	(0.13, −0.39)	(0.14, −0.69)	(−0.03, −0.58)	(13.50, −12.68)
alpha_MU_EFF_STAT	(0.14, −0.13)	(−0.23, −0.07)	(−0.34, −0.02)	(0.10, −0.10)	(0.23, −0.22)
alpha_MU_EFF_SYST	(0.16, −0.11)	(−1.30, 0.65)	(−2.35, 1.33)	(0.12, −0.08)	(0.27, −0.18)
alpha_MU_EFF_SYST_LOWPT	(0.14, −0.13)	(−0.18, −0.12)	(−0.24, −0.12)	(0.10, −0.10)	(0.23, −0.22)
alpha_MU_ID	(0.10, −0.13)	(−0.01, −0.26)	(−0.19, −0.23)	(0.10, −0.10)	(−0.17, −0.23)
alpha_MU_ISO_STAT	(0.14, −0.13)	(−0.24, −0.06)	(−0.36, −0.01)	(0.10, −0.10)	(0.23, −0.22)
alpha_MU_ISO_SYST	(0.15, −0.12)	(−0.50, 0.15)	(−0.89, 0.43)	(0.11, −0.09)	(0.24, −0.20)
alpha_MU_MS	(−0.08, −0.17)	(0.00, −0.26)	(−0.19, −0.19)	(0.10, −0.10)	(−0.27, −0.20)
alpha_MU_SCALE	(0.06, −0.08)	(−0.12, −0.15)	(−0.16, −0.21)	(0.10, −0.10)	(−0.23, −0.22)
alpha_MU_TTVA_STAT	(0.14, −0.13)	(−0.18, −0.13)	(−0.23, −0.12)	(0.10, −0.10)	(0.23, −0.22)
alpha_MU_TTVA_SYS	(0.14, −0.13)	(−0.24, −0.07)	(−0.40, 0.02)	(0.10, −0.09)	(0.23, −0.21)
alpha_PDF_Comb	(−0.69, 0.69)	(−0.70, 0.70)	(−0.73, 0.73)	(−0.74, 0.74)	(−0.61, 0.60)
alpha_PH_EFF	(1.80, −2.08)	(1.81, −2.12)	(1.85, −2.21)	(1.94, −2.15)	(1.95, −2.40)
alpha_PH_EFF_TRKISO	(0.13, −0.13)	(0.15, −0.15)	(0.18, −0.18)	(0.10, −0.10)	(0.22, −0.22)
alpha_PH_ISO_DD	(0.13, −0.13)	(0.15, −0.15)	(0.18, −0.18)	(0.10, −0.10)	(0.22, −0.22)
alpha_PRW_DATASF	(0.62, −0.47)	(0.39, −1.78)	(2.15, −3.52)	(1.37, −1.31)	(−5.73, 7.38)
alpha_syst_JetFake_ONEmuCR2	(0.00, 0.00)	(−2.91, 2.91)	(0.00, 0.00)	(0.00, 0.00)	(0.00, 0.00)
alpha_syst_JetFake_SR2	(−0.95, 0.96)	(0.00, 0.00)	(0.00, 0.00)	(0.00, 0.00)	(0.00, 0.00)
alpha_syst_JetFake_TWOeleCR2	(0.00, 0.00)	(0.00, 0.00)	(0.00, 0.00)	(−1.62, 1.89)	(0.00, 0.00)
alpha_syst_JetFake_TWOmuCR2	(0.00, 0.00)	(0.00, 0.00)	(−1.62, 1.42)	(0.00, 0.00)	(0.00, 0.00)
alpha_syst_PhJet_shape_SR2	(0.40, −0.40)	(0.00, 0.00)	(0.00, 0.00)	(0.00, 0.00)	(0.00, 0.00)

Table 54: Breakdown of the dominant systematic uncertainties expressed in % on background estimates before the simplified shape fit in the SR defined by $E_{\mathrm{T}}^{\mathrm{miss}} \in$ [225 GeV; 300 GeV] and its CRs for an integrated luminosity of 36.4 fb^{-1}. Note that the individual uncertainties can be correlated, and do not necessarily add up quadratically to the total background uncertainty. The percentages show the size of the uncertainty relative to the total expected background.

Systematic	SR	CR1mu	CR2mu	CR2e	CRgjet
alpha_EG_RESO	(0.03, 0.18)	(−0.40, 0.31)	(0.24, 0.20)	(0.41, 0.43)	(−0.69, 1.19)
alpha_EG_SCALE	(−2.52, 2.88)	(−2.62, 2.96)	(−3.21, 3.88)	(−1.96, 2.74)	(−7.21, 8.54)
alpha_EL_EFF_ID	(0.00, −0.00)	(0.00, 0.00)	(0.02, −0.04)	(−1.85, 3.97)	(0.04, −0.08)
alpha_EL_EFF_ISO	(0.00, −0.00)	(0.00, 0.00)	(0.02, −0.04)	(−1.90, 2.75)	(0.04, −0.07)
alpha_EL_EFF_RECO	(0.00, −0.00)	(0.00, 0.00)	(0.03, −0.03)	(−0.94, 1.19)	(0.05, −0.06)
alpha_EleFake_statCR_ONEmuCR3	(0.00, 0.00)	(−0.11, 0.11)	(0.00, 0.00)	(0.00, 0.00)	(0.00, 0.00)
alpha_EleFake_statCR_SR3	(−0.16, 0.16)	(0.00, 0.00)	(0.00, 0.00)	(0.00, 0.00)	(0.00, 0.00)
alpha_EleFake_statCR_TWOeleCR3	(0.00, 0.00)	(0.00, 0.00)	(0.00, 0.00)	(−0.14, 0.14)	(0.00, 0.00)
alpha_EleFake_statCR_TWOmuCR3	(0.00, 0.00)	(0.00, 0.00)	(−0.06, 0.06)	(0.00, 0.00)	(0.00, 0.00)
alpha_EleFake_stat_ONEmuCR3	(0.00, 0.00)	(−0.10, 0.10)	(0.00, 0.00)	(0.00, 0.00)	(0.00, 0.00)
alpha_EleFake_stat_SR3	(−0.61, 0.61)	(0.00, 0.00)	(0.00, 0.00)	(0.00, 0.00)	(0.00, 0.00)
alpha_EleFake_stat_TWOeleCR3	(0.00, 0.00)	(0.00, 0.00)	(0.00, 0.00)	(−0.02, 0.02)	(0.00, 0.00)
alpha_EleFake_stat_TWOmuCR3	(0.00, 0.00)	(0.00, 0.00)	(−0.01, 0.01)	(0.00, 0.00)	(0.00, 0.00)
alpha_EleFake_syst_ONEmuCR3	(0.00, 0.00)	(−0.20, 0.20)	(0.00, 0.00)	(0.00, 0.00)	(0.00, 0.00)
alpha_EleFake_syst_SR3	(−1.06, 1.06)	(0.00, 0.00)	(0.00, 0.00)	(0.00, 0.00)	(0.00, 0.00)
alpha_EleFake_syst_TWOeleCR3	(0.00, 0.00)	(0.00, 0.00)	(0.00, 0.00)	(−0.04, 0.04)	(0.00, 0.00)
alpha_EleFake_syst_TWOmuCR3	(0.00, 0.00)	(0.00, 0.00)	(−0.02, 0.02)	(0.00, 0.00)	(0.00, 0.00)
alpha_JER	(1.33, −1.41)	(1.51, −1.61)	(1.09, −1.16)	(0.99, −1.05)	(−10.96, 11.69)
alpha_JES	(1.74, −4.15)	(2.34, −3.84)	(2.68, −3.55)	(1.57, −1.64)	(−4.60, 2.31)
alpha_JVT_EFF	(0.12, −0.12)	(0.12, −0.12)	(0.14, −0.14)	(0.22, −0.23)	(0.22, −0.22)
alpha_JetFake_statCR_ONEmuCR3	(0.00, 0.00)	(−1.81, 1.81)	(0.00, 0.00)	(0.00, 0.00)	(0.00, 0.00)
alpha_JetFake_statCR_SR3	(−1.60, 1.61)	(0.00, 0.00)	(0.00, 0.00)	(0.00, 0.00)	(0.00, 0.00)
alpha_JetFake_statCR_TWOeleCR3	(0.00, 0.00)	(0.00, 0.00)	(0.00, 0.00)	(−4.54, 4.96)	(0.00, 0.00)
alpha_JetFake_statCR_TWOmuCR3	(0.00, 0.00)	(0.00, 0.00)	(−3.71, 3.46)	(0.00, 0.00)	(0.00, 0.00)
alpha_LUMI_SYST	(−3.77, 3.74)	(−3.95, 3.92)	(−3.93, 3.90)	(−3.83, 3.80)	(−4.12, 4.08)
alpha_MET_RESO_PARA	(0.29, −0.29)	(0.22, −0.21)	(−0.18, 0.18)	(0.06, −0.06)	(3.34, −3.31)
alpha_MET_RESO_PERP	(0.34, −0.35)	(0.14, −0.14)	(−0.59, 0.60)	(−0.00, 0.00)	(9.73, −9.96)
alpha_MET_SCALE	(−0.05, −0.40)	(0.09, −0.23)	(0.11, 0.03)	(0.05, −0.15)	(13.50, −12.68)
alpha_MU_EFF_STAT	(0.12, −0.11)	(−0.20, −0.04)	(−0.29, −0.00)	(0.23, −0.22)	(0.23, −0.22)
alpha_MU_EFF_SYST	(0.14, −0.09)	(−1.76, 1.02)	(−2.96, 1.81)	(0.27, −0.18)	(0.27, −0.18)
alpha_MU_EFF_SYST_LOWPT	(0.12, −0.11)	(−0.14, −0.10)	(−0.18, −0.10)	(0.23, −0.22)	(0.23, −0.22)
alpha_MU_ID	(0.11, −0.10)	(−0.10, 0.78)	(−0.06, −0.15)	(0.23, −0.22)	(−0.17, −0.23)
alpha_MU_ISO_STAT	(0.12, −0.11)	(−0.32, 0.07)	(−0.48, 0.17)	(0.23, −0.22)	(0.23, −0.22)
alpha_MU_ISO_SYST	(0.13, −0.11)	(−0.53, 0.23)	(−0.92, 0.52)	(0.25, −0.21)	(0.24, −0.20)
alpha_MU_MS	(0.13, −0.13)	(−0.14, −0.11)	(−0.25, −0.13)	(0.23, −0.22)	(−0.27, −0.20)
alpha_MU_SCALE	(0.12, −0.12)	(−0.12, −0.12)	(−0.20, −0.09)	(0.23, −0.22)	(−0.23, −0.22)
alpha_MU_TTVA_STAT	(0.12, −0.11)	(−0.14, −0.09)	(−0.20, −0.09)	(0.23, −0.22)	(0.23, −0.22)
alpha_MU_TTVA_SYS	(0.12, −0.11)	(−0.20, −0.04)	(−0.32, 0.02)	(0.24, −0.22)	(0.23, −0.21)
alpha_PDF_Comb	(−0.72, 0.72)	(−0.81, 0.81)	(−0.75, 0.75)	(−0.73, 0.73)	(−0.61, 0.60)
alpha_PH_EFF	(1.99, −2.23)	(2.07, −2.32)	(2.03, −2.32)	(1.82, −2.28)	(1.95, −2.40)
alpha_PH_EFF_TRKISO	(0.12, −0.12)	(0.12, −0.12)	(0.14, −0.14)	(0.22, −0.23)	(0.22, −0.22)
alpha_PH_ISO_DD	(0.12, −0.12)	(0.12, −0.12)	(0.14, −0.14)	(0.22, −0.23)	(0.22, −0.22)
alpha_PRW_DATASF	(0.35, −0.90)	(−0.34, 0.33)	(−0.15, 0.53)	(0.15, −0.89)	(−5.73, 7.38)
alpha_syst_JetFake_ONEmuCR3	(0.00, 0.00)	(−2.50, 2.50)	(0.00, 0.00)	(0.00, 0.00)	(0.00, 0.00)
alpha_syst_JetFake_SR3	(−3.29, 3.29)	(0.00, 0.00)	(0.00, 0.00)	(0.00, 0.00)	(0.00, 0.00)
alpha_syst_JetFake_TWOeleCR3	(0.00, 0.00)	(0.00, 0.00)	(0.00, 0.00)	(−6.44, 7.73)	(0.00, 0.00)
alpha_syst_JetFake_TWOmuCR3	(0.00, 0.00)	(0.00, 0.00)	(−3.41, 3.21)	(0.00, 0.00)	(0.00, 0.00)
alpha_syst_PhJet_shape_SR3	(0.27, −0.27)	(0.00, 0.00)	(0.00, 0.00)	(0.00, 0.00)	(0.00, 0.00)

Table 55: Breakdown of the dominant systematic uncertainties expressed in % on background estimates before the simplified shape fit in the SR defined by $E_{\mathrm{T}}^{\mathrm{miss}} > 300$ GeV and its CRs for an integrated luminosity of 36.4 fb^{-1}. Note that the individual uncertainties can be correlated, and do not necessarily add up quadratically to the total background uncertainty. The percentages show the size of the uncertainty relative to the total expected background.

F Signal region choice

The expected limit on the simplified DM model signal strength was computed for the various inclusive regions and for the multiple-bin fit in order to determine which strategy to adopt for limit setting. The resulting expected limits can be seen in Fig.54.

Of the inclusive regions, the $E_{\mathrm{T}}^{\mathrm{miss}} > 150$ GeV one is the best at very low DM/mediator masses, quickly superseded by the $E_{\mathrm{T}}^{\mathrm{miss}} > 225$ GeV region in the rest of the parameter space. The $E_{\mathrm{T}}^{\mathrm{miss}} > 300$ GeV , probably because of its larger associated uncertainty, is not able to set better constraints on high-mass models in spite of their harder $E_{\mathrm{T}}^{\mathrm{miss}}$ spectra. The multiple-bin fit allows to set better expected limits than any of the inclusive signal regions. It will thus be adopted to set model-dependent limits.

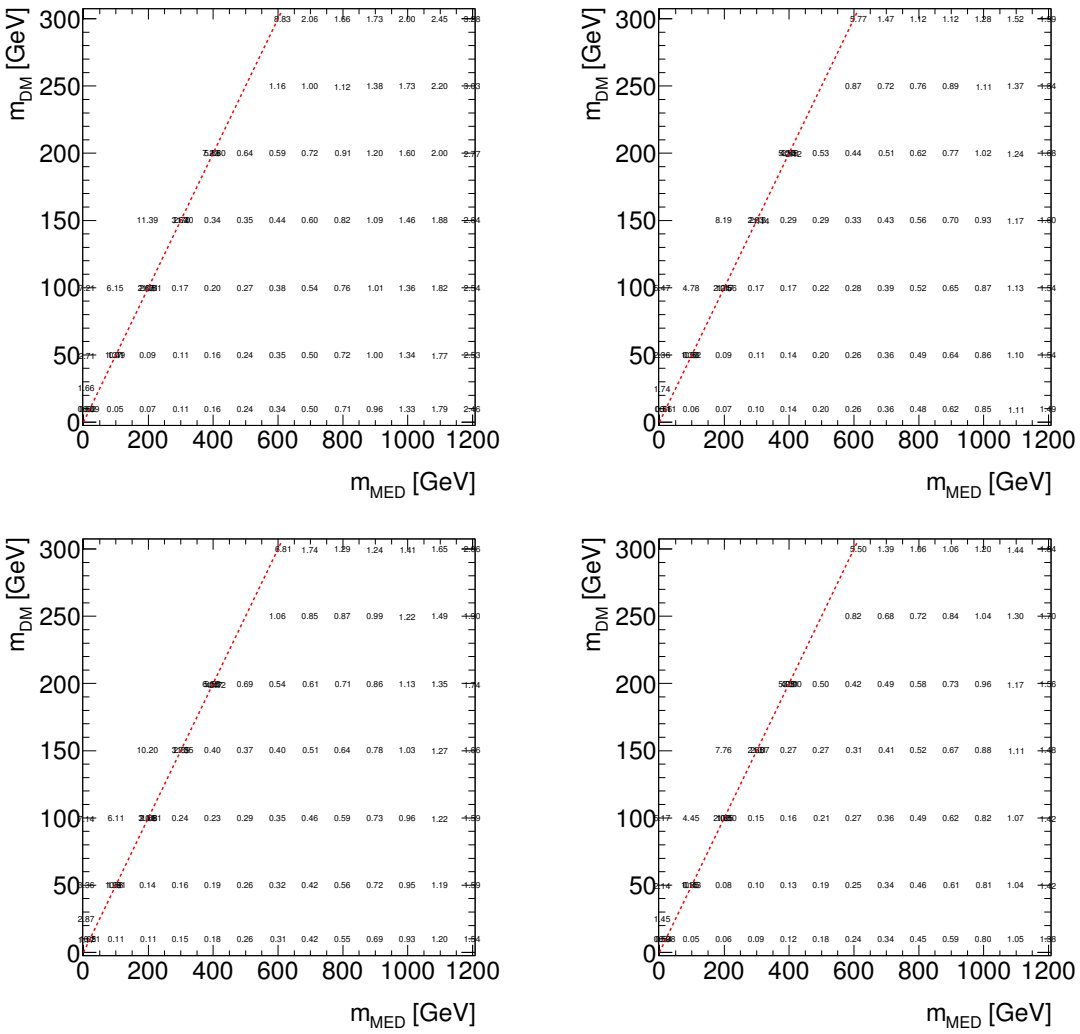

Figure 54: Expected upper limit on the signal strength for the simplified DM model with an axial-vector mediator for the inclusive signal region with $E_{\mathrm{T}}^{\mathrm{miss}}$>150 GeV (upper left), $E_{\mathrm{T}}^{\mathrm{miss}}$>225 GeV (upper right), and $E_{\mathrm{T}}^{\mathrm{miss}}$>300 GeV (lower left), and for the multiple-bin fit (lower right).

G Rescaling to other DM simplified models

The LHC Dark Matter Working Group recommends to present the results for both axial-vector and vector mediators, using the following couplings, to allow to show the complementarity of the direct searches, such as this one, and resonance searches looking for the mediator, such as dijet or dilepton resonance searches:

- V1: vector mediator with couplings only to quarks and DM: $g_q = 0.25$, $g_\chi = 1.0$, $g_\ell = 0$
- V2: vector mediator with small couplings to leptons as well: $g_q = 0.1$, $g_\chi = 1.0$, $g_\ell = 0.01$
- A1: axial-vector mediator with couplings only to quarks and DM: $g_q = 0.25$, $g_\chi = 1.0$, $g_\ell = 0$ (the one described in Section 2.1 and generated officially for this analysis).
- A2: axial-vector mediator with couplings also to leptons: $g_\chi = 1.0$, $g_q = g_\ell = 0.1$

It is expected that these various choices only affect the cross-section and not the acceptance of the analysis: once a model is generated (the A1 model in this case), it could then be simply re-used and re-scaled in order to present results for the other scenarios.

This assumption was tested and the results are shown in Fig. 55: the ratio of the acceptance of the various scenarios is seen to be compatible with 1 for all points checked in the plots, therefore validating the rescaling approach. The cross section for each scenario can be seen in Fig. 56.

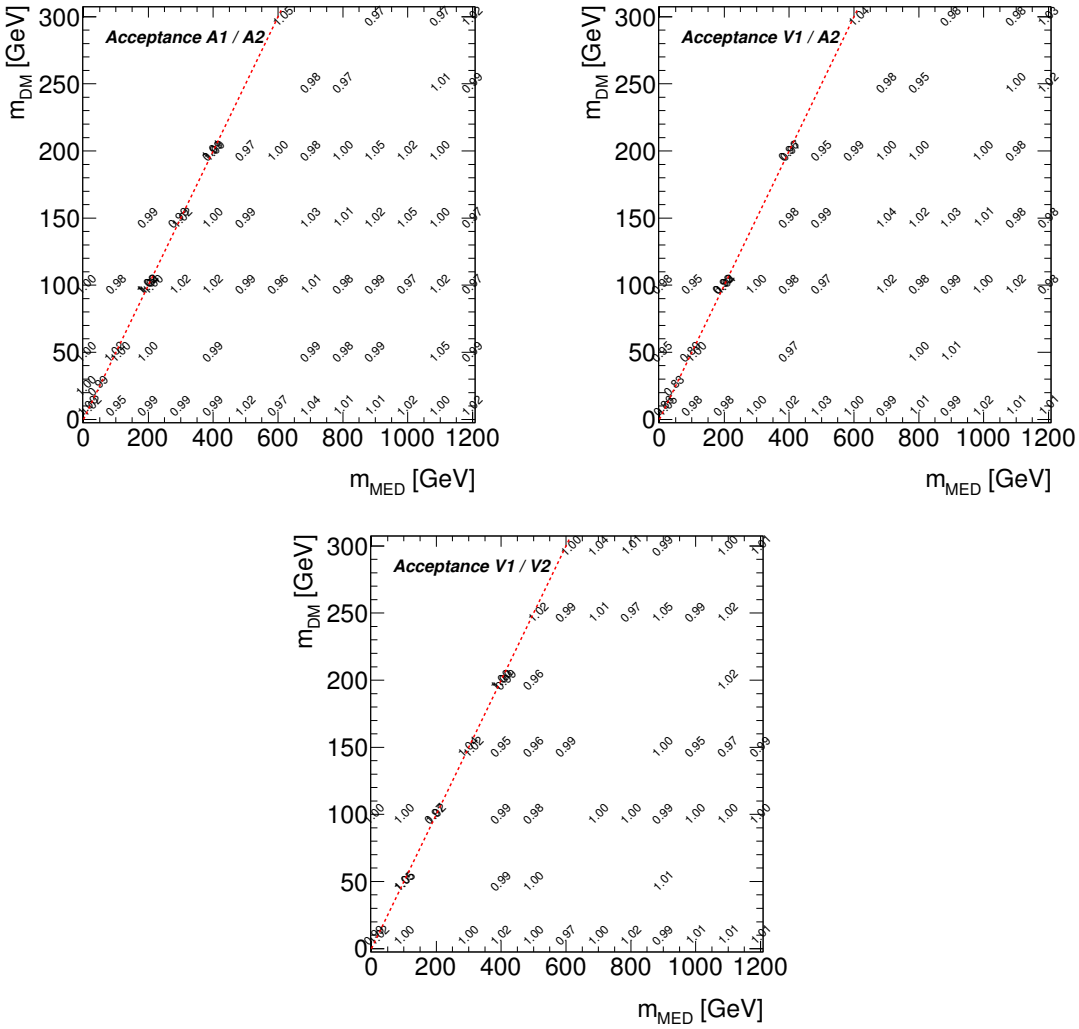

Figure 55: Ratio of the acceptance of the analysis for the various simplified DM scenarios, where the A1 scenario is the nominal one in this analysis: A1 over A2 scenarios (top left), V1 over A2 scenarios (top right) and V1 over V2 scenarios (bottom). All ratios are compatible with 1 within statistical uncertainty.

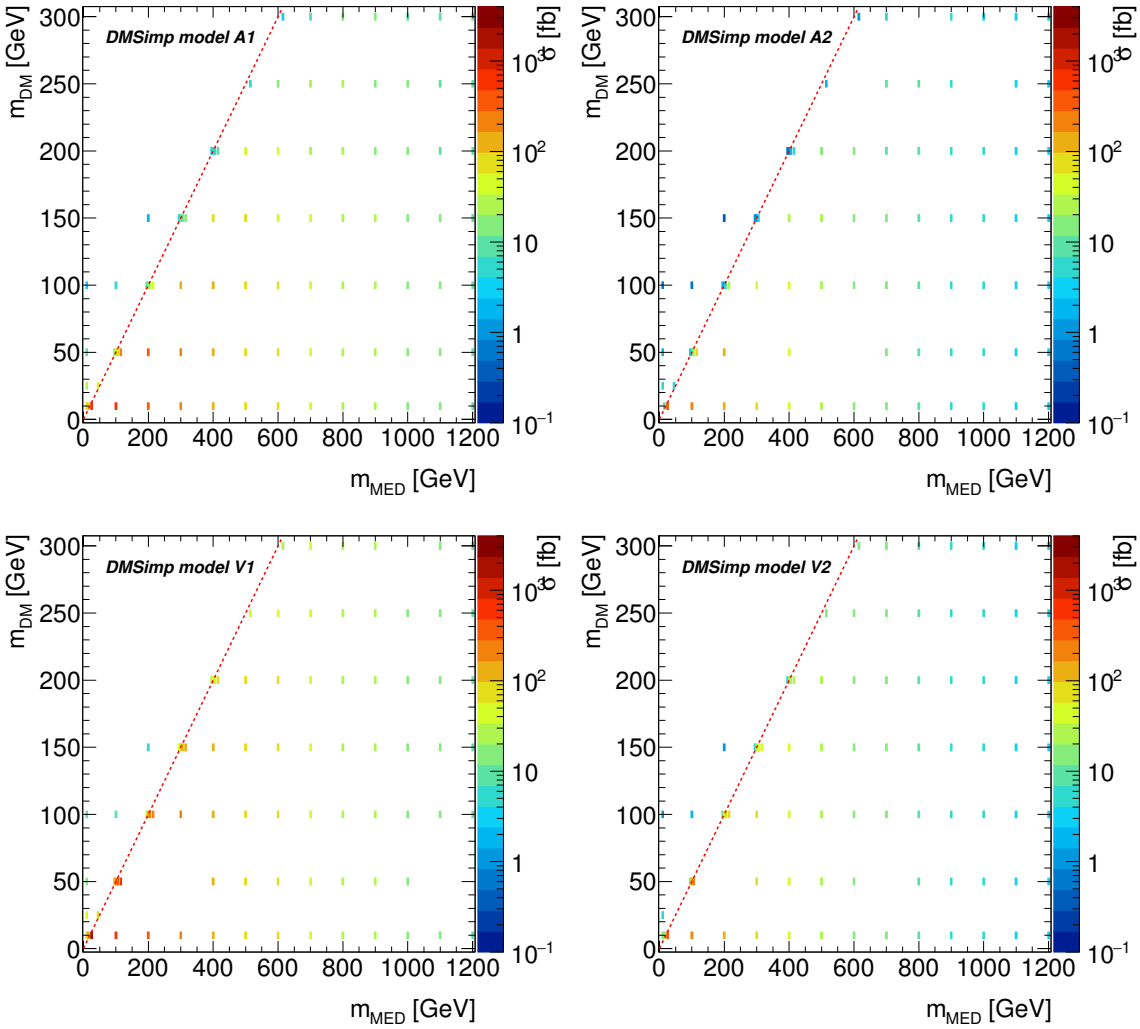

Figure 56: Cross section for the various simplified DM model scenarios: A1 (upper left), A2, (upper right), V1 (lower left) and V2 (lower right).

H Auxiliary material

Table 56 gives an example cutflow for the DMsimp point with m_{DM} = 10 GeV and m_{MED} = 800 GeV .

Cut	N_{events}
Nominal	1198
Skimming (incl. trigger)	858
$E_{\mathrm{T}}^{\mathrm{miss}} > 150$ GeV	736
At least one loose photon with $p_{\mathrm{T}}>$ 150 GeV (—η—¡2.37)	700
$z_0 < 250$ mm	696
The leading photon is tight	658
The leading photon is isolated	622
$\Delta\phi(\gamma, E_{\mathrm{T}}^{\mathrm{miss}}) > 0.4$	620
$E_{\mathrm{T}}^{\mathrm{miss}}/\sqrt{\Sigma E_T} > 8.5$ GeV$^{1/2}$	596
Jet veto	461
Lepton veto	460

Table 56: Number of events after each cut for 36.4 fb^{-1} for a simplified model of dark matter production involving an axial-vector operator, Dirac DM and couplings g_q= 0.25 and g_{DM} = 1 with m_{DM} = 10 GeV and m_{MED} = 800 GeV . The skimming requests at least one reconstructed photon with $p_{\mathrm{T}}>$ 125 GeV and $E_{\mathrm{T}}^{\mathrm{miss}}>$ 70 GeV .

The limit on the signal strength μ is shown in Figure 57 for various DMsimp points.

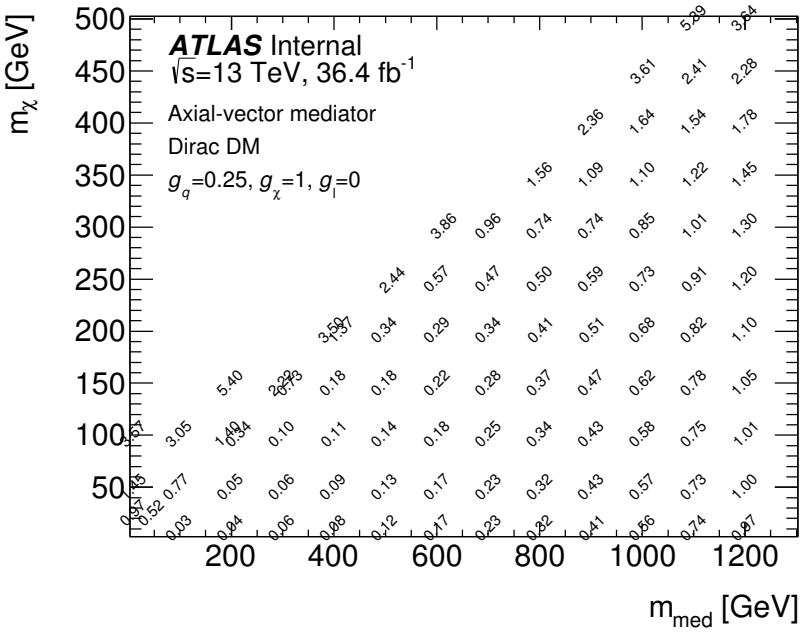

Figure 57: The observed 95% CL upper limits on signal strength μ, the ratio of the experimental limit to the predicted signal cross-section, for a simplified model of dark matter production involving an axial-vector operator, Dirac DM and couplings g_q= 0.25 and g_{DM} = 1 as a function of the DM and the axial mediator particle masses. The bound on μ only applies for choices of couplings that yield the same kinematic distributions as the benchmark model.

1262 The acceptance for various DMsimp points is shown in Table 57

m_{DM} (GeV)	m_{MED} (GeV)	$A^{E_{\mathrm{T}}^{\mathrm{miss}}>150\ \mathrm{GeV}}$ (%)	$A^{E_{\mathrm{T}}^{\mathrm{miss}}>225\ \mathrm{GeV}}$ (%)	$A^{E_{\mathrm{T}}^{\mathrm{miss}}>300\ \mathrm{GeV}}$ (%)
10	10	23.1	10.0	4.0
10	15	21.9	9.3	3.6
10	25	13.7	5.4	2.1
10	100	24.8	9.8	3.8
10	200	32.3	14.3	5.3
10	300	37.2	17.8	7.6
10	400	39.1	20.0	8.9
10	500	41.7	22.9	11.6
10	600	42.0	23.6	11.7
10	700	45.8	26.0	13.8
10	800	45.2	27.5	14.6
10	900	46.5	28.8	15.1
10	1000	47.3	30.0	16.8
10	1100	47.7	30.7	18.3
10	1200	48.3	31.4	18.5
100	10	38.8	19.7	8.9
100	100	39.3	19.9	9.6
100	195	37.5	18.3	8.2
100	200	37.8	18.2	8.4
100	205	34.4	16.0	6.7
100	215	33.6	14.9	6.9
150	200	41.3	22.6	11.8
150	295	40.4	20.5	10.2
150	300	38.8	20.9	9.1
150	305	39.3	20.5	8.9
150	315	38.6	19.8	8.7
200	395	42.9	24.9	12.3
200	400	42.2	23.0	10.8
200	405	41.5	22.1	10.5
200	415	41.6	23.1	10.4
25	10	30.7	13.6	5.2
25	45	28.1	11.5	4.7
250	515	43.9	25.1	11.9
300	615	44.3	25.9	13.6
50	10	34.2	16.7	7.4
50	95	32.2	14.1	5.6
50	100	30.3	13.4	5.3
50	105	28.9	12.2	4.4
50	115	27.1	11.6	4.6

Table 57: Acceptance, in %, for a simplified model of dark matter production involving an axial-vector operator, Dirac DM and couplings g_q= 0.25 and g_{DM} = 1 for various m_{DM} and m_{MED} values.

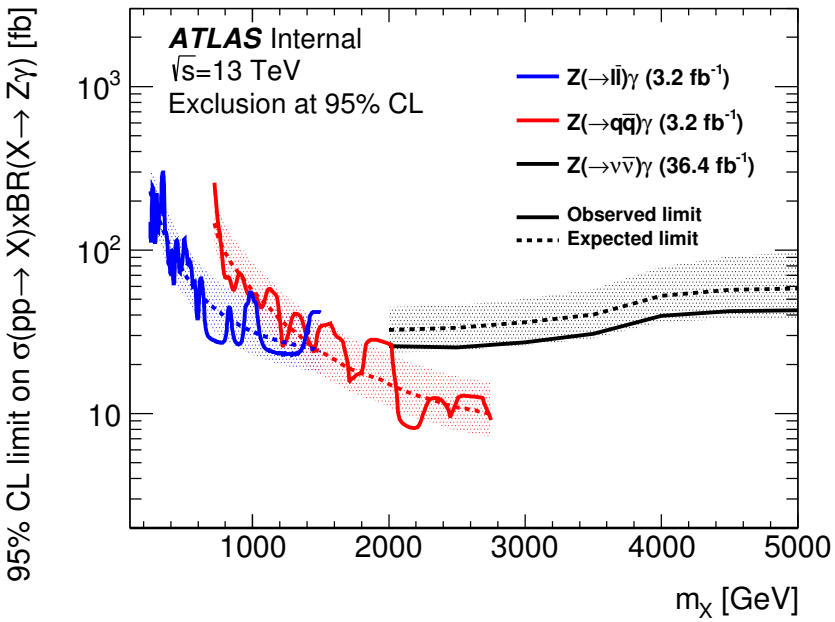

Figure 58: The observed (expected) limit at 95% CL on the production cross section of a $Z\gamma$ resonance as a function of its mass. The limits from the search in the $Z \to q\bar{q}$ and $Z \to \ell\ell$ channels with 3.2 fb^{-1}are also reported.